JUN 20 1982

E 1.28: ONWI-352/v.2

COMPLETED

211

ORIGINAL

ONWI-352
UCRL-53142

Uncertainties and Sensitivities in the Performance of Geologic Nuclear Waste Isolation Systems

Volume II

Technical Report

April, 1981

W. G. Sutcliffe
K. G. Feller
N. K. Madsen
G. D. Pollak

Lawrence Livermore National Laboratory
University of California
Livermore, CA 94550

ONWI
Office of Nuclear Waste Isolation

BATTELLE Project Management Division

BIBLIOGRAPHIC DATA

Sutcliffe, W. D., K. G. Feller, N. K. Madsen, and G. D. Pollak, 1981. *Uncertainties and Sensitivities in the Performance of Geologic Nuclear Waste Isolation Systems*, Volume II, ONWI-352 (UCRL-53142), Office of Nuclear Waste Isolation, Battelle Memorial Institute, Columbus, OH.

NOTICE

This report was prepared as an account of work sponsored by an agency of the United States Government. Neither the United States Government nor any agency thereof, nor any of their employees, makes any warranty, express or implied, or assumes any legal liability or responsibility for the accuracy, completeness, or usefulness of any information, apparatus, product, or process disclosed, or represents that its use would not infringe privately owned rights. Reference herein to any specific commercial product, process, or service by trade name, trademark, manufacturer, or otherwise, does not necessarily constitute or imply its endorsement, recommendation, or favoring by the United States Government or any agency thereof. The views and opinions of authors expressed herein do not necessarily state or reflect those of the United States Government or any agency thereof.

Printed in the United States of America
Available from
National Technical Information Service
U.S. Department of Commerce
5285 Port Royal Road
Springfield, VA 22161

NTIS price codes
Printed copy: A10
Microfiche copy: A01

ONWI-352
UCRL-53142

Uncertainties and Sensitivities in the Performance of Geologic Nuclear Waste Isolation Systems

Volume II

Technical Report

April, 1981

W. G. Sutcliffe
K. G. Feller
N. K. Madsen
G. D. Pollak

Lawrence Livermore National Laboratory
University of California
Livermore, CA 94550

This report was prepared by Lawrence Livermore National Laboratory under Contract No. W-7405-Eng-48 with the U.S. Department of Energy. This contract was administered by the Battelle Office of Nuclear Waste Isolation.

PREFACE

This report is being issued as two volumes. Volume II is the complete report. Volume I, Summary, is a reproduction of some parts of Volume II, and contains no additional information.

Those parts of Volume II which are reproduced in Volume I, Summary are:

- Section 1, Introduction and Summary
- Figures referenced in Section 1 (Appendix A in Volume I)
- Table of Contents of Volume II (Appendix B in Volume I).

BLANK PAGE

CONTENTS

Abstract 1

1. Introduction and Summary 1

1.1 Background and Purpose 2

1.2 Study Scope 2

1.3 Technical Approach 3

1.4 System Models 5

1.5 Parametric Analysis 7

1.6 Analysis of a Waste Isolation System in Bedded Salt 10

1.7 Hydrology with Branching 17

1.8 Conclusions 19

1.9 Additional Work 20

1.9.1 Site Specific Analysis 20

1.9.2 Development and Evaluation of Uncertainty Analysis Methods 20

1.9.3 Detailed Analysis of Subsystems 22

1.9.4 Validation of Models 22

2. Physical System and Model Descriptions 23

2.1 Models and Performance Measures 23

2.1.1 Properties and Processes 23

2.1.2 Sequence of Events and Processes 24

2.1.3 Activity and Dose 26

2.2 Waste Form and Package Subsystem 27

2.2.1 Inventory 27

2.2.2 Corrosion 32

2.2.3 Dissolution 32

2.2.4 Local Transport 34

2.2.5 Waste Form and Package Model 34

2.3 Repository 35

2.3.1 Definition 35

2.3.2 Characterization 35

2.3.3 Modeling 35

2.4 Site 37

2.4.1 Definition 37

2.4.2 Flow Paths 37

2.4.3 Parameters 39

BEST DOCUMENT AVAILABLE

CONTENTS (Continued.)

2.5 Regional Subsystem 39
2.5.1 Definition 39
2.5.2 Site Boundary Conditions 40
2.5.3 Solute Transport 40
2.6 Flow and Transport Equations and Parameters 41
2.6.1 Equations 41
2.6.2 Dispersion 42
2.6.3 Retardation 43
2.7 Subsystem Aggregation and Performance Measure Calculations . 43
2.7.1 Dissolution and Transport 43
2.7.2 Aggregation of Path Elements 45
2.7.3 Radioactive Decay 46
2.7.4 Peak Activity Rate 46
References 49
3. Methods of Analysis and Computation 50
3.1 Methods of Analysis 50
3.1.1 Deterministic Analysis 50
3.1.2 Uncertainty Analysis 51
3.1.3 Value of Information 54
3.2 MACRO Computer Code 55
References 59
4. Data Base 60
4.1 Waste Form/Package Data 60
4.2 Repository Site Data 66
4.2.1 Piezometric Data 67
4.2.2 Vertical Permeability 69
4.2.3 Dispersivity 70
4.2.4 Sorption 71
4.3 Repository Site Data--Salt 73
4.3.1 Dispersivity 75
4.3.2 Fission Products with Sorption 75
References 90
5. A Parametric Study of System Performance 99
5.1 Parameters 99
5.2 Deterministic Results 101

BEST DOCUMENT AVAILABLE

CONTENTS (Continued.)

5.3 Uncertainty Analysis Results 113

5.4 Summary 126

6. Probabilistic Consequence Analysis of Waste Isolation Systems 130

6.1 Purpose and Method of Analysis 130

6.2 System Model Description 132

6.3 MACRO Input Data 138

6.4 Subsystem Contributions to System Performance 141

6.5 Uncertainty Sensitivity Analysis 147

6.5.1 Complete System 147

6.5.2 Waste Form and Package 151

6.5.3 Repository Site Subsystem (Vertical Path through Repository) 153

6.5.4 Regional Subsystem (Upper Aquifer) 156

6.5.5 Pairs of Subsystems 158

6.5.6 Summary of Uncertainty Sensitivity Analysis 162

6.6 High-Level Waste Forms 166

6.7 Repositories in Basalt 174

6.7.1 Waste Form and Package in Basalt 175

6.7.2 Basalt Repository Site 175

6.7.3 Regional Transport at a Basalt Site 177

6.8 Application of Parametric System Performance Results to Bedded Salt Scenario 177

7. A Parallel Path Hydrology Study 184

7.1 Parameters and Equations 184

7.2 Analysis 187

7.3 Conclusions 197

Acknowledgments 198

BEST DOCUMENT AVAILABLE

UNCERTAINTIES AND SENSITIVITIES IN THE PERFORMANCE OF GEOLOGIC NUCLEAR WASTE ISOLATION SYSTEMS

ABSTRACT

This report presents an analysis of the long-term safety of geologic nuclear waste isolation systems. The study focuses on the effect of uncertainty about engineered and natural systems. We identify the subsystems and parameters that dominate the system performance under various conditions. We also consider the potential differences between waste forms, host media, and site characteristics, and how these differences affect the system's performance.

The scope of this study is limited to probabilistic analysis of nuclear waste migration via groundwater flow in assumed pathways. The primary measure of performance is the peak rate of activity release (Ci/yr) at the end point of a pathway.

As well as demonstrating methods for uncertainty analysis, we present specific results and conclusions. Deterministic and probabilistic parametric analyses cover a range of parameter values large enough to encompass significantly different waste forms, packages, and sites (in various media). The results are useful for the assessment of geologic waste isolation systems in general. We also analyze specific hypothetical systems using generic data.

The following are some general observations:

- A global, parametric analysis is more informative than a local sensitivity analysis.
- Individual contributions of "multiple barriers" (subsystems) are sometimes insignificant.
- Some uncertainties have little effect on system performance.

1. INTRODUCTION AND SUMMARY

This report analyzes the sensitivities and uncertainties in the long-term safety of geologic nuclear waste isolation systems. This section briefly describes the purpose and scope of the study, the technical approach and models, some results and conclusions, and recommendations for additional work.

1.1 BACKGROUND AND PURPOSE

This study was conducted for the Office of Nuclear Waste Isolation (ONWI) to provide information useful in the development and assessment of technology to isolate nuclear waste. Often the most complicating factor in making decisions in this area is the uncertainty about the isolation system and its predicted performance.

These uncertainties arise because of:

- New technology
- Geologic variability
- Required long-term safety

The importance of individual uncertainties is difficult to assess. Our overall goal is to demonstrate a method for quantifying and evaluating the importance of various uncertainties. Our particular objective is to identify which uncertainties about individual subsystems are important in terms of complete system. We identify the conditions under which various subsystems and parameters dominate. We also consider the potential differences between waste forms, host media, and site characteristics, and how these differences affect assessed system performance, particularly when uncertainties are considered.

1.2 STUDY SCOPE

The scope of this study is limited to the post-closure, radiologic safety of mined repositories for nuclear waste. Only leakage via groundwater was considered. The analysis assumed scenarios where hydrologic pathways exist. The study did not address specific mechanisms for creating these pathways or the probabilities that such pathways exist. Thus, the study focused on probabilistic analysis of the consequences.

Assuming significant pathways exist, we allowed probability distributions to represent uncertainties about the hydrologic and chemical properties that control vast transport along these paths. We also used probability distributions to represent uncertainty about the life of waste packages and the rate of waste leaching from degraded packages.

An analysis covered a range of parameter values large enough to encompass significantly different sites in various media, waste forms, and packages.

These results can be applied generally to isolation systems that we represented by a point source embedded in a sequence of serially connected pathways.

Specific hypothetical systems were analyzed using generic data to construct cases for analysis. Major emphasis was placed on spent-fuel repositories, in bedded salt. A less extensive analysis was also conducted to investigate the differences between bedded salt and basalt media, and to compare the effects of spent fuel (SF) and high-level waste (HLW). High-level waste was assumed to be in a glass or SYNROC waste form.

1.3 TECHNICAL APPROACH

Waste isolation systems were represented by simple models applied in parametric analyses over very broad ranges of values to specific, hypothetical systems. The study included both deterministic and probabilistic analyses.

This approach consisted of:

- Characterization of the system
- Data acquisition
- Performance analysis
- Interpretation of results

The characterization, as discussed in Section 2, consists of assuming performance measures, constructing appropriate models (identifying parameters), and combining them to obtain an algorithm for calculating the performance measures.

The need to encompass the complete system and to evaluate uncertainty dictates the detail in the models. Subsystem models are simple algebraic models with a small number of parameters. Transport was computed using analytic solutions of one-dimensional differential equations. More complex mathematical functions are represented by tables. This approach allows the large number of calculations necessary to accomplish the sensitivity and uncertainty analyses.

The data acquisition effort, discussed in Section 4, consisted of obtaining and interpreting raw data, transforming the data into the necessary input, and finally quantifying the uncertainty in the data. The data were based on a literature survey and questioning of experts. For the most part we chose ranges of numbers that would be representative of a repository in salt.

Uncertainties were quantified by associating the 1st and 99th percentiles of log-normal distributions with the limits chosen. We used log-normal distributions because the range of data usually covered several orders of magnitude.

The performance analyses compute sensitivity, uncertainty, and sensitivity of uncertainty. Both deterministic and probabilistic calculations were performed. The deterministic results follow from a direct application of the models to be discussed. The probabilistic or uncertainty calculations used discrete elements to represent probability distributions.

Deterministic analyses assessed performance sensitivity to model parameters. Local sensitivity analysis (achieved by small variations in parameters) proved to be potentially misleading. The large parameter ranges (encompassed by uncertainty in parameter values and different systems) required a more global analysis. The primary method of deterministic sensitivity analysis was a parametric study with a few high-level parameters. The results are presented as contour plots in Section 5. Performance sensitivity to each model parameter depends on the values of the other parameters. Each has domains of high and low sensitivity, depending on the values of all the model parameters. Thus, the uncertainty of a parameter is important in some regimes and unimportant in others.

The effect of each parameter's uncertainty was studied by:

- Associating probability distributions with the model parameters
- Computing probability distributions of the performance variables by using the system model
- Perturbating the distributions and observing the effect on the performance distributions

We computed the probability distributions by:

- Dividing the input and output variable spaces into finite intervals
- Computing the output values for every combination of input values (each variable interval is given a representative value)
- Summing the probabilities of input variable combinations to the appropriate output variable interval

In reviewing the study conclusions, one must keep in mind the limitations of this study, including the use of simple models and generic data.

1.4 SYSTEM MODELS

The system model used in this study is composed of three independent subsystems:

- The waste form and package
- The repository and nearby site
- The regional aquifer

These subsystems are pictured in Fig. 1-1. They are decoupled (independent) by assumption and the choice of variables.

The studies in Sections 5 and 6 consider nuclide transport through a system of serially connected flow path segments. Section 7 considers water flow through parallel paths.

To avoid the assumptions involved in modeling a water use system we chose to base our performance measure on activity. We used the peak (maximum over time) rate of activity release measured in curies per year (Ci/yr). We computed this peak rate of activity released for each of three groups of nuclides:

Group 1	^{99}Tc and ^{129}I
Group 2	Other fission products
Group 3	Actinides

The grouping is based on assumed similarity in retardation factors and dissolution (leach) rates. The disadvantages of using activity rather than dose as a basis for a performance measure are that the effect of the groups cannot be readily combined and that the output cannot be directly compared to other radiation standards.

Both spent fuel and high-level waste were considered as waste forms. The nuclide inventories were calculated using typical reactor parameters (Alexander et al., 1977).* Since the output scales with the amount of inventory, we arbitrarily chose an inventory resulting from the generation of 10^6 megawatt years of electricity (MWe·yr). This would be a typical

---

*Alexander, C. W., et al., 1977, "Projections for Spent Fuel to be Discharged by the U.S. Nuclear Power Industry," Oak Ridge National Laboratory, ORNL TM-6008.

BEST DOCUMENT AVAILABLE

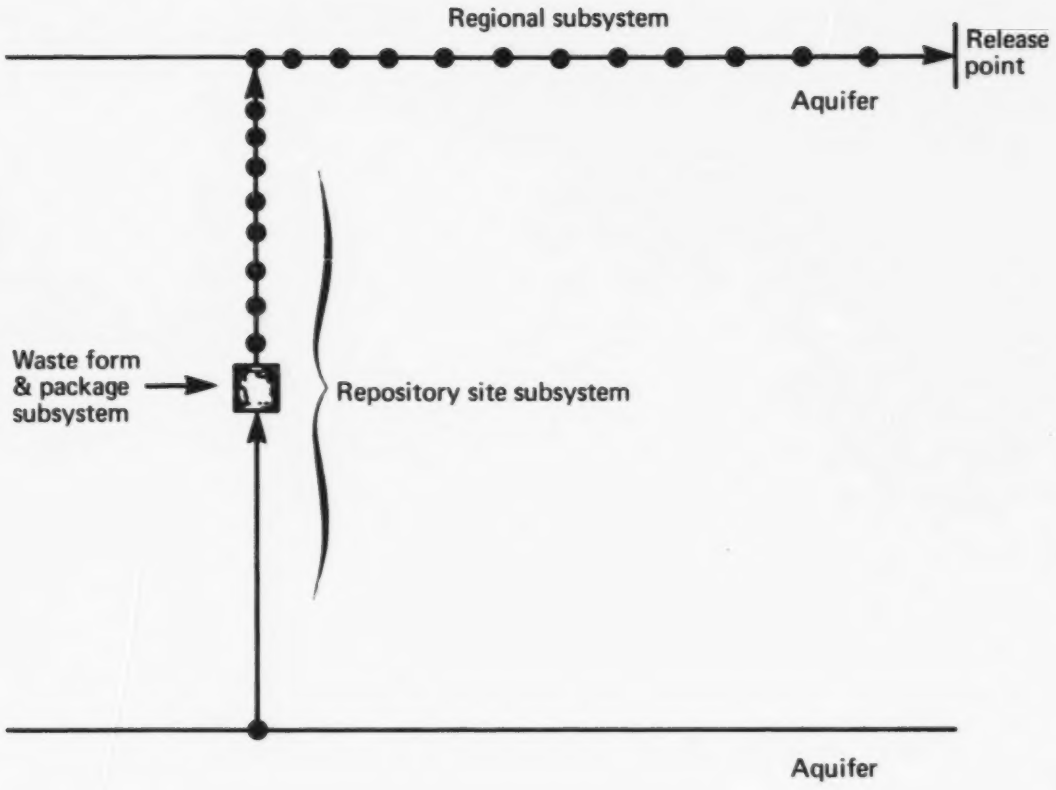

FIG. 1-1. Waste isolation subsystems.

inventory for a medium-size repository. The release from the waste form and package is assumed to be at a constant rate and is governed by two parameters, the release initiation time (t_0) and the release duration (t_D) (dissolution or leach time). Included in t_0 are the age of the waste at emplacement, the repository resaturation and repressurization time, and the canister life (corrosion) time. These terms, t_0 and t_D, could be a function of thermal effects, water chemistry, etc. These effects were not explicitly considered in this study. The entire inventory is represented as a point source. Refinement or more detail could be added to this model.

The water flow through the repository site or regional pathways is governed by D'Arcy's Law. The input parameters are head difference and length or head gradient, and hydraulic conductivity. The output is the D'Arcy velocity. The pore water velocity is then obtained by dividing by effective porosity. The transport of nuclides is assumed to be governed by the advection-dispersion (diffusion) equation. We assume one-dimensional pathways with longitudinal dispersion. The same retardation factor is assumed for all nuclides in the same decay chain. The transport equation is solved using Green's functions with semi-infinite boundary conditions. The input parameters are water velocity, retardation factor, dispersion constant, and path length. The output is the transit time and the spread. For serially connected pathways (repository site and regional aquifer) the total transit time is the sum of the transit times, and the square of the waste-pulse spread is the sum of the squares of the pulse spreads. To compute the flux of waste released we integrate over the path response and dissolution functions. The activity released is obtained by multiplying the flux by the activity function which depends on time. For our performance measure we took the maximum (over time) of this product.

1.5 PARAMETRIC ANALYSIS

The purpose of the analysis was to determine the areas of dominance for a few high-level parameters. We chose parameters primarily characteristic of the waste form and package (dissolution time) and the transport of nuclides through the site and region (transit time). This analysis is not limited to a specific example or scenario (as in Section 6) and could be used as a preliminary analysis for many different isolation systems. This general, high-level look provides basic understanding of the model behavior used to

BEST DOCUMENT AVAILABLE

interpret the analysis in Section 6 (see especially Section 6.8). The parameters and their ranges are listed in Table 1-1. The deterministic results of the analysis are presented in the form of contour plots as in Figs. 1-2 and 1-3. From Fig. 1-2, which is for actinides from spent fuel with little dispersion, we see that the peak activity released depends only on the transit time when the transit time is larger than the dissolution time. By comparing Figs. 1-2 and 1-3 we see that the actinide activity released is about an order of magnitude greater for spent fuel than for high-level waste. This is, of course, an obvious result since the high-level waste has most of the U and Pu removed. To put these results in perspective, a 100 Ci/yr release into a river flowing 10^{18} cm^3/yr (typical of the Colorado River) gives a concentration of 10^{-16} Ci/cm^3, which is three or four orders of magnitude less than the natural activity of the earth's surface.*

Some general conclusions can be drawn from the Parametric Analysis Results:

- Performance (peak activity release rate) is usually more sensitive to the larger of the transit time or dissolution time.
- Actinide release rate is greater for spent-fuel than for high-level waste.
- Dispersivity does not significantly influence performance.

A probabilistic parametric analysis was performed (Section 5.3) for the same parameters. An uncertainty of two orders of magnitude was assumed for

TABLE 1-1. Parameters and ranges for parametric analysis.

Transit time (T)	10^3 - 10^6 yr
Dissolution time (T_D)	10^3 - 10^6 yr
Release initiation time (T_D)	500 yr
Transit time/spread (T/S)	1, 10
Inventory type	Spent-Fuel (SF), High Level Waste (HLW)
Inventory amount	10^6 MWe·yr
Nuclide groups	I, Tc; other fission products; actinides

*M. Eisenbad, Environmental Radioactivity (Academic Press, New York, 1973), Chapter 7.

BEST DOCUMENT AVAILABLE

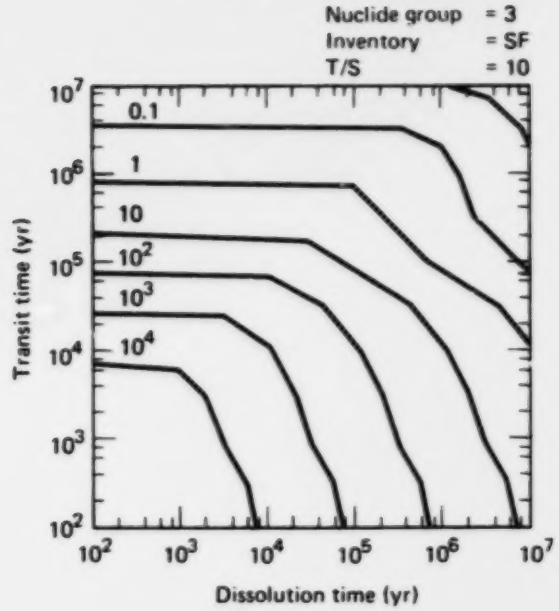

FIG. 1-2. Peak activity release rate (Ci/yr) for actinides from 10^6 MWe·yr of spent fuel as a function of dissolution and transit times.

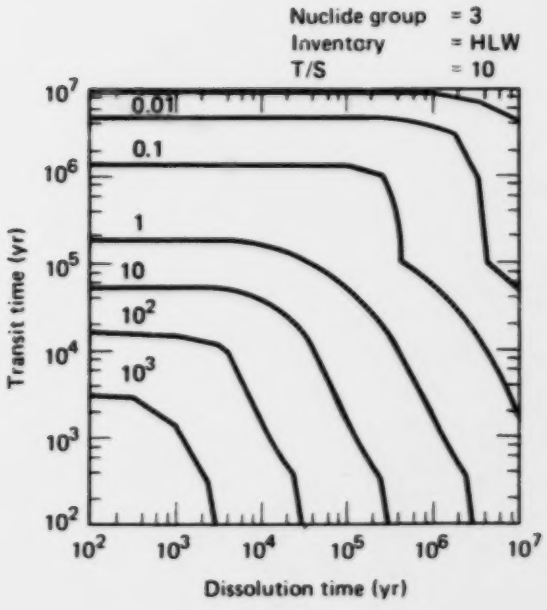

FIG. 1-3. Peak activity release rate (Ci/yr) for actinides from 10^6 MWe·yr of high-level waste as a function of dissolution and transit times.

the transit and dissolution time. The results confirmed the conclusions drawn from the deterministic analysis.

1.6 ANALYSIS OF A WASTE ISOLATION SYSTEM IN BEDDED SALT

We conducted a probabilistic analysis of a hypothetical repository for spent fuel in bedded salt (Section 6). The analysis assumed scenarios where the repository was substantially degraded below the nominal performance of a bedded salt repository. The system analyzed is shown in Fig. 1-1. The failure scenario assumes a flow path connecting the repository to an underlying aquifer and a fracture zone (associated with a sealed shaft and tunnel) connecting the repository to an overlying aquifer. The values of the parameters characterizing these pathways and the waste form/package are given in Table 1-2.

The purpose of the analysis is to determine how much each subsystem contributes to the system performance, and which parameters dominate the performance uncertainty. Given the flaws that allow substantial water flow through the repository, we computed probability distributions of the peak-release rates of activity for each nuclide group. In general, the uncertainty range (1st to 99th percentiles) of input parameters was an order of magnitude above and below the median values given in Table 1-2. The dominance of parameters was determined from uncertainty sensitivity analyses; that is, after the basic uncertainty calculation, the performance was recalculated setting the uncertain parameters to their median values one at a time.

The probability distributions of the outcomes (peak rate of activity release) are summarized using bar graphs (Fig. 1-4 is an example of a computed probability distribution). The horizontal bar below the curve corresponds to the vertical bars in Fig. 1-5. The percentile points are determined by adding the probabilities from the left. Figure 1-5 shows a bar graph for each of four cases. These cases are presented on the same graph for easy comparison. The horizontal ticks on each bar mark the 1st, 25th, 50th, 75th, and 99th percentile values of the computed distribution. The asterisk marks the mean value of the distribution.

An uncertainty sensitivity analysis was performed for each separate subsystem. This analysis identified the subsystem model parameters dominating the uncertainty about the performance of each subsystem.

BEST DOCUMENT AVAILABLE

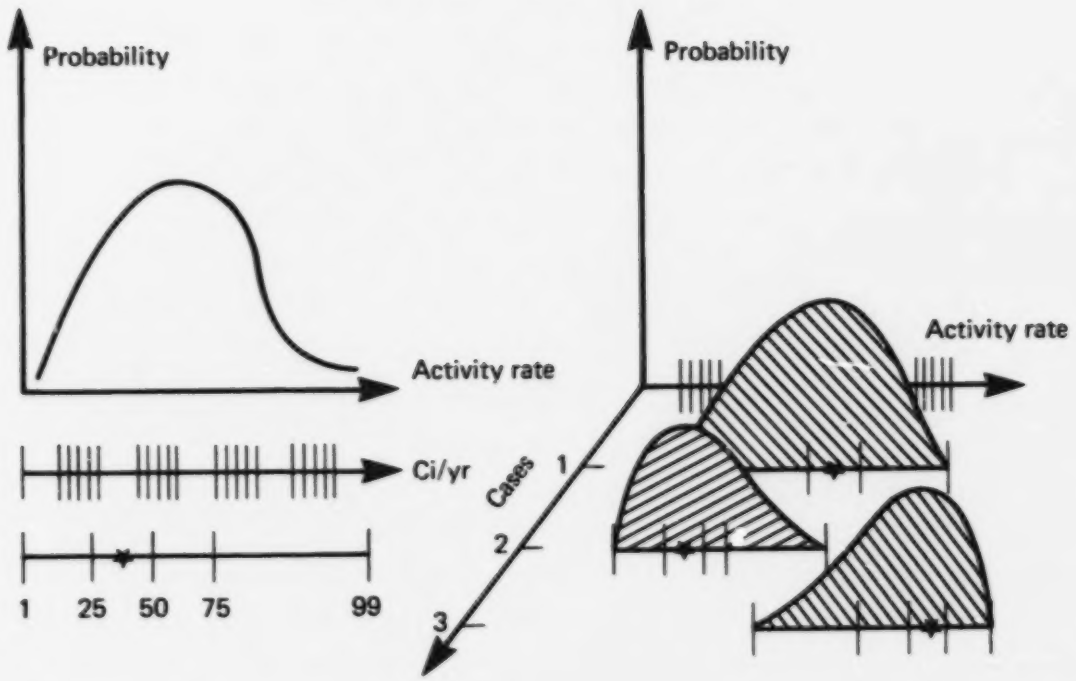

FIG. 1-4. Bar graph representation of a probability distribution.

BEST DOCUMENT AVAILABLE

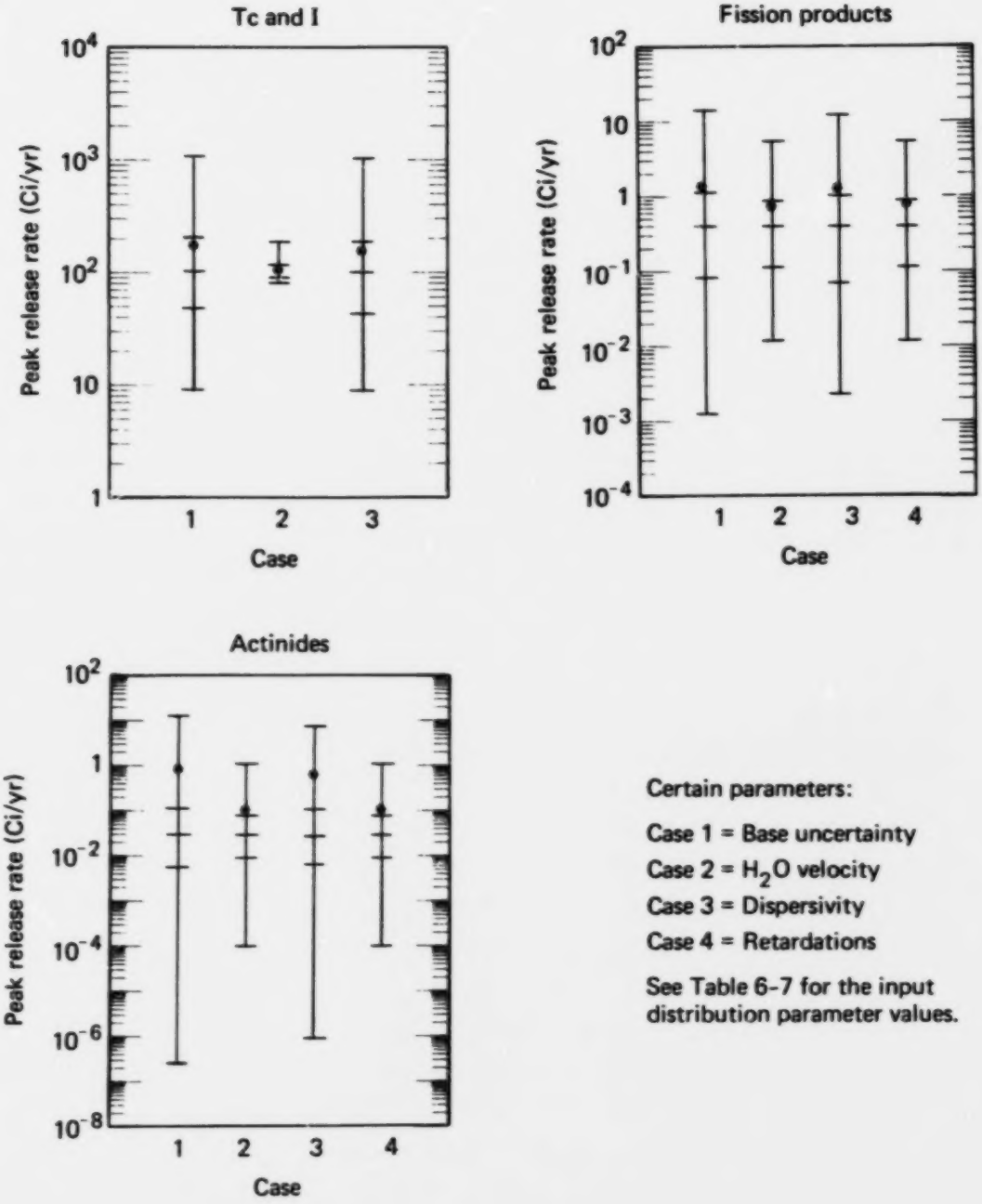

Certain parameters:

Case 1 = Base uncertainty
Case 2 = H_2O velocity
Case 3 = Dispersivity
Case 4 = Retardations

See Table 6-7 for the input distribution parameter values.

Horizontal bars represent the 1st, 25th, 50th, 75th and 99th percentiles.
*represents the mean value.

FIG. 1-5. Uncertainty sensitivity analysis of the aquifer (regional subsystem).

BEST DOCUMENT AVAILABLE

Figure 1-5 shows the performance of the aquifer assuming the whole inventory of 10^6 MWe·yr of spent fuel was instantaneously released at the input end of the aquifer 50 yr after being removed from reactors. The results show that an uncertainty in dispersivity of 400 m to 10 km has little effect on the performance of a 10-km aquifer.

TABLE 1-2. Subsystem parameters--median values.

Waste Form and Package	
Inventory type	Spent Fuel
Inventory amount	10^6 MWe·yr[a]
Release initiation time	500 yr
Dissolution time - Tc, I and fission products	5000 yr
Dissolution time, actinides	10^5 yr
Repository Site-Fracture Zone Below Repository	
Length	300 m[a]
Area	10^4 m^2
Hydraulic conductivity	0.1 m/yr
Repository Site-Fracture Zone Associated with Shaft and Tunnel	
Length	1200 m[a]
Area	100 m^2
Hydraulic conductivity	1 m/yr
Longitudinal dispersivity	50 m
Effective porosity	0.001
Retardation factor for Tc, I and fission products	10
Retardation factor for actinides	100
Regional Aquifer	
Length	10 m[a]
Water velocity	2 m/yr
Longitudinal dispersivity	2000 m
Retardation factor for Tc, I and fission products	100
Retardation factor for actinides	1000
Head difference between upper and lower aquifers	10 m[a]

[a]Indicates no uncertainty.

A similar analysis was conducted for the repository site subsystem. From results appearing in Section 6* we can see that the uncertainty in the hydraulic conductivity, porosity, and retardations of the flawed shaft dominated the uncertainty in the performance of the subsystem. Of course, this result depends on the relative values of the upper path and lower path parameter distributions chosen for this scenario.

The analysis of the waste form/package subsystem assumes no transit time. Waste is released at a constant rate beginning at t_0 and continuing for a duration t_D. Although the purpose of this assumption is to analyze this subsystem alone, we could think of this as a limiting case resulting from an extreme well intrusion scenario. From results presented in Section 6** we can see that the uncertainty in the peak-release rate of the fission products was sensitive to the uncertainty in the time-of-release initiation (t_0). The uncertainties in the technetium, iodine, and actinide outcomes were more sensitive to the uncertainty in the dissolution times (t_D).

The performances of the subsystems are compared in Fig. 1-6. The aquifer, case 3, is the same as the case 1 in Fig. 1-5. By comparing cases 1, 2, and 3 with case 4, the combined system, in Fig. 1-6, we see that for the fission products and actinides the regional aquifer is the dominant subsystem. The waste form and package subsystem is the most effective subsystem in reducing the peak-release rate of technetium and iodine. It is not surprising that the vertical path fails to dominate the performance of the system for any radionuclide group, since we assumed that the integrity of the host media is compromised by fractures. Any combination of one, two, or all three technetium and iodine subsystems (except the vertical path alone) produces distributions with percentiles and mean values within an order-of-magnitude range. For fission products and the actinides, any combination of two subsystems, or the aquifer alone, produces distributions with the 50th, 75th and 99th percentiles within an order-of-magnitude range.

Figure 1-7 gives the results of an uncertainty sensitivity analysis for the complete system. The sensitive parameters from each subsystem were included in the analysis. If a subsystem's performance was insensitive to a parameter's uncertainty, that parameter was set certain at its median value in

---

*See Fig. 6-6.

**See Fig. 6-5.

BEST DOCUMENT AVAILABLE

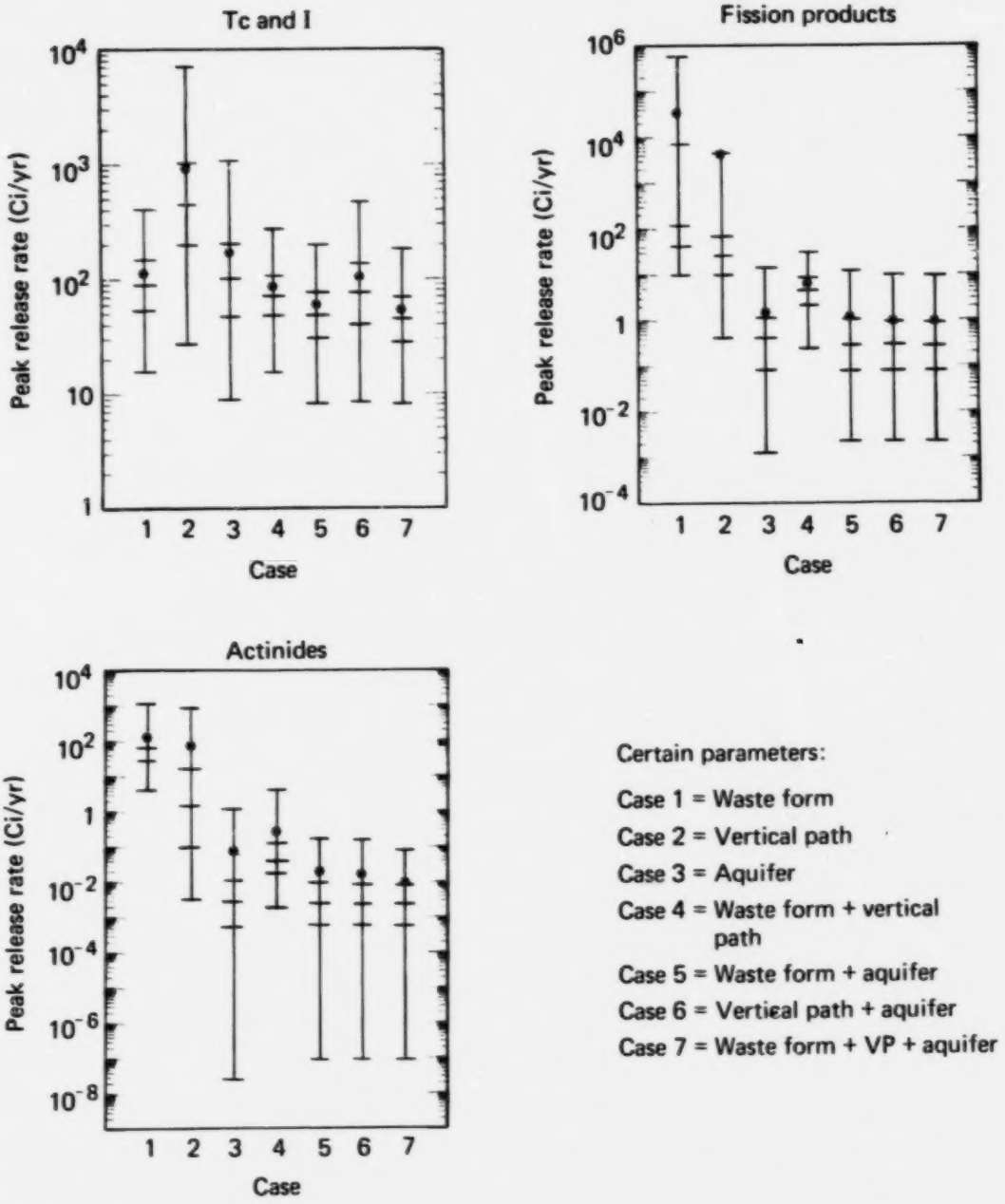

Horizontal bars represent 1st, 25th, 50th, 75th and 99th percentiles.
*represents the mean value.

FIG. 1-6. Comparison of probability distributions for peak release rates of separate subsystems and aggregated subsystems.

BEST DOCUMENT AVAILABLE

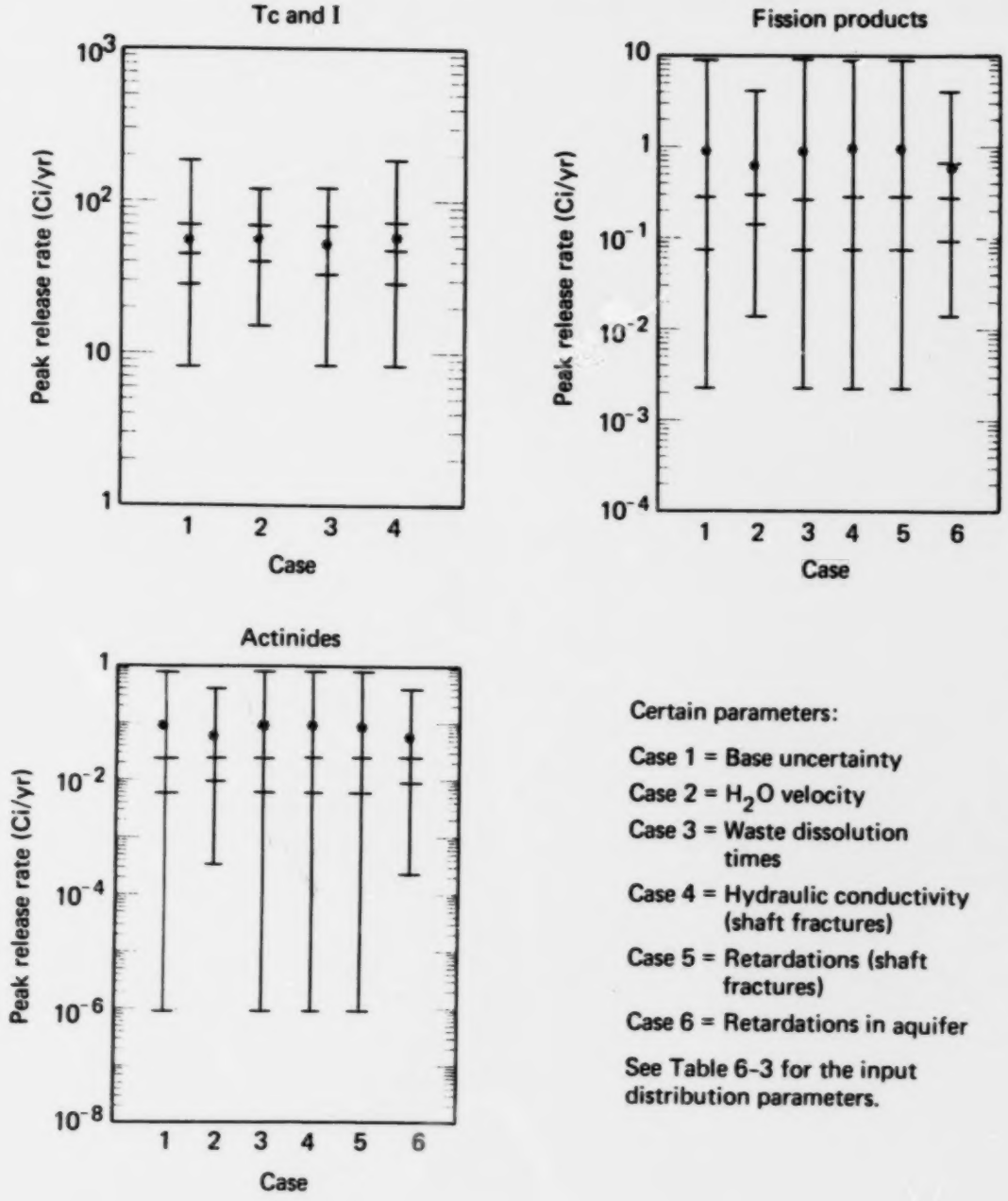

Certain parameters:

Case 1 = Base uncertainty

Case 2 = H_2O velocity

Case 3 = Waste dissolution times

Case 4 = Hydraulic conductivity (shaft fractures)

Case 5 = Retardations (shaft fractures)

Case 6 = Retardations in aquifer

See Table 6-3 for the input distribution parameters.

Horizontal bars represent the 1st, 25th, 50th, 75th and 90th percentiles.
*represents the mean value.

FIG. 1-7. Uncertainty sensitivity analysis of complete system.

the analysis of the complete system. To summarize the results, the parameters with greatest effect on the probability distributions of peak release rates were:

- Water velocity in the aquifer (Groups 1, 2, 3)
- Waste form dissolution time (Group 1)
- Waste particle retardations in the aquifer (Groups 2, 3)

The group numbers in parentheses indicate the groups most affected by the parameter.

Uncertainties about parameters for the repository site have little effect on system uncertainty, since system performance is dominated by the waste form subsystem for Tc and I, and by the regional subsystem for the other fission products and actinides. Again, this may be expected since the probability distributions for the vertical path parameters were selected to represent compromised repository barrier layers.

From Figs. 1-6 and 1-7 we can confirm the intuitive conclusion that when there is a dominant subsystem the uncertainty in the performance of the overall system is most sensitive to the uncertainty in parameters of that subsystem. It is difficult and, therefore, inadvisable to come to specific conclusions as to which parameter uncertainties are most important, in general, based on analysis of a single scenario. This is particularly true when the probability of that scenario has not been considered. Thus, conclusions based on specific quantitative results apply only to this system and scenario. The most limiting aspect of the analysis is that we studied only one flow network. On the other hand, the uncertainty associated with the network parameters allows various interpretations of the nature of the flow path.

1.7 HYDROLOGY WITH BRANCHING

The studies reported in Section 6 dealt only with series flow paths. Since branching flow is potentially important for modeling multiple shafts or shafts and flows, we undertook a study of parallel pathways. The study was limited to analysis of the flow (hydrology). A more detailed model of a repository would be necessary to determine the splitting fractions for an analysis of the transport of waste.

A simple network, Fig. 1-8, was used to model the flow. We determined the dependencies of the flow rates in terms of the transmissivities and the head differences.

BEST DOCUMENT AVAILABLE

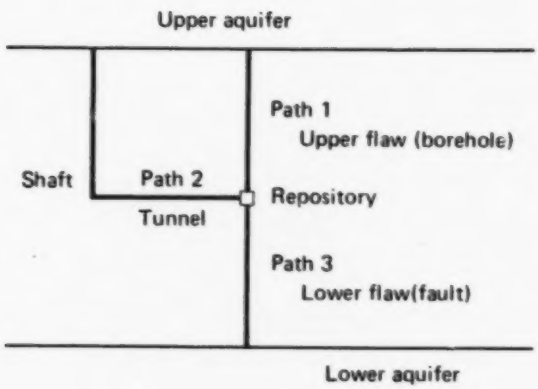

FIG. 1-8. Parallel path system.

Analytic results and contour plots are presented in Section 7. The numerical data allow us to confirm our intuition in many cases. In other cases nonintuitive results appear. For example, it is possible to have combinations of transmissivities and head drops where there is no flow in the upstream path. The conditions under which these combinations occur do not involve the transmissivity of the upstream path in question. If one of the flaws is a ventilation shaft, and the other is the main shaft, it might be possible to choose the relative positions of the two flowpaths so that the flow in the fast pathway would be zero. Careful consideration of such factors in repository design may significantly reduce the risk of waste migration.

1.8 CONCLUSIONS

Our work began by investigating the simple notion of ranking parameters, based on the effect changes in their values had on deterministic and probabilistic system performance. Over the range of possible parameter values, each parameter has regions of dominance and regions where the parameter has little effect. Our observations lead us to seriously doubt the value of any sensitivity analysis or response-surface technique based on small perturbations about a "base" point.

It is more useful to describe system performance in terms of a few high-level variables. The dependence of system performance on these variables can be ascertained from the plots presented in Section 5. Only in some limited regions is any kind of ranking meaningful.

In Section 6, instead of the higher-level variable, transit time, site and regional parameters are used. The results clearly illustrate how much each subsystem (waste form and package, repository site, and regional aquifer) contributes to the performance of the complete system. These specific results lead to some generalizations about the behavior of a waste isolation system; and illustrate the value of conducting such analysis for real sites and designs.

In the example systems analysis of a flawed repository, the waste form/package dominated the performance of the system in controlling Tc and I, and the regional aquifer dominated control of the other fusion products and actinides.

To realize a substantial improvement in overall system performance, we must improve a weaker subsystem to approximately the level of the dominant

subsystem. For example, increasing the value of the waste dissolution time had very little effect on the system's performance until the median time of the probability distribution was increased by three orders of magnitude (See Fig. 6-16).

There are cases where there are no dominant subsystems. If the transit or dissolution time is such that the activity is changing rapidly,* the performance of combined subsystems can be substantially better than that of the individual subsystems.

1.9 ADDITIONAL WORK

A perspective of how uncertainty analysis "fits in" can be obtained from Fig. 1-9. Our work has focused on those areas represented by boxes with shaded corners. Additional work in the following areas is suggested:

- Site specific analysis
- Development and evaluation of uncertainty analysis methods
- Detailed analysis of subsystems
- Validation of models

1.9.1 Site Specific Analysis

The methodology presented in this report was applied only to hypothetical systems and used generic data. This application is useful as a first step; however, the critical test of any method must be its usefulness in the real world. A site (and design) specific analysis could guide more detailed analysis necessary for a comprehensive performance assessment.

A necessary step in this analysis is the involvement of people intimately familiar with the site. Only with their help can consistent data and applicable models be developed for the analysis. This work would include the identification of failure scenarios and their relative likelihoods.

1.9.2 Development and Evaluation of Uncertainty Analysis Methods

In our analysis the probability distributions for model parameters were assumed to be independent. Decoupling systems can, in some cases, ignore

---

*See Figs. 5-15 through 5-19 in Section 5.

BEST DOCUMENT AVAILABLE

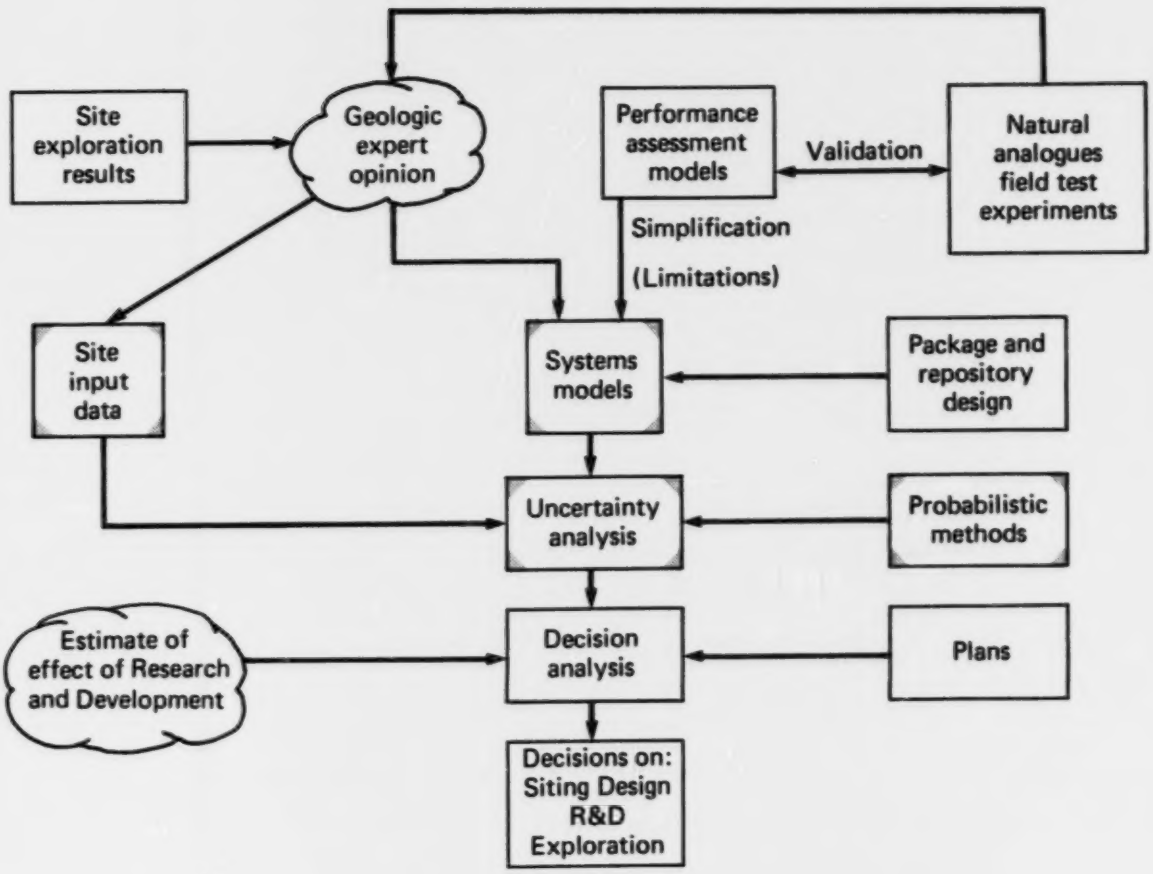

FIG. 1-9. Information flow through uncertainty analysis.

important effects. For example, waste dissolution rates may depend on the water-flow rate through the repository. Some correlations between subsystems, and between parameters of the same subsystem, could be included in further studies.

To properly develop and to evaluate probabilistic methods a knowledge of their intended use is necessary. Therefore, this effort should identify some of the decisions to be made and the framework (criteria, alternatives, etc.) in which they are to be made. In particular, estimates of the likelihood of R&D outcomes should be included.

1.9.3 Detailed Analysis of Subsystems

Our analysis made use of simple models, since we were interested in the performance of the total system. If attention is focused on a subsystem, we can afford to use more detailed models; for example, a detailed model of the waste form/package system must be used to investigate the feasibility of a 1000-yr canister.

A point source repository might be adequate to calculate performance at great distances; however, to calculate the hazard of a well-intrusion scenario a more detailed repository model is necessary. Repository-scale hydrology models have not received much attention and could be important in design decisions.

With the use of a water use model, our calculations could yield dose as a performance measure. With some development we could relax the nuclide group assumption and concentrate on selected nuclide chains.

1.9.4 Validation of Models

To place confidence limits on our results, an extensive effort involving more detailed models, experiments, and field tests should be undertaken. The first step in this direction should be to establish the quantitative effects of the simplifying assumptions made in going from detailed models to systems level models. In particular, the conditions under which, and the degree to which, the one-dimensional and isothermal assumptions are valid should be established.

2. PHYSICAL SYSTEM AND MODEL DESCRIPTIONS

This section describes the physical systems analyzed and the models used to represent them. The major subsystems described here (waste form and package, repository site, regional aquifer) do not represent any specific site. They are generic, representing a hypothetical system with properties typical to specific designs or locations. The models and methodology used could, of course, be applied to a specific system.

2.1 MODELS AND PERFORMANCE MEASURES

2.1.1 Properties and Processes

We characterize the systems and subsystems by identifying appropriate models and parameters. A model can be thought of as a representation of an object or system. The more properties that are represented, the more detailed the model is said to be. The first step in modeling is usually to describe the object or system by the use of words or pictures. In this section, we describe the waste form, the package, the repository, the repository site, and the regional aquifer to be studied. Next, we need to identify the processes that can change the properties of the object or system. Some of the processes considered here are: canister corrosion, waste form dissolution, groundwater flow and solute transport in groundwater.

The step to mathematical or quantitative modeling requires mathematics (e.g., numbers, functions, operators) to describe the properties of the object or system that we are modeling. In this work, we will associate numbers (i.e., parameters or variables) with the properties of the waste isolation system. The uncertainty in these parameters is represented by probability distributions. The state of a system is described by the specification of the properties or parameters that characterize the system. Processes govern the change of state. Processes are usually described by relationships among properties. These are often the dynamic or conservation laws. For example, we will assume that groundwater flow is governed by D'Arcy's Law (DeWiest [1969]).

The descriptions in the following sections are somewhat more detailed than necessary for the models used for the analyses.

The selection of models to represent the physical waste isolation system depends on the performance measure we select. The performance of a waste isolation system can be measured in many ways. We shall, however, restrict our attention to a few relevent measures. These measures consist of a quantitative measure of waste or its effect (e.g., mass, activity, dose) and a space-time element. The focus of much of our analysis is on the uncertainty associated with these measures. The space or position at which the output is calculated is some area of interest, such as the discharge end of an aquifer. Instead of the instantaneous value of a quantity, we are often interested in time at which the quantity reaches a maximum or in the integrated value over a period of time.

Once the performance measures have been specified, we can select those processes to be represented (or excluded) in the model. For example, since we are primarily concerned with the release of waste at some distance from the repository at some time in the far future, we have neglected all thermal effects.

2.1.2 Sequence of Events and Processes

We will assume that the following scenario occurs after the waste is emplaced and the repository is closed. The repository refills and repressurizes. The canister corrodes and the waste form dissolves. Dissolved waste is transported in groundwater flowing through the repository to a nearby aquifer through existing flaws in the repository medium. The waste is then transported in the aquifer to a point where it is a potential hazard. These processes may overlap as shown in Fig. 2-1.

Finally, for practical reasons, the models are not very detailed. The numerous calculations that are required for a sensitivity or uncertainty analysis dictate the use of simple models. The role of more detailed models is to validate and to establish the limitations of the simpler models.

In this work, no attempt is made to predict the occurrence of flaws. Further, we have assumed that such flaws are permanent; i.e., we do not consider healing or disruptive events.

BEST DOCUMENT AVAILABLE

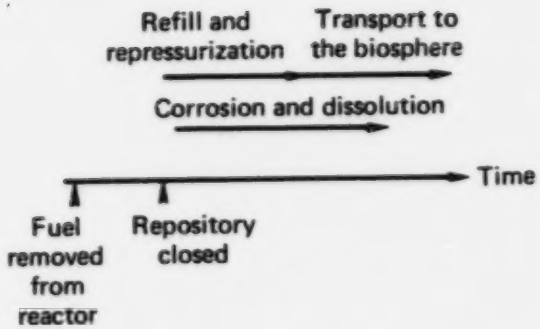

FIG. 2-1. Sequence of events and processes.

BEST DOCUMENT AVAILABLE

2.1.3 Activity and Dose

The choice of performance measure depends on the purpose of the performance assessment. We are primarily interested in comparing the influence of parameters and subsystems rather than evaluating the performance with respect to a given set of standards or criteria. By choosing activity (curies) rather than dose (REMS), we avoid a number of assumptions about water use systems.

Although it is possible to calculate the released activity or activity rate as a function of time, we found it sufficient to focus on the maximum or peak activity rate (Ci/yr) as the primary performance measure. The time of occurrence of this peak and the quantity of material released are also considered. In Section 7, the water flow out of the repository via a given pathway is used as a performance measure.

All of our calculations have assumed an inventory of high-level waste (HLW) or spent fuel (SF) from the generation of one million megawatt electric years (10^6 MWe•yr). This probably corresponds to somewhat less than half of the waste to be accumulated by the year 2000. It also corresponds to the inventory in a medium sized (regional) repository.

To form an idea of the levels of activity involved in our analysis, we look at a few examples. Since our results are in curies per year (Ci/yr), we present some examples in these units:

- The radon activity released from a uranium mine ventilating at 10,000 ft^3/min is about 50 Ci/yr (Eisenbad [1973], p. 208).
- The dietary intake of uranium for an individual is about 10^{-10} Ci/yr (Ibid. [1973], p. 169). The concentration (Ci/cm^3) is often a measure of interest.
- The approximate radium (^{226}Ra) content of granite is 2.7×10^{-12} Ci/cm^3 (Ibid. [1973], p. 171).
- The radium concentration of sea water near the surface is about 10^{-13} Ci/cm^3.
- The release of 100 Ci/yr into a river flowing at 10^{18} cm^3/yr (typical of the Colorado River) gives a concentration of 10^{-16} Ci/cm^3.

It should be kept in mind that not all activities are equivalent. The type and energy associated with decay of a given isotope determines its potential hazard.

BEST DOCUMENT AVAILABLE

To obtain a better idea of how the release of waste would effect man, we need to convert our results to dose or dose rate (Gladstone [1967]). As mentioned, this requires several assumptions. To calculate the rem dose to a human requires a knowledge of his intake of, or exposure to, the various radionuclides. To obtain this intake information it is in turn necessary to know the pathways which the nuclides take once they enter the surface water system. Direct exposure from swimming or boating in such waters is one source of dose, but a more common pathway is via food chains which depend at some point on water from these surface water bodies. The analysis of the transfer of these nuclides between the surface waters and various animal and plant forms ingested by humans is obviously a complicated process. Several models have been constructed for this process, see for example BIODOSE (Bonner and Ng [1980]). Dose has not been used as a performance measure in this study because of the necessary assumptions and parameter uncertainties, such as the long term variability of river flow rate, irrigation rate, and plant type.

We can, however, give some examples of dose received from natural sources:

- The γ doses in air over igneous rock from ^{226}Ra, ^{238}U, ^{232}Th, ^{40}K are 24, 26, 37, 35 mrem/yr, respectively (Eisenbad [1973], p. 191).
- The γ dose from external sources in normal areas is about 50 mrem/yr for terrestrial sources and 28 mrem/yr from cosmic radiation (Ibid. [1973], p. 189).

Again, we must keep in mind that dose depends on many things. The percent of activity and some potential doses due to the nuclides in spent fuel and high-level waste are presented in Tables 2-1 through 2-5.

2.2 WASTE FORM AND PACKAGE SUBSYSTEM

2.2.1 Inventory

The waste form and package subsystem is defined as the waste form itself (spent fuel assembly, glass matrix or synthetic mineral form), plus the canister, and any local backfill material in the canister niche. This is consistent with the NCR definitions:*

---

*Federal Register, Vol. 45, No. 94; Tues., May 13, 1980; Proposed Rules 31399.

BEST DOCUMENT AVAILABLE

- "Waste form"--means the radioactive waste materials and any associated encapsulating or stabilizing materials.
- "Waste package"--means the physical waste form, its container and any ancillary enclosures, including its shielding, packing, and overpack.

At the present time, the policy for civilian nuclear waste is that there be no reprocessing of the spent fuel, and that the spent fuel assemblies be emplaced in the niche surrounded by a suitable canister. However, it is possible that the current policy will have been changed by the time the repository is ready to receive the canisters. In that case, glass or synthetic minerals may be used as a suitable medium for embedding the reprocessed waste. Some of the salient differences in nuclide composition between the spent fuel and high-level waste are:

- Spent fuel contains 488 times as much ^{129}I as does high-level waste.
- The cladding and structure around the spent fuel contain small additional quantities of radioactive materials of which ^{59}Ni is the most important.

TABLE 2-1. Activity and dose for Nuclide Group 1 in spent fuel.

SF nuclide	Activity (%)		Specific hazard[a]
	10^2-10^5 yr	10^6 yr	
^{99}Tc	99.8	94	3.1×10^8 (GI-LLI)
^{129}I	0.2	6	3.6×10^{11} (T)
Weighted hazard[b]	1.0×10^9	2.2×10^{10}	

[a]Specific hazard = the 50-yr individual dose commitment (in mrem) to the body organ receiving the highest dose per curie ingested during the first year of the 50-yr period. Here T = thyroid, B = bone, K = kidney, and GI-LLI = gastrointestinal-lower large intestine. Does not take into account relative cancer risks for different organs.

[b]Weighted hazard = the 50-yr individual dose (mrem) per curie of the nuclides in a given group taking into account the relative amounts of each nuclide as a function of time.

BEST DOCUMENT AVAILABLE

TABLE 2-2. Activity and dose for nuclide Group 1 in high-level waste.

HLW nuclide	Activity (%) 10^2-10^5 yr	10^6 yr
^{99}Tc	100	100
^{129}I	0.0003	0.01
Weighted hazard[a]	3.1×10^8	3.5×10^8

[a]Specific hazard = the 50-yr individual dose commitment (in mrem) to the body organ receiving the highest dose per curie ingested during the first year of the 50-yr period. Here T = thyroid, B = bone, K = kidney, and GI-LLI = gastrointestinal-lower large intestine. Does not take into account relative cancer risks for different organs.

[b]Weighted hazard = the 50-yr individual dose (mrem) per curie of the nuclides in a given group taking into account the relative amounts of each nuclide as a function of time.

TABLE 2-3. Activity and dose for Nuclide Group 2 in SF and HLW [Group 2 (SF = HLW)].

Nuclide	Activity (%) 10^3 yr	10^4 yr	10^5 yr	10^6 yr	Specific hazard[a]
^{59}Ni	45	52	39	—	4.9×10^8 (B)
^{93}Zr	16	19	30	50	1.2×10^8 (GI-LLI)
^{93m}Nb	16	19	30	50	1.9×10^8 (GI-LLI)
^{14}C	23	10	—	—	1.4×10^8 (B)
Weighted[b] hazard	3.0×10^8	3.3×10^8	2.8×10^8	1.6×10^8	

[a]Specific hazard = the 50-yr individual dose commitment (in mrem) to the body organ receiving the highest dose per curie ingested during the first year of the 50-yr period. Here T = thyroid, B = bone, K = kidney, and GI-LLI = gastrointestinal-lower large intestine. Does not take into account relative cancer risks for different organs.

[b]Weighted hazard = the 50-yr individual dose (mrem) per curie of the nuclides in a given group taking into account the relative amounts of each nuclide as a function of time.

BEST DOCUMENT AVAILABLE

TABLE 2-4. Activity and dose for Nuclide Group 3 in SF (Group 3).

SF nuclide	Activity (%) 10^3 yr	10^4 yr	10^5 yr	10^6 yr	Specific hazard[a]
^{241}Am	48	--	--	--	4.1×10^{10} (B)
^{240}Pu	32	43	--	--	4.0×10^{10} (B)
^{239}Pu	20	55	72	--	4.0×10^{10} (B)
^{238}U	--	--	1.3	6	3.4×10^{10} (B)
^{237}Np	--	--	4	15	7.0×10^{10} (B)
^{234}U	--	--	5.6	8	4.2×10^{10} (B)
^{233}U	--	--	1.4	16	4.4×10^{10} (B)
^{230}Th	--	--	3.9	10	1.0×10^{11} (B)
^{229}Th	--	--	1.3	16	4.0×10^{11} (B)
^{226}Ra	--	0.03	3.6	10	1.5×10^{13} (B)
^{210}Po	--	0.03	3.6	10	1.3×10^{11} (K)
^{210}Pb	--	0.03	3.6	10	7.7×10^{11} (B)
Weighted hazard[b]	4.0×10^{10}	4.5×10^{10}	6.1×10^{11}	1.7×10^{12}	

[a]Specific hazard = the 50-yr individual dose commitment (in mrem) to the body organ receiving the highest dose per curie ingested during the first year of the 50-yr period. Here T = thyroid, B = bone, K = kidney, and GI-LLI = gastrointestinal-lower large intestine. Does not take into account relative cancer risks for different organs.

[b]Weighted hazard = the 50-yr individual dose (mrem) per curie of the nuclides in a given group taking into account the relative amounts of each nuclide as a function of time

BEST DOCUMENT AVAILABLE

TABLE 2-5. Activity and dose for Nuclide Group 3 in HLW.

HLW nuclide	Activity (%) 10^3 yr	10^4 yr	10^5 yr	10^6 yr	Specific hazard[a]
^{243}Am	28	52	--	--	4.1×10^{10} (B)
^{241}Am	56	--	--	--	
^{240}Pu	13	21	--	--	
^{239}Pu	3	27	48	--	
^{233}U	--	--	10	33	
^{237}Np	--	--	28	32	
^{229}Th	--	--	10	33	
^{226}Ra	--	--	1.7	0.6	
^{210}Po	--	--	1.7	0.6	
^{210}Pb	--	--	1.7	0.6	
Weighted[b] hazard	4.0×10^{10}	4.0×10^{10}	3.5×10^{11}	2.7×10^{11}	

[a]Specific hazard = the 50-yr individual dose commitment (in mrem) to the body organ receiving the highest dose per curie ingested during the first year of the 50-yr period. Here T = thyroid, B = bone, K = kidney, and GI-LLI = gastrointestinal-lower large intestine. Does not take into account relative cancer risks for different organs.

[b]Weighted hazard = the 50-yr individual dose (mrem) per curie of the nuclides in a given group taking into account the relative amounts of each nuclide as a function of time.

- Spent fuel initially contains about 200 times the plutonium in high-level waste.
- The peak ^{226}Ra content of spent fuel is 51 times the peak ^{226}Ra content of high-level waste.
- There is a fifth more ^{241}Am in spent fuel than in high-level waste at 100 yr. However, by 10,000 yr, the amount of ^{241}Am in the two types of waste are roughly equal.

Because of the difference in inventory, we expect spent fuel to be more hazardous than high-level waste (HLW).

2.2.2 Corrosion

The primary release mechanism for transporting nuclides to the biosphere is breach of the canister by water entering into the repository from the external rock environment, followed by aqueous leaching of the waste form and subsequent aqueous transport to the surface. The three characteristics of the waste form package that then need to be modeled are corrosion of the canister, leaching of the waste form, and transport of the nuclides out of the emplacement niche.

The corrosion of the canister will depend on its temperature, the flushing time of the canister niche, the amount of dissolved oxidizing agents in the water (O_2, Fe^{+3}), and type and amount of any other ionic species in the water (e.g., Na^{+}) and the metallic composition of the canister. The analysis of these dependencies is an on-going question (Lester et al. [1980]). Corrosion will presumably not be uniform over the surface of the canister, nor will the rate of corrosion in any one place be temporally constant. However, modeling these factors to the detail necessary for precise predictions would be almost impossible. Also, the corrosion has been modeled as a spatially and temporally uniform process, given the small time scales for corrosion compared to those for leaching (dissolution) and transport time. Thus, its only important parameter is the overall corrosion time. This may be correlated with such transport quantities as the retardation of the media or dissolution of waste form (both of these are correlated with water quality), or with the site hydrology (which determines canister niche flushing time). Both of these dependences could have been addressed but were not in this report.

2.2.3 Dissolution

The dissolution and leaching of the waste form itself will begin at the first breaching of the canister. Based on current experimental information (Coles [1980]), there will be a short period during which leaching is governed by surface-water interactions. This period will produce a comparatively fast initial leaching rate. After the surface kinetic phase is over, a diffusion dominated process can be expected. This process depends on the same physical characteristics as the corrosion. In addition, it is predominantly dependent on the waste form material and the effective surface area exposed. As in

corrosion, leaching can be expected to be spatially and temporally inhomogeneous. Unlike corrosion, this inhomogeneity is likely to be of major significance in determining final curie output for any given canister. However, a precise deterministic analysis is not possible nor needed. Since a large number of canisters are involved, a reasonable representation of the leaching should be obtainable using a statistical description. Since canisters will become wet at widely varying times, corrode at widely varying rates, and crack to varying degrees, individual variations in leach rate and starting time can be smoothed out in a global description. The effects of temporal variation of the leaching should be well-approximated by a constant leach rate. Even long-term changes (e.g., variation of niche flushing time, long term temperature variation, etc.) can be conservatively modeled by a constant leach rate.

The individual nuclides must be distinguished when modeling spent fuel leaching, since radial distribution of the various radionuclides across a spent fuel rod is nonuniform. This is due to thermally driven diffusion of the lighter nuclides towards the cooler outer edge of the rod during reactor operation. The diffusion rate is a function of the mass of the nuclide species and the melting/boiling points of the various elements or compounds. Therefore, a higher proportion of the lighter elements (fission products) will exist near the surface of the rod cladding.

It has been found that up to 30% of the volatile fission products are actually on the surface of the cladding (Coles [1981]). Leaching studies of spent fuel have concentrated on the leach rate of uranium, since this is the most abundant element and would, therefore, presumably be rate-determining if the nuclide distributions were uniform. However, for those nuclides which reside on the surface of the cladding, leaching will presumably be very fast once corrosion has advanced to the point where the canister is breached.

To model this phenomenon, a rough distinction has been drawn between the fission products, most of which are reasonably volatile, and the actinides. The fission products have all been modeled as having the same dissolution rate. This is certainly an approximation since not all the fission product nuclides are present in the same proportions on the surface of cladding, nor is the total inventory of any of them present. However, it is certainly conservative to assume this, and improved answers may be obtained by scaling the computed curie output by the various percentages. The actinides are modeled separately and given a uniform leach rate appropriate to that of

uranium. This is an approximation too, since the actinides are not uniformly distributed.

It is not necessary to make a distinction between actinide and fission product leach rates for solidified high-level waste forms, such as glass or SYNROC, since these presumably have uniform waste matrices. The dissolution or leach time used in this report is the inverse of the assumed fractional dissolution rate.

2.2.4 Local Transport

The third aspect of the waste form subsystem which may need to be modeled is the migration of the nuclides out of the canister niche once they have been leached into solution. This can occur through any of three possible mechanisms: thermal convection, natural convection, and molecular diffusion.

The first mechanism requires only that the canister niche have water in it; i.e., that there exist some pathway for water to enter the repository. The corridors then serve as conduits to disperse the water throughout the repository.

The second mechanism requires water flow through the canister niche. There will presumably be only a few such niches in the entire repository where this might occur during the pre-emplacement phase. However, after emplacement, thermal effects may alter this by inducing cracks in the media causing subsequent large scale convection. In salt, brine migration may be an important initial source of fluid.

The third mechanism, diffusion, can always be expected to occur, but will be negligible if either of the other two mechanisms are operating. In the scenarios are used in this study, only the natural convective mechanism has been assumed. It has further been assumed that the time it takes for nuclides to be transported out of the niche can be ignored in comparison with the dissolution time.

2.2.5 Waste Form and Package Model

For our analysis, we will characterize the waste form and package according to:

- Type of nuclide inventory, spent fuel (SF) or high-level waste (HLW)
- Amount of inventory in megawatt electric years (MWe•yr)

- Age of inventory in years
- Corrosion time in years
- Dissolution leach time (t_d) in years.

The age of the inventory, the corrosion time, and the refill and repressurization time are combined into one parameter, the initial release time (t_0).

2.3 REPOSITORY

2.3.1 Definition

The term repository (as used in this report) refers to underground excavations for nuclear waste disposal. As such, this usage is synonymous with the term depository. Surface facilities are not considered in this report.

2.3.2 Characterization

The repository will probably consist of an array of corridors parallel to each other and connected to exterior shafts by at least one central corridor. Many factors of the repository can directly and indirectly affect the transport of nuclides from the canister. Specifically, the repository characteristics will affect hydrology and transport, both within the repository and in the nearby vicinity (called the site). Such characteristics as the excavation method, extraction ratio, backfill permeability and porosity, overall dimensions, corridor placement, and tunnel and shaft locations will affect both transient (refill and repressurization) and steady-state hydrology. This hydrology, along with the backfill characteristics, will determine the transport.

2.3.3 Modeling

Detailed modeling of the dependence of the physical processes on the site characteristics is an immense task. Although the repository significantly affects the waste migration, the complexity of the problem and the resource constraints of this project preclude its detailed analysis.

Instead, because the site hydrology is modeled as a three-dimensional array of one-dimensional paths (see next section), this report's final outputs

of interest from the repository-scale transport should be splitting ratios for the waste into the various outflow paths as a function of time, with the repository treated as a point source. The outflow paths might be, for instance, the tunnel/shaft path(s), through the backfill or a fracture zone around the mined section, interstitial flow through the surrounding host rock, or fracture flow through jointing or other flaws near the repository. During the initial phase of repository transport the splitting fractions may be time-dependent. After repressurization and steady state has been reached, the splitting fractions of waste should be constant, provided no new pathways occur and the hydraulic parameters in the old pathways do not change.

The primary question then is what algorithm can be used to determine these fractions. If the waste is uniformly distributed in the repository, the splitting fractions for waste are the same as those for water outflow. If total leaching time* of the canisters is shorter than the characteristic times for nuclide transport within the repository, then the repository will eventually uniformly saturate with the various nuclides, independent of any outflow paths (such as interstitial or fracture flow through the host rock) other than tunnels and shafts. The presence of these other outflow paths can significantly affect the time necessay for saturation. However, this significance is reduced as the leach time becomes much shorter than repository transport times. If the leach time is longer than the repository flushing time, a state of uniform repository saturation will never be reached and the waste placement, corridor arrangement, as well as the hydrotransport characteristics of outflow paths through nonengineered features, can be important determinants of the splitting fractions. Some modeling of this dependence has been performed under the assumption that the only pathway to aquifers other than tunnel/shaft paths is flow in a strictly vertical direction. This is probably not true for the highly anisotropic, hydrologic environments characteristic of bedded media. Since hydrologic modeling in a setting primarily characterized by horizontal (either porous or fracture) flow through the host rock to the repository is not sufficiently far advanced to be of use to this study, a second approach could be made in conjunction with the water-splitting algorithms appropriate to the uniform saturation case. First,

---

*In this report no distinction is made between leaching and dissolving.

a baseline case would be run with the waste splitting equal to the water splitting. A second case would then be run, treating the splitting fraction as an uncertain variable correlated to the splitting fractions for the water. The first procedure is appropriate to the case in which leach time is less than repository flushing time, while the second approach is more appropriate in cases in which the leach time is longer.

In this report, the repository is modeled as a point source of nuclides or waste. The repository is combined with the site in a subsystem which models the flow into and out of the aquifers near the repository. The studies in Section 6 consider only a single path through the repository so that there is no splitting. The studies in Section 7 consider only the branching flow of water, so that there is again no modeling of splitting.

2.4 SITE

2.4.1 Definition

A technical definition of the site (suitable for this report) is that region which encompasses the repository and all its shafts and tunnels, and any significant natural water transmitting features (such as major jointing) in the vicinity of the repository. Typically, this region might be several kilometers in radial extent. From an operational point of view, the distinguishing feature of the site should be that it contains all potentially major outflow paths from the repository to the aquifers. It would not, however, contain the entire aquifer(s).

2.4.2 Flow Paths

For a given site, exploration and construction will disclose the existence and nature of some natural or man-made flaws, but there is always the possibility that the exploration has failed to discover other flaws or flow along bedding planes. The usual method of handling this uncertainty is to list all the possible types of flow paths and evaluate or estimate the probability that these paths exist at various locations.

Since real sites have not been considered in this study, no probability estimates can be made concerning the number and nature of any flow paths.

Only a list of possible path types can be made. See, for example, Carpenter et al. [1979]. (Typical values are given in Appendix E of the Bedded Salt report by Kovar and Steinborn [1980].) The various flow paths listed have in common that they are one- or two-dimensional in their major extent.

These flow paths are generally surrounded by host rock of low permeability and low porosity, and they are likely to conduct all the water flow through the site. In addition, the flow of paths which are two-dimensional in nature, tends to be reasonably constant in direction, and of finite extent perpendicular to the flow. These considerations imply that, for our purposes, the flow paths can be treated to a good approximation as one-dimensional paths or "pipes" in a three-dimensional array or network.

The simplest network consists of a source and a single path leading to a discharge point. Physically, this might correspond to transport from repository to discharge via a permeable interbed. It could also represent an effective path system with the indicated path representing an aquifer that ignores any vertical paths between the repository and the aquifer. This is because the transit time and pulse spreading associated with the vertical pipes are negligible compared to the contributions of the aquifers. In either of these cases, the site subsystem can be lumped together with the regional subsystem.

The path network most often analyzed in this work is depicted in Fig. 6-1. It is actually a generic network applicable to any set of paths connected in series. The vertical path through the repository can correspond to a flaw which extends from (at least) a lower to an upper aquifer and intersects the repository (e.g., a deep borehole). Equivalently, it can also represent two flaws, one of which extends from the repository down to a lower aquifer, the connection to the upper aquifer being a second, distinct flow path, such as a shaft. We usually assume conditions in which the water flows upward to the top aquifer and hence, out to a surface discharge point. However, the same analysis applies to the case where the water flows downward and through a lower aquifer, to some surface discharge point. The fact that the discharge is directly from the lower aquifer to surface waters implies that erosion has removed the various layers down to the lower aquifer, over the horizontal distance between the repository and the discharge point. (This is known to happen in some sedimentary basins.)

In a simple parallel path network (see Fig. 7-1), one flaw extends between the lower aquifer and the repository, and two between the upper aquifer and the repository. Depending on the magnitudes and signs of various

head differences and transmissivities, there may be either one or two outflow paths. This network is sufficiently general that it can be used to identify many of the potentially interesting facets of much more complicated networks. These include such aspects as competition among different pathways and groups for maximum impact, interpath correlations for different variables, and the ability to see how the number of paths that are outflow is related to parameter values. This site structure may in turn be connected to surface waters by a regional aquifer.

2.4.3 Parameters

Determination of the appropriate network is only part of the characterization task. We must also determine the parameters associated with each element of the network.

The parameters necessary to characterize site (and regional) flow paths are those that appear in D'Arcy's Law and the advection-diffusion equation. These are discussed in Subsection 2.6.

The site model allows calculation of the water flow into and out of the repository as in Section 7, and the activity released into the regional aquifer as in Section 6.

2.5 REGIONAL SUBSYSTEM

2.5.1 Definition

The region is usually defined as that geographical area which surrounds the site, both horizontally and vertically, and includes all water bearing formations which are hydrologically connected to the site. In particular, it includes all aquifers. In fact, in the work reported here, the regional subsystem is just a single pathway connecting the repository site to the biosphere. In this context, the biosphere includes surface waters such as rivers and lakes.

Water flow in sedimentary basins is generally along bedding planes, although vertical flow may be significant in some areas. In crystalline rock formations, there are no well defined bedding planes, and so water will generally follow joint formations. However, crystalline formations often occur as intrusive zones embedded within a larger sedimentary basin. For the purposes of this study, the region will be assumed to be sedimentary in nature. This implies that the site is sufficiently large so that any intrusive bodies containing the repository are within the site.

2.5.2 Site Boundary Conditions

Although our studies assume that the heads in the aquifers are part of the specification of the site subsystem, it is an analysis of the region that provides this input. Because the flow of water within the formation is generally dictated by gravity, lower aquifers will often be at a lower head than overlying aquifers and if any flaws exist in between the two, the water flow will be down. To obtain an upward flow, either the flaw must be located reasonably near a large water body in the recharge zone, or an "obstacle" must exist in the lower aquifer, which effectively adds an additional force (besides gravity) and redirects the water upward.

This "obstacle" can be either a real obstruction of the aquifer by a low-permeability zone, or it may be water moving into a discharge zone from the opposite direction. Although the downward flow case is the more common, most of the analyses in this report will use an upward flow, primarily because the typical transit times are shorter than those of the downward flow case. Therefore, the doses are generally higher (i.e., conservative).

2.5.3 Solute Transport

Unlike most vertical flow paths, the transport of solute within the aquifers is not constrained perpendicular to one-dimensional flow paths. Horizontal transverse dispersion can be expected to disperse the solute over a wide front. This can be important if the aquifer is being used as a source of well water, or if the total water flow splits to two different water-use systems at some point downstream from the repository. If neither happens, then all the solute eventually reaches the same water system. Although there may be some time-lag for various portions of the pulse, it should not be significant, and the horizontal transverse dispersion can often be ignored. In this report, the above conditions of no wells and no splitting will be assumed and transverse dispersion will be ignored.

In some cases, transverse dispersion in the vertical cross-sectional plane may be significant. This will be the case if the aquifer actually consists of several adjacent water bearing layers of differing permeability or porosity. This will mean that, as the solute disperses among these layers, its velocity changes, inducing an additional horizontal spreading of the

BEST DOCUMENT AVAILABLE

pulse. This spreading can be modeled as an effective longitudinal dispersion (Pollack [1980]), provided certain assumptions are satisfied.

2.6 FLOW AND TRANSPORT EQUATIONS AND PARAMETERS

2.6.1 Equations

The dynamic equations used for the hydrology and transport calculations for the flow path network are the traditional ones of water conservation and D'Arcy's Law for the hydrology, and the advection-dispersion equation for the transport of waste. [See for example the book edited by DeWiest (1969) or the report by TASC (1978).] The parameters that appear in D'Arcy's Law are:

$$q = K \frac{\Delta H}{L} \tag{2-1}$$

$$Q = qA \tag{2-2}$$

and the advection-diffusion equation:

$$\frac{\partial C}{\partial t} + \frac{u}{B} \frac{\partial C}{\partial X} = \alpha \frac{u}{B} \frac{\partial^2 C}{\partial X^2} , \tag{2-3}$$

where

$$u = q/\theta \tag{2-4}$$

characterizes the flow path segment in the site or regional network. These parameters or variables are identified in Table 2-6.

TABLE 2-6. Parameters in flow and transport equations.

Symbol	Name	Units
q	D'Arcy velocity	m/yr
K	Hydraulic conductivity	m/yr
ΔH	Head difference	m
L	Path length	m
Q	Flow rate	m^3/yr
A	Cross-sectional path area	m^2
C	Solute concentration	[illegible]ry[a]
u	Pore velocity	m/
B	Retardation factor	--
α	Longitudinal dispersion	m
θ	Effective porosity	--

[a] For example, $\frac{Ci/(MWe \cdot yr)}{m^3}$

As will be seen in Subsection 2.7, the concentration is not calculated explicitly. The flow rate, decay rate, and concentration are combined into the variable we use, the activity rate, J. The units of J are curies per year, Ci/yr.

Since these equations have been validated only for media admitting porous (or interstitial) flow, rather than the case of fracture flow, it is reasonable to question their appropriateness in all cases. Defense of their use rests on the fact that for those paths suspected of admitting fracture flow (such as the fracture zone around mined pathways or through jointing), the fracturing is fairly extensive. This means that on spatial scales greater than the cross-sectional flow path dimensions, the fracture zone appears as almost interstitial.

Since D'Arcy's Law can be derived by averaging the Navier-Stokes fluid flow equations over some scale, its validity is independent of the scale of the fractures, as long as this scale is less than that for gross variability of the driving force (hydraulic head). Similar reasoning applies to the advection-dispersion equation, although here the dispersion is often dictated by the largest inhomogeneities in the system. Thus, its usefulness (as opposed to validity) is much more seriously open to question.

In general, it is necessary to solve for some of the path-hydraulic gradients by requiring conservation of water at each path connection point (node) and zero-total head drop for any closed set of paths (along with one or two boundary conditions on regional recharge rate or aquifer head). This leads to a set of simultaneous linear equations which are straightforward to solve.

2.6.2 Dispersion

When a pulse of solute travels through a porous media, the differential flow velocities (both magnitude and direction) associated with the various microscopic channels cause the pulse to be spread out, both in the direction of flow (longitudinal dispersion) and perpendicular to the flow (lateral dispersion). The amount of dispersion is assumed proportional to the average velocity of the water. Given the one-dimensional nature of the hydrology modeling used for this report, transverse dispersion is ignored.

BEST DOCUMENT AVAILABLE

To model the effects of longitudinal dispersion, the fundamental assumption is made that the main features of the transport are adequately described by two quantities:

- Average time taken to traverse the sequence of path segments (note that the average time is not necessarily the transit time for the peak).
- Variance of the pulse at its exit point.

When Laplace transform techniques are used, it may be seen that the following relationships hold for a series of one-dimensional flow paths:

$$T_T = \sum T_j \tag{2-5}$$

$$S_T^2 = \sum_j S_j^2 \tag{2-6}$$

where T_j is the average transit time for the jth segment, $T_j = L_j/u_j$; T_T is the average total transit time; S_j^2 is the variance induced by transit through the jth path;

$$S_j^2 = 2\alpha_j L_j/u_j^2 = 2\alpha_j T_j^2/L_j$$

where

α_j = dispersivity of the jth path, and
S_T^2 = the total variance.

2.6.3 Retardation

The u_j which appears in these formulas may be scaled by a factor of $1/B^i$, where B^i is the retardation of nuclide type i in path segment j. This retardation is due to the variety of ion-rock interactions such as ion adsorption onto rock surfaces, ion-ion-rock complexes, etc. These retardation factors have their own probability distributions dependent on groundwater chemistry and rock type, as well as nuclide type.

2.7 SUBSYSTEM AGGREGATION AND PERFORMANCE MEASURE CALCULATIONS

2.7.1 Dissolution and Transport

There are two major calculations which must be performed to evaluate the activity rate released from a system or subsystem. The first integrates the waste form dissolution model with a transport model. If $R^i(t)$ is the dissolution rate for nuclide type i as a function of time and $G_j^i(t)$ is

BEST DOCUMENT AVAILABLE

the Green's function (output flux for an instantaneous input of solute) for nuclide type i and pathway j, then the output flux is given by:

$$j_j^i(t) = \int_0^t R^i(t')\, G_j^i(t - t')\, dt'. \tag{2-7}$$

At this point, the units of j and G are arbitrary. Anticipating the next calculation, we usually assign units of Ci/yr to G and j.

As mentioned in previous sections, the waste form dissolution is assumed to start at the initial release time as canister breach occurs ($t = t_0$), and to continue at a constant rate until the dissolution is complete. Thus, assuming a unit inventory and ignoring decay:

$$R^i(t) = \begin{cases} 0 & t < t_0^i \\ \dfrac{1}{t_d^i}, & t_0^i \le t \le t_d^i + t_0^i \\ 0, & t > t_d^i + t_0^i, \end{cases} \tag{2-8}$$

where t_d^i is the dissolution time for nuclide type i. Decay will be incorporated below. For a single pathway that starts at x = 0 and extends to $x = +\infty$, it may be shown that:

$$G(t) = \frac{L}{[4\,ut^3]^{1/2}} \exp[-(L-ut)^2/4\alpha ut], \tag{2-9}$$

where

L = position along path
α = longitudinal dispersity
u = velocity
t = time.

It can be shown (Oston [1979]) that our results are not sensitive to this semi-infinite boundary condition.

The integral in Eq. (2-7) can be performed analytically for the case when R(t) is given by Eq. (2-8). The result can be written in terms of Error Functions, but the exact expression is of little interest except to note that it exists; therefore, the form will not be given here.

BEST DOCUMENT AVAILABLE

2.7.2 Aggregation of Path Elements

The aggregation of path elements is the second calculation necessary to evaluate the performance measure. The essence of the procedure is to find an approximation to the integral:

$$G_T(t) = \int_0^t G_2(t - t')\, G_1(t')\, dt' \qquad (2\text{-}10)$$

which mathematically represents the output from two paths whose Green's functions are G_1 and G_2, assuming an instantaneous impulse of solute into the first. If the pulse spread S, associated with each path is less than the corresponding average transit time T, the integral can be approximated by the expression:

$$G_T(t) = \frac{1}{\sqrt{2\pi S_T^2 t^3 / T_T^3}} \exp\left[-(T_T - t)^2 / \left(2S^2 t / T_T^3\right)\right] \qquad (2\text{-}11)$$

or

$$G(t/T) = \frac{1}{\sqrt{2\pi\beta^2 T_T^2 (t/T_T)^3}} \exp\left[-(T_T - t)^2 / 2\beta^2 (t/T_T)\right] \qquad (2\text{-}12)$$

where:

$$T_T = T_1 + T_2$$
$$S_T = S_1^2 + S_2^2$$
$$\beta = S_T / T_T \quad .$$

The expression generalizes for any number of paths in series. This approximation allows the subsystems to be characterized by the parameters (T_j, S_j), which are combined to give (T_T, S_T), for the total system. The validity of the approximation becomes tenuous as the S/T ratio for any single pipe becomes larger than one. Since the analytic form of the answer is the same as Eq. (2-9), the integration over the square-pulse dissolution function again yields Error Functions.

BEST DOCUMENT AVAILABLE

2.7.3 Radioactive Decay

The incorporation of inventory and decay into this aggregation procedure is straightforward. Since the decay of the solute is independent of its location, tables can be made for the activity of the various nuclides at specific times. The nuclide activity flux as a function of time will then be given by:

$$J^i(t) = H^i(t)\ j^i(t) \qquad (2\text{-}13)$$

where

$j^i(t)$ = output flux for the system for nuclide i, assuming unit input and no decay (nondecayed flux),

$H^i(t)$ = activity (hazard) of nuclide i as a function of time,

$J^i(t)$ = total output flux for nuclide i (decayed flux).

Values of $H^i(t)$ are approximated by interpolation between points in the tables.

2.7.4 Peak Activity Rate

As mentioned earlier (Subsection 2.1), we have focused on the peak activity rate (flux) as a primary measure of an isolation system's performance. The calculation of the peak activity rate (decayed flux) could conceivably be done directly by computing the product of j(t) and H(t) at several discrete times, and selecting the maximum of these products. However, this is a laborious procedure and is not suitable for extensive computer simulations; therefore, an approximation is used.

As discussed above, the time dependence of the released activity rate (decayed flux) is a function of the dissolution time, the total transit time, and the dispersion. When the dissolution time is much less than the dispersion pulse spreading, the nondecayed flux is approximately equal to the Green's function multiplied by the quantity of waste released.

BEST DOCUMENT AVAILABLE

When the dissolution time is much longer than the pulse spreading, the shape of the nondecayed flux is approximately rectangular with some spreading only along the leading and trailing edges of the pulse. If the total temporal spread (dissolution plus dispersion) of j(t) is less than the time for any major variations in H(t), then the peak of the product will occur at a time close to that of j(t).

The approximate time of peak converges to the exact solution as the total pulse width tends to zero. In many cases, when H(t) varies significantly over the time equivalent to the total pulse width, the dissolution times are large and the the peak of j(t) occurs almost at the tail end of the (almost square) pulse. Since H(t) is generally monotonically decreasing, and j(t) is almost flat (nonvarying) over the length of the pulse, the peak of the product probably occurs near the beginning of the pulse, totally separated from the time j(t) peaks. The essence of the approximation procedure is to accurately answer questions about the maximum of the product, and the associated time, by looking at only the function j(t). For the case of long dissolution times, the single procedure of taking the maximum of j(t) and evaluating the product at that peak time, thus will not yield correct answers. However, a minor modification of this procedure will work. Specifically, since j(t) is almost flat over its duration for the long dissolution case, the time at which the pulse first reaches 90% of its maximum value will occur near the beginning of the pulse. This is also the time region where H(t) is likely to have its maximum. Therefore, the algorithm for the peak:

$$J_{max} = H(t_{90})\, j(t_{90}) \qquad (2\text{-}14)$$
$$t_{peak} = t_{90} \ ,$$

with t_{90} defined by:

$$j(t_{90}) = 0.9\ j(t_{max}) \qquad (2\text{-}15)$$

and t_{max} is the time of the peak of the nondecayed flux.

This gives accurate results for J_{max} and t_{peak}, when the dissolution time is much longer than the average transit time. It will also yield accurate answers for the other dissolution times. Thus, this is a unified algorithm for peak flux, provided only that the dispersion-induced pulse

spreading is not greater than the transit time. In practice, a table of values for $j(t_{90})$ and t_{90} is constructed and table lookups performed for the various computations. The validity of the approximation rests on the monotonic decrease in inventory activity with time. This is rigorously true for the fission products (Groups 1 and 2), but there is a local maximum for the actinides, due to the decay of the fuel mixture into radium daughter products. This buildup occurs between 10,000 and 100,000 yr and causes a very slight increase in activity. This error is considered negligible compared to that of other approximations.

REFERENCES

Analysis of Some Nuclear Waste Management Options, Vol. II: Appendix F, 1978, Lawrence Livermore National Laboratory, Livermore, CA, UCRL-13917.

Bonner, N. A. and Y. C. Ng, 1980, BIODOSE, Lawrence Livermore National Laboratory, Livermore, CA, UCID-18562.

Carpenter, D., T. L. Steinborn, L. D. Thorson, 1979, Groundwater Recharge and Discharge Scenarios for a Nuclear Waste Repository in Bedded Salt, Lawrence Livermore National Laboratory, Livermore, CA, UCID-18119.

Coles, D. G., 1980, Continuous-Flow Leach Testing Method for Various Nuclear Waste Forms, Lawrence Livermore National Laboratory, Livermore, CA, UCRL-85006.

Ibid., 1981, Single-Path, Continuous-Flow Leach Test, PNL 76-68 GLASS: Selected Bead Leach I Results, Lawrence Livermore National Laboratory, Livermore, CA, UCRL-85405.

DeWiest, J. M., 1969, Flow Through Porous Media (Academic Press, New York).

Eisenbad, M., 1973, Environmental Radioactivity (Academic Press, New York), p. 208.

Glasstone, S., 1967, Sourcebook on Atomic Energy, (Van Nostrand Co., Inc., Princeton), Chapter 18.

Kovar, F. R., and T. L. Steinborn, 1980, The Bedded Salt Report, Lawrence Livermore National Laboratory, Livermore, CA, UCRL-52737.

Lester, D. H., et al., 1980, "Waste Package Performance Analysis," Proceedings of the 1980 National Waste Terminal Storage Program Information Meeting, Office of Nuclear Waste Isolation, Battelle Memorial Institute, Columbus, OH, ONWI-212.

Osten, S. G., 1979, Finite Medium Green's Function Solutions to Nuclide Transport in Porous Media, Lawrence Livermore National Laboratory, Livermore, CA, UCRL-15040.

3. METHODS OF ANALYSIS AND COMPUTATION

This section describes the methods of analysis and computation used to investigate the behavior of the simple models of nuclear waste isolation systems. We present the rationale for the methods of deterministic and probabilistic analysis by relating the analysis methods to the primary goal of the study. This section also describes how probability distributions of model parameters were propagated through the deterministic models.

3.1 METHODS OF ANALYSIS

A major purpose of the research and development funded by ONWI is to reduce uncertainties about the performance of engineered and natural systems. The primary goal of this study was to identify parameters of waste isolation systems, whose uncertainties greatly affect predictions about long-term performance. Conversely, we identified parameters whose uncertainties contribute very little to the uncertainty about long-term performance. This type of information can be useful in judging which research and development may significantly reduce the uncertainty about the long-term performance of repositories.

Subsection 3.1.1 describes the role of deterministic analysis in this study, and Subsection 3.1.2 deals with the methods of uncertainty analysis and the validity of the approach to identifying important uncertainties.

3.1.1 Deterministic Analysis

Three major purposes for conducting deterministic analysis with the systems models are to:

- Determine which parameter uncertainties are likely to have the greatest effect on the uncertainty in model outputs.
- Select variables for probabilistic treatment in uncertainty analyses.
- Make the results of uncertainty analyses easier to understand and explain.

The deterministic analysis is presented in Sections 5 and 7. A parametric study with general applicability is presented in Section 5. Contour plots are also used in this section to show how the magnitude and time of the peak activity release rate depend on the time for waste to dissolve and travel from the waste form to the release point. These contour plots identify the regimes where one or both parameters have a significant effect on the value of the performance measure.

Section 7 presents a deterministic analysis of water flow in a network composed of parallel paths. The sensitivity of water flow to the model parameters was investigated by computing first derivatives. The results show which parameter variations have the greatest effect on flow and demonstrate that sensitivity to parameters can depend on the values of the model parameters.

3.1.2 Uncertainty Analysis

The major objective of the uncertainty analysis was to determine which model parameters have the greatest effect on the probability distributions of the outcomes when the probability distributions of those parameters are perturbed. Research that could affect the uncertainty about these parameters could modify the uncertainty assessment of the outcomes.

In this study, probability distributions were used to represent uncertainty about the model input parameters. Probabilities are used to quantitatively state the degree-of-belief with respect to a proposition, based on a given state of information. This definition is also extended to continuous variables, if the proposition is that the value of a variable is less than or equal to a number. The probability of the variable X having a value less than or equal to x is a cumulative distribution function, $F_X(x)$. The derivative of $F_X(x)$ with respect to x is the probability density function.

Section 5 analyzes the effects of the probability distributions for waste transit and dissolution times on the probability distributions for performance variables. This is a parametric analysis of the model without explicit association between the parameter distributions and particular waste forms, repository designs, and media. The parametric study results are presented as

graphs. These results are broadly applicable to a wide range of systems. The graphs are applied in an example analysis of a system in Subsection 6.8.

For the analysis in Section 6, probability distributions of the model parameters represent particular types of waste forms, geologic media, and flow pathways. This is an example of a systems analysis of a hypothetical system. We emphasize that the uncertainty analysis in Section 6 does not constitute a risk assessment since:

- The analysis considers only a single relatively severe scenario, without considering the probability of that scenario, and
- Experts were not extensively involved in assigning probability distributions to the model parameters.

The analysis in Section 6 assumes that existing flaws connect a lower and upper aquifer. A hydraulic gradient establishes the water flow necessary to dissolve and transport the waste to the upper aquifer leading to the surface. All parameter probabilities are conditional probabilities given this scenario. These conditional probabilities were <u>not</u> multiplied by the probability of the scenario; therefore, this approach may overestimate the importance of the conditional probability of some model parameters if this scenario is very unlikely.

The probability distributions were assigned to the model parameters without conducting statistical analyses of data, or formal interviews of experts. Distributions were assigned based on reviews of reported data and on brief consultations with experts at LLNL. These initial probability assignments are appropriate for the general purpose of this study. Of course, gross misstatements of the uncertainty represented by the parameter distributions can lead to erroneous conclusions.

The approach used in investigating the importance of parameter uncertainties can be called an uncertainty-sensitive method. Figure 3-1 summarizes data from such an analysis. Case 1 is the base uncertainty case, computed with all five model parameters (listed on the figure) input as uncertain and represented by probability distributions. In Cases 2 through 6, each uncertain parameter was set certain at its median value. The bar graphs summarize the probability distributions computed for each case. The horizontal bars are placed at the 1st, 25th, 50th, 75th and 99th percentiles

BEST DOCUMENT AVAILABLE

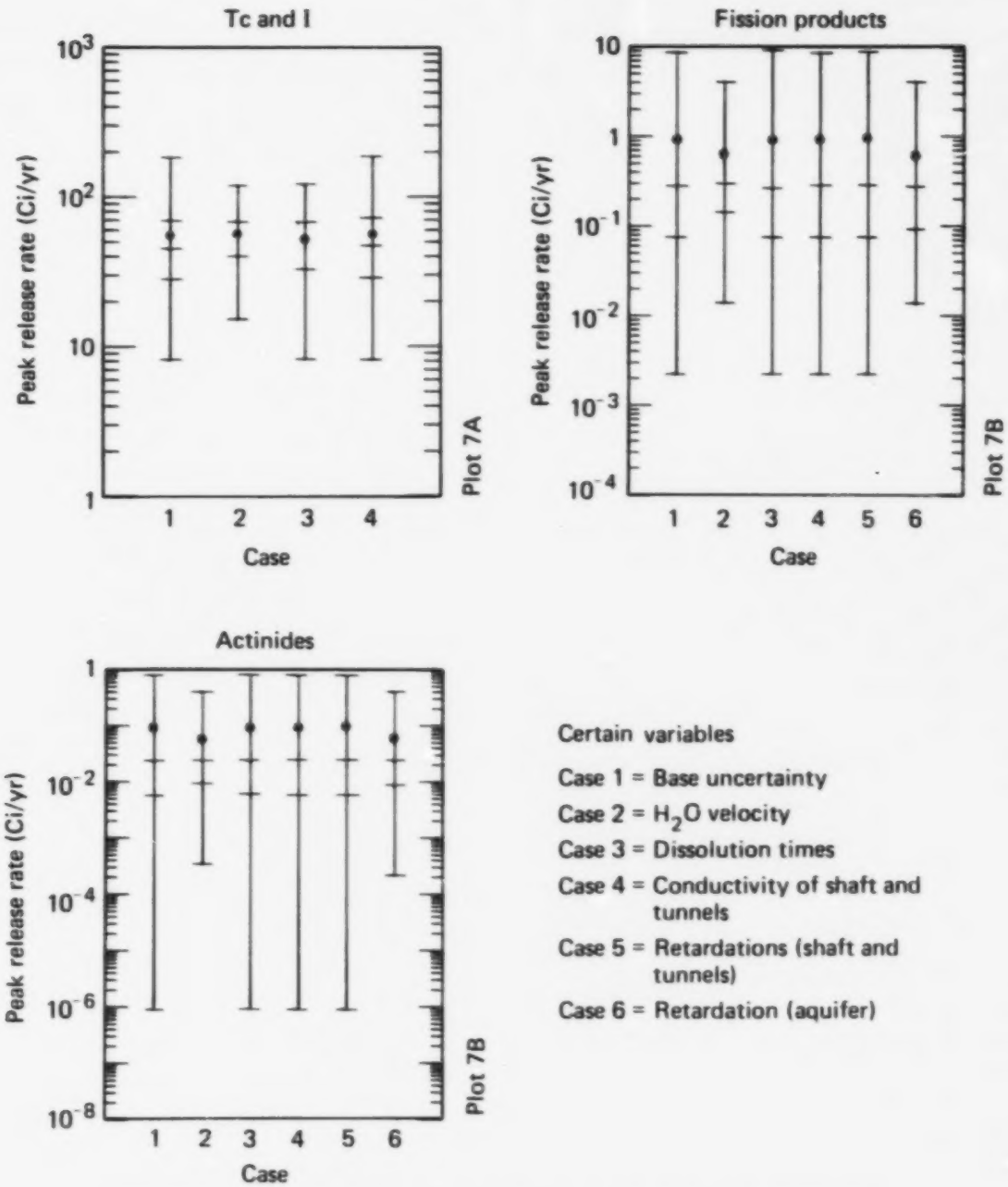

FIG. 3-1. Uncertainty sensitivity analysis of a waste isolation system.

of the outcome variables (peak rate of activity release). The asterisk shows the mean value of the outcome.

Note that there is no Case 5 or Case 6 for Tc and I since these nuclides were assigned a constant retardation factor of 1.0. Several other parameters were also input as certain for all cases. These parameters were set certain in the uncertainty analysis of the complete system based on analyses of separate subsystems.

The differences between the percentiles and means of the base case and other cases indicate the sensitivity of probability distributions to those of the model parameters. For those cases where the distributions changed, the first and 99th percentiles were affected more than the 50th percentiles. This is understandable since the parameters were set certain at their median values. Since this can be misleading, it will be discussed in the next section.

3.1.3 Value of Information

The theory of the value of information (Howard [1966, 1967]) provides one of the best conceptual constructs for choosing between several research strategies. We did not conduct a value of information (VOI). We compare the methods in this study with those of the VOI to point out the limitations of the results.

VOI theory is based on the assumption that research can have a positive value only if the findings can result in a different action than would have been taken without doing any research. For example, suppose waste form A will be chosen over B if no additional research is performed. Then, additional research can have positive value only if there are research outcomes that would result in changing the selection to B. Waste form B would be selected for those research findings which change the information to make the predicted performance of the system look more favorable with B than with A.

Some of the information necessary for conducting a VOI study are:

- Clearly defined alternative actions (the choice of which can be influenced by the information from the tests).
- Clearly defined alternative test strategies (or research activities).

• Statements about the effectiveness of the tests in terms of likelihood functions (examples of such statements would be: the probability of a false negative, and the probability of a false positive).

This study has not considered specific means of reducing uncertainties about the performance of the elements of waste isolation systems. Therefore, VOI methods are not applicable. However, some VOI concepts do apply. Additional information from tests and research may affect the probability distributions of parameters represented in our models. For research to have value, it must affect information about a parameter to which the model is sensitive.

Our uncertainty sensitivity analysis sets each parameter at the median value (50th percentile) of the parameter distribution. A true VOI study actually accounts for the fact that the outcome of a test, even a perfect one, is not predictable. Consider a test which could provide "perfect information." After completion of the test, we would know the exact value of a parameter under a specific set of conditions. However, it is important to note that the test could produce any result within the range of the distribution function. The method applied here is actually equivalent to investigating the value of a guaranteed test outcome.

3.2 MACRO COMPUTER CODE

The MACRO computer code developed at LLNL was designed as a tool for systems analysts in performing uncertainty and sensitivity analyses of systems models using uncertain values of input or physical parameters. The uncertainty in the value of a parameter is described by a probability distribution over the parameter values. If a model of a physical system requires an uncertain parameter as input, the output of the model will then be described by a probability distribution.

MACRO was specifically designed to coordinate and execute a sequence of user-supplied models where the input parameters of the models may be uncertain. It is explicitly capable of handling the general case where some of the inputs to models are the outputs from one or several of the other models. Its main capability is propagation of the input distributions through a sequence of deterministic models, thereby producing probability distributions for the model outputs.

BEST DOCUMENT AVAILABLE

The current version of MACRO has built-in models specifically designed to analyze the post-closure performance of a nuclear waste repository. These models include the physical systems model used in this study and described in Section 2.

MACRO propagates probabilities through models by converting continuous probability-density functions to finite probability distributions and applying the laws of probability to these distributions. The probability distribution of a variable, X, is represented by doublets (p_i, x_i) where p_i is the probability that X is contained in an interval whose representative value is x_i. Intervals are assigned for every uncertain variable of interest. In MACRO, several different methods for choosing the intervals are available. One choice could be to choose the intervals on an equal ratio basis with five intervals per decade. For example, we might calculate the x_i from the formula:

$$x_i = 10^{i/5}, \tag{3-1}$$

where x_i would be the representative value for the interval:

$$(x_{i-1/2}, x_{i+1/2}). \tag{3-2}$$

The calculation rules from probability theory are used to compute the distribution of a model output variable. Suppose we wish to calculate the probability distribution of a model output variable Z where the function f(X,Y) is the model:

$$Z = f(X,Y), \tag{3-3}$$

and the model inputs X and Y are independent with finite probability distributions represented by the doublets

$$(p_i, x_i) \qquad i = 1,\ldots,n$$

and

$$(q_j, y_j) \qquad j = 1,\ldots,m. \tag{3-4}$$

BEST DOCUMENT AVAILABLE

Then, we form the probability distribution for Z, (r_k, z_k), using the rule:

$$r_k = \sum p_i q_j, \tag{3-5}$$

where the sum is over all indices i and j such that $f(x_i, y_j)$ is in the interval:

$$(z_{k-1/2}, z_{k+1/2}). \tag{3-6}$$

MACRO is not limited to the assumption that X and Y are independent. Several models within MACRO have two dependent output variables. These models generate a joint probability mass function for X and Y. The function is represented by n × m doublets:

$$(p_{ij}; x_i, y_j) \text{ for } i = 1,\ldots n \text{ and } j = 1,\ldots m, \tag{3-7}$$

where p_{ij} is the probability of X having value x_i and of Y having value y_j. If X and Y are used in a subsequent model to compute Z, then

$$r_k = \sum p_{ij}, \tag{3-8}$$

with the sum over all indices i and j such that $f(x_i, y_j)$ is in the kth interval for Z.

An example of this procedure for independent variables appears in Figs. 3-2 and 3-3. Figure 3-2 shows the finite probability distributions of the variables K = permeability, and dH/dx = (hydraulic gradient). Figure 3-3 shows the resultant probability distribution of the D'Arcy velocity Q given by the simple product model Q = K(dH/dx) (D'Arcy's Law).

Through the use of an interpretive language, MACRO actually allows the analyst considerable flexibility in choosing, modifying and sequencing the calculations, programming special sensitivity procedures, manipulating probability distributions and producing output edits and plots.

BEST DOCUMENT AVAILABLE

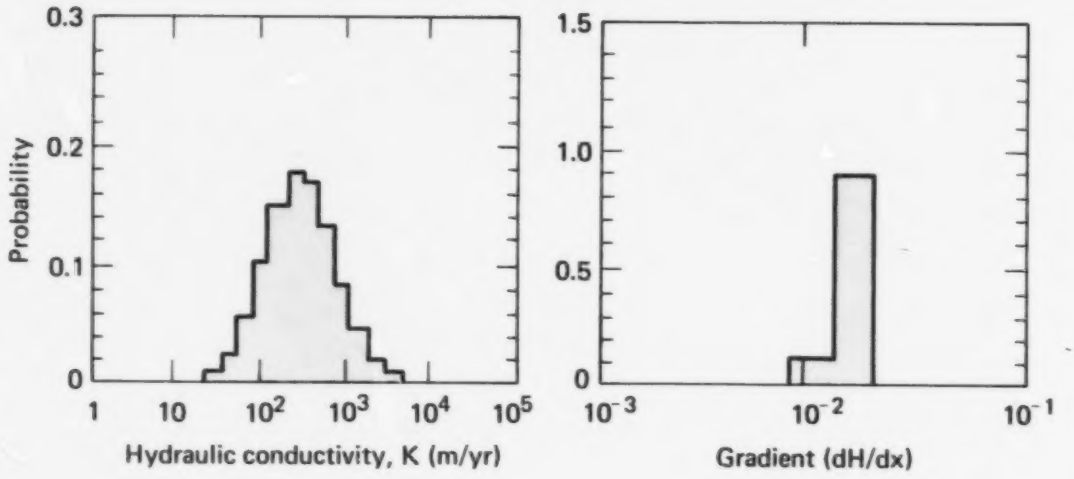

FIG. 3-2. Finite probability distribution of input variables K and dH/dx.

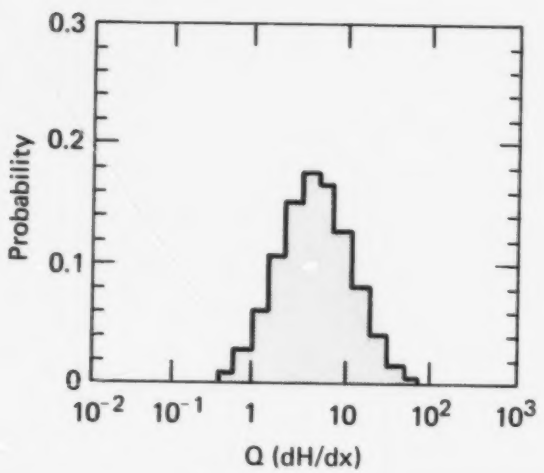

FIG. 3-3. Finite probability distribution of output variable Q, the D'Arcy velocity.

REFERENCES

Howard, R. A., "Information Value Theory," IEEE Transactions on Systems Science Cybernetics, Vol. SSC-2, No. 1 (Aug. 1966).

Ibid., "Value of Information Lotteries," IEEE Transactions on Systems Science and Cybernetics, Vol. SSC-3, No. 1 (June 1967).

4. DATA BASE

This section provides the data used to generate the inputs for the calculations contained in this report. Three types of sources were used in arriving at the information contained in this section:

- Previously published data
- Private communications with knowledgeable experts
- Our own estimates when no other source was available.

To obtain a list of potentially useful published reports, a RECON computer search of an extensive data base was performed at LLNL using the keywords: basalt, salt, deposits, boreholes, shafts, seals, fracture, breccia, jointing, permeability, and porosity. These reports were then individually searched to obtain the desired data. When the desired data was not found in existing reports, knowledgeable experts were consulted to obtain reasonable values for the needed information. Donald Jackson, Willard Murray, Frederick Kovar and Terry Steinborn were the individuals contacted.

4.1 WASTE FORM/PACKAGE DATA

In this study, we have assumed that the type of nuclear waste (nuclear inventory) was either spent fuel (SF) or high-level waste (HLW). The total amount of the inventory was assumed to be that which would result from generating 10^6 MWe·yr. The inventories were calculated using standard PWR reactor parameters (Alexander et al. [1977]). The uranium fuel (enriched to 3.2% U^{235}) was used for 1100 days at an average power of 30 MW/MT. For the plutonium-storage fuel cycle, the high-level waste was derived from fuel reprocessed 160 days after removal from the reactor. Reprocessing was assumed to remove all the Kr and Xe, 99.9% of the I, 99.5% of the U and Pu. The waste was also taken to include core structural materials, such as cladding and spacers. Summaries of the inventories used in the computations are shown in Tables 4-1 (SF) and 4-2 (HLW).

For the analysis in this report, we have divided the biologically significant nuclides in the waste into three major groups: (1) fission products with no sorption, (2) fission products with sorption; and (3) the

BEST DOCUMENT AVAILABLE

TABLE 4-1. Inventory of radionuclides in spent fuel.

	Radionuclides in spent fuel (Ci/MWe·yr)				
Radionuclide	1.0E2 yr	1.0E3 yr	1.0E4 yr	1.0E5 yr	1.0E6 yr
AM243	5.53E-01	5.19E-01	2.26E-01	6.50E-05	6.58E-09
AM241	0.04E+01	2.16E+01	4.09E-03	2.06E-06	3.66E-39
PU240	1.49E+01	1.36E+01	5.40E+00	5.32E-04	6.81E-11
PU239	8.88E+00	8.66E+00	6.79E+00	5.35E+00	6.51E-09
PU238	3.76E+01	3.86E-02	7.42E-21	0.0	0.0
NP237	1.24E-02	2.65E-02	3.08E-02	2.99E-02	2.23E-02
U238	9.84E-03	9.84E-03	9.84E-03	9.84E-03	9.84E-03
U235	4.71E-04	4.78E-04	5.46E-04	7.64E-04	7.81E-04
U234	3.93E-02	5.28E-02	5.18E-02	4.24E-02	1.24E-02
U233	6.08E-06	8.70E-05	1.24E-03	1.05E-02	2.37E-02
PA231	1.72E-06	1.07E-05	9.87E-05	6.32E-04	7.81E-04
TH232	4.40E-11	4.42E-10	5.10E-09	6.19E-08	6.29E-07
TH230	2.86E-05	4.24E-04	4.31E-03	2.70E-02	1.37E-02
TH229	3.55E-08	3.53E-06	4.27E-04	9.60E-03	2.40E-02
AC227	1.39E-06	1.07E-05	9.87E-05	6.32E-04	7.81E-04
RA228	3.98E-11	4.42E-10	5.10E-09	6.19E-08	6.29E-07
RA226	5.75E-07	7.60E-05	3.36E-03	2.74E-02	1.37E-02
PD210	3.23E-07	7.60E-05	3.36E-03	2.74E-02	1.37E-02
PB210	3.23E-07	7.60E-05	3.36E-03	2.74E-02	1.37E-02
EU154	2.69E+00	3.17E-17	0.0	0.0	0.0
SM151	1.73E+01	1.33E-02	9.77E-34	0.0	0.0
CS137	3.35E+02	3.13E-07	0.0	0.0	0.0
CS135	8.31E-03	8.31E-03	8.30E-03	8.12E-03	6.60E-03
I129	1.17E-03	1.17E-03	1.165-03	1.16E-03	1.12E-03
SN126	1.70E-02	1.69E-02	1.58E-02	8.49E-03	1.66E-05
PD107	3.42E-03	3.42E-03	3.42E-03	3.39E-03	3.10E-03
TC99	4.48E-01	4.47E-01	4.34E-01	3.23E-01	1.71E-02
NB93M	5.88E-02	5.91E-02	5.89E-02	5.65E-02	3.73E-02
ZR93	5.91E-02	5.91E-02	5.89E-02	5.65E-02	3.73E-02
SR90	2.07E+02	4.75E-08	0.0	0.0	0.0
SE79	1.25E-02	1.23E-02	1.125-02	4.29E-03	2.92E-07
NI59	1.72E-01	1.71E-01	1.58E-01	7.25E-02	2.98E-05
C14	9.62E-02	8.63E-02	2.90E-02	5.44E-07	2.93E-54

BEST DOCUMENT AVAILABLE

TABLE 4-2. Inventory of radionuclides in high-level waste.

	Radionuclides in high-level waste (Ci/MWe·yr)				
Radionuclide	1.0E2 yr	1.0E3 yr	1.0E4 yr	1.0E5 yr	1.0E6 yr
AM243	5.53E-01	5.10E-01	2.26E-01	6.50E-05	6.51E-09
AM241	4.26E+00	1.02E+00	4.08E-03	2.06E-06	3.66E-39
PU240	2.57E-01	2.38E-01	9.46E-02	9.31E-06	6.81E-11
PU239	4.61E-02	5.83E-02	1.22E-01	1.75E-02	6.51E-09
PU238	1.42E-00	5.90E-03	7.42E-21	0.0	0.0
NP237	1.00E-02	1.07E-02	1.09E-02	1.06E-02	7.90E-03
U238	4.92E-05	4.92E-05	4.92E-05	4.92E-05	4.92E-05
U235	2.34E-06	2.40E-06	3.26E-06	9.30E-06	9.89E-06
U234	6.90E-04	1.27E-03	1.24E-03	9.76E-04	1.23E-04
U233	4.28E-06	4.43E-05	4.53E-04	3.73E-03	8.38E-03
PA231	7.26E-07	7.57E-07	1.11E-06	7.04E-06	9.89E-06
TH232	1.18E-12	3.30E-12	3.62E-11	5.46E-10	5.70E-09
TH230	1.03E-06	1.01E-05	1.04E-04	6.36E-04	1.59E-04
TH229	2.15E-08	2.02E-06	1.61E-04	3.41E-03	8.50E-03
AC227	6.97E-07	7.58E-07	1.11E-06	7.05E-06	9.89E-06
RA228	1.16E-12	3.30E-12	3.62E-11	5.46E-10	5.70E-09
RA226	3.44E-08	1.84E-06	8.06E-05	6.44E-04	1.59E-04
PO210	2.34E-08	1.84E-06	8.06E-05	6.44E-04	1.59E-04
PB210	2.34E-08	1.84E-06	8.06E-05	6.44E-04	1.59E-04
SU154	2.69E+00	3.17E-17	0.0	0.0	0.0
SM151	1.73E+01	1.33E-02	9.77E-34	0.0	0.0
CS137	3.35E+02	3.13E-07	0.0	0.0	0.0
CS135	8.31E-03	8.31E-03	8.30E-03	8.12E-03	6.60E-03
I129	1.54E-06	1.54E-06	1.54E-06	1.54E-06	1.48E-06
SN126	1.70E-02	1.69E-02	1.58E-02	8.49E-03	1.66E-05
PD107	3.42E-03	3.42E-03	3.42E-03	3.39E-03	3.10E-03
TC99	4.48E-01	4.47E-01	4.34E-01	3.23E-01	1.71E-02
NB934	5.88E-02	5.91E-02	5.89E-02	5.65E-02	3.73E-02
ZR93	5.91E-02	5.91E-02	5.89E-02	5.65E-02	3.73E-02
SR90	2.07E-02	4.75E-08	0.0	0.0	0.0
SE79	1.25E-02	1.23E-02	1.23E-02	4.29E-03	2.92E-07
NI59	1.72E-01	1.71E-01	1.58E-01	7.25E-02	2.98E-05
C14	9.62E-02	8.63E-02	2.90E-02	5.44E-07	2.93E-54

BEST DOCUMENT AVAILABLE

TABLE 4-3. Fission products grouping.

Group I	^{129}I, ^{99}Tc
Group II	^{154}Eu, ^{151}Sm, ^{137}Cs, ^{135}Cs, ^{126}Sn, ^{107}Pd ^{93m}Nb, ^{93}Zr, ^{90}Sr, ^{79}Se, ^{59}Ni, ^{14}C
Group III	^{243}Am, ^{241}Am, ^{240}Pu, ^{238}Pu, ^{238}Pu, ^{237}Np ^{238}U, ^{235}U, ^{234}U, ^{233}U, ^{231}Pa, ^{232}Th ^{230}Th, ^{229}Th, ^{227}Ac, ^{228}Ra, ^{226}Ra, ^{210}Po ^{210}Pb

actinides and their daughter products. The fission product/actinide division separates the β-emitters from the α-emitters. The specific grouping of the nuclides is shown in Table 4-3.

Additional details and rationale for this treatment can be found in Ross et al. [1979].

Throughout this study, we assume that the nuclear waste (whether SF or HLW) is placed in canisters that will completely contain it. The canisters are emplaced in the repository which is eventually decommissioned and abandoned. The regional hydrological mechanisms refill and repressurize the repository, resulting in water contact with the canister which then corrodes and allows the release of waste into the regional groundwater system.

Of particular use for the calculations performed is the time quantity t_0, which is the actual age of the waste at the time of its initial release to the regional groundwater system. This time t_0 is an obvious function of the waste age at emplacement, the repository operational lifetime, refill and repressurization times and the canister corrosion time. For the calculations, we have assumed that the uncertain t_0 is lognormally distributed with a median value of 500 yr and 1st and 99th percentile values of 50 and 5000 yr, respectively.

BEST DOCUMENT AVAILABLE

Once the canister has corroded, we assume that the dissolution of the waste begins and continues at a constant rate until all of the waste has been dissolved. Data on the exact rates of dissolution of the various waste nuclides in spent fuel and HLW are neither extensive nor very precise. Numerous leaching-rate studies have been performed for some HLW elements in various types of glass at 25-75°C. The reported values for the leaching rates range from less than 10^{-9} to 10^{-4} g • cm^{-2} • day^{-1}. Fewer studies have been performed on the more recent SYNROC HLW forms. Reported leaching rates are in the range from less than 10^{-12} to 10^{-5} g • cm^{-2} • day^{-1}.

Figure 4-1 shows the leaching rate ranges reported for various waste glasses.

Figures 4-2 and 4-3 and Table 4-4 show leaching rate results for SYNROC-C and SYNROC-D waste forms.

TABLE 4-4. Leach rates from SYNROC-D[a] (distilled water at 300°C and 1 kbar for 1 day).

Element	g(SYNROC) • cm^{-2} • day^{-1}
Al	5.9×1^{-7}
Ca	9.0×10^{-9}
Ce	ND (not detected)
Fe	3.2×10^{-9}
Mn	7.9×10^{-11}
Na	3.8×10^{-5}
Ni	ND
Si	9.0×10^{-8}
Sr	ND
Ti	1.2×10^{-10}
U	ND
Zr	ND
Cs	8.2×10^{-6}
Gd	ND

[a]These are the first leaching results of SYNROC-D and must be considered as preliminary (Kovar, [1980]).

BEST DOCUMENT AVAILABLE

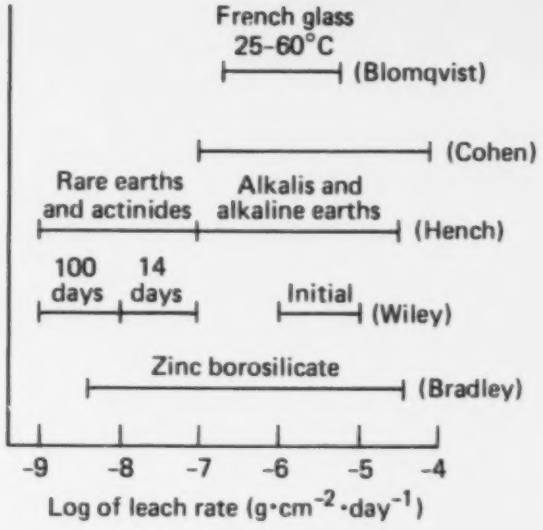

FIG. 4-1. Ranges of measured leach rates for waste glasses.

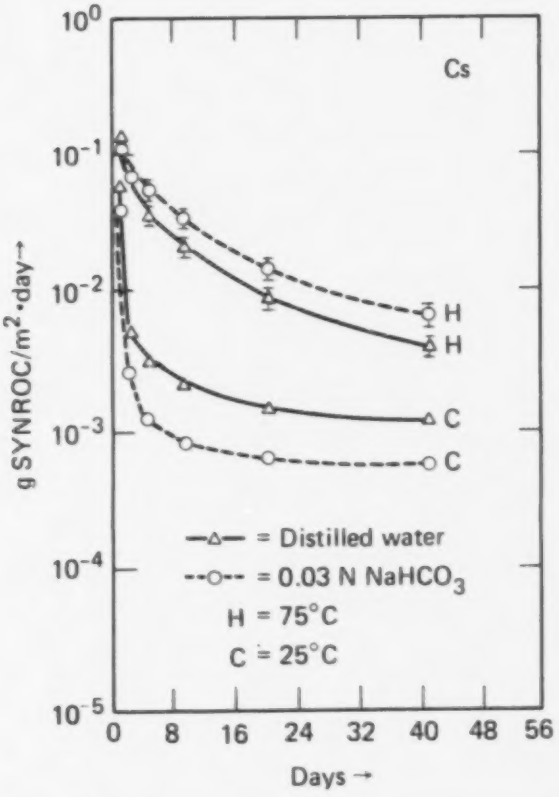

FIG. 4-2. Leaching rates for Cs from SYNROC-C (from Coles and Bazan [1980]).

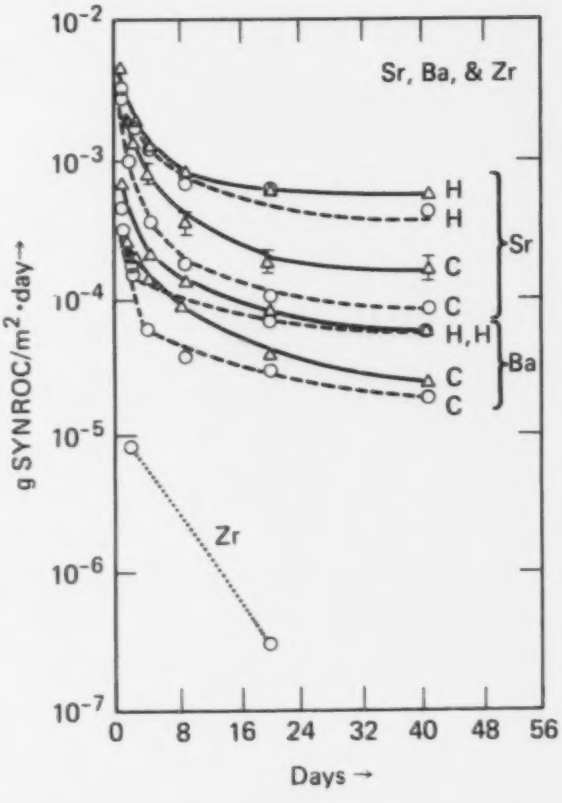

FIG. 4-3. Leaching rates for Sr, Ba, and Zr from SYNROC-C (from Coles and Bazan [1980]).

Leaching rates are clearly dependent on temperature and also on the quality or type of solution dissolving the waste. Some experiments have been performed to assess their dependencies, but comprehensive and conclusive data are not yet available. Also, leach rate data for all the nuclides present in spent fuel or HLW are not available.

4.2 REPOSITORY SITE DATA

The following information has been largely extracted from Walton et al. [1980].

The Columbia River basalt, centered near the semi-arid Pasco Basin, is considered by many to be typical basalt repository host rock. The repository might be located about 1000 m below the surface.

A 1500-m thick sequence of Columbia River basalt apparently overlies a series of older basalts beneath the Pasco Basin. Individual basalt units range in thickness from more than 100 m to a fraction of a meter. The Columbia River basalt covers an area of more than 155,000 km^2 in Washington, Oregon and Idaho. The flow in deep basalt is generally toward the Columbia River. Horizontal hydraulic conductivities in the deeper basalts are low and range from 2.6×10^{-12} to 3.5×10^{-8} m/s. Vertical hydraulic conductivities of dense basalt range from 3.5×10^{-12} to 1.4×10^{-8} m/s. The average porosity of basalt rocks is 2%.

Major layering exists in the basalt geologic column with numerous possible deposit types, of varying hydraulic conductivities and thicknesses, and a wide variety of boundary conditions. Interbedded high-low hydraulic conductivity sequences occur within the major layers as complex intraformational aquifer-aquitard features. Waste-transport routes will be determined by these sequences and gross transmissivities will have limited meaning.

Detailed descriptions of the flow system, including flow velocities with high-low hydraulic conductivity sequences, are not possible with existing data. However, according to theory, waste-transport routes are ultimately towards the Columbia River and the lengths of flow paths from the repository to the biosphere may be relatively short.

Great difficulty is encountered in evaluating basalt-vertical hydraulic conductivity and its variation in space. The list of vertical-hydraulic conductivity values for basalts determined with available measurement techniques is short. Vertical hydraulic conductivity is one of the weakest links in the chain of predictable parameters. Vertical hydraulic gradients are very difficult to identify and quantify, especially in relatively impermeable basalt rocks. Sampling techniques often significantly disturb artesian pressure heads, and reestablishment of static conditions may require excessively long periods of recovery.

4.2.1 Piezometric Data

The piezometric surface in the uppermost basalt rocks (to depths of about 518 m) is trough-shaped in the vicinity of the Hanford Site, about an axis coinciding roughly with the course of the Columbia River (Liverman, [1975]). Recharge to upper basalts occurs where the water table is higher than the piezometric surface and from outside the Hanford Site including regional recharge from irrigation. Discharge is ultimately into the Columbia River with a mean stage elevation of 107 m. Elevations of piezometric head range from 152 to 107 m above MSL within the Hanford Site.

Available water level data for deep wells, DC-1 and DC-6, within the Hanford Site are summarized in Table 4-5. Well DC-6 is near the Columbia River and DC-1 is about 8 km east of the river. No continuous trend associated with the depth of piezometric heads is apparent. Apps et al. [1979] have suggested that there are errors in the DC-1 readings that have been caused by leaky seals. In general, piezometric heads at greater depths than 518 m are above the water table and the mean stage of the Columbia River. Theoretically, the Columbia River is a discharge area and piezometric heads should increase with depth. The piezometric surface in the lowermost basalt rocks should be trough-shaped in the vicinity of the Hanford Site about an axis coinciding roughly with the course of the Columbia River. More must be learned to complete our understanding of the regional system of horizontal and vertical movement in the basalt rock.

BEST DOCUMENT AVAILABLE

TABLE 4-5. Piezometric heads in selected deep basalt wells within the Hanford Site (after Deju and Fecht [1979]; Piper [1975]).

Number	Depth interval (m)	Piezometric head elevation[a] (m) MSL	Water table elevation (m) MSL	River mean stage elevation (m) MSL
DC-1	110-127	123	123	107
	334-363	122		
	600-658	124		
	832-887	125 (Grande Ronde above Umtanum)		
	1024-1096	119 (Grande Ronde above Umtanum)		
	1150-1200	116		
	1244-1305	112		
DC-6	683-692	137 (Grande Ronde)	110	107
	732-741	136		
	748-757	139		
	825-835	129		
	883-895	138		
	922-931	140 (top of Umtanum)		
	1019-1028	135 (below Umtanum)		
	1103-1113	128		
	1113-1122	132		
	1123-1131	131		
	1125-1134	132		

[a]Heads determined by packer tests within the depth intervals noted.

Information concerning the hydrogeological properties of sediments and rocks beneath the Pasco Basin is listed in Table 4-6 (Deju and Summers [1975]; Deju and Ledgerwood [1976]; La Sala and Doty [1970]; Price [1960]; Agapito et al. [1977]; Summers [1978]; Raymond and Tillson [1968]; Gephart et al. [1979]; Rockwell [1978]; Tanaka [1977]; and MacNish and Barker [1973]).

BEST DOCUMENT AVAILABLE

4.2.2 Vertical Permeability

Little work has been done to determine the vertical component of permeability in the Columbia basalts. Vertical permeability is difficult to evaluate *in situ*, since deep wells run parallel to vertical joint systems.

TABLE 4-6. Summary of hydrogeologic properties of sediments and rocks beneath the Pasco Basin (after Deju and Fecht [1979]).

Material	Horizontal hydraulic conductivity (m/s)	Porosity (%)	Remarks
Unconfined aquifer	4.2×10^{-3} - 4.2×10^{2}	Estimated	Mostly dry (above water table)
Glaciofluvial sediments	2.1×10^{-2}	5-20	
Unconfined aquifer	3.5×10^{-6} - $7 \times 1 \times 10^{-4}$	Estimated	--
Upper and middle Ringold sediments	2.1×10^{-4}	12	
Confined aquifer	3.5×10^{-7} - 2.5×10^{-5}	Estimated	Mostly clayey material
Lower Ringold	7.1×10^{-6}	5-20	
Saddle Mountain basalt	1.1×10^{-7} - 3.5×10^{-5}	1.00-3.95	Most of hydraulic conductivity is in interflow zones
Dense basalts	1.1×10^{-7}		
Brecciated basalts	1.1×10^{-7}	(2.00)	
Interflow zones	7.1×10^{-6}		
Wanapum basalt	7.1×10^{-8} - 3.5×10^{-8}		Most of hydraulic conductivity is in interflow zones

BEST DOCUMENT AVAILABLE

TABLE 4-6. (Continued.)

Material	Horizontal hydraulic conductivity (m/s)	Porosity (%)	Remarks
Dense basalt	7.1×10^{-8}		
Brecciated basalts	2.8×10^{-7}	(2.00)	
Interflow zones	3.5×10^{-6}		
Grande Ronde basalt	2.6×10^{-12} - 3.5×10^{-8}		Lowest hydraulic conductivity found
Umtanum	3.5×10^{-12}		
Dense basalt	1.1×10^{-8}		
Brecciated basalts	3.5×10^{-8}		
Interflow zones	1.1×10^{-8}		

Deju and Ledgerwood [1976], using data obtained by La Sala et al. [1972], suggested that the vertical components of permeability were approximately one-tenth the horizontal permeability.

Tanaka et al. [1974] attempted in a modeling study of an area north of Hanford to match hydraulic conductivity to head response to develop a suitable value for vertical conductivity. Tanaka concluded that the vertical component of K should be between 3.5×10^{-12} and 1.3×10^{-10} m/s.

Deju et al. [1977] concluded that hydraulic conductivities in the central volume of a dense, thick basalt are usually about 10^{-11} or 10^{-12} m/s. An understanding of permeability anisotropies is critical to effective modeling of a deep repository. Further work on directional components of permeability needs to be done.

4.2.3 Dispersivity

Values of dispersivities determined from field studies involving well tests and areal models are several orders of magnitude greater than laboratory dispersivities. Where known, field longitudinal dispersivities normally range from 5 to 100 m and field transverse dispersivities normally range from 1 to 35 m (Anderson [1979]). Well test dispersivities are commonly one-half the values of

BEST DOCUMENT AVAILABLE

areal model dispersivities. Table 4-7 summarizes reported values of regional dispersivity for basalts. The degree of certainty in estimating values for this parameter is highly uncertain.

4.2.4 Sorption

Sorption includes the attenuation processes that cause the flowrate of radionuclides through porous media to be much slower than the flowrate of the water itself. Sorption encompasses a set of extremely complicated physiochemical processes which depend on many variables; e.g., bulk density, void fraction, cation exchange capacity, destribution coefficient, etc. The combined effects and interactions of these variables are not well understood and are beyond the scope of this report.

Use of the distribution coefficient in simulating ion exchange has been emphasized. Distribution coefficients are commonly determined in the laboratory where it is difficult, if not impossible, to maintain or simulate the physical and chemical field integrity of a sample. Use of the distribution coefficient approach is limited because it takes into account only relatively fast mass transfer processes. Reported distribution coefficients for selected radionuclides and the Umtanum member of the Columbia

TABLE 4-7. Regional dispersivity for basalts.

Basalt	Longitudinal dispersivity (m)	Reference
Columbia River basalt		
Dense basalt	0.34	Hill and Grimwood [1978]
Vesicular basalt	3.35	
Fractured basalt (Hanford site)	30.4	Anderson [1979]

BEST DOCUMENT AVAILABLE

River basalt in the Pasco Basin are provided in Table 4-8, and for selected radionuclides and the sediments above the Columbia River basalt at the Hanford site in Table 4-9.

For calculations, the distribution coefficients K_d are converted to retardation factors (B) by the following relationship (Duguid [1976]).

$$B = 1 + \frac{\rho}{\theta} K_d \qquad (4\text{-}1)$$

where ρ is the bulk density and θ is the porosity of host rock. The reader should refer to Section 2 for additional details on distribution coefficient and retardation factors.

TABLE 4-8. Laboratory tests simulating distribution coefficients for selected radionuclides and the Umtanum member of the Columbia River basalt in the Pasco Basin.

Radionuclide	Distribution coefficient, K_d (ml/g)	Reference
^{137}Cs	296 + 31	Serne [1978]
^{90}Sr	151 + 18	
^{106}Ru	38.0 + 8.1	
Pu	19.8 + 4.0	
^{241}Am	231 + 18	
^{85}Sr	120.4 + 11.6	Ames [1978]
^{237}Pu	6.5 + 2	
^{226}Ra	731 + 327	
^{60}Co	315 + 45.8	
U	3.09 + 15.8	
^{125}I	6.2 + 2.3	
^{75}Se	11.1 + 0.8	

BEST DOCUMENT AVAILABLE

4.3 Repository Site Data--Salt

A primary reference on salt deposits in the United States is the Summary of Rock Salt Deposits in the United States as Possible Storage Sites for Radioactive Waste Materials, by Pierce and Rich [1962]. This report is a compilation of data on the distribution and geology of salt deposits known at that time. Figure 4-4 (Evenson [1979]) illustrates a typical geohydraulic cross section containing a bedded salt deposit. The illustration shows a typical layer of salt that exists in the geologic column alongside numerous types of deposits with varying hydrologic properties.

As was the case for basalt, the hydraulic conductivity in horizontal and vertical directions can vary significantly in the stratified sedimentary rock. Again, few field tests of entire rock masses have been conducted to evaluate vertical conductivity. Table 4-10 lists horizontal and vertical conductivities calculated from pumping tests in the Uinta and Green River formations, Piceance Basin, Colorado.

TABLE 4-9. Laboratory tests simulating distribution coefficients for selected radionuclides and sediments above Columbia River basalt at the Hanford Site.

Type of test	Radionuclide	Distribution coefficient, K_d (ml/g)	Reference
Laboratory	^{90}Sr	5-38	Deju and Fecht [1979]
	^{137}Cs	12-200	
	Pu	200	
	U	<1	
	^{241}Am	1200	
	^{99}Tc	Very low (<<1)	
	^{89}Ru	26-750	
Laboratory	^{239}Pu	1980	Rhodes [1957]
Field	^{90}Sr	5-25	Deju [1974]

BEST DOCUMENT AVAILABLE

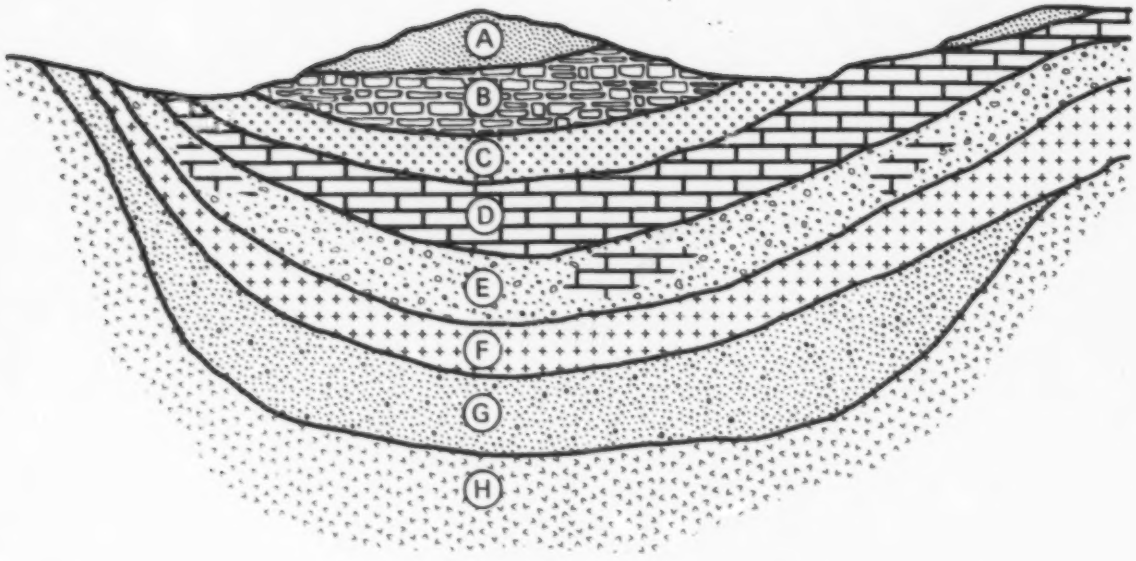

Explanation Symbol	Hydrogeological characteristics		
A	Medium to high permeability deposits – typically sands, gravels, glacial materials.	E	Very low to low to medium permeability – typically combinations of interbedded shales, sandstones and limestones.
B	Low to medium permeability deposits – typically salts, clays and shales.	F	Very low permeability bedded salt deposits.
C	Medium to high permeability deposits – typically sandstones and basalts.	G	Low to medium permeability deposits – typically sandstones.
D	Low to high permeability deposits – typically dolomite and limestone.	H	Very low to low permeability deposits – typically basement rocks, granites.

FIG. 4-4. Typical cross section of hydrogeologic environment.

BEST DOCUMENT AVAILABLE

TABLE 4-10. Variability in horizontal and vertical conductivities (from Golder Associates [1977]).

Rock types	K_H (cm/s)	K_V (cm/s)	K_V/K_{vH}
Shale	2×10^{-6}	1×10^{-6}	0.5
Siltstone-shale	2.1×10^{-4}	2.1×10^{-5}	0.1
Siltstone-shale	2.8×10^{-5}	3.0×10^{-6}	0.107
Sandstone	3.4×10^{-5}	3.4×10^{-5}	1.0

Compilation of porosity and conductivity data for sedimentary rocks commonly associated with salt deposits are found in Table 4-11. This table is taken directly from Isherwood [1979]. The porosity values are for effective porosity rather than total porosity. Effective porosity is a measure of the void space that actively contributes to flow through a porous medium. Fine-grained rocks such as siltstones and shales can have total porosities of 30-50%, with only a very small fraction of the void space contributing to the flow. Table 4-12 shows the values for salt compared to other rocks.

4.3.1 Dispersivity

Summaries of dispersivity values obtained by field methods are included in Tables 4-13 and 4-14. The ratios of these values to typical laboratory dispersivity values are of the order of 10^2 to 10^3. These high ratios indicate that large scale effects dominate the dispersion process in regional groundwater transport and should receive more attention in future studies.

4.3.2 Fission Products with Sorption

The following material has been extracted from Isherwood [1979]. The fission products with sorption characteristics that are present in high-level waste are ^{90}Sr, ^{90}Y, ^{93}Zr, ^{93}Nb, ^{126}Sn, ^{134}Cs and ^{137}Cs. Of these, only strontium and cesium are major contributors to the waste inventory. Yttrium-90, which is in secular equilibrium with ^{90}Sr, has a half-life of only 64 h. In 10-yr-old waste, the inventory of the ^{93}Zr, ^{93}Nb pair is 2×10^{-5} (that of the combined inventory of ^{90}Sr plus ^{137}Cs); the ^{126}Sn inventory is even less.

BEST DOCUMENT AVAILABLE

TABLE 4-11. Conductivity and porosity values for sandstone and conglomerates (Isherwood [1979]).

Description	Conductivity (cm/s)	Effective porosity (%)	Reference
Sandstone, mudstone conglomerate, Triassic basin	10^{-11} to 10^{-9}		Marine [1973]
Sandstone, Spraberry oil field, W. Texas	9.7×10^{-10}	13	Streltsova [1976]
Sandstone, sandy shales, East Carpathians:			
Primary	$<10^{-6}$	8-10	
Secondary	10^{-4}		
Sandstone, Shelbelinsky gas field: secondary	10^{-4} to 10^{-3}	5-27	Wyllie and Spangler [1952]
Bradford sandstone (Devonian)	2.7×10^{-6}	14.8	Wyllie and Spangler [1952]
Berea sandstone (Mississippian)	3.83×10^{-4}	19	Wyllie and Spangler [1952]
Oil Creek sandstone (Ordovician)	4×10^{-6}	6.7	Winsauer et al. [1952]
Woodbine sandstone (Cretaceous)	4.4×10^{-3}	25.6	Winsauer et al. [1952]
Repetto sandstone (Pliocene)	3.6×10^{-5}	19.1	Winsauer et al. [1952]
Wilcox sandstone (Eocene)	3×10^{-7}	15.3	Archie [1950]
Cambrian-Ordovician	1.3×10^{-7}		Maxey [1964]
Catahoula sandstone	4.4×10^{-2} to 3.3×10^{-2}		Lang [1972]

BEST DOCUMENT AVAILABLE

TABLE 4-11. (Continued.)

Description	Conductivity (cm/s)	Effective porosity (%)	Reference
Cretaceous sandstone	1.5×10^{-4} to 4.8×10^{-2}		Davis [1969]
Cretaceous sandstone	1.5×10^{-4} to 4.8×10^{-2}		Davis [1969]
Cromwell sandstone	4.1×10^{-1}	16.6	Muskat [1937]
Gilcrest sandstone	8×10^{-1}	27.4	Muskat [1937]
Prue sandstone	3.4×10^{-3}	11.4	Muskat [1937]
Wilcox sandstone	7.6×10^{-2} to 8.8×10^{-2}		Muskat [1937]
Converse sand	4.1×10^{-3} 1.2×10^{-3} 1×10^{-3}		Welder and Weeks [1965]
Hartsville Formation	3.3×10^{-5}		Welder and Weeks [1965]
Ft. Union sandstone	3.7×10^{-4} 1.2×10^{-4}		Lowry [1966]

Table 4-15 shows the distribution coefficients of strontium and cesium. (This compilation is not meant to be an exhaustive listing of K_d's), but rather a representative selection of those commonly found in the literature. The same is true for the actinide K_d's compiled in Table 4-16. The values in Table 4-15 range from 0.19 in salt to 4,000 in tuff for strontium, and from 0.027 in salt to 17,800 in tuff for cesium.

From the values shown in Table 4-15, a conservative estimate for an average strontium distribution coefficient in relatively dilute groundwater is approximately 10 (which gives a retardation factor of 100). Since distribution coefficients for cesium are often as much as an order of magnitude larger than those for strontium under the same experimental conditions, the average retardation factor for cesium in dilute groundwater should be greater than 100. Retardation factors for both strontium and cesium

BEST DOCUMENT AVAILABLE

in brines would be substantially smaller. These retardation factors are estimates for use in modeling a generic repository and are not site-specific.

Table 4-16 is a compilation of K_d's reported in the literature for americium, neptunium, thorium, plutonium and uranium sorption experiments using geologic materials. The K_d values vary greatly in the pH range of natural waters (5 to 8). For example, the values for americium range between 8 and 5×10^4; for plutonium, between 20 and 3.8×10^5; and for thorium, between 40 and 10^5. The primary reason for this wide range of values is that there are differences in experimental conditions and in the sorption characteristics of the rock sample. A good example of the effect of experimental conditions can be found in the work of Seitz et al. [1978], where K_d's for americium varied between 10 (for a rock tablet) to 8.92×10^3 (for crushed rock).

Based on this range of values, an average K_d for the actinides and their daughter products is conservatively estimated at 200 to 300, which yields a retardation factor of approximately 10^4. Minimum and maximum K_d values of 10 and 10^4 give K_f's of 10^2 and 10^5. These estimated retardation factors are useful only for modeling a generic repository, and are not site-specific.

TABLE 4-12. Range of conductivity and porosity for principal rock types (after Ekren [1974]).

Rock type	Total porosity (%)	Interstitial conductivity (cm/s)
Volcanic	<1	10
Granite	0.05--3	5×10^{-11} to 2×10^{-10}
Metamorphic	0.02--2.4	5×10^{-11} to 2×10^{-6}
Basalt	0.9	2×10^{-9} to 5×10^{-6}
Sandstone	0--51	10^{-7} to 10^{-2}
Shale	0.7--45	4×10^{-11} to 2×10^{-4}
Salt	<1	7×10^{-9} to 4×10^{-6}

BEST DOCUMENT AVAILABLE

TABLE 4-13. Values for longitudinal and transverse dispersity, obtained by fitting model parameters to observed phenomena (Isherwood [1979]).

Setting	a_L (m)	a_T (m)	Reference
Rocky Mt. arsenal alluvial sediments	30.5	30.5	Konikow [1977]
Arkansas River Valley, Colo., alluvial sediments	30.5	9.1	Konikow and Bredehoeft [1974]
Calif.	30.5	9.1	Helweg and Labadie [1977]
Sutter Basin, Calif., alluvial sediments	80-200	8-20	Gupta et al. [1975]
Long Island glacial deposits	21.3	4.3	Pinder [1973]
Brunswick, Ga. limestone	61	20	Bredehoeft and Pinder [1973]
Snake River, Idaho, fractured basalt	91	136.5	Robertson [1974]
Idaho, fractured basalt	91	91	Grove [1977]
Hanford Site, Wash., fractured basalt	30.5	18	Ahlstrom et al. [1977]
Barstow, Calif.,	61	0.18	Robson [1978]
Alsace, France alluvial sediments	15	1	Fried [1975]
Alberta glacial till	3.0-6.1	0.6-1.2	Schwartz [1977]
Florida (SE) limestone	6.7	0.7	Segal and Pinder [1976]
Barstow, Calif., alluvial deposits	61	18	Robson [1974]
Lyons, France, alluvial aquifer	12	4	Fried [1975]
Roswell Basin, N. Mex.	21.3	[a]	Rabinowitz and Gross [1972]
Idaho Falls, Idaho, lava flows and sediments	91	137	Robertson and Barraclough [1973]

[a]Not reported.

BEST DOCUMENT AVAILABLE

TABLE 4-14. Values for longitudinal and transverse dispersivity, obtained from single-well, two-well, and multi-well tracer tests (no entry indicates that no value was reported), (Isherwood [1979]).

Setting	a_L (m)	a_T (m)	Method	Reference
Chalk River Ontario:				Pickens et al. [1977]
alluvial aquifer	0.034		Single-well tracer test	
strata of high velocity	0.1		Single-well tracer test	
strata of high velocity	0.5		Two-well tracer test	
strata of high velocity	0.1		Two-well tracer test	
Lyons, France:				Fried [1975]
alluvial aquifer (stratum)	1-0-0.5		Single-well tracer test	
alluvial aquifer (full aquif)	5		Single-well tracer test	
alluvial aquifer (full aquif)	12.0	3.1-14	Single-well test with resistivity	
alluvial aquifer (full aquif)	8	0.015-1	Single-well test with resistivity	
alluvial aquifer (full aquif)	7	0.009-1	Single-well test with resistivity	
Carlsbad, N. Mex. fractured dolomite	38.1		Two-well tracer test	Grove and Beetem [1971]

BEST DOCUMENT AVAILABLE

TABLE 4-14. (Continued.)

Setting	a_L (m)	a_T (m)	Method	Reference
Savannah River, SC, fractured schistgneiss	134.1		Two-well tracer test	Webster et al. [1970]
Barstow, Calif., alluvial sediments	15.2		Two-well tracer test	Robson [1974]
Dorset, England:				Ivanovich and Smith [1978]
fractured chalk	3.1		Two-well tracer test	
intact chalk	1.0		Two-well tracer test	
Berkeley, Calif., sand/gravel	2-3		Multiwell tracer test	Lau et al. [1957]
Mississippi, limestone	11.6		Single-well tracer test	Fenske [1973]
Nevada Test Site, carbonate aquifer	15		Two-well tracer test	Classen and Cordes [1975]

BEST DOCUMENT AVAILABLE

TABLE 4-15. Distribution coefficients for strontium and cesium (taken in part from Borg et al. [1976], Table 23, and Isherwood [1979]).

K_d (ml/g)			
Sr	Cs	Conditions	Reference
16-135	792-9520	Basalt, 32-80 mesh, prep. groundwater	Angelo et al. [1962]
1.7-3.8	22-314	Quartz sand, pH 7.7	Baetsle and Djonghe [1962]
4-9	8-9	Granodiorite, 100-200 mesh, prep. groundwater	Beetem et al. [1962]
11-23	1020-1810	Granodiorite, 0.5-1 mm, prep. groundwater	
50	300	Hanford sediments	Brown [1967]
45-75	800-1000	Tuff	Dlouhy [1967]
1	1-15	Dolomite, 200 mesh, brine, pH 6.7	Dosch and Lynch [1978]
3-5	7-125	Dolomite, 200 mesh, sim. groundwater, pH 7.9	
1	1-9	Clay, 20-45 mesh, brine, pH 6.8	
3-45	30-120	Clay, 20-45 mesh, sim. groundwater, pH 7.7	
5-22	<1	Polyhalite, 200 mesh, brine, pH 6.8	
<1	14-16	Sandstone, 200 mesh, brine, pH 7.0	
1-5	130-140	Sandstone, 200 mesh, sim. groundwater, pH 7.7	
220	39	Basalt, 0.5-4 mm, 300 ppm TDS	Essington and Nork [1969]
1220	280	Basalt, 0.5-4 mm, 300 ppm TDS	
1.1	6.5	Basalt, 0.5-4 mm, seawater	

BEST DOCUMENT AVAILABLE

TABLE 4-15. (Continued.)

Conditions	K_d (ml/g) Sr	K_d (ml/g) Cs	Reference
Soil, pH 6.8	143-282	617-1053	Godse et al. [1967]
Tuff, 100-200 mesh, prep. groundwater	2070-3480	12,000-17,800	Goldberg et al. [1962]
Soils	19-43	189-420	Hajek and Knoll [1966]
Tuff, chimney rubble, groundwater	400	5000-8000	Borg et al. [1976]
Soils, Ca groundwater	9.4-71	250-1000	Inoue [1967]
Tuff, 0.4 mm, prep. water	260	1020	Nork and Fenske [1970]
Carbonate, 4 mm, prep. water	9.19	13.5	
Granite, 4 mm, groundwater	1.7	34.3	
Shaley siltstone, 4 mm, well water	8.32	39	
Sandstone, 4 mm, well water	1.37	102	
Salt, 4 mm, saturated salt water	0.19	0.027	
Alluvium, 0.5-4 mm groundwater	48-2454	121-3165	Nork et al. [1971]
Sands	13-43	100	Parsons [1962]
Basalt, in site measurements	3	—	Robertson and Barraclough [1973]
Dolomite, 100-325 mesh, dist. water, pH 8.3	5.6-12.4	110-2656	Serne et al. [1977]
Dolomite, 100-325 mesh, brine, pH 6.5-6.9	-0.8-1.0	-0.3-0.3	
Limestone, 100-170 mesh, dist. water, pH 8.3	9.0-13.0	6540-7518	

BEST DOCUMENT AVAILABLE

TABLE 4-15. (Continued.)

Conditions	K_d, ml/g		Reference
	S_r	C_s	
Limestone, 100-170 mesh, brine, pH 6.5-6.9	-0.4-0.9	-0.8-0.2	
Sandstone, 100-170 mesh, dist. water, pH 8.3	22-37.5	12,195-18,567	
Sandstone, 100-325 mesh, dist. water, pH 8.3	12.0-19.2	5248-6855	
Sandstone, 100-170 mesh, brine, pH 6.5-6.9	-0.3-1.1	-0.1-0.5	
Sandstone, 100-325 mesh, brine, pH 6.5-6.9	-0.5-0.7	-0.3-0.8	
Dolomite, 4000 ppm TDS	5-14	—	Stead [1963]
Tuff	4000	--	

BEST DOCUMENT AVAILABLE

TABLE 4-16. Actinide distribution coefficients (Isherwood [1979]).

Conditions	K_d (ml/g)	Reference
	Americium	
Anhydrite, 200 mesh, brine, pH 6.5-7.9	290	Dosch and Lynch [1978]
Anhydrite, 200 mesh, sim. groundwater, pH 6.5-7.9	2200	
Clay, 20-45 mesh, brine, pH 6.5-7.8	310	
Clay, 20-45 mesh, sim. groundwater, pH 7.4-8.4	2300	
Dolomite, 200 mesh, brine, pH 6.5-7.8	2600	
Dolomite, 200 mesh, sim. groundwater, pH 7.5-8.3	22,000	
Limestone, pH 6.7	($K_f = 10^4$)	Fried et al. [1977]
Sand, 5N NO_3, oil, org., pH 3	1	Hajek and Knoll [1966]
Sand, 5N NO_3, oil, org., pH 7	200	
Sand, sludge, pH 7	500	
Desert sand, 0.001 M Ca, pH 2.5-3.1	>1200	Routson et al. [1975]
Desert sand, 0.02 M Ca, pH 2.5-3.1	>1200	
Sandy clay, 0.002 M Ca, pH 2.5-3.1	67	
Sandy clay, 0.2 M Ca, pH 2.5-3.1	1	
Sandy clay, 3 M Na, pH 2.5-3.1	1.6	
Sandy clay, 0.015 M Na, pH 2.5-3.1	280	
Basalt, pre-equilibrated water, pH 7		Seitz et al. [1978]
Eh = 293 mV:		
16-20 mesh	70-98	
30-40 mesh	97-148	
50-70 mesh	115-280	
60-100 mesh	101	
Rock tablet	135-280	
Dolomite, pre-equilibrated water, pH 8.5, Eh = 274 mV:		
60-100 mesh	3470-8920	
100-325 mesh	653	
Rock tablet	10-150	
	Americium	
Granite, pre-equilibrated water, pH 8.5, Eh = 261 mV:		Seitz et al. [1978]
60-100 mesh	21	
Rock tablet	5-18	

BEST DOCUMENT AVAILABLE

TABLE 4-16. (Continued.)

Conditions	K_d (ml/g)	Reference
Limestone, pre-equilibrated water, pH 7.6, Eh = 277 mV:		
60-100 mesh	2230	
Rock tablet	135-280	
Sandstone, rock tablet, pre-equilibrated water, pH 6.8	8-11	
Tuff, rock tablet, pre-equilibrated water, pH 7.9, Eh = 282 mV	23-370	
Illite/kaolinite, 90% sat. NaCl, pH 7-8	50,000	Van Dalen et al. [1975]
River sand, 90% sat. NaCl, pH 7-8	400	
	Neptunium	
Clay soil, 5 m M Ca $(NO_3)_2$, pH 6.5	320	Dahlman et al. [1976]
Sand, 0.002 M Ca, pH 2.5-3.1	2.37	Routson et al. [1975]
Sand, 0.2 M Ca, pH 2.5-3.1	0.36	
Sand, 0.15 M Na, pH 2.5-3.1	3.9	
Sand, 3.0 M Na, pH 2.5-3.1	3.2	
Sandy clay, 0.002 M Na, pH 2.5-3.1	0.25	
Sandy clay, 0.2 M Na, pH 2.5-3.1	0.16	
Sandy clay, 0.015 M Na, pH 2.5-3.1	0.7	
Sandy clay, 3.0 M Na, pH 2.5-3.1	0.4	
Granite, 60-100 mesh, pre-equilibrated water	21	Seitz et al. [1978]
	Neptunium	
Dolomite, 60-100 mesh, pre-equilibrated water	395	Seitz et al. [1978]
Argillite, 60-100 mesh, pre-equilibrated water	27	
Apatite, 60-100 mesh, pre-equilibrated water	1280	
Limestone, 60-100 mesh, pre-equilibrated water, pH 7.6, Eh = 277 mV	7540	
Tuff, 60-100 mesh, pre- equilibrated water, pH 7.9, Eh = 282 mV	8	

BEST DOCUMENT AVAILABLE

TABLE 4-16. (Continued.)

Conditions	K_d (ml/g)	Reference
Dolomite, 100-325 mesh, brine, pH 7.0	22	Serne et al. [1977]
Limestone, 100-170 mesh, brine, pH 6.9		
	Plutonium	
Clay soil, Pu(IV), 5 m M Ca, pH 6.5	300,000	Dahlman et al. [1976]
Anhydrite, 200 mesh, brine, pH7.9	6700-7700	Dosch and Lynch [1978]
Clay, 20-45 mesh, brine, pH 6.8-7.9	40,000-72,000	
Clay, 20-45 mesh, sim. groundwater, pH 8.0	180,000	
Dolomite, 200 mesh, sim. groundwater, pH 7.9	2400-7300	
Dolomite, 200 mesh, brine, pH 7.2	2100-5400	
Mediterranean sediment	10,000-90,000	Dursuma and Parsi [1974]
Tuff, Pu(IV), pH 6.7	($K_f = 10^4$)	Fried and Friedman [1976]
Tuff, Pu(VI), pH 6.7	($K_f = 300$)	
	Plutonium	
Limestone, Pu(IV), pH 6.7	($K_f = 3 \times 10^4$)	Fried et al. [1977]
Basalt "fissure," Pu(IV), pH 6.7	($K_f = 2 \times 10^4$)	
Soil clays, Pu(IV), 5 m M Ca, pH 6.5	100,000-170,000	Gast et al. [1977]
Soil clays, Pu(VI), 5 m M Ca, pH 6.5	75,000	
Montmorillonite, Pu(IV), 5 m M Ca, pH 6.5	21,000	
Montmorillonite, Pu(IV), 5 m M Ca, pH 6.5	250	
17 soil samples, 10^{-6}, 10^{-7}, 10^{-8} M Pu	35-14,000	Glover et al. [1976]
Surface soil, groundwater	($K_f = 10^4$)	Hajek and Knoll [1966]
5% clay, 50% silt, 45% sand	20,000-48,000	Hetherton et al. [1975]
Soils	>430	Miner et al. [1975]

BEST DOCUMENT AVAILABLE

TABLE 4-16. (Continued.)

Conditions	K_d (ml/g)	Reference
Calcareous sediment	16,000-380,000	Mo and Lowman [1975]
Av value for Enewitak groundwater particulates	250,000	Noshkin et al. [1976]
Av value for suspended silt	90,000	Pillai and Mathew [1976]
Anhydrite, pre-equilibrated water, pH 7.6, Eh = 275 mV:		Seitz et al. [1978]
167-20 mesh	678-819	
30-40 mesh	946-1040	
50-70 mesh	1550-2840	
	Plutonium	
Basalt, pre-equilibrated water, pH 7.0, Eh = 293 mV:		Seitz et al. [1978]
16-20 mesh	62-27	
30-40 mesh	54-86	
50-70 mesh	49-53	
Rock tablet	99	
Dolomite, rock tablet, pre-equilibrated water, pH 8.5, Eh = 273 mV	13-34	
Granite, pre-equilibrated water, pH 8.5, Eh = 261 mV;		
60-100 mesh	2050	
Rock tablet	40	
Limestone, pre-equilibrated water, pH 7.6, Eh = 277 mV:		
60-100 mesh	293	
Rock tablet	16-710	
Sandstone, rock tablet, pre-equilibrated water, pH 6.8	20-64	
Lake Michigan particulates	300,000	Wahlgren et al. [1976]
Silt loam, Ca sat. clay, pH 6.5	160,000	Bondietti et al. [1976]
Montmorillonite, Ca sat., clay pH 6.5	400,000	
Clay soil, 5 m M Ca $(NO_3)_2$, pH 6.5	160,000	Dahlman et al. [1976]

BEST DOCUMENT AVAILABLE

TABLE 4-16. (Continued.)

Conditions	K_d (ml/g)	Reference
Med. sand, pH 8.15	40-130	Nishiwaki et al. [1976]
Very find sand, pH 8.15	310-470	
Silt/clay, pH 8.15	2,700-10,000	
	Plutonium	
Schist soil, 1 g/liter Th, pH 3.2	8	Rancon [1973]
Schist soil, 0.1 g/liter Th, pH 3.2	60	
Illite, 1 g/liter Th, ph 3.2	120	
Illite, 0.1 g/liter Th, pH 3.2	1000	
Illite, 0.1 g/liter Th, pH 6	>100,000	
	Uranium	
Silt loam, U(VI), Ca sat., pH 6.5	62,000	Bondetti et al. [1976]
Clay soil, U(VI), 5 m M Ca $(NO_3)_2$, pH 6.5	4400	Dahlman et al. [1976]
Clay soil, 1 ppm UO^{+2}, pH 5.5	300	Rancon [1973]
Clay soil, 1 ppm UO^{+2}, pH 10	2000	
Clay soil, 1 ppm UO^{+2}, pH 12	270	
Dolomite, 100-325 mesh, brine, pH 6.9	4.5	Serne et al. [1977]
Limestone, 100-170 mesh, brine, pH 6.9	2.9	

BEST DOCUMENT AVAILABLE

REFERENCES

Agapito, J. F. T., M. P. Hardy, and D. R. St. Laurent, 1977, Geo-Engineering Review and Proposed Program Outline for the Structural Design of a Radioactive Waste Repository in Columbia Plateau Basalts, Rockwell Hanford Operations, Richland, WA, RJO-ST-6.

Ahlstrom, S. W., H. P. Foote, R. C. G. Arnett, C. R. Cole, and R. J. Serne, 1977, Multicomponent Mass Transport Model: Theory and Numerical Implementation (Discrete-Parcel-Random-Walk Version), Battelle Pacific Northwest Laboratories, Richland, WA, BNWL-2127.

Alexander, C. W., C. W. Kee, A. G. Croff, and J. O. Blomeke, 1977, Projections for Spent Fuel to be Discharged by the U.S. Nuclear Power Industry, Oak Ridge National Laboratory, Oak Ridge, TN, ORNL/TM-6008.

Ames, L. L., 1978, "Radionuclide Bath K_d Values on Basalt, Heulandite and Nontronite," in Basalt Waste Isolation Program Annual Report--Fiscal Year 1978, Rockwell Hanford Operations, Richland, WA, RHO-BWI-78-100.

Anderson, M. P., 1979, "Using Models to Simulate the Movement of Contaminants through Groundwater Flow Systems," critical reviews in Environ. Control 9(2).

Angelo, C., M. Goldberg, V. Janzer, and W. Beetem, 1962, Geology of the U18a Site, Buckboard Mesa, NTS, Part IV: Summary of K_ds for Fission Products between Groundwater and Basaltic Rocks, U.S. Geological Survey, Report WT-1828, pp. 66-81.

Apps, J., T. Doe, B. Doty, S. Doty, R. Galbraith, A. Kearns, B. Kohrt, J. Long, A. Monroe, T. N. Narasimhan, P. Nelson, C. R. Wilson, and P. A. Witherspoon, 1979, Geohydrological Studies for Nuclear Waste Isolation at the Hanford Reservation, Volume II: Final Report, Lawrence Berkeley Laboratory, Berkeley, CA, LBL-8764.

Archie, G. E., 1950, "Introduction to Petrophysics of Reservoir Rocks," Bull. Am. Assoc. Petrol. Geol. 34, 943.

Baetsle, L., and P. Djonghe, 1962, "Investigations on the Movement of Radioactive Substances in the Ground, Part III: Practical Aspects of the Program and Physicochemical Considerations," in Proc. 2nd Conference on Ground Disposal of Radio-active Wastes, Chalk River, Canada, J. Morgan, D. Jamison and J. Stevenson, Eds., U.S. Atomic Energy Commission, Washington, D.C., TID-7628, pp. 198-210.

Beetem, W., V. J. Janzer, C. G. Angelo, and M. Goldberg, 1962, Summary of Distribution Coefficients for Fission Products between Groundwater and Granite Rocks. Climax Stock, U.S. Geological Survey, Nevada Test Site, Technical Letter NTS-13.

Blomqvist, G., 1978, "Leaching of Active French Glasses at Studsvik: Progress Report 1978-06-01," Kaernbraenslesaekerhet, Stockholm, Sweden, Report KBS-TR-99.

BEST DOCUMENT AVAILABLE

Bondietti, E., S. Reynolds, and M. Shanks, 1976, "Interactions of Plutonium with Complexing Substances in Solid and Natural Waters," in Proc. Symposium on Transuranium Nuclides in the Environment, San Francisco, Nov. 17-21, 1976, International Atomic Energy Agency, Vienna.

Borg, I., R. Stone, H. Levy, and L. Ramspott, 1976, Information Pertinent to the Migration of Radionuclides in Groundwater at the Nevada Test Site: Part 1: Review and Analysis of Existing Information, Lawrence Livermore National Laboratory, Livermore, CA, UCRL-52078, Part 1.

Bradley, D. J., 1978, Leaching of Fully Radioactive High Level Waste Glass, Battelle Pacific Northwest Laboratories, Richland, WA, Report PNL-2664.

Bredehoeft, J. D., and G. F. Pinder, 1973, "Mass Transport in Flowing Groundwater," Water Resources Res. 9(1), 194.

Brown, D., 1967, "Migration Characteristics of Radionuclides through Sediments Underlying the Hanford Reservation," in Proc. Symposium on Disposal of Radioactive Wastes into the Ground, Vienna, May 29-June 2, 1967, International Atomic Energy Agency, Vienna.

Burkholder, H. C., 1976, Methods and Data for Predicting Nuclide Migration in Geologic Media, International Symposium on Management of Wastes from the LWR Fuel Cycle, Denver, CO, Battelle Pacific Northwest Laboratories, Richland, WA, BNWL-SA-5523.

Burkholder, H. C., M. O. Cloninger, and D. A. Baker, 1976, "Incentives for Partitioning High-Level Wastes," Nucl. Technol. 31, pp. 202-217.

Classen, H. C., and E. H. Cordes, 1975, "Two-Well Recirculating Tracer Test in Fractured Carbonate Rock, Nevada," Hydrol. Sci. Bull. 20, 3.

Cohen, J. J., 1977, Determination of Performance Criteria for High-Level Solidified Nuclear Waste, University of California, Lawrence Livermore National Laboratory, Livermore, CA, Report NUREG-0279.

Coles, D. G., and F. Bazan, 1980, Continuous-Flow Leaching Studies of Crushed and Cored SYNROC, Lawrence Livermore National Laboratory, Livermore, CA, UCRL-84679.

Dahlman, R., E. Bondietti, and L. Eyman, 1976, "Biological Pathways and Chemical Behavior of Plutonium and Other Actinides in the Environment," in Proc. Symposium on Transuranium Nuclides in the Environment, San Francisco, Nov. 17-21, 1976, International Atomic Energy Agency, Vienna.

Davis, S. N., 1969, "Porosity, Permeability of Natural Materials," in Flow Through Porous Media, R. J. M. DeWiest, Ed. (Academic Press, New York), pp. 54-88.

Deju, R. A., and K. R. Fecht, 1979, Preliminary Description of Hydrologic Characteristics and Contaminant Transport Potential of Rocks in the Pasco Basin South-Central Washington, Rockwell International, Rockwell Hanford Operations, Richland, WA, RHO-BWI-LD-20.

BEST DOCUMENT AVAILABLE

Deju, R. A., and R. K. Ledgerwood, 1976, Hydrogeology of the Uppermost Confined Aquifers Underlying the Hanford Reservation, Atlantic Richfield Hanford Company, Richland, WA, ARH-SA-253.

Deju, R. A., and W. K. Summers, 1975, Transmissivity and Hydraulic Conductivity of Saturated Sedimentary Rocks in the Hanford Reservation, Atlantic Richfield Hanford Company, Richland, WA, ARH-C-00007.

Deju, R. A., 1974, A Comprehensive Review of Mathematical Models Construction to Describe the Hydrology of the Hanford Reservation, Atlantic Richfield Hanford Company, Richland, WA, ARH-C-00003.

Deju, R. A., 1974, The Hanford Field Testing Program, Atlantic Richfield Hanford Company, Richland, WA, ARH-C-0004.

Deju, R. A., P. A. Eddy, M. W. Grutzeck, and C. W. Myers, 1977, Environmental Factors Needed to Establish the Geotechnical Feasibility of Storing Radioactive Waste in Columbia River Basalts, Rockwell International, Hanford, WA, RHO-ST-8.

Dlouhy, Z., 1967, "Movement of Radionuclides in the Aereated Zone," in Proc. Symposium on Disposal of Radioactive Wastes into the Ground, Vienna, May 29-June 2, 1967, International Atomic Energy Agency, Vienna, pp. 241-249.

Dosch, R., and A. Lynch, 1978, Interaction of Radionuclides with Geomedia Associated with the Waste Isolation Pilot Plant (WIPP) Site in New Mexico, Sandia National Laboratories, Albuquerque, NM, SAND 78-0297.

Duguid, J., and H. Reeves, 1976, Material Transport through Porous Media: A Finite-Element Galerkin Model, Oak Ridge National Laboratory, Oak Ridge, TN, ORNL 4928.

Dursuma, E., and P. Parsi, 1974, "Distribution Coefficients of Plutonium between Sediment and Seawater," in Activities of the International Laboratory of Marine Radioactivity, International Atomic Energy Agency, Vienna, Report 163, pp. 94-96.

Ekren, E. R., 1974, Geologic and Hydrologic Considerations for Various Contents of High-Level Radioactive Waste Disposal in Conterminous U.S., U.S. Geological Survey, Open Field Report 74-158.

Essington, E., and W. Nork, 1969, Radionuclide Contamination Evaluation-Milrow Event, Teledyne Isotopes, Nevada Operations Office, Las Vegas, NV, NVO-1229-117.

Evenson, D. E., T. A. Pickett, and P. A. Showalter, 1979, Processes and Parameters Involved in Modeling Radionuclide Transport from Bedded Salt Repositories, Camp, Dresser & McKee, Boston, Mass., Report to Lawrence Livermore National Laboratory, Livermore, CA (UCRL-15095).

Fenske, P. R., 1973, Hydrology and Radionuclide Transport Monitoring Well HT-2m, Tatum Dome, Mississippi, Desert Research Institute, University of Nevada, Project Report No. 25, NVO-1253.

BEST DOCUMENT AVAILABLE

Fried, J. J., 1975, Groundwater Pollution (Elsevier Scientific, Amsterdam).

Fried, S., A. Friedman, R. Atcher, and J. Hines, 1977, "Retention of Plutonium and Americium by Rock," Science 196, 1087.

Fried, S., and A. Friedman, 1976, "The Retention of Plutonium (VIO) on Los Alamos Tuff," in Proc. Symposium on Waste Management, Tucson, Oct. 3-6, 1976.

Gast, R., E. Landa, and L. Thornigm, 1977, The Behavior of Technetium-99 in Soils and Plants, Progress Report COO-2447-5 (April 1-March 31, 1977), prepared by Minnesota University, St. Paul, Department of Soil Sciences, p. 76.

Gephart, R. E., R. A. Deju and P. A. Eddy, 1979, Geophysical Logging and Hydrologic Testing of Deep Basalt Flows in the Rattlesnake Hills, Well Number One, Rockwell Hanford Operations and Battelle Pacific Northwest Laboratories, Richland, WA, RHO-BEW-ST-1.

Glover, P., F. Miner, and W. Polzer, 1976, Plutonium and Americium Behavior in the Soil/Water Environment I. Sorption of Plutonium and Americium by Soils, Battelle Pacific Northwest Laboratories, Hanford, WA, BNWL-211, pp. 224-0254.

Godse, V., A. Mohan, M. Singh, R. Amlray, and K. Thomas, 1967, "Characterization of Trombcy Soils for Disposal of Radioactive Wastes," in Proc. Symposium on Disposal of Radioactive Wastes into the Ground, Vienna, 1967, International Atomic Energy Agency, Vienna.

Goldberg, M., V. J. Janzer, C. G. Angelo, and W. Beetem, 1962, The Effects of Sodium Ion Concentration on Distribution Coefficients for Tuffs from NTS, U.S. Geological Survey, Nevada Test Site, Technical Letter NTS-16.

Golder Associates, 1977, Development of Site Suitability Criteria for a High Level Waste Repository, published as Lawrence Livermore National Laboratory, Livermore, CA, report UCRL-13793.

Grove, D. B., 1977, The Use of Galerkin Finite-Element Methods to Solve Mass Transport Equations, U.S. Geological Survey, Denver, Colo., Water Resources Division, Water Res. Inv. 77-49, p. 61.

Grove, D. B., and W. A. Beetem, 1971, "Porosity and Dispersion Constant Calculations for a Fractured Carbonate Aquifer Using the Two-Well Tracer Method," Water Resources Res. 7(1), 128.

Gupta, S. K., K. K. Tanji and J. N. Luthin, 1975, A Three-Dimensional Finite Element Groundwater Model, California Water Res. Center, Univ. of California, Davis, Contribution 152.

Hajek, B., and K. Knoll, 1966, Disposal Characteristics of Plutonium and Americium in a High Salt Waste, Battelle Pacific Northwest Laboratories, Hanford, WA, BNWL-CCG-649.

Helweg, O. J., and J. W. Labadie, 1977, "Linked Models for Managing River Basin Salt Balance, Water Resources Res. 13, 329.

Hench, L. L., D. E. Clark, and E. L. Yen-Bower, 1978, "Surface Leaching of Glasses and Glass Ceramics," Proc. Conf. on High Level Solid Waste Forms, Denver, CO, Dec. 19-21, 1978.

Hetherington, J., L. D. Jefferies, N. Mitchell, R. Pentreath, and D. Woodhead, 1975, Environmental and Public Health Consequences of the Controlled Disposal of Transuranic Elements to the Marine Environment, International Atomic Energy Agency, Vienna, SM-199/11.

Hill, M. D., and P. D. Grimwood, 1978, Preliminary Assessment of the Radiological Protection Aspects of Disposal of High Level Waste in Geological Formations, National Radiological Protection Board Report, United Kingdom, R69.

Howard, R. A., 1966, "Information Value Theory," IEEE Transactions on Systems Science and Cybernetics, Vol. SSC-2, No. 1.

Howard, R. A., 1967, "Value of Information Lotteries," IEEE Transactions on Systems Science and Cybernetics, Vol. SSC-3, No. 1.

Inoue, Y., 1967, "Prediction of Radionuclide Migration in Groundwater at the Japan Atomic Energy Research Institute," in Proc. Symposium on Disposal of Radioactive Wastes into the Ground, Vienna, May 29-June 2, 1967 (International Atomic Energy Agency, Vienna).

Isherwood, D., 1979, Geosciences Data Base Handbook for Modeling a Nuclear Repository, Lawrence Livermore National Laboratory, Livermore, CA, UCRL-52719, Vol. 1.

Ivanovich, M., and D. B. Smith, 1978, "Determination of Aquifer Parameters by a Two-Well Pulsed Method Using Radioactive Tracers," J. Hydrol. 36, 35.

Kaufman, A. M., 1978, Waste Pipe Calculus, Lawrence Livermore National Laboratory, Livermore, CA, UCID-17953.

Konikow, L. F., 1977, Modeling Chloride Movement in the Alluvial Aquifer at the Rocky Mountain Arsenal, Colorado, U.S. Geological Survey, Denver, Colo., Water Supply Paper 2044.

Konikow, L. F., and J. D. Bredehoeft, 1974, "Modeling Flow and Chemical Quality Changes in an Irrigated Stream-Aquifer System," Water Resources Res. 10, 546.

Kovar, F. R., 1980, Lawrence Livermore National Laboratory Internal Technical Memo, "Dissolution Rates of Various Waste Forms" WFA 8D-12-D.

Lang, J. W., 1972, Geohydrologic Summary of the Pearl River Basin, Mississippi and Louisiana, U.S. Geological Survey, Water Supply Paper 1899-M.

La Sala, A. M., Jr., and G. C. Doty, 1970, Preliminary Evaluation of Hydrologic Factors Related to Radioactive Waste Storage in Basaltic Rocks at the Hanford Reservation, Washington Open File Report, U.S. Geologic Survey in cooperation with the U.S. Atomic Energy Commission, Washington, D.C.

BEST DOCUMENT AVAILABLE

Lau, L. K., W. J. Kaufman, and D. K. Todd, 1957, Dispersion Phenomena in Flow through Porous Media, Sanitary Engineering Research Laboratory, University of California, Berkeley, CA, Progress Report 3.

Liverman, J. L., 1975, Final Environmental Statement--Waste Management Operations--Hanford Reservation, Richland, WA, U.S. Energy Research and Development Administration, Washington, D.C., ERD-1538.

Lowry, M. E., 1966, Groundwater Resources of Sheridan County, Wyoming, U.S. Geological Survey, Water Supply Paper 1807.

MacNish, R. D., and R. S. Barker, 1973, Digital Simulation of a Basalt Aquifer System, Walla Walla River Basin, Washington and Oregon, Washington State Department of Ecology, Olympia, WA.

Marine, I. W., 1973, "Geohydrology of Buried Triassic Basin at Savannah River Basin at Savannah River Plant, South Carolina," in 2nd International Symposium on Underground Waste Management and Artificial Recharge, New Orleans, LA, Am. Assoc. Petrol. Geol., Tulsa, OK, Vol. 1, pp. 481-504.

Maxey, G. B., 1964, "Hydrostratigraphic Units," J. Hydrol. 2, 124.

Miner, F., P. Glover, and W. Polzer, 1974, "Plutonium Behavior in the Soils," Agron. Abst., p. 35.

Mo, T., and F. Lowman, 1975, Laboratory Experiments on the Transfer Dynamics of Plutonium from Marine Sediments to Seawater and to Marine Organisms, CONF-750503-5, p. 35.

Muskat, M., 1937, Flow of Homogeneous Fluids through Porous Media (McGraw-Hill, NY).

Nishiwaki, Y., Y. Honda, Y. Kimura, H. Morishima, T. Koga, Y. Miyaguchi, and H. Kawai, 1972, "Behavior and Distribution of Radioactive Substances in Coastal and Estuarine Environments," in Radioactive Contamination of the Marine Environment, International Atomic Energy Agency, Vienna, SN-158/11, pp. 177-193.

Nork, W., and P. Fenske, 1970, Radioactivity in Water--Project Rulison, NVO-1229-131.

Nork, W., E. Forslow, and E. Essington, 1971, Radioactivity in Water, Central Nevada Test Area, NVO-1229-175.

Noshkin, V., K. Wong, K. Marsh, R. Eagle, G. Halladay, and R. Buddemeier, 1976, "Plutonium Radionuclides in the Groundwaters at Eniwetak Atoll," in Proc. Symposium on Transuranium Nuclides in the Environment, San Francisco, Nov. 17-21, 1976, International Atomic Energy Agency, Vienna, pp. 517-543.

Parsons, P., 1962, "Underground Movement of Radioactive Wastes at Chalk River," in Proc. 2nd Conference on Groundwater Disposal of Radioactive Wastes, Chalk River, Canada, J. Morgan, D. Jamison and J. Stevenson, Eds., Atomic Energy Commission, Washington, D.C., TID-7628.

BEST DOCUMENT AVAILABLE

Pickens, J. F., W. F. Merritt, and J. A. Cherry, 1977, "Field Determination of the Physical Contaminant Transport Parameters in a Sandy Aquifer," in Proceedings of the IAEA Advisory Ground Meeting on the Use of Nuclear Techniques in Water Pollution Studies, Poland, International Atomic Energy Agency, Vienna.

Pierce, W. G., and E. I. Rich, 1962, Summary of Rock Salt Deposits in the United States as Possible Storage Sites for Radioactive Waste Materials, U.S. Geological Survey, Bulletin 1148.

Pillai, K., and E. Mathew, 1976, "Plutonium in the Aquatic Environment: Its Behavior, Distribution and Significance," in Proc. Symposium on Transuranium Nuclides in the Environment, San Francisco, Nov. 17-21, 1976, International Atomic Energy Agency, Vienna, pp. 24-45.

Pinder, G. F., 1973, "A Galerkin Finite-Element Simulation of Groundwater Contamination of Long Island, New York," Water Resources Res. 9, 6.

Price, C. W., 1960, Artificial Recharge of Well Tapping Basalt Aquifers, Walla Walla Area, Washington, Washington State Department of Ecology, Olympia, WA, Water-Supply Bulletin 7.

Rabinowitz, D. D., and G. W. Gross, 1972, Environmental Tritium as a Hydrometeorologic Tool in the Roswell Basin, New Mexico, New Mexico Water Resources Research Institute, Las Cruces, NM, Project No. OWRR A-0037-NMEX.

Rancon, D., 1973, "The Behavior in Underground Environments of Uranium and Thorium Discharged by the Nuclear Industry," in Environmental Behavior of Radionuclides Released in the Nuclear Industry, International Atomic Energy Agency, Vienna, SM-172/55, pp. 333-346 (in French).

Raymond, J. R., and D. D. Tillson, 1968, Evaluation of a Thick Basalt Sequence in South-Central Washington, Battelle Pacific Northwest Laboratories, Richland, WA, BNWL-776.

Rhodes, D. W., 1957, "The Effects of pH on the Uptake of Radioactive Isotopes from Solution by a Soil," in Soil Science Society of America Proceedings, Vol. 21.

Robertson, J. B., 1974, Digital Modeling of Radioactive and Chemical Waste Transport in the Snake River Plain Aquifer at the National Reactor Testing Station, Idaho, U.S. Geological Survey, Idaho Falls, Idaho, Water Resources Division, Open File Report IDO-22054.

Robertson, J. B., and J. T. Barraclough, 1973, "Radioactive and Chemical Waste Transport in Groundwater at National Reactor Testing Station, Idaho: 20-Year Case History and Digital Model," in Int. Symp. on Underground Waste Management and Artificial Recharge, J. Braunstein, Ed., American Association of Petroleum Geologists, Tulsa, Okla., pp. 291-322.

Robson, S. G., 1974, Feasibility of Digital Water Quality Modeling Illustrated by Application at Barstow, California, U.S. Geological Survey, Menlo Park, CA, Water Res. Inv. Report 46-73.

BEST DOCUMENT AVAILABLE

Robson, S. G., 1978, Application of Digital Profile Modeling Techniques to Groundwater Solute Transport at Barstow, California, U.S. Geological Survey, Water Suply Paper 2050.

Rockwell, International, 1978, Basalt Waste Isolation Program Annual Report--Fiscal Year 1978, Rockwell Hanford Operations, Richland, WA, RHO-BWI-78-100.

Ross, B., et al., 1979, NUTRAN: A Computer Model of Long-Term Hazards from Waste Repositories, The Analytic Sciences Corporation Report TR-1797-7.

Rouston, R., G. Jansen, and A. Robinson, 1975, Sorption of ^{99}Tc, and ^{237}Np and Am on Two Subsoils from Differing Weathering Intensity Areas, Battelle Pacific Northwest Laboratories, Richland, WA, BNL-1889, p. 15.

Schwartz, F. W., 1977, "Macroscopic Dispersion in Porous Media: The Controlling Factors," Water Resources Res. 13(4), 743.

Segal, G., and G. F. Pinder, 1976, "Transient Simulation of Salt Water Intrusion in Southeastern Florida," Water Resources Res. 12, 65.

Seitz, M. G., P. G. Rickert, S. M. Fried, A. M. Friedman and M. J. Steindler, 1978, Studies of Nuclear Waste Migration in Geologic Media, Argonne National Laboratory, Argonne, IL, Annual Report (November 1976-October 1977), ANL-78-8.

Serne, R. J., D. Rai, M. J. Mason, and M. A. Molecke, 1977, Batch K_d Measurements of Nuclides to Estimate Migration Potential at the Proposed Waste Isolation Pilot Plant in New Mexico, Battelle Pacific Northwest Laboratories, Richland, WA, PNL-2448.

Stead, F., 1963, "Tritium Distribution in Groundwater Around Large Underground Fusion Explosions," Science 142, 1163.

Streltsova, T. D., 1976, "Hydrodynamics of Groundwater Flow in a Fractured Formation," Water Resources Res. 12(3), 405.

Summers, W. D. and Associates, 1978, A Survey of the Groundwater Geology and Hydrology of the Pasco Basin, Washington, Rockwell Hanford Operations, Richland, WA, RHO-BWI-C-41.

Tanaka, H. H., 1977, Aquifer Test of Well 18/25/I5E in Grant County, Washington, Washington State Department of Ecology, Olympia, WA.

Tanaka, H. H., A. J. Hansen, and J. A. Skrivan, 1974, Digital Model of Groundwater Hydrology, Columbia Basin Irrigation Project Area, Washington, Washington State Department of Ecology, Olympia, WA, Water Supply Bulletin 40.

Van Dalen, A., F. deWitte, and J. Wiskstra, 1975, "Distribution Coefficients for Some Radionuclides Between Saline Water and Clays, Sandstones and Other Samples from the Dutch Subsoil," Reactor Centrum Nederland, pp. 75-109.

Wahlgren, J., J. Alberts, D. Nelson, and K. Orlandi, 1976, "Study of the Behavior of Transuranics and Possible Chemical Homologues in Lake Michigan Water and Bota," in Proc. Symposium on Transuranium Nuclides in the Environment, San Francisco, Nov. 17-21, 1975, International Atomic Energy Agency, Vienna, pp. 9-23.

BEST DOCUMENT AVAILABLE

Walton, W. C., M. L. Voorhees, and T. A. Prickett, 1980, "Conceptual Model for Regional Radionuclide Transport from a Basalt Repository Site," Camp, Dresser and McKee Inc., Champaign, IL. Water Resources Div., report to Lawrence Livermore National Laboratory, Livermore, CA (also, UCRL-15252, May 1980).

Webster, D. S., J. F. Proctor, and I. W. Marine, 1970, Two-Well Tracer Test in Fractured Crystalline Rock, U.S. Geological Survey, Water Supply Paper 1544-1.

Welder, G. E., and E. P. Weeks, 1965, Hydrologic Conditions Near Glendo, Platte County, Wyoming, U.S. Geological Survey, Water Supply Paper 1971.

Wiley, J. R., 1979, "Leach Rates of High Activity Waste from Borosilicate Glass," Nucl. Technol 43, 268.

Winsauer, W. O., H. H. Shearin, Jr., P. H. Masson, and M. Williams, 1952, "Resistivity of Brine-Saturated Sands in Relation to Pore Geometry," Bull. Am. Assoc. Petrol. Geol. 36, 253.

Wyllie, M. R. J., and M. B. Spangler, 1952, "Application of Electrical Resistivity Measurements to Problem of Fluid Flow in Porous Media," Bull. Am. Assoc. Petrol. Geol. 36, 359.

BEST DOCUMENT AVAILABLE

5. A PARAMETRIC STUDY OF SYSTEM PERFORMANCE

This section presents a parametric analysis of the central mathematical model used to represent waste isolation systems. The parametric deterministic analysis of this model is described in Subsection 5.3, with the results presented in the form of contour plots. The parametric uncertainty analysis is presented in Subsection 5.4.

The mathematical model used to estimate the long-term performance of deep geologic repositories is described in Subsection 2.6. This 1-D Green's function approach represents a network of series path segments as an equivalent 1-D single-segment path. The release into this system is characterized as a square pulse. Thus, a multicomponent system is represented by the parameters of this equivalent system.

This section investigates deterministic and probabilistic behavior of this model. The two purposes of this analysis are:

- To develop an understanding of the model behavior, that is necessary to evaluate analyses of specific systems (such as in Section 6).
- To develop a set of graphs that can be used in future to conduct preliminary analyses of isolation systems.

5.1 PARAMETERS

As discussed in Section 2, the subsystems considered in this report can be characterized by the following variables:

• Waste form and package	Initial release time, dissolution times.
• Repository site pathways	Splitting fraction, average transit time, dispersion-induced spreading.
• Regional aquifer pathway	Average transit time, dispersion-induced spreading.

For a series system with no branching, the transit times and dispersive spreading associated with each segment may be added linearly and quadratically, respectively, to produce an effective total transit time and dispersive spreading (Kaufman, 1978).* This approximation is reasonably good if the temporal spread S of a pulse is less than the transit time T for that pulse in any segment. T is the first moment and S is the square root of the second central moment of the normalized waste pulse.

For a group of serially connected flow paths, the performance of the waste isolation system can be analyzed in terms of the six fundamental variables:

1) Waste inventory (SF or HLW).
2) Initial release time (start of pulse).
3) Dissolution time (duration of the pulse).
4) Total transit time (for the segments of the system).
5) Dispersive spreading (for the segments of the system).
6) Nuclide group.

Since the results scale with the amount of the inventory, an inventory of 10^6 MWe•yr was arbitrarily chosen. In the analysis that follows, the initial release time was considered to be small compared to the dissolution and transit times and nominally set to 500 yr. The performance was calculated for all combinations of inventory type and nuclide group. Rather than consider all possible values for dispersive spreading, it is possible to bracket the performance of the system by considering only the physically realistic limits. It is reasonable to treat the effects of dispersion in this manner because the performance is not particularly sensitive to the dispersion over a wide range of values. Further, the dispersive pulse spread associated with a given flow path segment can be written as proportional to the transit time for the path:

$$S = T\sqrt{2\alpha/L}$$

---

*Kaufman, A. M., Waste Pipe Calculus, Lawrence Livermore National Laboratory, Livermore, Calif., UCID-17953, 1978.

where

α = longitudinal dispersity

L = path length

T = transit time

S = induced pulse spread.

The proportionality constant does not depend on the velocity of flow but only on the ratio of α to L. The constant α is one of the uncertain parameters in geologic transport. Typically α is dictated by the size of the largest inhomogeneity in the flow path, that, at most, is the length of the flow path. Real field tests generally indicate a value of 100 m or larger, and nearly always larger than 50 m. If one assumes a value of 10 km as a total flow path length (considered typical), and takes a maximum value of $\alpha = L/2$ and a minimum value of 50 m, then the range of the ratio of transit time to pulse spread, T/S, is from 1.0-10.0.

For a given inventory (nuclide group and dispersion), performance can be calculated as a function of two variables: dissolution time, t_d, and transit time, T.

The primary performance measure calculated was the peak rate of release of activity (Ci/yr). Two intermediate variables of interest were also plotted, namely, peak normalized flux (with no decay) and time of the peak of normalized flux. The normalized flux differs from the activity release rate (flux) in that the normalized flux does not take into account decay. It is the fractional release rate of the emplaced inventory.

The activity flux must also take into account the differing inventories of spent fuel (SF) and high level waste (HLW).

5.2 DETERMINISTIC RESULTS

Contour plots (plots of equal values of the performance measures) show how the system performance depends on the dissolution and transit times for various inventory types, nuclide groups and dispersive spread.

The results of the deterministic analysis are reproduced in Figs. 5-1 through 5-14. Figures 5-1 and 5-2 show contours of equal time of (90%) peak

BEST DOCUMENT AVAILABLE

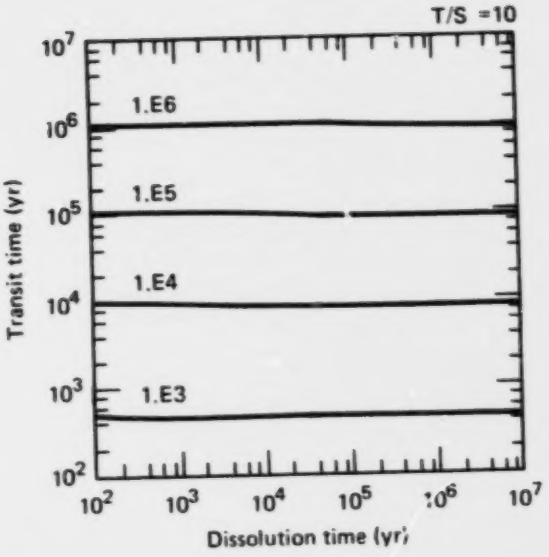

FIG. 5-1. Time of peak normalized flux (yr); (T/S = 10).

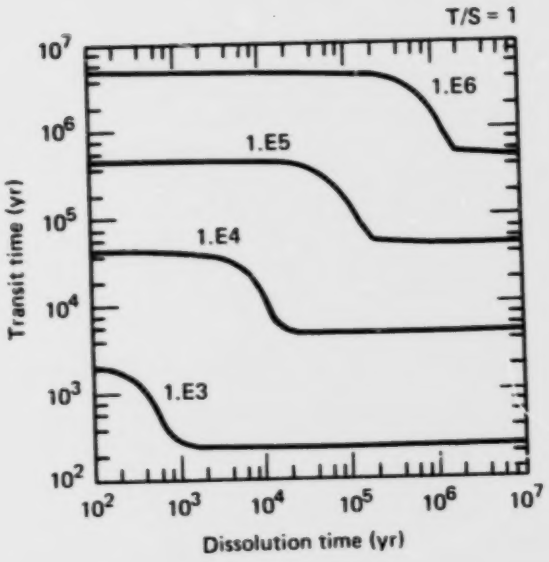

FIG. 5-2. Time of peak normalized flux (yr); (T/S = 1).

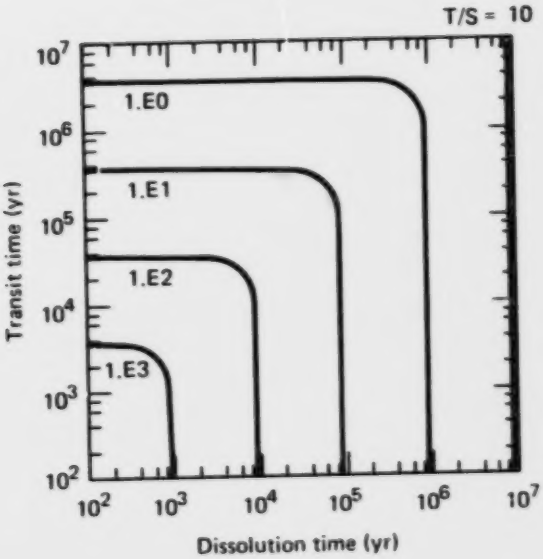

FIG. 5-3. Peak normalized flux (1/yr); (T/S = 10).

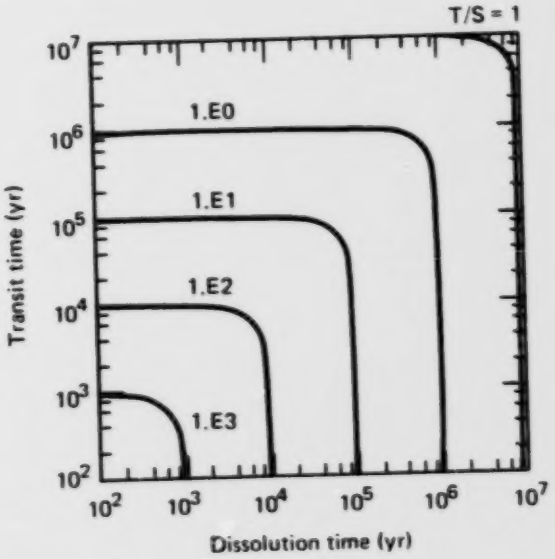

FIG. 5-4. Peak normalized flux (1/yr); (T/S = 1).

BEST DOCUMENT AVAILABLE

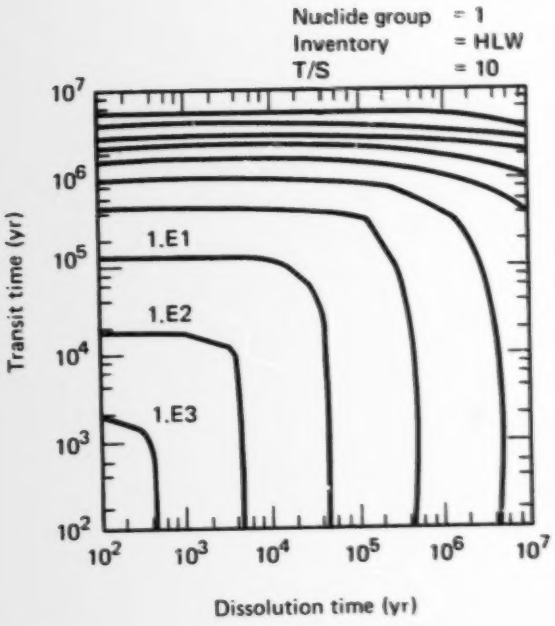

FIG. 5-5. Peak activity rate (Ci/yr)--Nuclide Group 1, HLW inventory, T/S = 10.

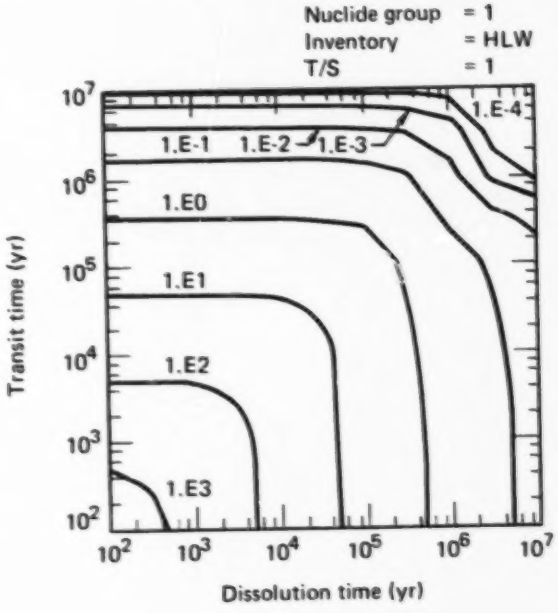

FIG. 5-6. Peak activity rate (Ci/yr)--Nuclide Group 1, HLW inventory, T/S = 1.

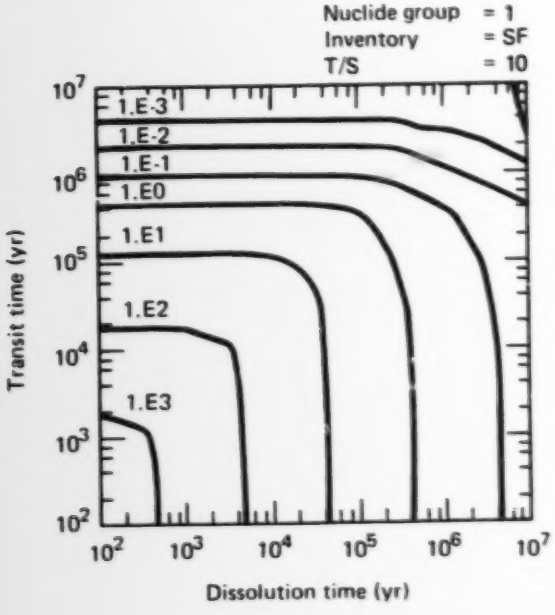

FIG. 5-7. Peak activity rate (Ci/yr)--Nuclide Group 1, SF inventory, T/S = 10.

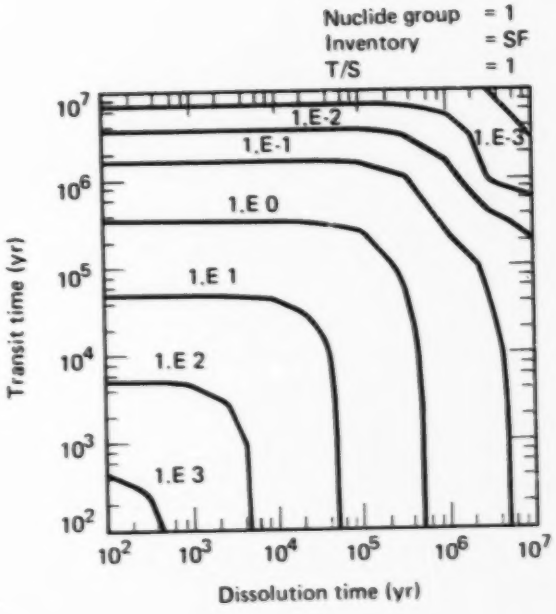

FIG. 5-8. Peak activity rate (Ci/yr)--Nuclide Group 1, SF inventory, T/S = 1.

BEST DOCUMENT AVAILABLE

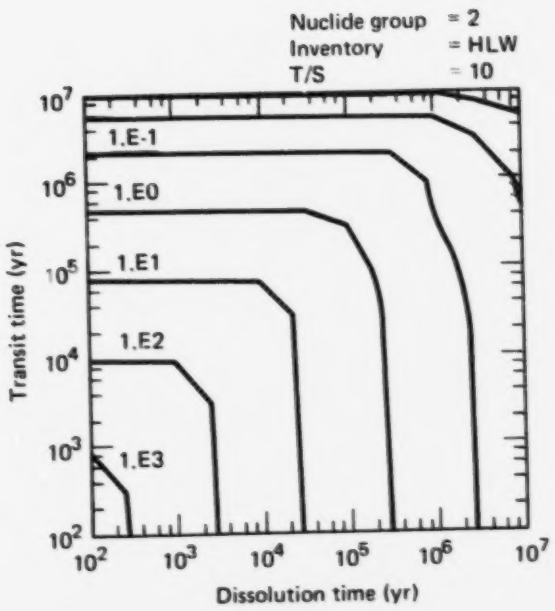

FIG. 5-9. Peak activity rate (Ci/yr)—Nuclide Group 2, HLW inventory, T/S = 10.

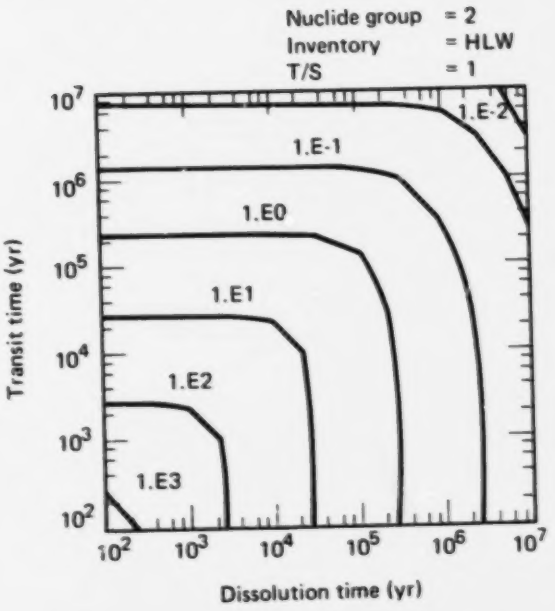

FIG. 5-10. Peak activity rate (Ci/yr)—Nuclide Group 2, HLW inventory, T/S = 1.

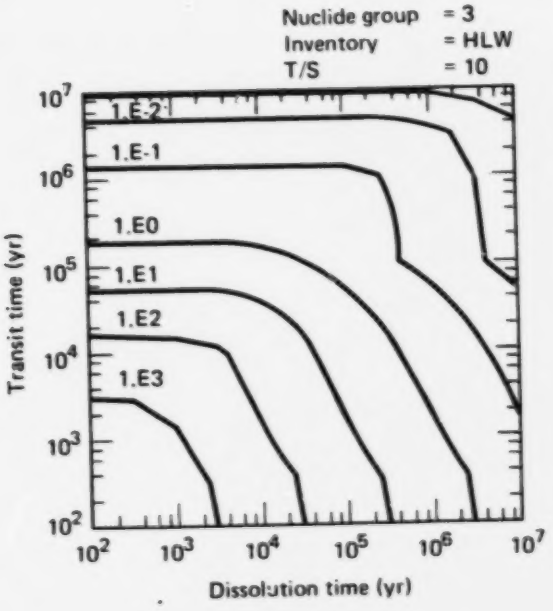

FIG. 5-11. Peak activity rate Ci/yr—Nuclide Group 3, HLW inventory, T/S = 10.

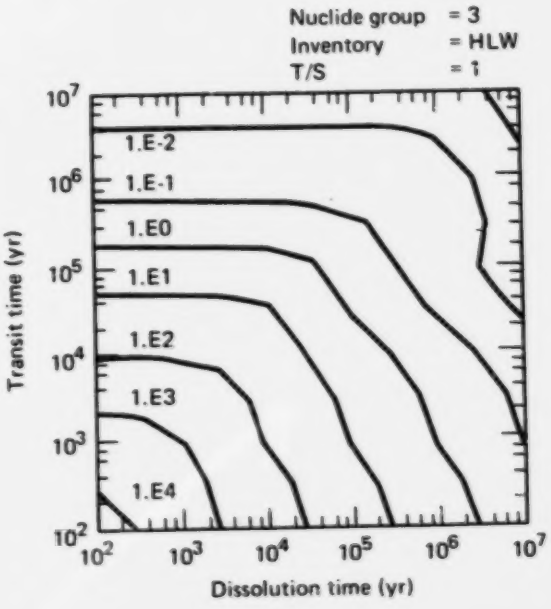

FIG. 5-12. Peak activity rate Ci/yr--Nuclide Group 3, HLW inventory, T/S = 1.

BEST DOCUMENT AVAILABLE

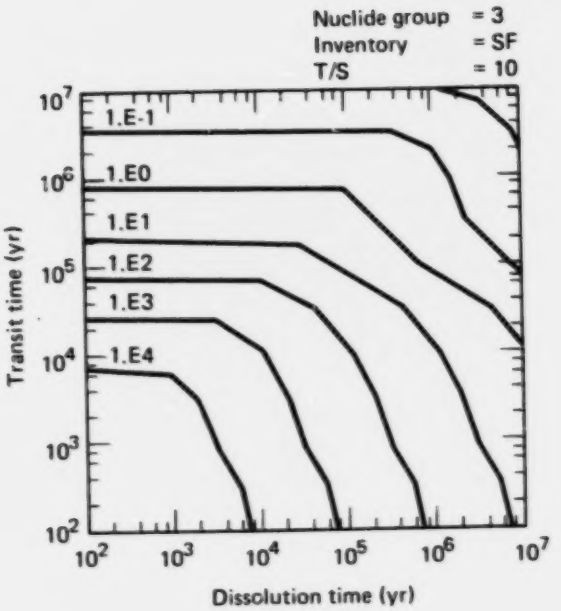

FIG. 5-13. Peak activity rate Ci/yr—Nuclide Group 3, SF inventory, T/S = 10.

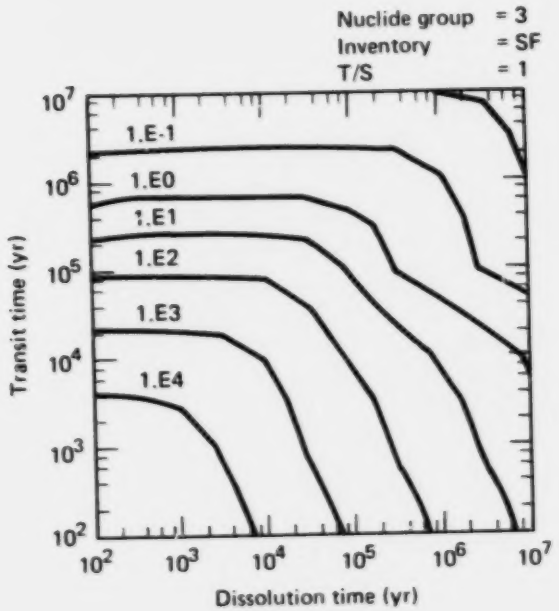

FIG. 5-14. Peak activity rate Ci/yr--Nuclide Group 3, SF inventory, T/S = 1.

normalized flux, with the two plots having values of T/S of 10 and 1, respectively. The first indicates that when dispersion is not large, the peak time is given by $T + t_0$, where

T = transit time

and

t_0 = initial release time.

The peak time is essentially independent of dissolution time, as expected since the leading edge of the pulse is quite sharp. The second plot (high dispersion) indicates that the time of peak flux, increases with the dissolution time when dissolution time and transit time are about equal. When the dissolution time is much smaller than transit time, the time of peak decreases as dispersion increases. This is reflected in the second plot by the higher position of the left hand segment of the contours relative to the same contours on the first plot. When dissolution time is much longer than transit time (so that the pulse is approximately a step-function), the time of 90% peak arrival again becomes independent of dissolution time. The form of the leading edge is only dependent on the dispersion, not on how long the step-function lasts.

In the region where $t_d \gg T$, the time of 90% peak is a decreasing function of dispersion (the leading edge becomes more spread out and moves forward). In terms of contours, this means that the right hand segments of the contours in Fig. 5-2 are lower than the corresponding ones in Fig. 5-1.

Figures 5-3 and 5-4 show the corresponding contour plots for the 90% peak normalized flux for the cases when T/S = 10 and T/S = 1, respectively. In both calculations, the quantity of waste was 10^6 MWe•yr. When transit time is negligible compared to dissolution, the output flux should be

$$j = 10^6/t_d \text{ (MWe•yr waste/yr)}, \tag{5-1}$$

exactly what is observed, independent of dispersion. For regions where dissolution times are much shorter than S (the dispersive pulse spread), the peak flux is determined from Eq. (2-12). In particular, when $T/S = 1/3 = 10$

BEST DOCUMENT AVAILABLE

in Eq. (2-12), then $T = t_p$ to 2% accuracy (t_p being the time at which the peak flux occurs). Thus, the exponential in Eq. (2-12) is approximately 1, and

$$j(t_p) = \frac{10^6}{0.1\ T\sqrt{2}} \approx 4 \cdot 10^6/T$$

so contours at $j(t_p) = 10^n$ will have y-axis intercepts at $4 \times 10^{6-n}$, which is what is observed in Fig. 5-3. For Fig. 5-4 ($\beta = 1$), the equation above has a correction to it. This correction is due to the fact that

$$t_p = 0.3T$$

when

$$\beta = 1 .$$

From Eq. (2-11) the normalized flux is:

$$\frac{1}{(2\pi S^2 t_p^3/T^3)^{1/2}} \exp -(t_p - T)^2/(2S^2 t_p/T)$$

$$= \frac{\exp -[(1 - 0.3)^2/2\ (0.3)]}{S(2.5)\sqrt{0.028}} = \frac{1.06}{S} . \qquad (5\text{-}2)$$

Hence, y-intercepts of contours 10^n occur at approximately $T = 10^{6-n}$.

Given the y-intercept of a contour (i.e., the value of transit time when $t_d = 0$) for a given value of $\beta << 1$, the value of the y-intercept of the same contour level for any other value of $\beta' << 1$ is obtained by the simple scaling formula:

$$T\beta = T'\beta' .$$

This formula is a direct result of Eq. (2-12).

BEST DOCUMENT AVAILABLE

From the graphs, it can be seen that the peak of normalized flux (j_p) is only a function of transit time (T) when $t_d \ll 10^6$. Likewise, j_p is only a function of t_d when $T \ll 10^6 C(\beta)/2.5 j_p \beta$. Here, $C(\beta)$ is an increasing function of β with the properties that

$$C(1) = 2.5 \text{ and } \lim_{\beta \to 0} C(\beta) = 1 \quad .$$

One final important point is emphasized concerning these two plots. There are only minor changes in the positions of the contours between T/S = 1 and T/S = 10. This fact substantiates the choice of using contour plots as a function of T and t_d and indicates that dispersion is not particularly important for the range of values that can be presumed physically reasonable.

From Eqs. (2-11) and (2-12), the value of peak normalized flux for a short impulse input is inversely proportional to T, with a proportionally constant which is a function only of T/S. The first row of Table 5-1 lists the ratio of the time of peak normalized flux (t_p) to the average transit time (T), as a function of T/S. The second row is the value of the peak normalized flux for each value of T/S, computed with the values of t_p/T and β in Eq. (2-12). The third row gives the normalized flux if $t_p = T$, and S/T = β. As T/S gets larger, the approximation that $t_p = T$ improves, so that at T/S = 5 there is only a 3% error in peak release rate.

TABLE 5-1. Time and magnitude of peak-normalized flux as a function of T/S [$j(1,\beta)$ is the flux at T].

	T/S = 1/β				
	1	2	3	4	5
t_p/T	0.30	0.69	0.83	0.91	0.94
$j(t_p/T,\beta)$	1.06/T	1.06/T	1.32/T	1.72/T	2.07/T
$j(1,\beta) = \frac{1}{\sqrt{2\pi\beta T}}$	0.40/T	0.80/T	1.20/T	1.60/T	2.00/T

The remaining 10 contour plots (Figs. 5-5 through 5-14) are plots of peak activity rates (Ci/yr) for each of the three nuclide groups, two inventory types (HLW or SF), and two values of T/S. The inventory for Group-2 nuclides is the same in HLW and SF, so only one inventory set is reproduced.

The analysis and interpretation of the various plots is necessarily based on the total activity as a function of time. Figures 5-15 through 5-19 indicate the activity of waste for each group and type of inventory as a function of time.

Several features of these plots should be noticed. Plots 5-15 and 5-16 illustrate the decay of the Group-1 nuclides (Tc^{99} and I^{129}). Spent fuel and HLW have the same amounts of Tc^{99}, but reprocessing removes 99.9% of the iodine. The initial inventory of Tc and I in SF are 0.45 and 1.2×10^{-3} Ci/Mwe·yr, respectively. Furthermore, the half-lives of Tc^{99} and I^{129} are 2.17×10^{-5} and 1.6×10^{7} yr respectively. Thus, the form of the activity curves for Group 1 are totally dominated by Tc out to about (at least) 2 million yr. After this, the Tc has decayed to a level less than that of the iodine. The transition point is quite clear in SF. In HLW, it occurs at a later time since the iodine level is three orders of magnitude less than in SF. For all practical purposes, we may consider the activity curves for Groups 1 and 2 to be identical for SF and HLW.

The major differences in inventory between the two forms is, of course, in the actinide levels. The various peaks that are present in the hazard curves of Figs. 5-19 and 5-20 are due to a variety of nuclides. The dominant nuclides are listed (in order) at the appropriate times on the figures.

Around 10^{6} years, the radioactivity of the actinides actually increases in HLW (and decreases more slowly in SF) due to the production of U^{233} and Th^{229} from alpha decay of Np^{237}. In SF at 10^{6} yr there are equally important additional contributions from the decay of U^{234} to Th^{230} to Ra^{226}, Po^{210}, and Pb^{210}. The U^{234} is primarily present due to alpha decay of Pu^{238} during the early phase of the decay cycle.

In general, the identification of the dominant species in the waste is important because the transit time is a strong function of retardation, and the retardation factors differ widely among the various chemical elements. For example, the retardation factor for uranium, rather than plutonium, may be appropriate for transit times in excess of 10^{5} yr.

BEST DOCUMENT AVAILABLE

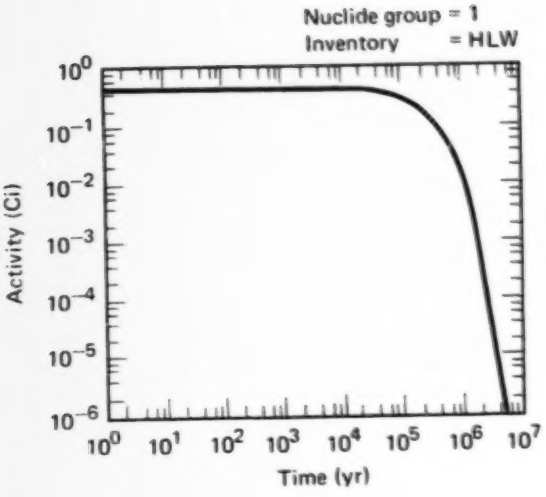

FIG. 5-15. Activity per MWe·yr vs time (Nuclide Group 1, HLW inventory).

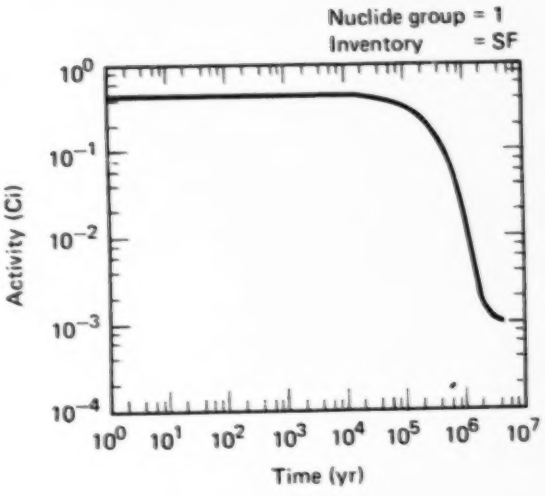

FIG. 5-16. Activity per MWe·yr vs time (Nuclide Group 1, SF inventory).

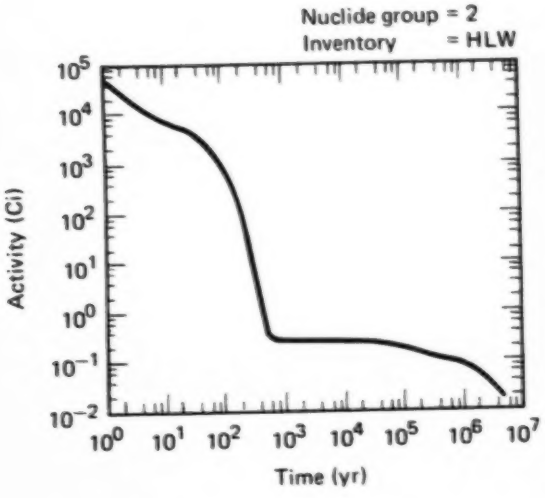

FIG. 5-17. Activity per MWe·yr vs time (Nuclide Group 2, HLW inventory).

BEST DOCUMENT AVAILABLE

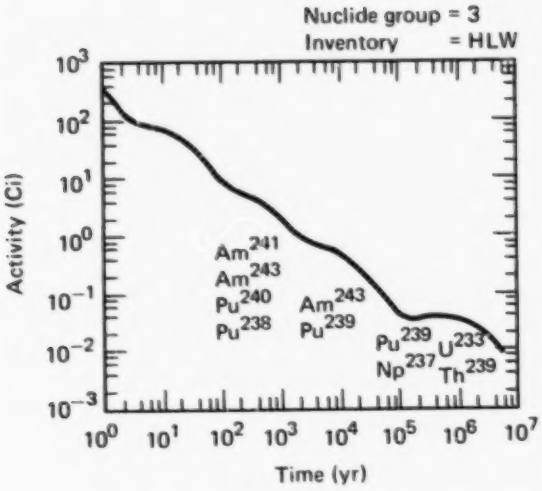

FIG. 5-18. Activity per MWe·yr vs time (Nuclide Group 3, HLW inventory).

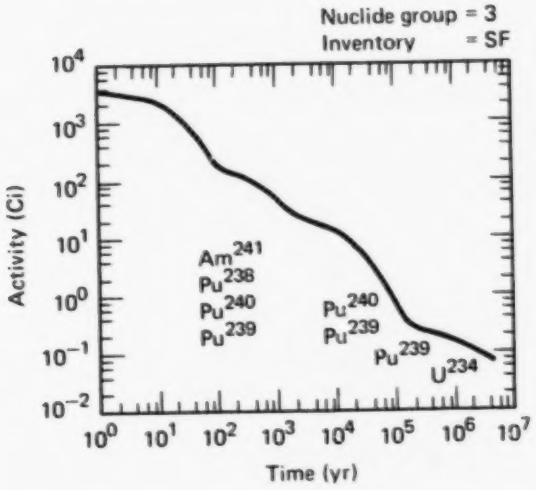

FIG. 5-19. Activity per MWe·yr vs time (Nuclide Group 3, SF inventory).

BEST DOCUMENT AVAILABLE

Given these considerations, it is now possible to discuss the effects decay and inventory have on the flux contours. In all cases, the initial amount of emplaced waste was 10^6 MWe•yr and the output plotted in units of Ci/yr. Figures 5-5 and 5-6 present the two plots of Group 1 for HLW with T/S = 10 and T/S = 1, respectively. Figures 5-7 and 5-8 are the corresponding ones for SF. Comparing Figs. 5-5 with 5-3 and 5-6 with 5-4 indicates that the primary effect of decay on the form of the contours is to increase the importance of transit time relative to dissolution time for the region where $T > 5 \times 10^5$ yr = twice the Tc^{99} lifetime. For transit times in excess of 10^6 yr, the dissolution time is no longer very important. In Figs. 5-7 and 5-8, the effect of the transition from Tc^{99} to I^{129} dominates after 10^6 yr can be seen as the discontinuity in the slopes of some of the contours. Comparing HLW to SF, it is clear that the only differences in peak activity rate for Group 1 occur after 10^6 yr when the relative quantities of I^{129} become important.

Figures 5-9 and 5-10 present the results for Group-2 nuclides (fission products) for T/S = 10 and 1, respectively. As mentioned, there is no difference between HLW and SF for this group. Since there is very little decay in the Group-2 nuclides between 500 and 10^5 yr, these contour plots are not significantly different from the normalized flux plots.

Figures 5-11 and 5-12 present the Group-3 contours for HLW with T/S = 10 and T/S = 1, respectively, while Figs. 5-13 and 5-14 give the corresponding results for SF. For this group, unlike the other two, there is a fairly continuous reduction in activity as a function of time. This causes the peak activity release rate to decrease as the transit time increases, even when the transit time is short compared to the dissolution time. The impact of the "hump" in the activity-vs-time curve between 10^5 and 5×10^6 yr shows up as discontinuities in the contour slopes for dissolution and transit times in this region. From the activity-vs-time curves, we see that the actinides in SF are generally more than an order of magnitude more radioactive (per MWe•yr) than the actinides in HLW. This difference shows up in the contour plots for both values of T/S as a shift in the y-intercepts of the contours. It takes a considerably longer dissolution time to make SF have the same performance as HLW.

BEST DOCUMENT AVAILABLE

It is important to note that, in all but one region of these contour plots, the change in T/S from 10 to 1 never produces a shift in the y-intercepts of the contours by more than a factor of three. The one exception is the short transit time ($\sim 10^3$ years) region of Group 2, where the effect is on the order of a factor of 4 or 5 due to the rapid fall off in the hazard as Cs^{137} and Sr^{90} decay. The x-intercepts, and thus the position of the roughly vertical segments of the contours, are independent of the value of T/S.

5.3 UNCERTAINTY ANALYSIS RESULTS

In this section, we look at the effect of the uncertainties in the transit and dissolution times on the uncertainty in peak activity rate. This is accomplished by comparing the results when both variables are uncertain, with those when only dissolution time or transit time are uncertain.

The results are presented in Figs. 5-20 through 5-31 in the form of bar graphs. The bar graphs represent the 1st- to 99th-percentile spread in the peak activity rate. The cross marks indicate the 25th, 50th, and 75th percentile positions. The (log) scale on either side is in Ci/yr. The bar graphs appear in sets of three.

The Case 1 results on each graph are computed with both the transit time and the dissolution time uncertain. The distribution for each is assumed to be lognormal with a 1st- to 99th-percentile spread of two decades. Case 2 is computed with the transit time certain at the median value and the dissolution time uncertain. Case 3 is computed with the dissolution time certain at the median value and the transit time uncertain. Results are computed with the median values at 10^3, 10^4, 10^5, and 10^6 yr for both the dissolution and transit times. The calculations with both values at 10^6 were not performed due to a computer program constraint. These 15 sets of bar graphs are presented in Figs. 5-20 through 5-31. As in the previous section, the 12 figures correspond to the combinations of the three nuclide groups, SF and HLW inventories, and T/S = 1 and T/S = 10.

In studying the results, several conclusions can be drawn. When the median value of transit time is much less than the median value for dissolution time, setting the dissolution time certain drastically reduces the spread of the peak activity flux. In the same regime, setting the transit time certain has virtually no effect on peak-activity flux uncertainty.

BEST DOCUMENT AVAILABLE

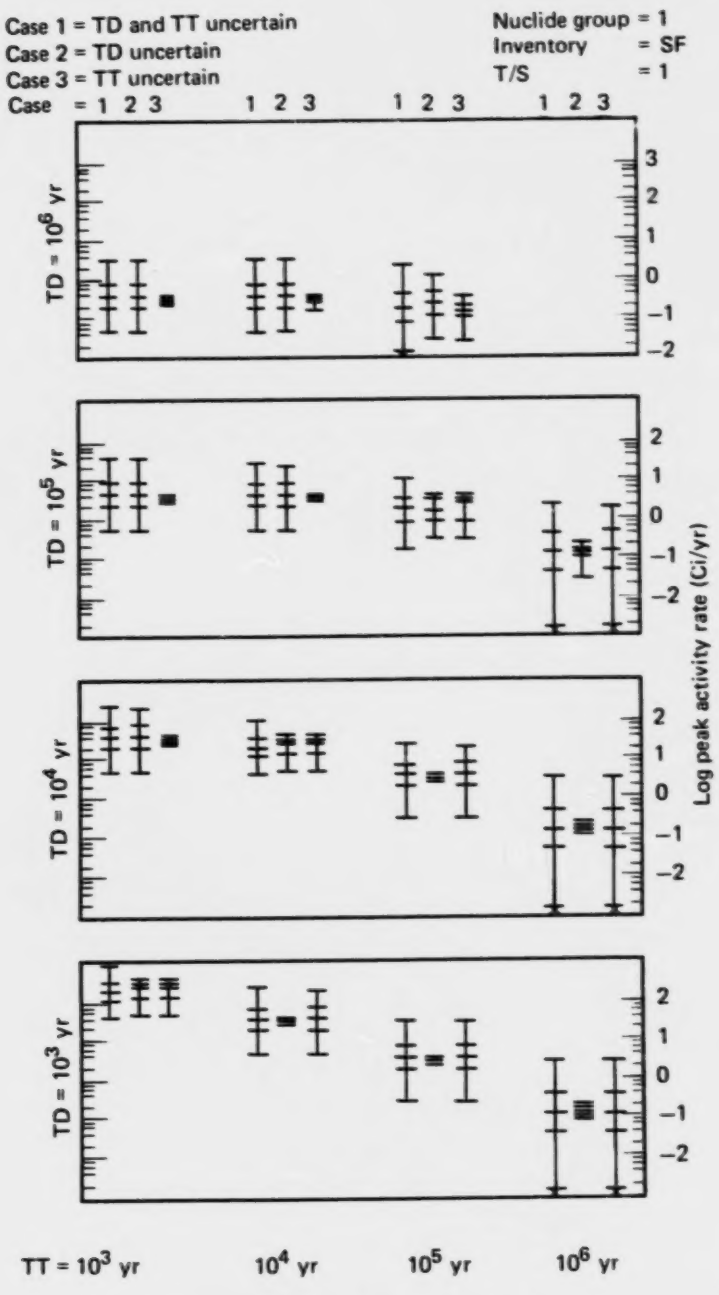

x indicates that part of graph is below the scale

FIG. 5-20. Distribution of peak activity rate--Nuclide Group 1; SF inventory; T/S = 1.

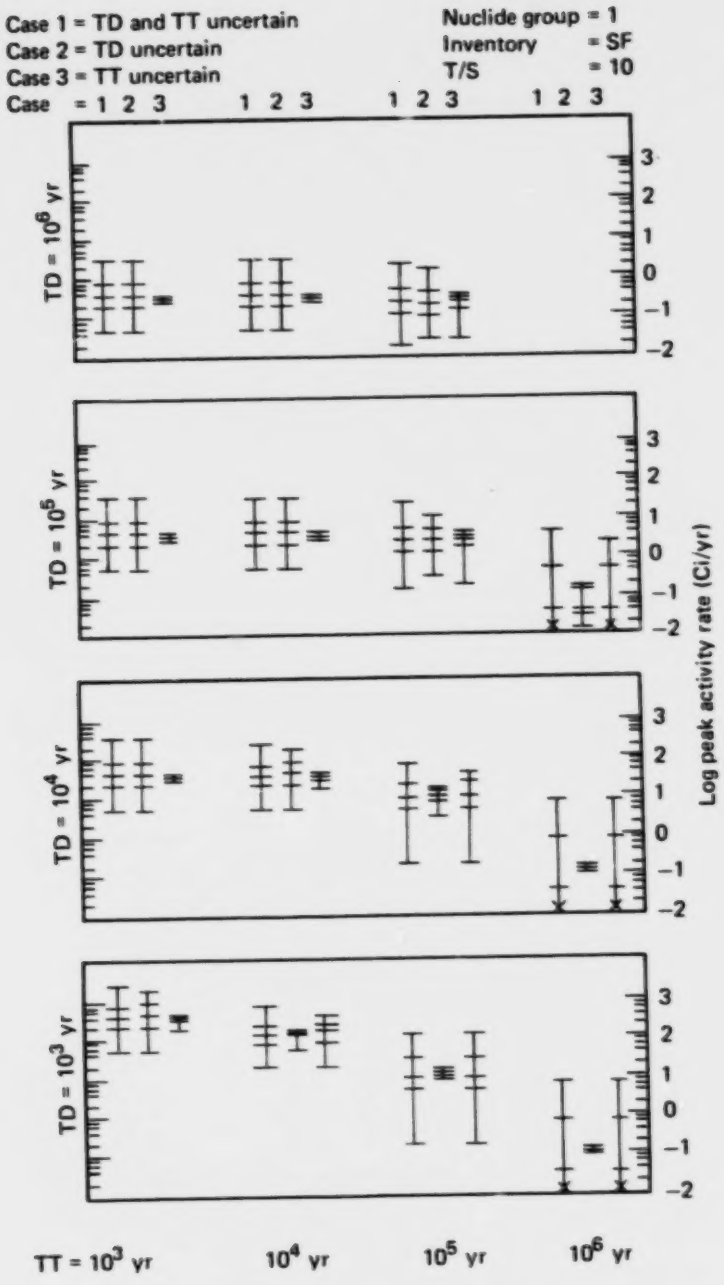

FIG. 5-21. Distribution of peak activity rate--Nuclide Group 1; SF inventory; T/S = 10.

BEST DOCUMENT AVAILABLE

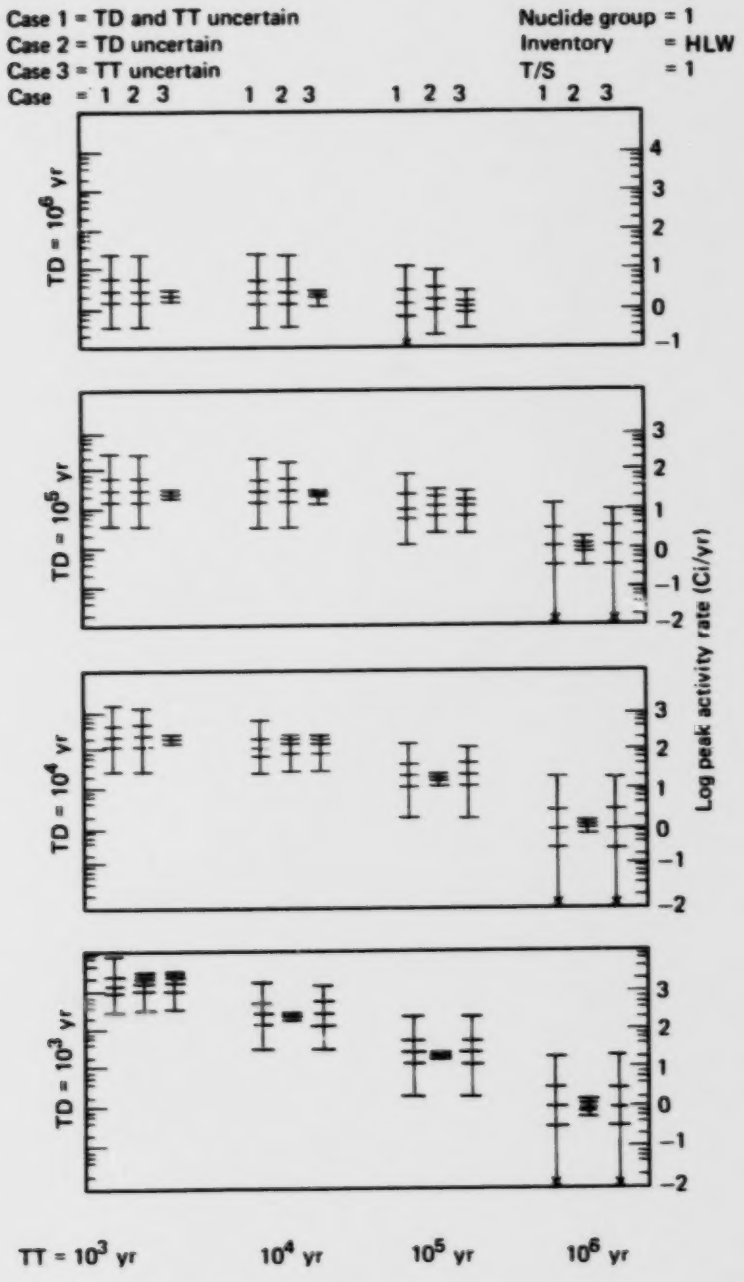
Case 1 = TD and TT uncertain
Case 2 = TD uncertain
Case 3 = TT uncertain
Case = 1 2 3 1 2 3 1 2 3 1 2 3
Nuclide group = 1
Inventory = HLW
T/S = 1
TD = 10^6 yr
TD = 10^5 yr
TD = 10^4 yr
TD = 10^3 yr
Log peak activity rate (Ci/yr)
TT = 10^3 yr
10^4 yr
10^5 yr
10^6 yr
x indicates that part of graph is below the scale

FIG. 5-22. Distribution of peak activity rate--Nuclide Group 1; HLW inventory; T/S = 1.

BEST DOCUMENT AVAILABLE

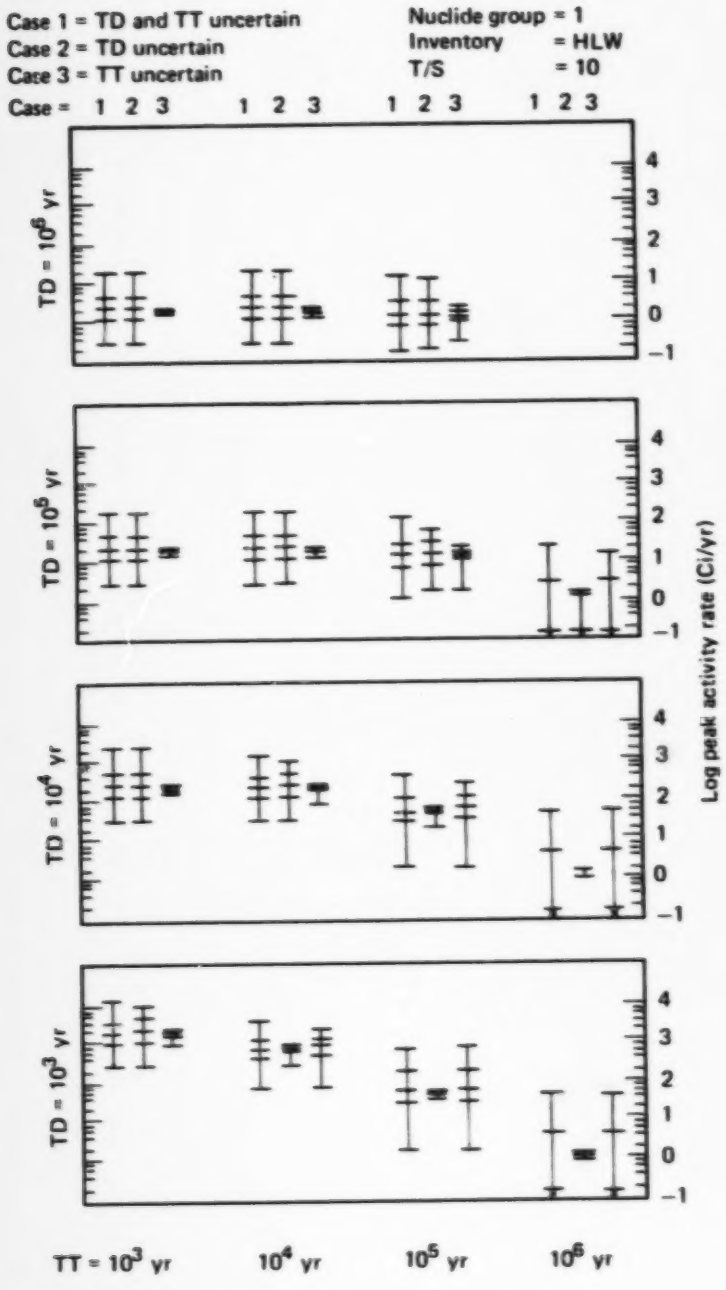

FIG. 5-23. Distribution of peak activity rate--Nuclide Group 1; HLW inventory; T/S = 10.

BEST DOCUMENT AVAILABLE

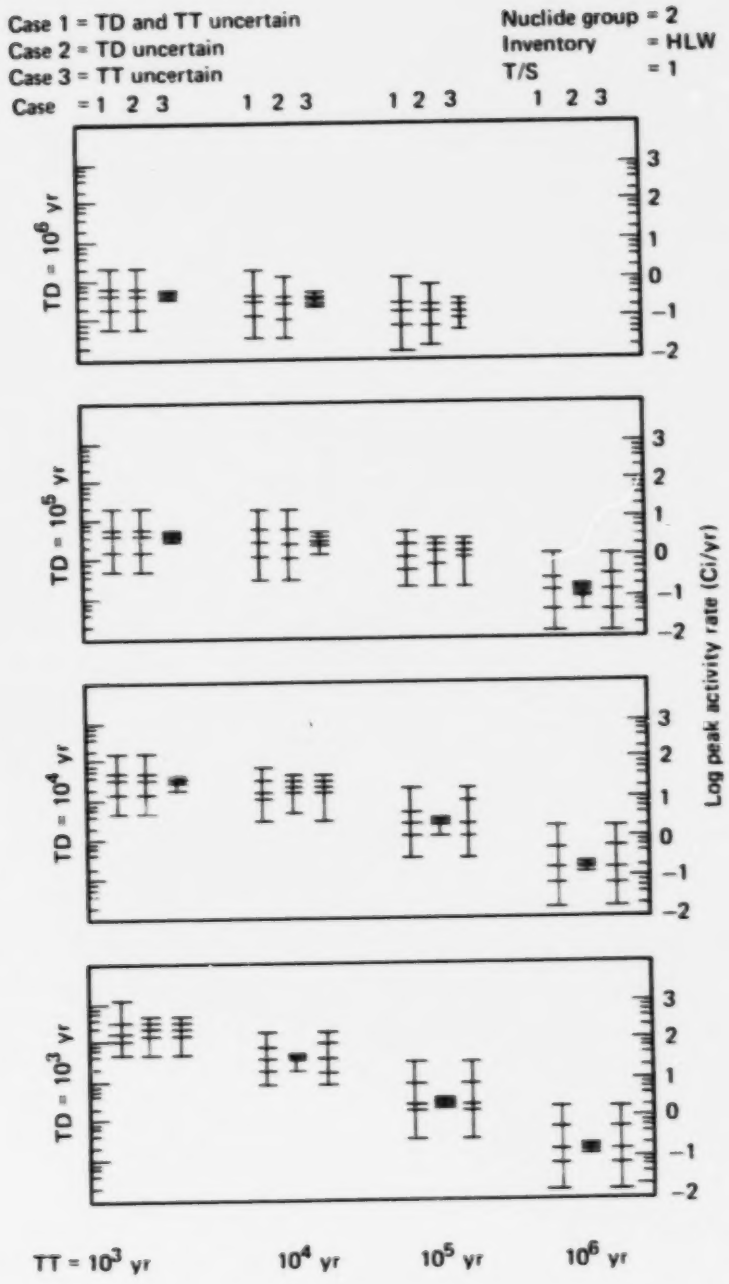

FIG. 5-24. Distribution of peak activity rate--Nuclide Group 2; HLW inventory; T/S = 1.

BEST DOCUMENT AVAILABLE

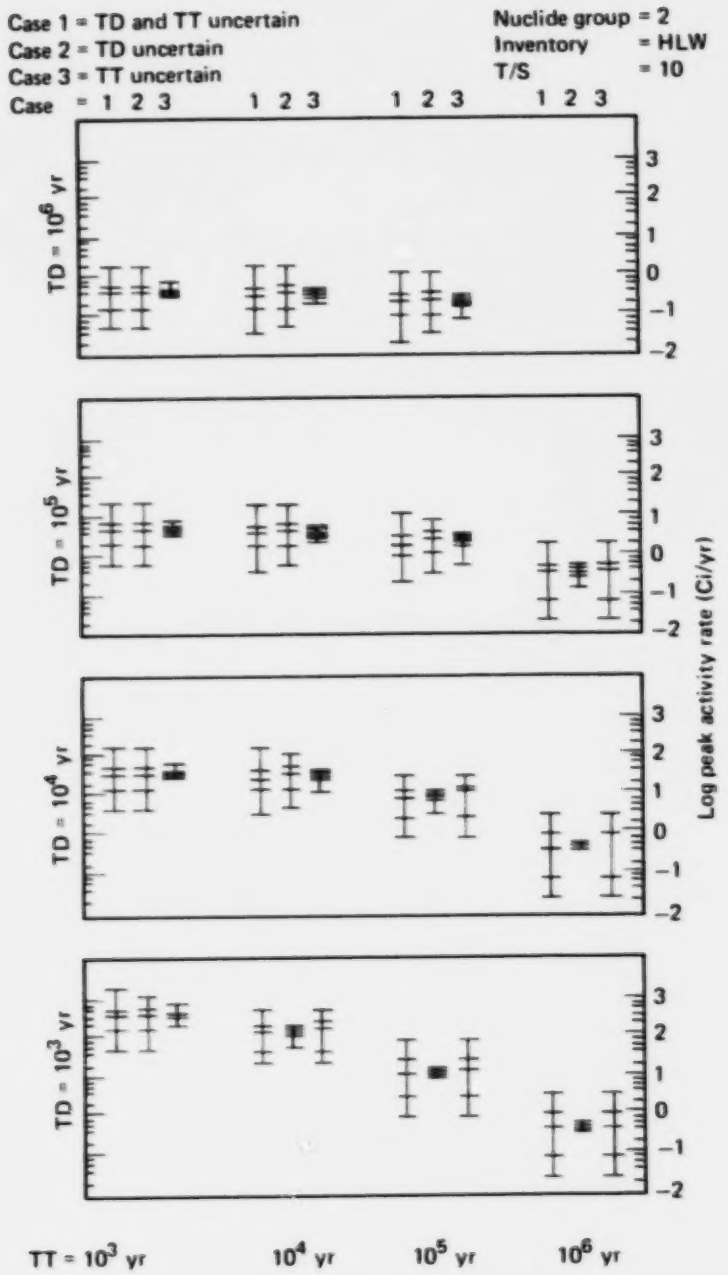

x indicates that part of graph is below the scale

FIG. 5-25. Distribution of peak activity rate--Nuclide Group 2; HLW inventory; T/S = 10.

BEST DOCUMENT AVAILABLE

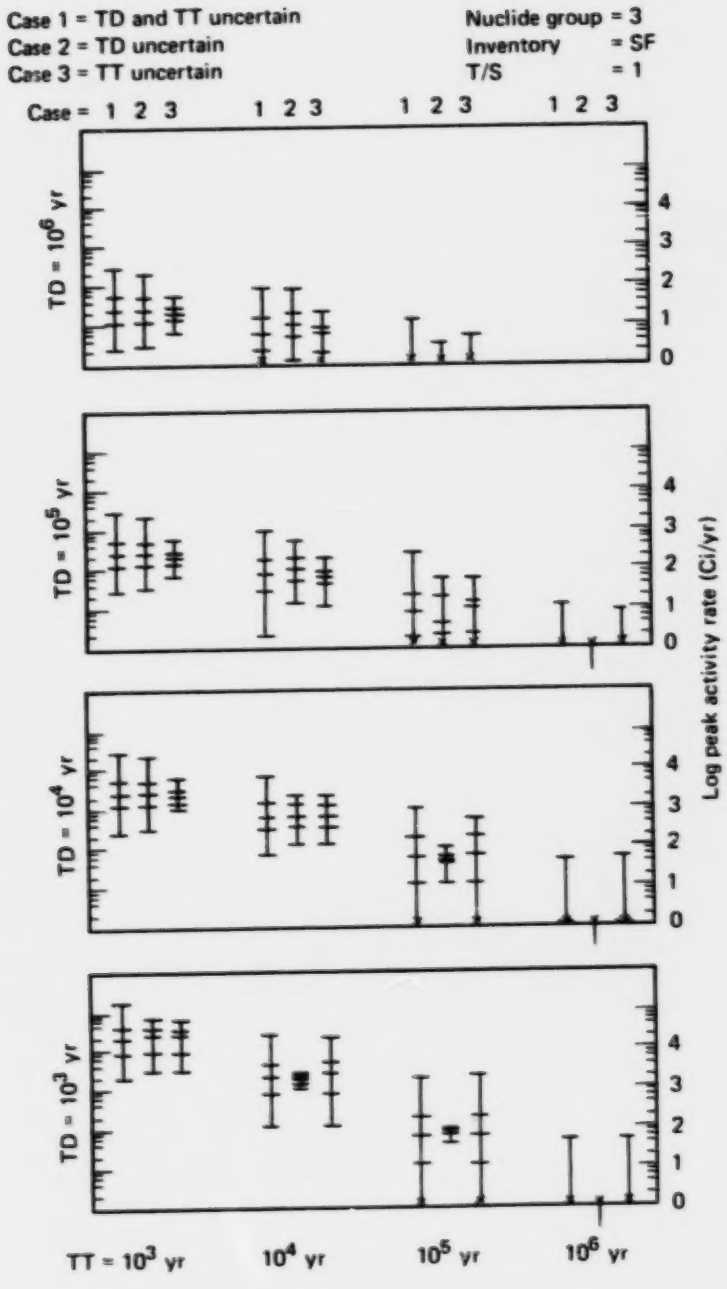
Case 1 = TD and TT uncertain
Case 2 = TD uncertain
Case 3 = TT uncertain
Nuclide group = 3
Inventory = SF
T/S = 1
Case = 1 2 3 1 2 3 1 2 3 1 2 3
TD = 10^6 yr
TD = 10^5 yr
TD = 10^4 yr
TD = 10^3 yr
0
1
2
3
4
Log peak activity rate (Ci/yr)
TT = 10^3 yr
10^4 yr
10^5 yr
10^6 yr
x indicates that part of graph is below the scale

FIG. 5-26. Distribution of peak activity rate--Nuclide Group 3; SF inventory; T/S = 1.

BEST DOCUMENT AVAILABLE

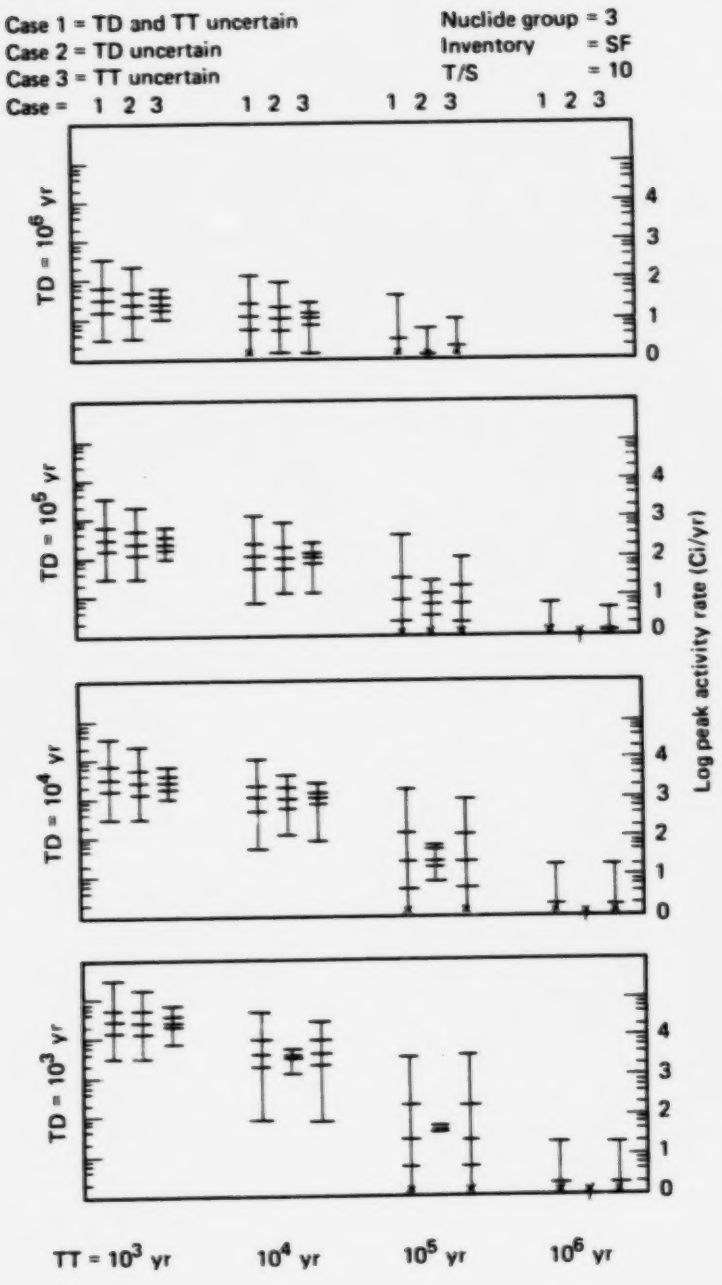
Case 1 = TD and TT uncertain
Case 2 = TD uncertain
Case 3 = TT uncertain
Nuclide group = 3
Inventory = SF
T/S = 10
Case = 1 2 3 1 2 3 1 2 3 1 2 3
TD = 10^6 yr
TD = 10^5 yr
TD = 10^4 yr
TD = 10^3 yr
0
1
2
3
4
Log peak activity rate (Ci/yr)
TT = 10^3 yr
10^4 yr
10^5 yr
10^6 yr
x indicates that part of graph is below the scale

FIG. 5-27. Distribution of peak activity rate--Nuclide Group 3; SF inventory; T/S = 10.

BEST DOCUMENT AVAILABLE

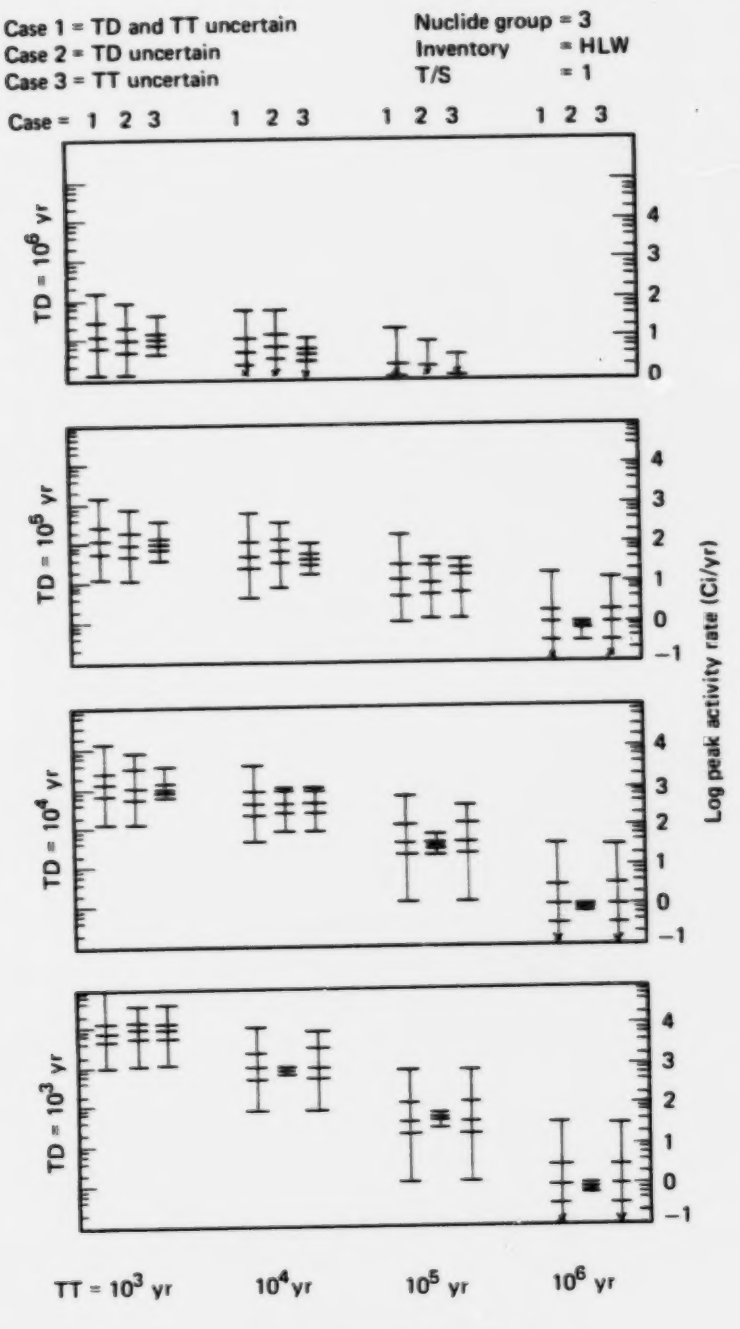

FIG. 5-28. Distribution of peak activity rate--Nuclide Group 3; HLW inventory; T/S = 1.

BEST DOCUMENT AVAILABLE

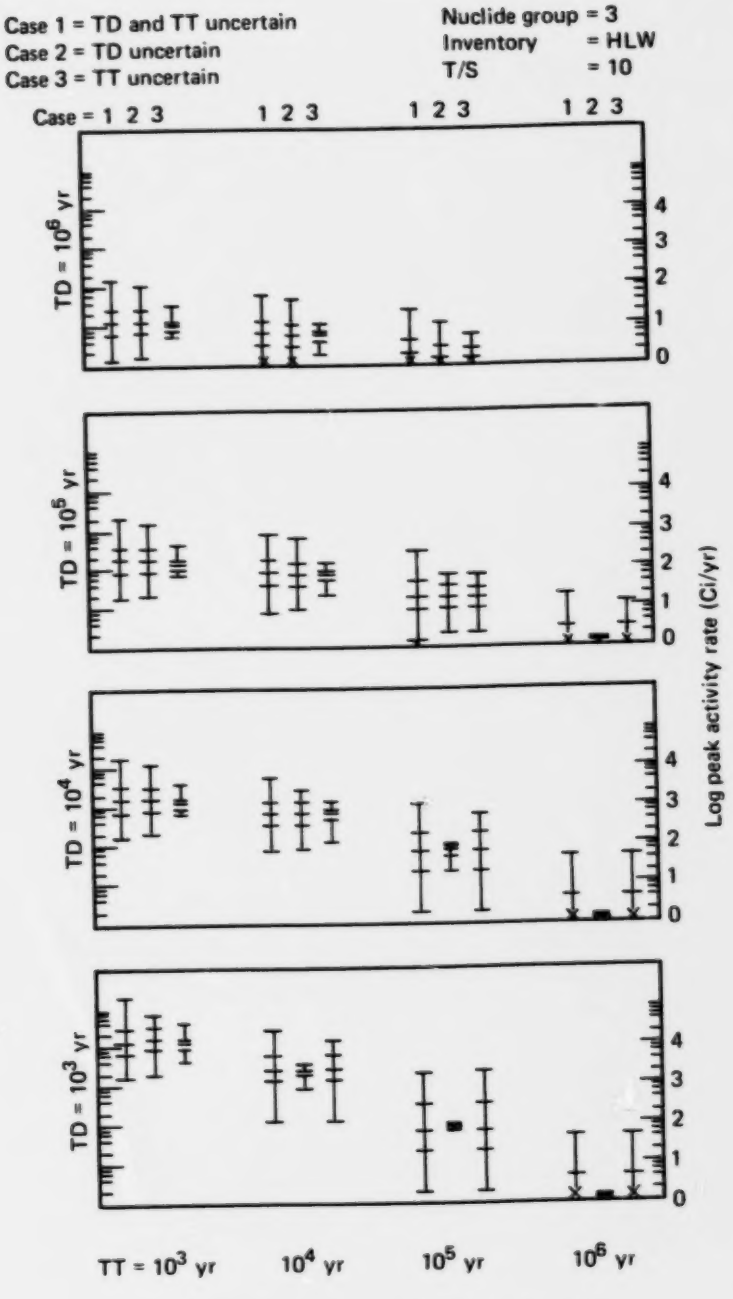
Case 1 = TD and TT uncertain
Case 2 = TD uncertain
Case 3 = TT uncertain
Nuclide group = 3
Inventory = HLW
T/S = 10
Case = 1 2 3 1 2 3 1 2 3 1 2 3
TD = 10^6 yr
TD = 10^5 yr
TD = 10^4 yr
TD = 10^3 yr
0 1 2 3 4
Log peak activity rate (Ci/yr)
TT = 10^3 yr
10^4 yr
10^5 yr
10^6 yr
x indicates that part of graph is below the scale

FIG. 5-29. Distribution of peak activity rate--Nuclide Group 3; HLW inventory; T/S = 10.

BEST DOCUMENT AVAILABLE

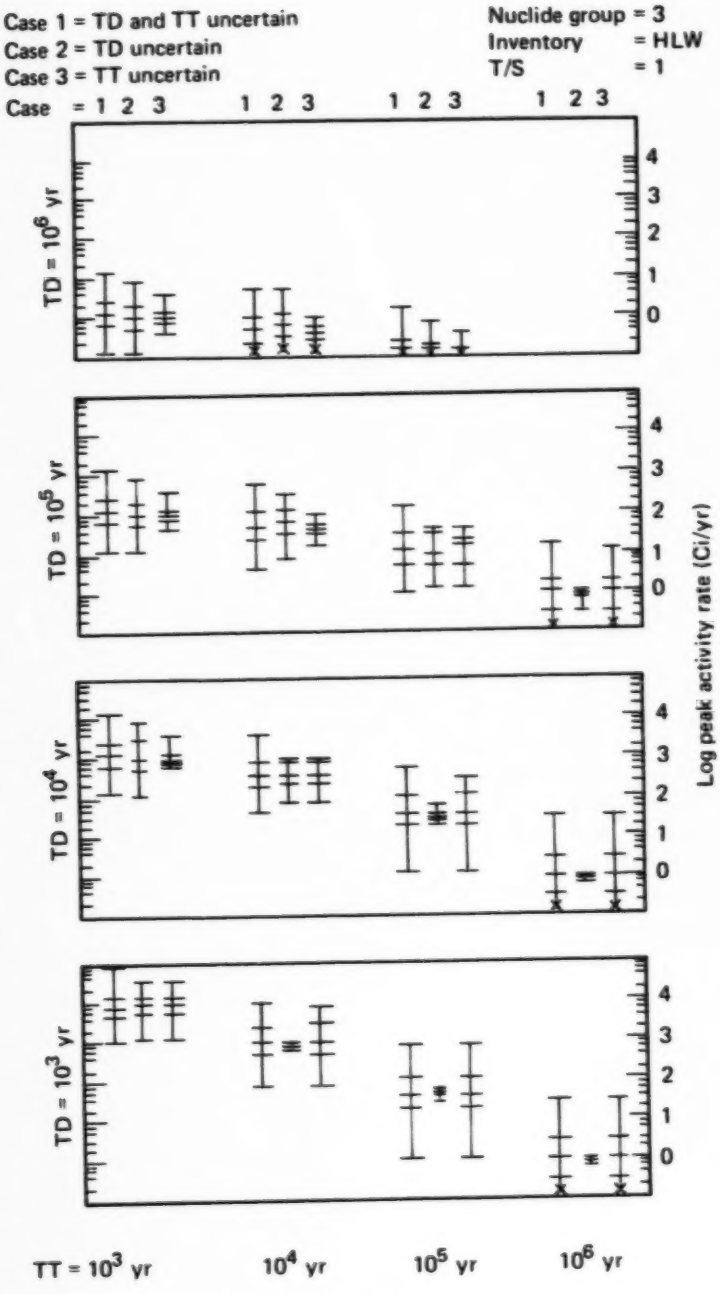
Case 1 = TD and TT uncertain
Case 2 = TD uncertain
Case 3 = TT uncertain
Nuclide group = 3
Inventory = HLW
T/S = 1
Case = 1 2 3 1 2 3 1 2 3 1 2 3
TD = 10^6 yr
TD = 10^5 yr
TD = 10^4 yr
TD = 10^3 yr
0
1
2
3
4
Log peak activity rate (Ci/yr)
TT = 10^3 yr
10^4 yr
10^5 yr
10^6 yr
x indicates that part of graph is below the scale

FIG. 5-30. Distribution of peak activity rate--Nuclide Group 3; HLW inventory; T/S = 1.

BEST DOCUMENT AVAILABL

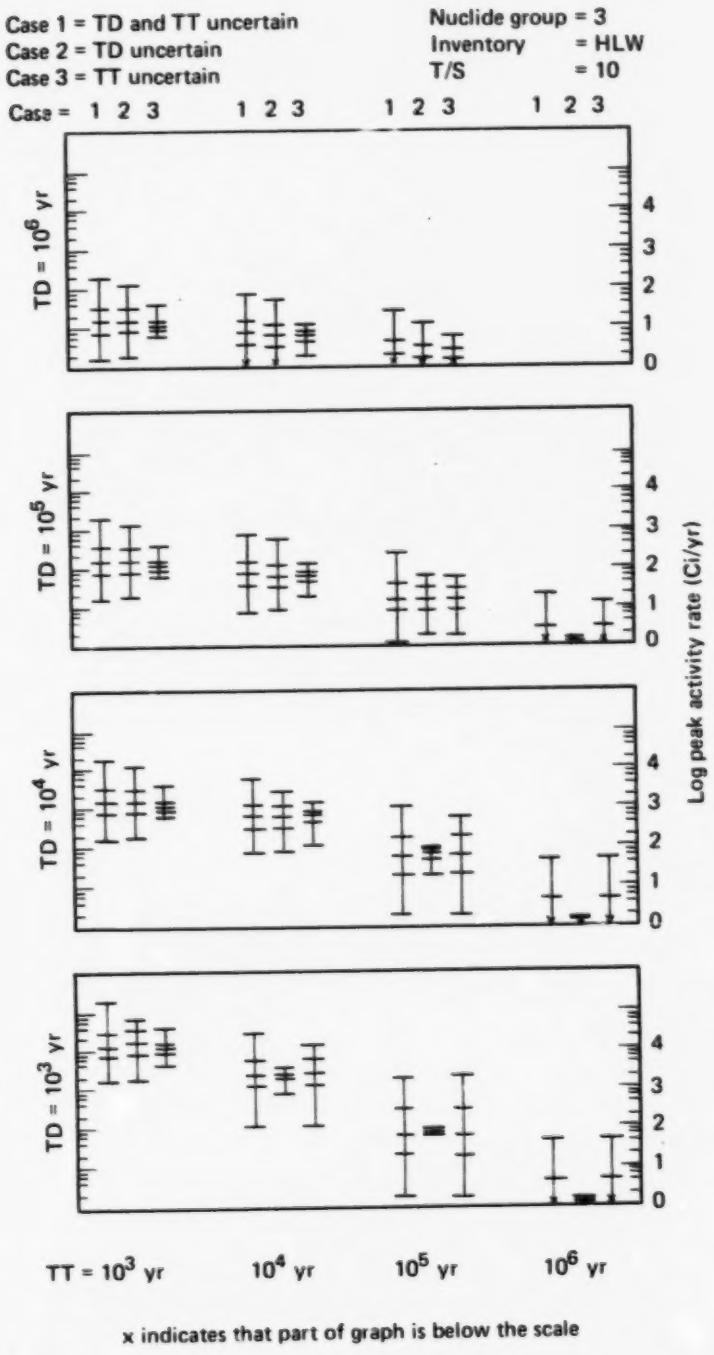
Case 1 = TD and TT uncertain
Case 2 = TD uncertain
Case 3 = TT uncertain
Nuclide group = 3
Inventory = HLW
T/S = 10
Case = 1 2 3 1 2 3 1 2 3 1 2 3
TD = 10^6 yr
TD = 10^5 yr
TD = 10^4 yr
TD = 10^3 yr
Log peak activity rate (Ci/yr)
TT = 10^3 yr
10^4 yr
10^5 yr
10^6 yr
x indicates that part of graph is below the scale

FIG. 5-31. Distribution of peak activity rate--Nuclide Group 3; HLW inventory; T/S = 10.

BEST DOCUMENT AVAILABLE

activity. This effect is not as pronounced in SF, because the hazard curve is not as variable in this region.

A significant variation in the size of comparable bars as a function of inventory type occurs in two places. The first is the difference in the median $T = 10^6 >>$ median t_d in cases in Group 1. The 1% levels in HLW are several orders (~8) of magnitude lower than in SF. This is due to the presence of I^{129} in SF, which limits the decrease in the hazard curve for times longer than 10^6 yr. The second area where a major difference in the size of the bars occurs is in Group 3 for $T = 10^6 >> t_d$. The difference is again due to the much more rapid variation of the HLW hazard curve from 5×10^5 yr onward.

The sizes of comparable bars between different groups can also be analyzed. The variations can essentially always be explained in terms of the degree of variation of the hazard curves. Thus, for median times between 10^3 and 10^5, Groups 1 and 2 can be expected to show smaller bars than the corresponding bars for Group 3, simply because the hazard curves for Groups 1 and 2 vary much more slowly than for Group 3.

5.4 SUMMARY

Before summarizing the results, it is important to review some of the fundamental assumptions.

1. The performance of an underground nuclear waste repository can be evaluated in terms of four primary variables: initial release time (breach time of the canisters), dissolution rate of given nuclides from the waste form, average transit time for a given nuclide type to be transported from the repository to the biosphere, and the dispersive spreading that a pulse of nuclides will experience during transport.

2. If the geologic environment of a repository is well chosen, the flow of groundwater will probably be dominated by flow along cross-sectionally constrained pathways such as shafts, boreholes, faults, discrete joints or fracture sets, rather than interstitial flow in an unconstrained environment. In such a case, the hydrology and transport can be considered 1-D in character and the dispersive spreading can be approximated as purely longitudinal. Even if the laterally-constrained flow assumption is not exactly satisfied (such as for horizontal flow in interbeds), then the results of this study may be

BEST DOCUMENT AVAILABLE

considered conservative rather than realistic in their interpretation, because lateral dispersion will have been ignored.

3. If the assumptions of pure longitudinal dispersion and discrete 1-D flow paths are made, then the transport may be characterized by two parameters, T and S, which have units of time and represent the average transit time and dispersive spreading associated with a given sequence of path segments. Most important for any segment, the ratio of $T/S = \sqrt{2\alpha/L}$ is independent of velocity.

4. The nuclides are divided into three groups whose members are assumed to have the same retardation factors and dissolution rates.

The main results of the deterministic analysis are:

1. For values of T/S in the neighborhood of 10, the time of peak of normalized flux (i.e., no decay) is independent of dissolution time and, in fact, is given by $T + t_0$, where t_0 = initial release time (see Fig. 5-1). For values of T/S near 1, the time of peak flux shows an increasing dependence on dissolution time in the region where $T = t_d$. For dissolution times much shorter or longer than T, the time of peak is again independent of t_d. (See Fig. 5-2.)

2. The value of peak normalized flux j_p, is independent of t_d for $t_d < t_d^* = 10^6/j_p$ and independent of T for $T < T^*$. T^* is an increasing function of T/S and has the value

$$T^* = 10^6/j_p$$

when

$$T/S = 1.$$

For values of $T/S \gg 1$:

$$T^* = \frac{10^6}{2.5\ j_p}\frac{T}{S} \quad , \tag{5-3}$$

where j_p is the value of peak of normalized flux under consideration. In graphical terms, T^* is the value of the y-intercept of a constant j_p contour. (See Figs. 5-3 and 5-4.) The actual values of the flux when $T = 0$ or $t_d = 0$ are given by

$$j_p = \frac{10^6}{T_d} , \quad (T = 0)$$

$$j_p = \frac{10^6}{\sqrt{2\pi S^2 T_p^3/T^3}} \exp -(T_p - T)^2/(2S^2 T_p/T) , \quad (t_d = 0) ,$$

with $\frac{T_p}{T} = \frac{\sqrt{9\beta^4 + 4} - 3\beta^2}{2}$, $T_p = t_p - T_0$, and $\beta = S/T$. (5-4)

For $\beta << 1$ $(T/S >> 1)$, $T_p = T$ and $j_p = \frac{10^6}{\sqrt{(2\pi S^2)}} = \frac{10^6}{\sqrt{(2\pi T^2)}} \left(\frac{T}{S}\right)$. (5-5)

3. The peak activity rate or flux is dependent on T (even when $T << t_d$) when T is greater than or equal to the half-life of a dominant contributor to the activity. This dependence is reflected in the slant of the vertical segments of the contours when decay is included.

For Group I (where almost all the activity is due to Tc^{99}), the contours with decay are quite similar to the contours without decay for dissolution and transit times less than 10^5 yr (Figs. 5-5 through 5-9) similarly for Group II (Figs. 5-10 and 5-11). For Group III, decay is occurring continuously from the onset, and therefore has a nontrivial effect on the contour structure for all transit times and all dissolution times greater than the transit time. (See Figs. 5-11 through 5-14.)

4. The activity-vs-time curves for the actinides indicate that SF is somewhat more than an order of magnitude more radioactive than HLW at any given time (see Figs. 5-18 and 5-19.) Therefore, to obtain the same peak flux from the two inventories, it is necessary to have a longer dissolution time or a longer transit time (or both) for SF compared to HLW. Specifically, for a given T/S ratio, the differences in the T-axis contour intercepts ($t_d = 0$) are on the order of a factor of 5-10. The shifts in the t_d-axis intercepts ($T = 0$) between the two inventories are on the order of a factor of 20-30 (Figs. 5-11 through 5-14). Thus, it is easier to equalize the hazard by modifying the transit time rather than the dissolution time.

BEST DOCUMENT AVAILABLE

5. Changing the ratio of T/S from 1 to 10 never produces a shift in the T-axis intercept of a contour of more than a factor of three, with the one exception of the Group 2 results when $T < 10^3$ years. The t_d axis intercepts are independent of T/S.

The following are the main results of the uncertainty sensitivity analysis:

1. When the median value of transit time is much less than the median value of dissolution time, removing the uncertainty in dissolution essentially removes the uncertainty in the peak activity rate. The uncertainty in the transit time has no effect on peak activity uncertainty.

2. The relative effects of dissolution and transit-time uncertainty on peak-activity-rate uncertainty are interchanged from Item 1, when the median value of dissolution time is less than the median value of transit time.

3. When the median values of the two times are the same, the relative impact of their uncertainties is a function of the ratio of T/S. When T/S is near one, reducing the uncertainty of either of the two times reduces the uncertainty in the peak activity rate by equal amounts. When T/S is large, reducing uncertainty in dissolution time has a greater impact than reducing uncertainty of transit time, although the difference is less pronounced for larger values of median transit time.

4. Decay has the effect of increasing the uncertainty in peak activity rate when either median transit or dissolution time is greater than or equal to the half-life of any important species in the waste. Decay has the effect of increasing the importance of transit-time uncertainty over dissolution time uncertainty. The effect becomes more important for larger-median transit times.

5. Variations in the ratio T/S do not have any significant effect on the high-activity portion distributions for peak flux, but can have a significant effect on the low-activity part when the median transit time is comparable to the half-life of an important species.

6. The degree to which the hazard curves vary as a function of time determines the relative importance of uncertainty in inventory or in different nuclide groups.

6. PROBABILISTIC CONSEQUENCE ANALYSIS OF WASTE ISOLATION SYSTEMS

This section presents uncertainty analyses of the long-term performance of hypothetical waste isolation systems for scenarios where the repository has been degraded substantially. Compared to the nominal performance of a repository, these are severe scenarios, characterized by water flow through the repository layer into an overlying aquifer that leads to the biosphere.

Subsection 6.2 describes the subsystem models and the aggregation of these models into an overall system model. Subsection 6.3 presents the input data used in the subsystem and system analyses of a hypothetical bedded salt repository. Subsection 6.4 compares the performances of the separate subsystems and the complete system, and Subsection 6.5 presents the uncertainty sensitivity analysis of the system.

Subsection 6.6 presents probabilistic analyses for SYNROC and glass forms of high-level waste, and Subsection 6.7 presents a more limited analysis of differences between repositories in bedded salt and basalt. Subsection 6.8 presents an analysis of selected problems, demonstrating the use of the parametric tables from Section 5.

6.1 PURPOSE AND METHOD OF ANALYSIS

Emphasis was placed on analyzing a hypothetical repository for spent fuel constructed in bedded salt. Less detailed analyses consider high-level waste in glass and SYNROC forms, and a repository in basalt. The waste isolation systems were represented by three subsystem models, combined to constitute the system model. These subsystem models were the waste form and package, repository site, and regional subsystem models.

The major reason for analyzing a bedded salt repository was to investigate the contribution of:

- Each subsystem to reducing the peak release rate of radionuclides to the biosphere.
- Subsystem model parameters to the uncertainty in the performance of each subsystem.
- Subsystem model parameters to the uncertainty in the performance of the overall system.

All of the analyses in this section assume scenarios with the repository site subsystem degraded substantially below a nominal performance level. That is, the site probably would not be a viable candidate if it were known that it would perform in this state following repository closure. Thus, the system is in a failed state.

The repository site subsystem model is used to represent a vertical sequence of rock types that contains the repository layers and acts as a barrier between a lower and an upper aquifer. The barrier layers of salt are assumed to be severely fractured, possibly as a result of earthquakes. Assuming that the repository site subsystem is in a failed state, we investigate how much it still contributes to the performance of the system, and how much the waste form and package and the regional subsystems are able to mitigate the consequences of such a failure.

This analysis does not consider the probability that the repository site would ever be in a state characterized by the parameter distributions used in this analysis. Conclusions are made about the relative importance of the uncertain parameters that characterize the waste form and package, the repository site and the regional transport system. However, these conclusions may not apply if the scenario has a very low probability.

In the bedded salt repository analysis, the performance of each subsystem is assessed by assuming an instantaneous input of the complete waste inventory to the subsystem and computing the probability distributions of peak values (over time) of the resulting rates of radionuclide releases from the subsystem.

Such analysis of the repository site subsystem or the regional subsystem is equivalent to assuming no waste holdup by the waste form and instantaneous transport through the regional subsystem or repository site subsystem, respectively. Such analysis of the waste form and package subsystem is equivalent to assuming instantaneous transport to the biosphere after radionuclides are released into the repository water.

There are two major advantages in performing separate subsystem analyses in addition to overall system analysis. Some radionuclides are effectively contained by more than one subsystem. For example, the peak release rate for the fission products group (excluding Tc and I) is effectively controlled by each subsystem. Such redundancy is one approach to improving the overall

functional reliability of a system. However, one important caveat applies to this analysis. Apparent redundancies do not necessarily exist if there are dependencies between subsystems. All three subsystems are essentially assumed to be independent in this analysis. The assumption is violated to some degree in reality, since the three abstract subsystems extracted for this analysis are interrelated in a real physical system.

The second advantage of performing subsystem analyses is to reduce the number of uncertain variables in the analysis of the aggregated system. Uncertainty sensitivity analyses of the subsystems models identified several variables whose uncertainty had no effect on the uncertainty in subsystem performance. These variables were set to a certain value for the aggregated systems analysis.

6.2 SYSTEM MODEL DESCRIPTION

The system model is briefly described here, primarily to summarize the flow of variable values between subsystem models and define the model inputs to MACRO. Section 2 presents a more detailed description of the physical systems represented by these models and discusses the model approximations and assumptions.

The system model represents a physical situation where water is flowing from a lower to upper aquifer through a repository. The series pathway model used to represent this situation is depicted in Fig. 6-1.

The repository site subsystem model consists of Pathway Segments 2 and 3, which connect the two aquifers. Segment 2 is used to represent flow through the fractures associated with a shaft while Segment 3 represents fracture flow from the lower aquifer to the repository.

The waste form and package subsystem is depicted by the circle at the intersection of Flow Path Segments 2 and 3. This model provides the waste input term into the repository site subsystem model.

The regional subsystem model consists of Pathway Segment 1, representing an aquifer flowing to a release point.

The waste form subsystem model does not contain any internal structure (i.e., the output of this model is directly specified). It is not computed by a mathematical model. The release of radionuclides to Pathway Segment 2 is

BEST DOCUMENT AVAILABLE

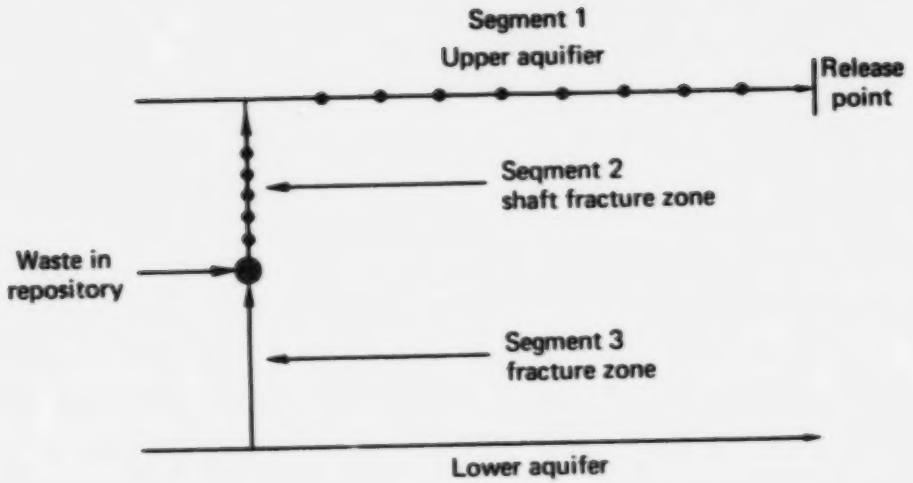

FIG. 6-1. Waste isolation system flow path model.

modeled as a square-wave release of the complete waste inventory, starting at time t_0 (initial release time) and persisting for time t_d (dissolution time). These parameters are specified for each radionuclide group with the superscript denoting the group:

t_0^1, t_0^2, t_0^3 = initial release time,

t_d^1, t_d^2, t_d^3 = dissolution times.

In addition, the type of waste inventory must be specified as either high-level waste or spent fuel. Also, the quantity of energy generated in producing the waste (MWe•yr) must be given. Radionuclide activity tables for each type of waste reside within the MACRO code. These are summarized in Tables 4-1 and 4-2.

The repository site subsystem model uses D'Arcy's Law (with retardation factors for Group-2 and -3 radionuclides) to compute the parameters for the Green's functions [see Eq. (2-37) in Section 2] of Pathway Segment 2. The waste particle velocity for radionuclide Group i in pathway Segment 2 is computed as:

$$u_2^i = \frac{Q_2}{A_2 \Theta_2 B_2^i} \qquad (6\text{-}1)$$

where

u_2^i = Group i velocity (m/yr),

Q_2 = water flow (m^3/yr),

A_2 = area of Segment 2 (m^2),

Θ_2 = effective porosity in Segment 2,

B_2^i = retardation factor for Group i in Segment 2.

Computing Q_2 using D'Arcy's Law,

$$Q_2 = \frac{\Delta H}{\frac{L_2}{A_2 K_2} + \frac{L_3}{A_3 K_3}}$$

BEST DOCUMENT AVAILABL

and substituting this expression into Eq. (6-1) gives,

$$u_2^i = \frac{\Delta H}{\frac{L_2}{K_2} + \frac{L_3 A_2}{K_3 A_3}\,\theta_2 B_2^i}\,, \qquad (6\text{-}2)$$

where

ΔH = head difference between the aquifers (m),

L_2 = length of Segment 2 (m),

L_3 = length of Segment 3 (m),

A_2 = area of the fractured zone below the repository (m^2),

A_3 = area of the fractured zone associated with the sealed shaft (m^3),

K_2 = hydraulic conductivity in Segment 2 (m/yr),

K_3 = hydraulic conductivity in Segment 3 (m/yr).

The output variables of the repository site subsystem model are the mean transit time (first time moment of the waste pulse) and the variance of the transit time (second central time moment of the pulse) for each radionuclide:

T_2^i = first moment of transit time for the waste pulse of the output of Segment 2, for radionuclide Group i.

S_2^i = square root of the second central moment of transit time for the waste pulse at the output of Segment 2, for radionuclide Group i.

These are computed from the velocities given by Eq. (6-2) as:

$$T_2^i = L_2/u_2^i\,, \qquad (6\text{-}3)$$

$$S_2^i = \sqrt{2\alpha_2 L_2}/u_2^i = T_2^i\sqrt{2\alpha_2/L_2}\,, \qquad (6\text{-}4)$$

where

α_2 = dispersivity (m) in Segment 2.

BEST DOCUMENT AVAILABLE

The input data to the regional subsystem model are the real velocity for water, the effective longitudinal dispersivity, and the retardation factors. The subsystem output variables are T and S for Path Segment 1, computed as:

$$T_1^i = L_1 B_1^i / u_1 \tag{6-5}$$

$$S_1^i = 2\alpha_1 L_1 B_1^i / u_1 = T_1^i \; 2\alpha_1 / L_1 \tag{6-6}$$

where

L_1 = length of upper aquifer (m),

B_1^i = retardation factor for Group-i radionuclides in the upper aquifer,

u_1 = water velocity in upper aquifer (m/yr),

α_1 = effective longitudinal dispersivity in the upper aquifer (m).

Figure 6-2 presents the system model that combines the output of each subsystem model to compute the peak release rate for each radionuclide. T and S from the repository site and regional subsystem models are summed by adding T's and the squares of the S's (see Section 2) to give T and S for each nuclide group for the total series system. The initial release time, dissolution time, and T and S for the system are input to the model. The model computes the time and magnitude of the waste flux, when the waste flux out of the upper aquifer is at a maximum.

The time and magnitude of the peak waste flux (t_p^i, j_p^i), and type and quantity of initial waste inventory are input to the final model to compute the peak rate of radionuclide activity release from the upper aquifer. The peak flux and peak-activity-release-rate models are described in Subsection 2.6.

Each subsystem's performance is investigated by setting the output time parameters (t_0^i, t_d^i, T_1^i, S_1^i, T_2^i, S_2^i) of the other two subsystems at a very small value or at zero. The initial release times (t_0^i) for the waste form subsystem are set at 50 yr (when analyzing the other subsystems) to represent the age of the waste at the time of repository closure.

BEST DOCUMENT AVAILABLE

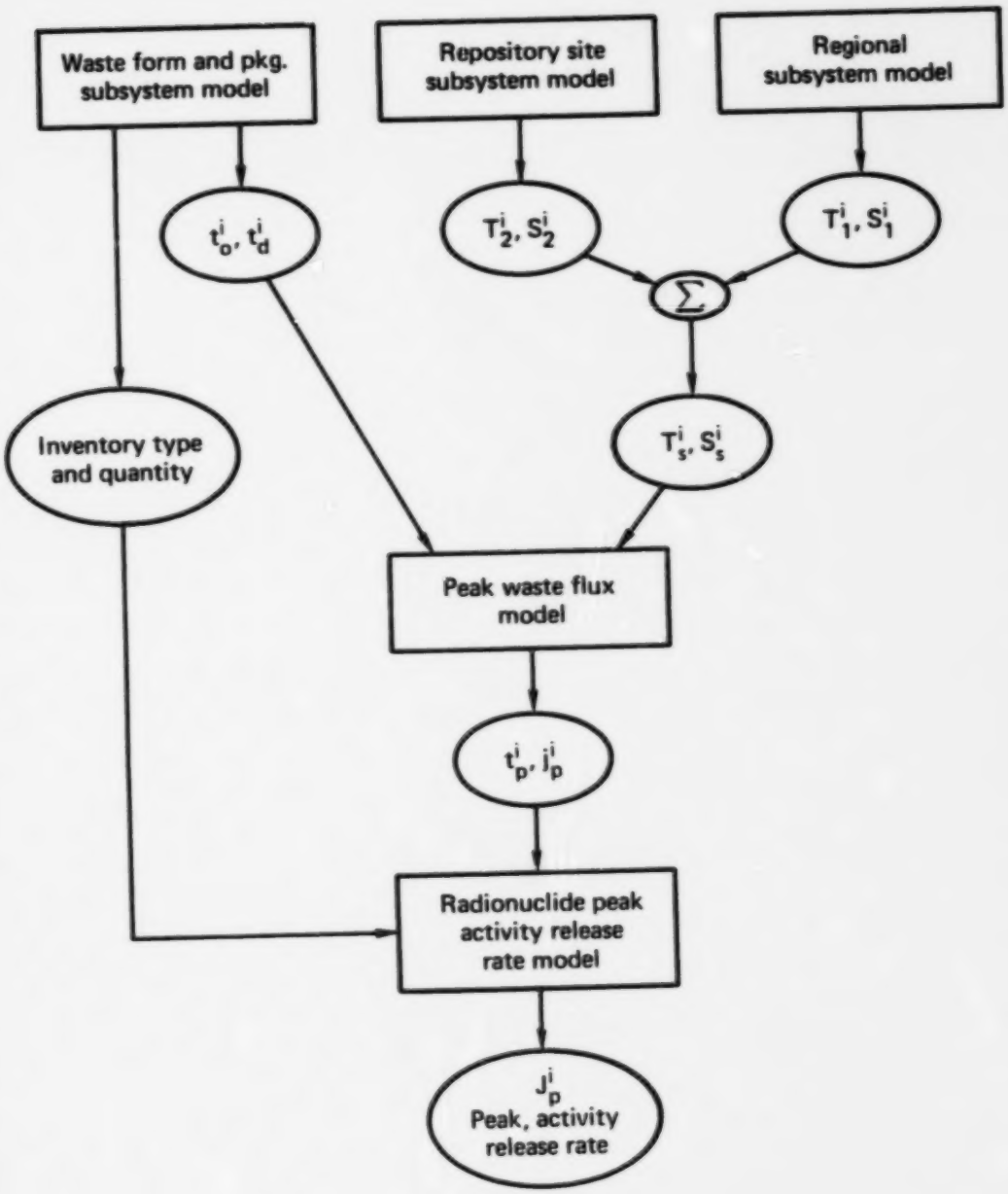

FIG. 6-2. Aggregated system model for series system analysis.

BEST DOCUMENT AVAILABLE

6.3 MACRO INPUT DATA

This subsection tabulates the data input to MACRO for the analysis of spent fuel in a bedded salt repository. The bases for the data are presented and discussed in Section 4. Specific data were changed for cases representing high-level waste in glass, SYNROC, and host-rock media other than bedded salt. These data are presented with those cases in later subsections.

Tables 6-1, 6-2 and 6-3 present data for each of the three subsystem models. All uncertain variables were input as truncated lognormal

TABLE 6-1. Input data for waste form subsystem model (yr).

Variable	Median 50th percentile	Low 1st percentile	High 99th percentile
t_0 (initial release time[a])	5.0×10^2	5.0×10^1	5.0×10^3
t_d^1 (dissolution time of Group 1)	5.0×10^3	1.0×10^3	2.5×10^4
t_d^2 (dissolution time of Group 2)	5.0×10^3	1.0×10^3	2.5×10^4
t_d^3 (dissolution time of Group 3)	1.0×10^5	1.0×10^4	1.0×10^6
Waste inventory	Spent fuel, 1.0×10^6 MWe•yr of waste		

[a]Initial release time is identical for all three radionuclide groups.

BEST DOCUMENT AVAILABLE

TABLE 6-2. Input data for repository subsystem model.

Variable	Median 50th percentile	Low 1st percentile	High 99th percentile
Head difference between aquifers:			
ΔH (m)	1.0×10^{1}	Certain variable	
Segment 2:			
Length L_2 (m)	1.2×10^{3}	Certain variable	
Area A_2 (m^2)	1.0×10^{2}	1.0×10^{1}	1.0×10^{3}
Conductivity K_2 (m/yr)	1.0×10^{-1}	1.0×10^{-2}	1.0
Dispersivity α_2 (m)	5.0×10^{1}	Certain variable	
Effective porosity θ^2	1.0×10^{-3}	2.0×10^{-4}	5.0×10^{-3}
Retardation fission products B_2^2	1.0×10^{1}	1.0[a]	1.0×10^{2}
Retardation actinides B_2^3	1.0×10^{2}	1.0×10^{1}	1.0×10^{3}
Segment 3:			
Length L_3 (m)	3.0×10^{2}	Certain variable	
Area A_3 (m^2)	1.0×10^{4}	1.0×10^{3}	1.0×10^{5}
Conductivity K_3 (m/yr)	1.0×10^{-1}	1.0×10^{-2}	1.0
System characteristics (computed using median values):			
First moment of transit time T_2 = 1440 yr			
Square root of second central moment of transit time S_2 = 415 yr.			

[a]Truncated lognormal distribution with minimum value of 1.0.

BEST DOCUMENT AVAILABLE

distributions. The distribution parameters were assigned so that the 1st, 50th, and 99th percentile values of the continuous lognormal distribution would equal those in the tables. The MACRO code converts the continuous lognormal distribution into a finite probability distribution (FPD) for discrete random variables (see Subsection 3.2). The FPD's were each truncated at the variable values $e^{\mu-3\sigma}$ and $e^{\mu+3\sigma}$, where μ is the mean of the natural log of the variable and σ is its standard deviation. These correspond to the 0.13-percentile and 99.87-percentile values of the continuous distributions. The

TABLE 6-3. Input data for regional subsystem model.

Variable	Median 50th percentile	Low 1st percentile	High 99th percentile
Aquifer length L_1 (m)	1.0×10^4	Certain variable	
Water velocity u_1 (m/yr)	2.0	2.0×10^{-1}	2.0×10^1
Effective longitudinal dispersivity α_1 (m)	2.0×10^3	4.0×10^2	1.0×10^4
Fission product retardation factor B_1^2	1.0×10^2	1.0×10^1	1.0×10^3
Actinide retardation factor B_1^3	1.0×10^3	1.0×10^2	1.0×10^4

Systems characteristics (computed using median values):

First moment of transit time T_1 = 5000 yr

Square root of second central moment of transit time, S_1 = 3162 yr.

BEST DOCUMENT AVAILABLE

FPD is renormalized to this closed interval. All FPDs for input parameters have 19 points. This number is set by the code user.

6.4 SUBSYSTEM CONTRIBUTIONS TO SYSTEM PERFORMANCE

This subsection presents our analysis of the waste isolation system model to determine the individual contribution of each subsystem to reducing the peak rate of release of radionuclides into the biosphere. The entire analysis assumes that the salt and shale layers have been degraded by fractures to allow substantial flow through the repository. Each subsystem contributes to the performance of the total system by delaying the transport of radionuclides into the biosphere and spreading their release over time. The delay allows radionuclides to decay, while spreading reduces the peak and average values of waste release rates. The major observations of this analysis are summarized at the end of this subsection.

We investigated the performance of each separate subsystem by assuming that the other subsystems do not retard the transport of radionuclides. Combinations included pairs of subsystems as well as all three subsystems. These analyses show the marginal improvement or detriment from the addition or loss of function of each subsystem, under the assumed degraded conditions of the repository site subsystem.

For the cases that combined two or three subsystem models, we assumed independence between subsystems. The random variables input to each subsystem model were assumed to be independent and were input to MACRO as marginal distributions.

This assumed independence may not apply in some important situations. For example, the hydraulic conductivities in Flow Segments 2 and 3 may be probabilistically dependent. Mathematically stated, the conditional probability density of the hydraulic conductivity in Segment 2, given the hydraulic conductivity in Segment 3, $g(K_2|K_3)$ is not equal to the unconditional probability density, $f(K_2)$.

No correct general statement can be made about the effect of ignoring dependencies between the model input variables. The question is, "Does the independence assumption shift particular percentiles (or the mean value) up or down relative to percentiles computed using a more accurate representation of dependencies?"

The bar graphs in Fig. 6-3 characterize the probability distributions of the peak release rates for each combination of subsystems. The horizontal bars on each bar graph represent the 1st, 25th, 50th, 75th, and 99th percentile values of the probability distributions, and the square represents the mean value of the peak release rate.

The first three cases in Fig. 6-3 were computed with the MACRO code input data presented in Subsection 6.3. Cases 1, 2, and 3 analyzed single subsystem models for the waste form and package, repository site, and regional subsystem models, respectively. The results from the uncertainty sensitivity analyses presented in Subsection 6.5 were the bases for setting some model input variables to a certain value, when the subsystems were combined. Subsystem input variables were set at their median values if the 99th percentile of the peak release rates were not sensitive to the uncertainty in the variables. This reduced the number of uncertain variables in the aggregated systems model, which in turn reduced the computation time. The sensitivity analyses in Subsection 6.5 indicate which variables were uncertain in each of the aggregated system analyses.

The remainder of this subsection discusses the results displayed in Fig. 6-3. We consider the results for each radionuclide group and present reasons for the major differences between the performance of subsystems.

The results of Cases 1, 2, and 3 in Fig. 6-3 indicate that for the assumed, degraded state of the repository site subsystem, the waste form and package is the most effective subsystem in reducing the peak release rate of radioactive Tc and I. The performance of the aquifer (constituting the regional subsystem) is slightly worse than the performance of the waste form from the viewpoint of the 50th, 75th, and 99th percentiles. However, the 25th and 1st percentiles of the aquifer alone are slightly smaller (better) than for the waste form. The vertical path, representing the repository site subsystem, is the least effective subsystem with the 99th percentile over an order of magnitude greater than for the waste form subsystem case.

These results can be explained using the graph of activity versus time for Tc and I (Fig. 5-16). Tc dominates the combined activity of Tc and I for about 10^6 yr. Tc activity is essentially constant for about 10^5 yr. Therefore, if Tc is released before this break in the curve, the spreading of the pulse time is the primary mechanism of reducing the peak release rates. The approximate median values of T^1 and S^1 for the vertical path are

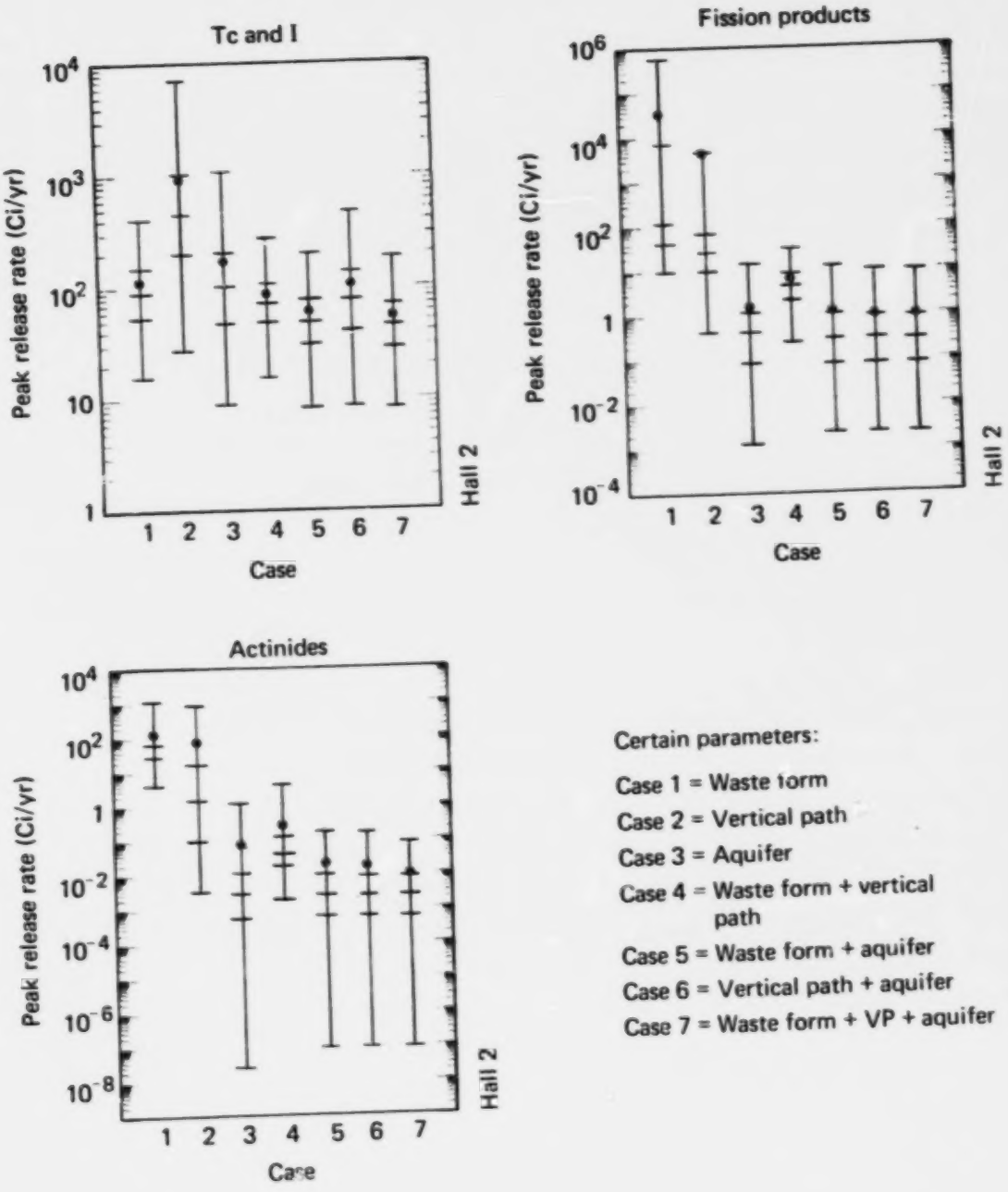

FIG. 6-3. Comparison of the probability distributions for the peak release rates of separate subsystems and aggregated subsystems.

BEST DOCUMENT AVAILABLE

T_2^1 = 1440 yr and S_2^1 = 415 yr, and for the aquifer T_1^1 = 5000 yr and S_1^1 = 3162 yr. This result indicates that the primary reason the aquifer performs better is the larger spreading of the waste pulse. The median values of the waste form parameters result in a square pulse release between 500 and 5500 yr. Again, the greater temporal spread of the pulse is primarily responsible for the relatively better performance of the waste form compared to the other two subsystems.

The Tc and I results provide a good example of how the conclusions depend on the data. For example, suppose that the probability distribution for the effective porosity in Flow Segment 2, θ_2, was shifted by a factor of 10; i.e., the median value is increased from 10^{-3} - 10^{-2}. By Eqs. (6-2), (6-3), and (6-4), it can be shown that the approximate median value of S_2^1 increases from 415 to 4150 yr. In this case, the performance of the repository site subsystem would be better than the aquifer performance.

Cases 4, 5, and 6 for Tc and I indicate that the combined pairs of subsystems perform better than any individual subsystem; i.e., the 99th and 1st percentiles are about equal to or smaller than the same percentiles for either single subsystem. As expected, there are no large synergistic effects from combining subsystems. A comparison of Cases 4, 5, and 6 to Case 7 indicates some system redundancy. That is, the complete failure of any one subsystem does not increase the 99th percentile of the peak release rate by more than a factor of 2 to 3.

The bar graphs for the peak release rates of the fission product activity (other than Tc and I) indicate that the aquifer is substantially superior to the waste form and package or the vertical path (repository site subsystem) in reducing the peak rate of release. This is explained by examining the activity-vs-time curve for fission products (Fig. 5-16). The delay of the waste pulse in the aquifer results in a high probability of the peak arriving during the flat portion of the activity curve (500-10^6 yr), or beyond the knee located between 10^6 and 10^7 yr. The median values for the waste pulse parameters of the fission products in the aquifer are $T_1^2 = 5.0 \times 10^5$ yr, and $S_1^2 = 3.1 \times 10^5$ yr. However, for both the waste form and the vertical path, there is a significant probability that the peak arrives during the rapid drop-off of the activity curve, between 100 and 500 yrs. This large slope of the activity curve is responsible for the skewness of the probability distributions for Cases 1 and 2. Note the large spread from the 50th-99th

percentile for Case 1. Note also that the mean is greater than the 99th percentile for Case 2. If the median dissolution times were increased by an order of magnitude, then the probability of releasing Cs and Sr (which dominate the early activity) during the first 500 yrs would be very small. Thus, the 99th percentile and mean would be substantially reduced.

Case 4 combines the waste form and the vertical path, resulting in a system performance substantially better than either subsystem. The combined transit time shifts the release peak into the flat portion of the activity curve, reducing the 99th percentile by two orders of magnitude. However, the first percentile is not reduced significantly, indicating that the probability of the peak occurring beyond the second activity knee (10^6 yr) is small.

Cases 5, 6, and 7 indicate that the performance of systems containing the aquifer and one or both of the other subsystems is not substantially better than for the aquifer alone, because of the relatively large values of the aquifer transit time. Comparisons between Cases 4, 5, 6, and 7 indicate that the overall system performance at the 99th percentile is insensitive to the complete failure of a single system, while the first percentile is sensitive to the failure of the aquifer.

The waste isolation system is relatively more effective at reducing the peak release rate of the fission products (other than Tc and I) than it is at reducing the rate of release for Tc and I. The 99th percentile of the release rate is nine orders of magnitude lower than the initial activity. The retardation of fission products in the aquifer delays their arrival to the biosphere until after the initial inventory decays by about five orders of magnitude. Since dispersion is proportional to transit time, the retardation of fission products also causes their increased dispersion over time, reducing the peak proportionately.

It is noted that the first percentile for the aquifer subsystem (Case 3) is less than the first percentile for any combination of the aquifer with other subsystems. This was caused by setting the dispersivity of the aquifer model to a certain value (the median) for Cases 5, 6, and 7. The dispersivity was set to a certain value on the basis of its very small effect on the 99th percentile, from the Case 3 uncertainty sensitivity analysis. This also caused the first percentile of Case 3 to be less than the first percentile of Cases 5, 6, and 7 for the actinide group.

The relative effects of the subsystems on the actinides are very similar to their effects on the fission products. The aquifer is also the most

effective subsystem for reducing the peak release rate of the actinides. The peak release rate for the aquifer subsystem (Case 3) has a 99th percentile, which is five orders of magnitude less than for the waste form or vertical path subsystems (Cases 1 and 2).

The waste form performs better in reducing the 99th percentile of the peak release rate of the actinides than it did in reducing the 99th percentile of the peak release rate of the fission products. This is due to an increase in the median of the input probability distribution for waste dissolution times. The median value for the waste dissolution time was 5.0×10^3 yr for fission products and 1.0×10^5 yr for actinides. Both fission product and actinide dissolution times allow for substantial decay of radionuclides; however, the spread of the waste pulse is greater for actinides.

The combined waste form and vertical path subsystems (Case 4) increase the transit time sufficiently to allow significant decay of the actinides (Fig. 5-19). Again, the performance of the combined systems is significantly better than either subsystem (on the basis of the mean and the 99th percentile). Cases 5 and 6 indicate that adding the waste form and the vertical path subsystems to the aquifer does not improve the performance substantially over that of the aquifer by itself (Case 3).

Comparing Case 7 with Cases 3 and 4 indicates that there is some redundancy in the system for this scenario. Complete failure of only the aquifer, or of only the vertical path and the waste form, results in about the same performance as the complete system (Case 7) based on mean values or 99th percentiles.

To summarize the results of the subsystem and system performance analysis: the waste form and package subsystem is the most effective in reducing the peak release rate of technetium and iodine; the aquifer is the most effective in reducing the peak release rate of the fission products and actinides. It is not surprising that the vertical path does not dominate the performance of the system for any radionuclide group, since we assumed a scenario where the integrity of the host media is compromised by fractures.

For technetium and iodine, any combination of one, two, or all three subsystems (except the vertical path alone) produces distributions with their percentiles and mean values within an order-of-magnitude range.

For fission products and the actinides, any combination of two subsystems or the aquifer alone produces distributions with the 50th, 75th, and 99th

percentiles within an order-of-magnitude range. The waste form or vertical path alone reduces the peak release rates several orders of magnitude over a release of the inventory at its maximum activity level.

The waste form does not perform as well in reducing the fission-product release rate as it does with the actinide release rate, primarily due to the shorter dissolution times for fission products. (The shorter time was used to represent the migration of fission products to the surface of spent fuel pellets during irradiation.)

6.5 UNCERTAINTY SENSITIVITY ANALYSIS

This subsection presents the results of a sensitivity analysis to determine which model parameter uncertainties have the greatest effect on the uncertainties in the outcomes. The method applied here is described in more detail in Subsection 3.1, which also identifies limitations of this approach.

An uncertainty sensitivity analysis was performed for each separate subsystem by setting each uncertain parameter for the single subsystem model at its median value one parameter at a time. If a parameter's uncertainty had only a small effect on the probability distribution of subsystem performance, then it was set certain at its median value in the analysis of the complete system.

Subsection 6.5.1 presents the uncertainty sensitivity analysis of the complete system model. The complete system model is composed of the waste form and package, repository site, and regional subsystem models. Subsections 6.5.2 through 6.5.4 present the analysis of single subsystems, and Subsection 6.5.5 presents the analysis of pairs of subsystems. The results of the uncertainty sensitivity analyses are summarized in Subsection 6.5.6.

6.5.1 Complete System

The results of the uncertainty sensitivity analysis for the complete system (comprising the waste form, repository site, and regional subsystems) are presented in Fig. 6-4. Case 1 is the base uncertainty case. The probability distributions of the peak release rates were computed with the parameter probability distributions given in Table 6-4. For each subsequent case (2 through 6), one parameter was input as certain and equal to its median value.

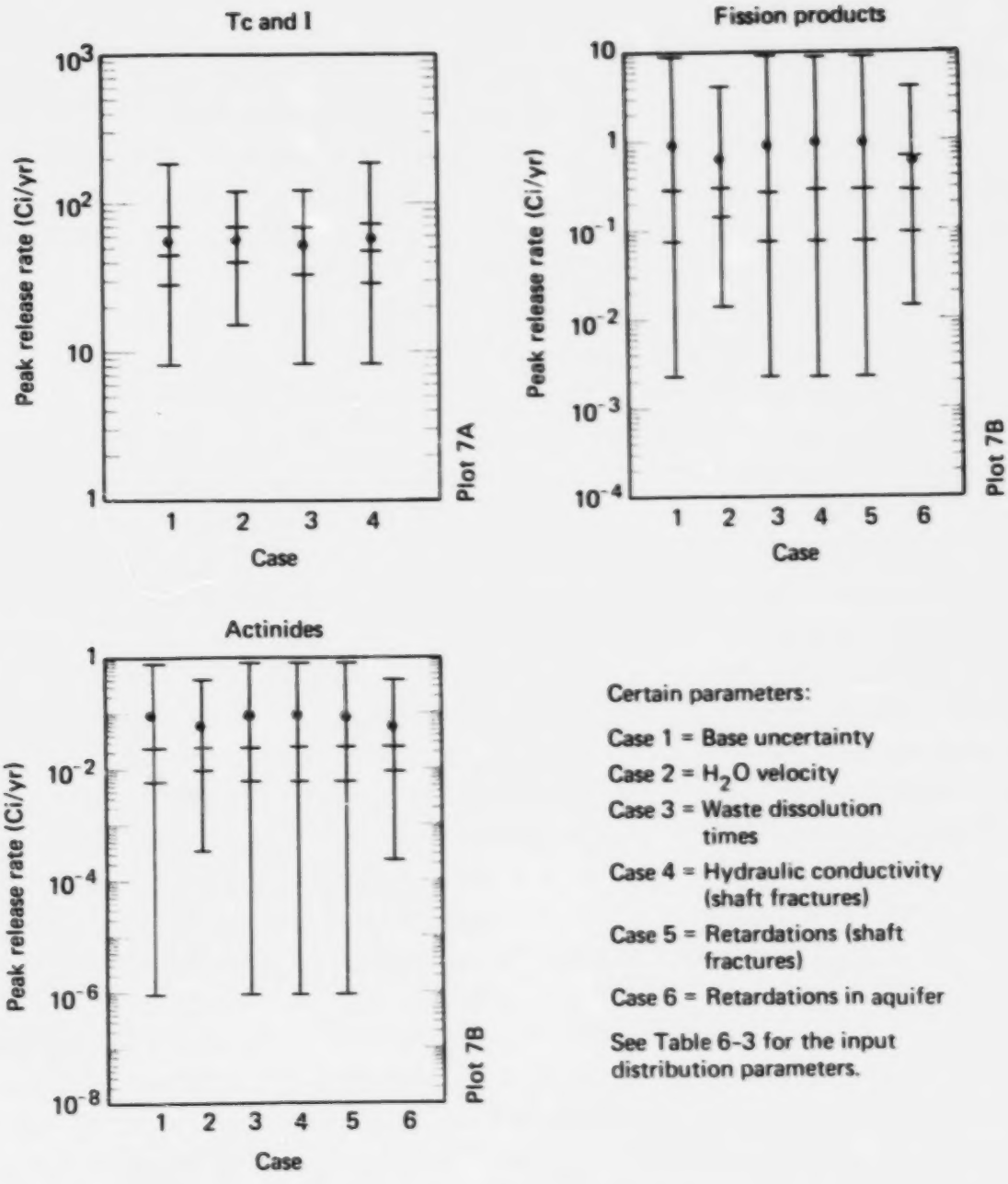

Certain parameters:

Case 1 = Base uncertainty

Case 2 = H_2O velocity

Case 3 = Waste dissolution times

Case 4 = Hydraulic conductivity (shaft fractures)

Case 5 = Retardations (shaft fractures)

Case 6 = Retardations in aquifer

See Table 6-3 for the input distribution parameters.

Horizontal bars represent the 1st, 25th, 50th, 75th and 90th percentiles.
*represents the mean value.

FIG. 6-4. Uncertainty sensitivity analysis of the complete system.

BEST DOCUMENT AVAILABLE

TABLE 6-4. Uncertain parameters for the complete waste system uncertainty sensitivity analysis (Fig. 6-4).[a,b]

Parameter	Percentile			Certain parameter for case number
	50th	1st	99th	
Water velocity (m/yr)	2.0	2.0×10^{-1}	2.0×10^{1}	2
Dissolution times (yr):				
Groups 1 and 2	5.0×10^{3}	1.0×10^{3}	2.5×10^{4}	3
Group 3	1.0×10^{5}	1.0×10^{4}	1.0×10^{6}	3
Conductivity of shafts and tunnels (m/yr)	1.0×10^{-1}	1.0×10^{-2}	1.0	4
Retardations in shafts and tunnels:				
Fission products	1.0×10^{1}	1.0[c]	1.0×10^{2}	5
Actinides	1.0×10^{2}	1.0×10^{1}	1.0×10^{3}	5
Retardations in aquifer:				
Fission products	1.0×10^{2}	1.0×10^{1}	1.0×10^{3}	6
Actinides	1.0×10^{3}	1.0×10^{2}	1.0×10^{4}	6

[a]All parameter uncertainties are represented with truncated lognormal probability distributions.

[b]All other model parameters were certain, using the median values given in Tables 6-1, 6-2, and 6-3.

[c]Minimum value of 1.0.

BEST DOCUMENT AVAILABLE

Cases 4 and 5 show that the system performance uncertainty is not sensitive to setting the repository site parameters certain at their median values. This is due to the relatively small values of T (transit time) and S (spread) for the vertical path, as compared to the values for the aquifer (see Table 6-5).

The velocity of water in the aquifer and the fission product and actinide retardations (Cases 2 and 6), had the greatest effect on the outcome distributions when each was set to a certain value.

Uncertainty in the waste form dissolution time (Case 3) affected the Tc and I outcome distribution, but had little effect on the peak release rates of the fission products and the actinides. This result is obtained because Group 3 is the only group for which the dissolution time is comparable to the transit time (see Table 6-5).

Setting the water velocity or the actinide retardation in the aquifer to their median values has a nonsymmetric effect on the outcome distributions for actinides. The log of the 1st percentile increases much more than the log of the 99th percentile decreases. Figure 5-19 shows that this is caused by the rapid drop-off of the actinide activity curve near 1.0×10^7 yr. The median value of T is 5×10^6 yr, which is near this knee of the curve.

TABLE 6-5. Median values of the model parameters for the complete system analysis (yr).

	Aquifer		Vertical path		Waste form	
Radionuclide group i	T_1^i	S_1^i	T_2^i	S_2^i	t_0^i	$t_0^i + t_d^i$
Tc and I	5.0×10^3	3.2×10^3	1.4×10^3	4.1×10^2	500	5.5×10^3
Fission products	5.0×10^5	3.2×10^5	1.4×10^5	4.1×10^4	500	5.5×10^3
Actinides	5.0×10^6	3.2×10^6	1.4×10^6	4.1×10^5	500	5.0×10^5

BEST DOCUMENT AVAILABLE

In summary, when set to the median values, the parameters with the greatest effect on the probability distributions of the peak release rates were:

- Water velocity in the aquifer (Groups 1, 2, and 3),
- Waste form dissolution time (Group 1),
- Waste particle retardations in the aquifer (Groups 2 and 3).

The group numbers in parentheses indicate the groups affected by the parameter.

Uncertainties about the vertical pathway input variables have little effect on system uncertainty, because system performance is dominated by the waste form subsystem for Tc and I, and by the regional subsystem for the other fission products and the actinides (see Fig. 6-3). Again, this may be expected since the distributions for the vertical path parameters were selected to represent compromised repository barrier layers.

It is important to note the possible effects of using different probability distributions in the analysis. If the vertical hydraulic conductivity used in Segment 2 were decreased, the vertical path could then dominate the system performance. For example, if the distribution of K_2 was shifted by a factor of 0.1 (decreased), the probability distributions for the outcomes would be more sensitive to the other parameters for the vertical path. Decreasing the median of θ_2 by a factor of 0.1 would increase the median values of T_2^i and S_2^i (in Table 6-5) by a factor of 10.

6.5.2 Waste Form and Package

The results of the uncertainty sensitivity analysis of the waste form and package subsystem are presented in Fig. 6-5. The cases were computed with the data in Table 6-6.

Setting the time-of-release initiation (for the waste form and package) to a certain value has the greatest effect on the peak release rate of the fission product group. Case 2 for the fission product graph (Fig. 6-5) shows that the 99th percentile was reduced by three orders of magnitude and the mean was reduced by over two orders of magnitude. This reduction results from setting the release initiation time to 500 yr; thus, the release is certain to occur after the fission products decay to the plateau level of the activity curve (Fig. 5-17).

In Case 2 for the Tc and I group and the actinide group, the uncertainty in the initial release time had little effect on the peak release rate

BEST DOCUMENT AVAILABLE

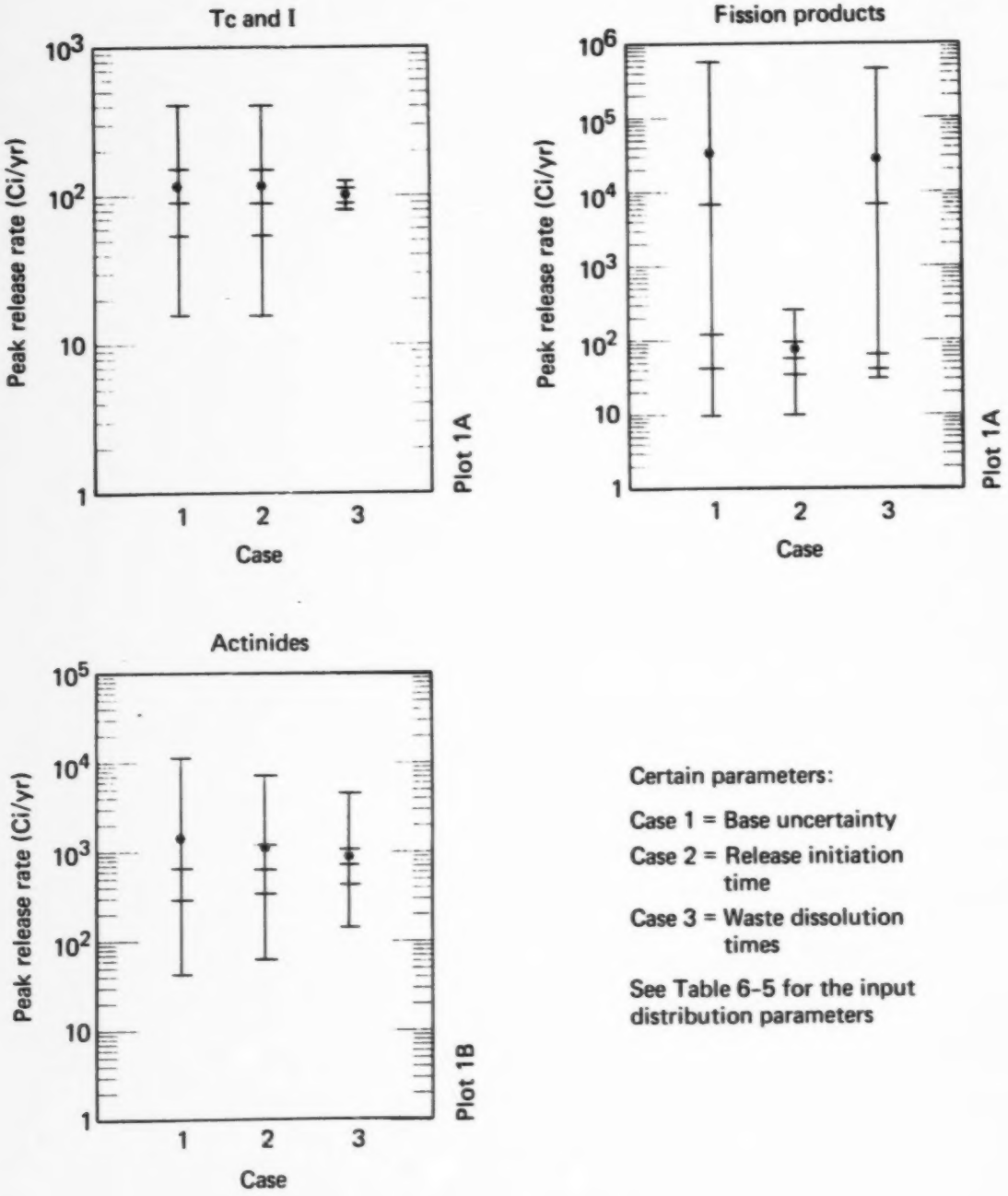

Horizontal bars represent the 1st, 25th, 50th, 75th and 99th percentiles.
*represents the mean value.

FIG. 6-5. Uncertainty sensitivity analysis of the waste form system.

TABLE 6-6. Uncertain parameters for waste form subsystem analysis (Fig. 6-5).

Parameter	Percentile			Certain parameter for case number
	50th	1st	99th	
Initial release time (yr):				
Groups 1, 2, and 3	5.0×10^2	5.0×10^1	5.0×10^3	2
Dissolution time (yr):				
Groups 1 and 2	5.0×10^3	1.0×10^3	2.5×10^4	3
Group 3	1.0×10^5	1.0×10^4	1.0×10^6	3

[a]All uncertainties of parameters are represented with truncated lognormal probability distributions.

distributions. Case 3 shows that the dissolution time changed the percentile and mean values by less than a factor of four.

6.5.3 Repository Site Subsystem (Vertical Path through Repository)

The results of the uncertainty sensitivity analysis for the repository site subsystem are presented in Fig. 6-6. The cases were computed with the data in Table 6-7.

The hydraulic conductivity of the path (associated with the fracture zone around a repository shaft) had the greatest effect of any parameter when it was set certain at its median value (Case 4). The reason is evident from examining the equation for the water velocity in Flow Segment 2:

$$u_2 = \frac{\Delta H}{\left(\frac{L_2}{K_2} + \frac{L_3 A_2}{K_3 A_3}\right)\Theta_2} \qquad (6\text{-}7)$$

BEST DOCUMENT AVAILABLE

BEST DOCUMENT AVAILABLE

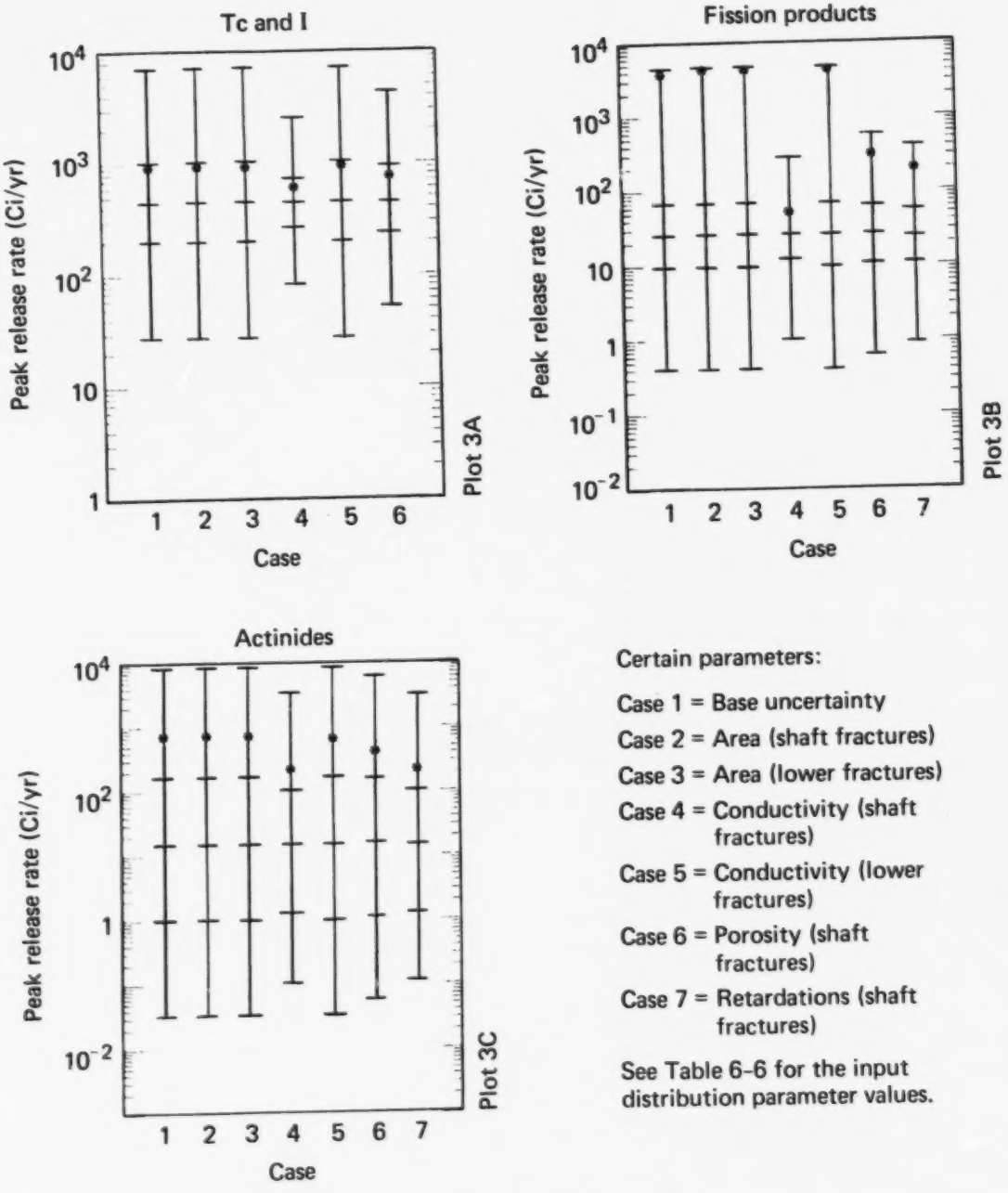

FIG. 6-6. Uncertainty sensitivity analysis of the vertical path through the repository (repository site subsystem).

Using median values for the parameters,

$$u_2 = \frac{10}{(1200 + 30) \cdot 10^{-3}} \qquad (6\text{-}8)$$

we can see that the water velocity is dominated by the term L_2/K_2 (value of 1200), relative to the term L_3A_2/K_3A_3 (value of 30). Thus, changes in the areas A_2 and A_3, and the hydraulic conductivity K_3 have a relatively small effect on u_2. This is due to the relatively large area of the fracture zone below the repository, A_3, compared to the fracture area associated with the shaft, A_2.

TABLE 6-7. Uncertain parameters for repository site subsystem analysis (Fig. 6-6).[a]

Parameter	Percentile			Certain parameter for case number
	50th	1st	99th	
Segment 2:				
Area (m^2)	1.0×10^2	1.0×10^1	1.0×10^3	2
Conductivity (m/yr)	1.0×10^{-1}	1.0×10^{-2}	1.0	4
Porosity	1.0×10^{-3}	1.0×10^{-4}	1.0×10^{-2}	6
Retardations:				
Fission products	1.0×10^1	1.0[b]	1.0×10^2	7
Actinides	1.0×10^2	1.0×10^1	1.0×10^3	7
Segment 3:				
Area (m^2)	1.0×10^4	1.0×10^3	1.0×10^5	3
Conductivity (m/yr)	1.0×10^{-1}	1.0×10^{-2}	1.0	5

[a]All parameter uncertainties represented with truncated lognormal probability distributions.

[b]Distribution truncated at minimum value of 1.0.

BEST DOCUMENT AVAILABLE

The effect of setting K_2 certain is to narrow the probability distribution of u_2 about its median value. This narrows the probability distributions for T_2 and S_2 (the parameters for the waste pulse). The greatest effect is observed for the results of the fission product group. Narrowing the probability distribution of the waste pulse parameters increases the probability that the peak of the pulse arrives well after the initial rapid decay of the fission products.

Equations (6-7) and (6-8) show that the porosity, θ_2, has approximately the same effect on u_2 as the hydraulic conductivity, K_2, if they are changed by equal percentages in opposite directions. For example, a 10% increase in θ_2 has about the same effect on u_2 as a 10% decrease in K_2. Case 6 shows that setting θ_2 certain has a smaller effect than setting K_2 certain (Case 4), because the base case probability distribution of θ_2 is narrower.

Setting the fission product and actinide retardations certain has about the same effect on the outcome distributions as the hydraulic conductivity. This is expected since each parameter has approximately the same effect on the retarded velocity of both radionuclide groups.

To summarize, since a large fracture zone was assumed beneath the repository, the uncertainty about the flow velocity from the waste canisters to the upper aquifer is dominated by uncertainty about the conductivity and porosity of the fracture zone associated with the shafts. The uncertainty in the waste particle velocity is also about equally affected by the uncertainty about retardations through such fracture zones.

6.5.4 Regional Subsystem (Upper Aquifer)

The results of the uncertainty sensitivity analysis for the regional subsystem are presented in Fig. 6-7 and the input data are listed in Table 6-8.

The water velocity and the waste particle retardations have identical effects on the outcome distributions when they are set certain at their median values. This is explained by the form of the mathematical expressions for the waste pulse parameters and by the fact that both parameters have distributions of the same shape. Equations (6-5) and (6-6) show that the expressions for the waste pulse parameters contain products or quotients of these parameters.

The uncertainty in the dispersivity has a relatively minor effect on the uncertainty in the outcomes (compared to the effect of water velocity or waste

BEST DOCUMENT AVAILABLE

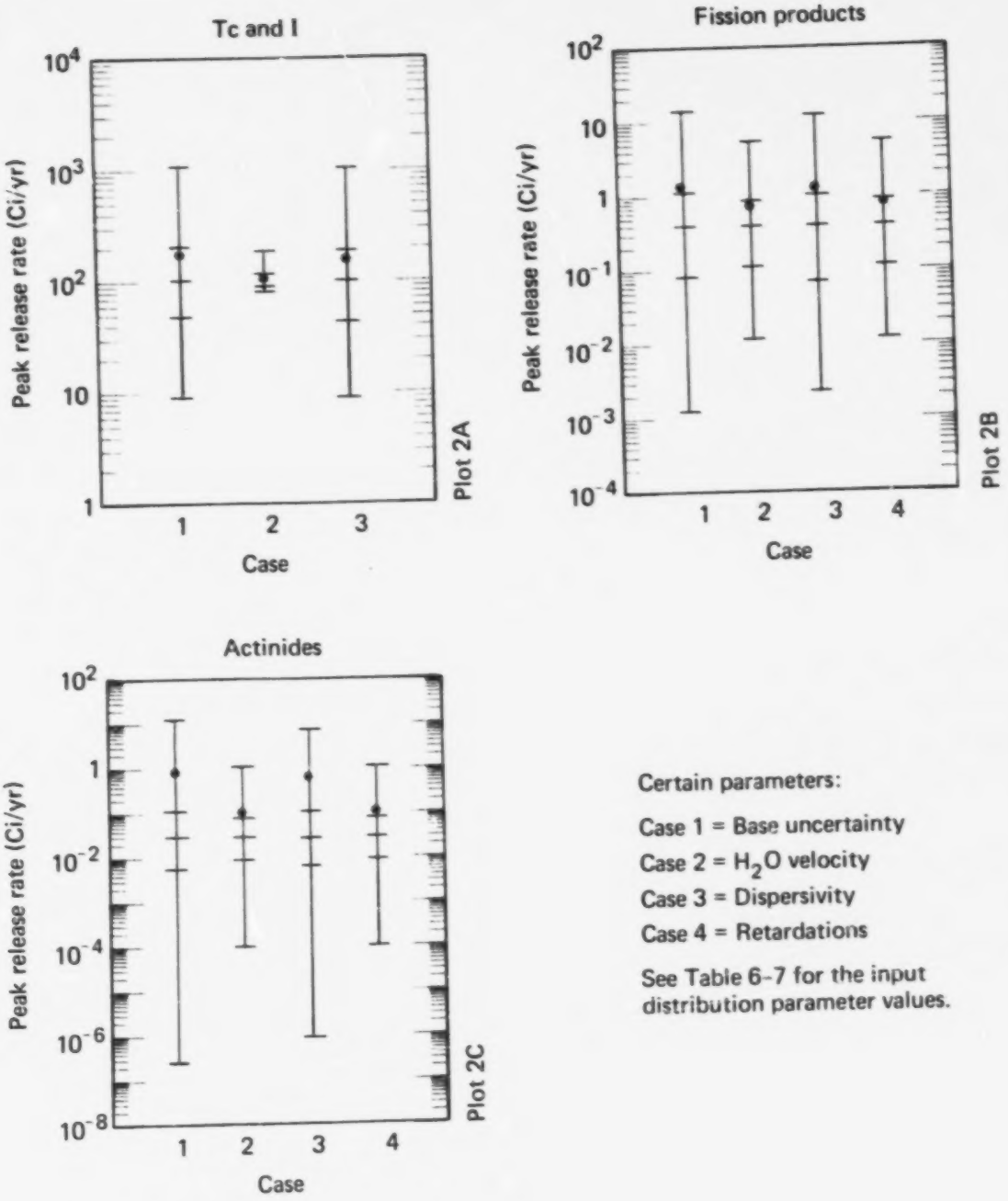

Certain parameters:

Case 1 = Base uncertainty

Case 2 = H_2O velocity

Case 3 = Dispersivity

Case 4 = Retardations

See Table 6-7 for the input distribution parameter values.

Horizontal bars represent the 1st, 25th, 50th, 75th and 99th percentiles.
*represents the mean value.

FIG. 6-7. Uncertainty sensitivity analysis of the aquifer (regional subsystem).

BEST DOCUMENT AVAILABLE

TABLE 6-8. Uncertain parameter for regional subsystem analysis (Fig. 6-7).[a]

Parameter	Percentile			Certain parameter for case number
	50th	1st	99th	
Water velocity (m/yr)	2.0	2.0×10^{-1}	2.0×10^{1}	2
Dispersivity (m)	2.0×10^{3}	4.0×10^{2}	1.0×10^{4}	3
Retardations:				
Fission products	1.0×10^{2}	1.0×10^{1}	1.0×10^{3}	4
Actinides	1.0×10^{3}	1.0×10^{2}	1.0×10^{4}	4

[a]All parameter uncertainties are presented by truncated lognormal probability distributions.

particle retardations) because the pulse parameter, S_1, is proportional to the square root of the dispersivity and proportional to the first powers of velocity and retardations.

6.5.5 Pairs of Subsystems

Figures 6-8 through 6-10 represent the uncertainty sensitivity analysis for system models composed of two subsystems. We present these results for completeness, with a few observations. The cases were run using the data in Tables 6-1 through 6-3. The parameters (which were set certain for each case) are listed on the figures.

The waste form and vertical path models are a particularly interesting subsystem pair. This subsystem pair models releases of radionuclides into the upper aquifer (which is significant if the water there is accessible by wells). The measure of particular interest is the concentration of radionuclides in the aquifer, which this model does not predict. Further modeling would be necessary to convert the peak release rates into estimates of peak concentrations.

The results of the combined waste form and regional (upper aquifer) subsystem models (Fig. 6-9) were the basis for not treating the time of waste release initiation (from the waste form) as an uncertain variable in the

BEST DOCUMENT AVAILABLE

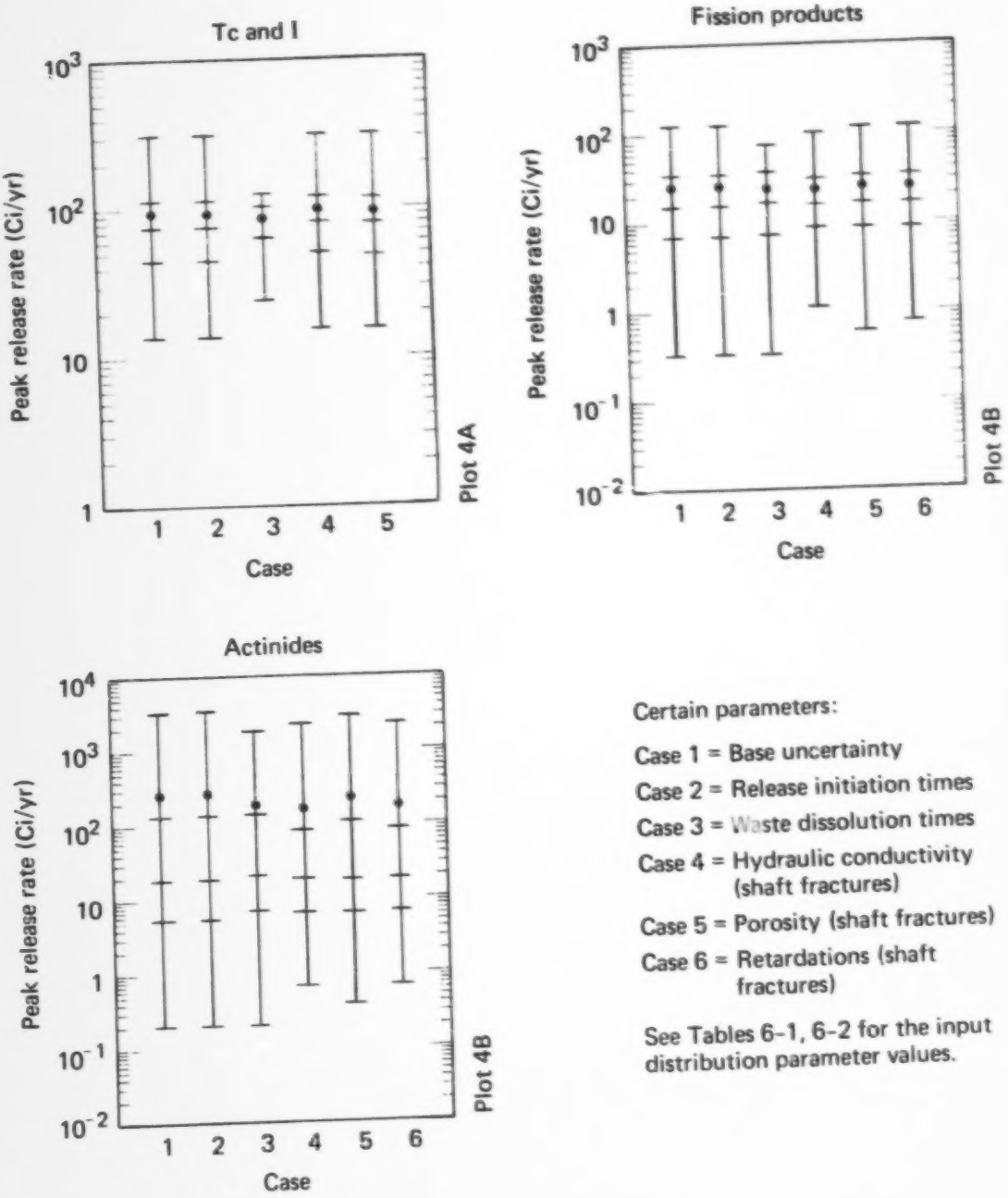

Certain parameters:

Case 1 = Base uncertainty

Case 2 = Release initiation times

Case 3 = Waste dissolution times

Case 4 = Hydraulic conductivity (shaft fractures)

Case 5 = Porosity (shaft fractures)

Case 6 = Retardations (shaft fractures)

See Tables 6-1, 6-2 for the input distribution parameter values.

Horizontal bars represent the 1st, 25th, 50th, 75th and 99th percentiles.
*represents the mean value.

FIG. 6-8. Uncertainty sensitivity analysis of the combined waste form and vertical path subsystems.

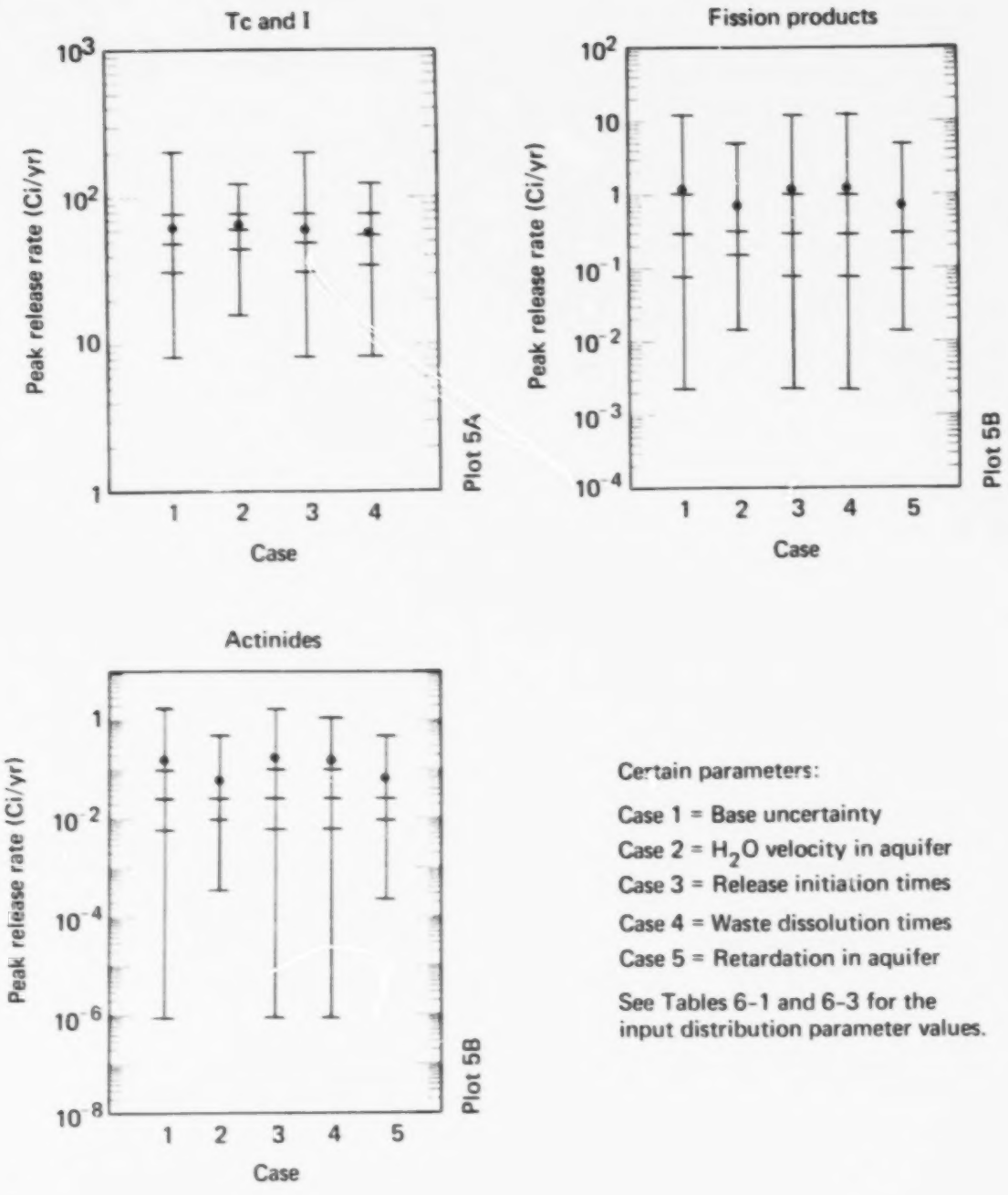

Horizontal bars represent the 1st, 25th, 50th, 75th and 99th percentiles.
*represents the mean values.

FIG. 6-9. Uncertainty sensitivity analysis of the combined waste form and regional (upper aquifer) subsystem models.

BEST DOCUMENT AVAILABLE

BEST DOCUMENT AVAILABLE

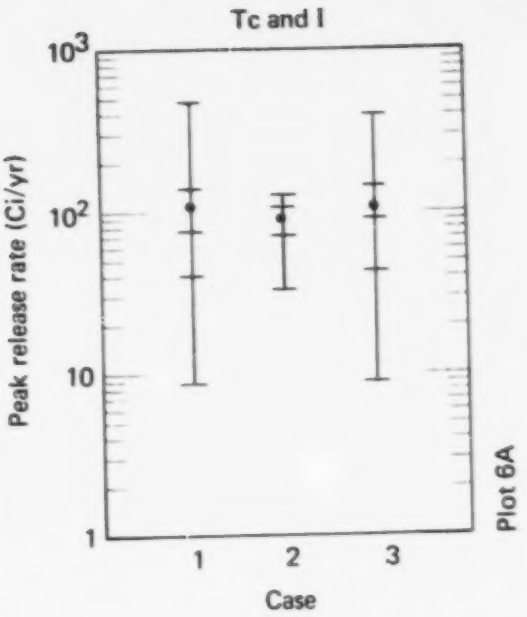

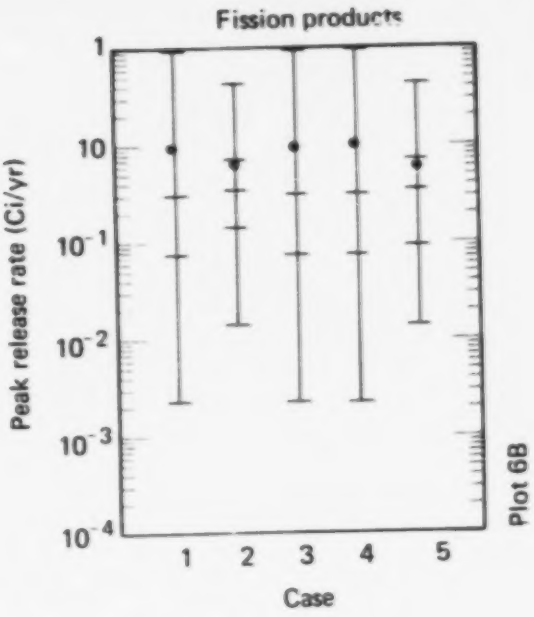

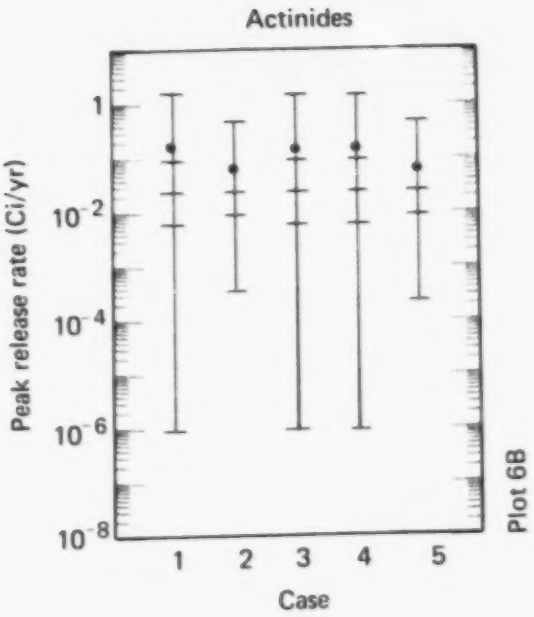

Certain parameters:

Case 1 = Base uncertainty

Case 2 = H_2O velocity in aquifer

Case 3 = Hydraulic conductivity (shaft fractures)

Case 4 = Retardation (shaft fractures)

Case 5 = Retardations in aquifer

See Tables 6-2 and 6-3 for the input distribution parameter values.

Horizontal bars represent the 1st, 25th, 50th, 75th and 99th percentiles.
*represents the mean value.

FIG. 6-10. Uncertainty sensitivity analysis of the combined vertical path and regional (upper aquifer) subsystem models.

complete system model (Fig. 6-4). Case 3 in Fig. 6-9 shows that the outcome distributions were insensitive to setting the release initiation time certain at its median value. Case 2 in Fig. 6-5 shows that the outcome distributions for fission products and actinides were sensitive to setting the release initiation times certain for the single subsystem model of the waste form and package.

6.5.6 Summary of Uncertainty Sensitivity Analysis

The purpose of the uncertainty sensitivity analysis was to gain an understanding of which model parameters tend to dominate the probability distributions of the outcomes. Figures 6-11 and 6-12 summarize the results presented in the section.

Before discussing these summaries, we emphasize that the results are specific to the models, the certain and probabilistic data used in them, and the assumed independence between the model parameters.

The graphs in Fig. 6-11 present the ratios of the 99th percentiles (computed with the model parameters on the abscissa set certain) to the 99th percentiles for the base uncertainty cases. The points connected with a solid line were computed with the results from the complete system model. The points connected with a dashed line were computed with the results from a single subsystem model run. For example, the point above u_1 on the dashed line for Tc and I was computed using the results from the regional (upper aquifer) subsystem model. The 99th percentile with u_1 certain, and t_d^1 and K_2 uncertain was about 0.19 of the 99th percentile computed with all three parameters uncertain. If the ratio of the percentile for a model parameter is much less than 1.0, then the 99th percentile of the outcome distribution is very sensitive to setting that parameter certain at its median value.

Figure 6-12 shows the spreads of the outcome distributions, including their sensitivities to the model parameter distributions. A distribution spread is defined as the ratio of the 99th to the 1st percentile. For

BEST DOCUMENT AVAILABLE

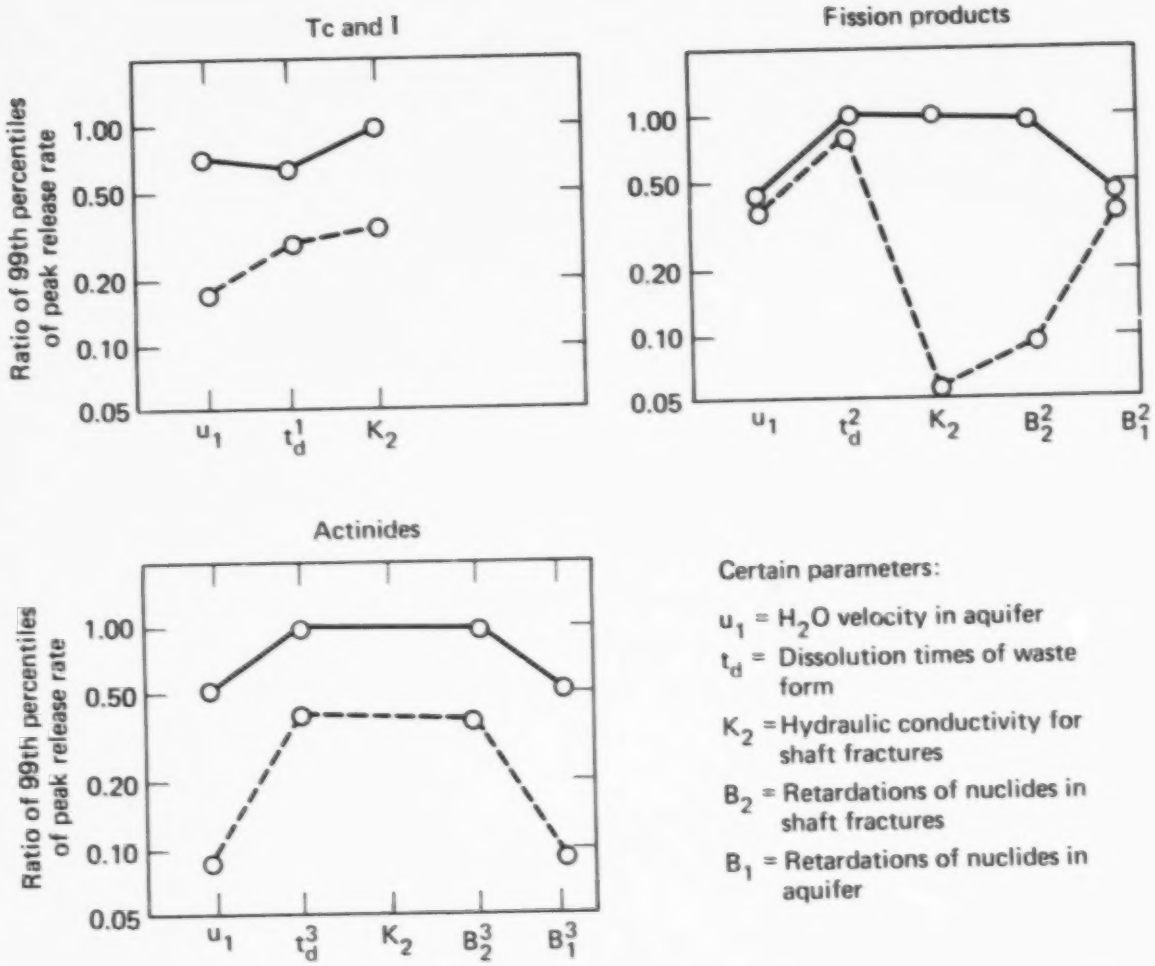

FIG. 6-11. Ratio of the 99th percentile with each parameter certain to the 99th percentile for the base case (solid line connects results for the complete system model; dashed line connects results for the single subsystems models, which contain the parameters on the abscissa).

BEST DOCUMENT AVAILABLE

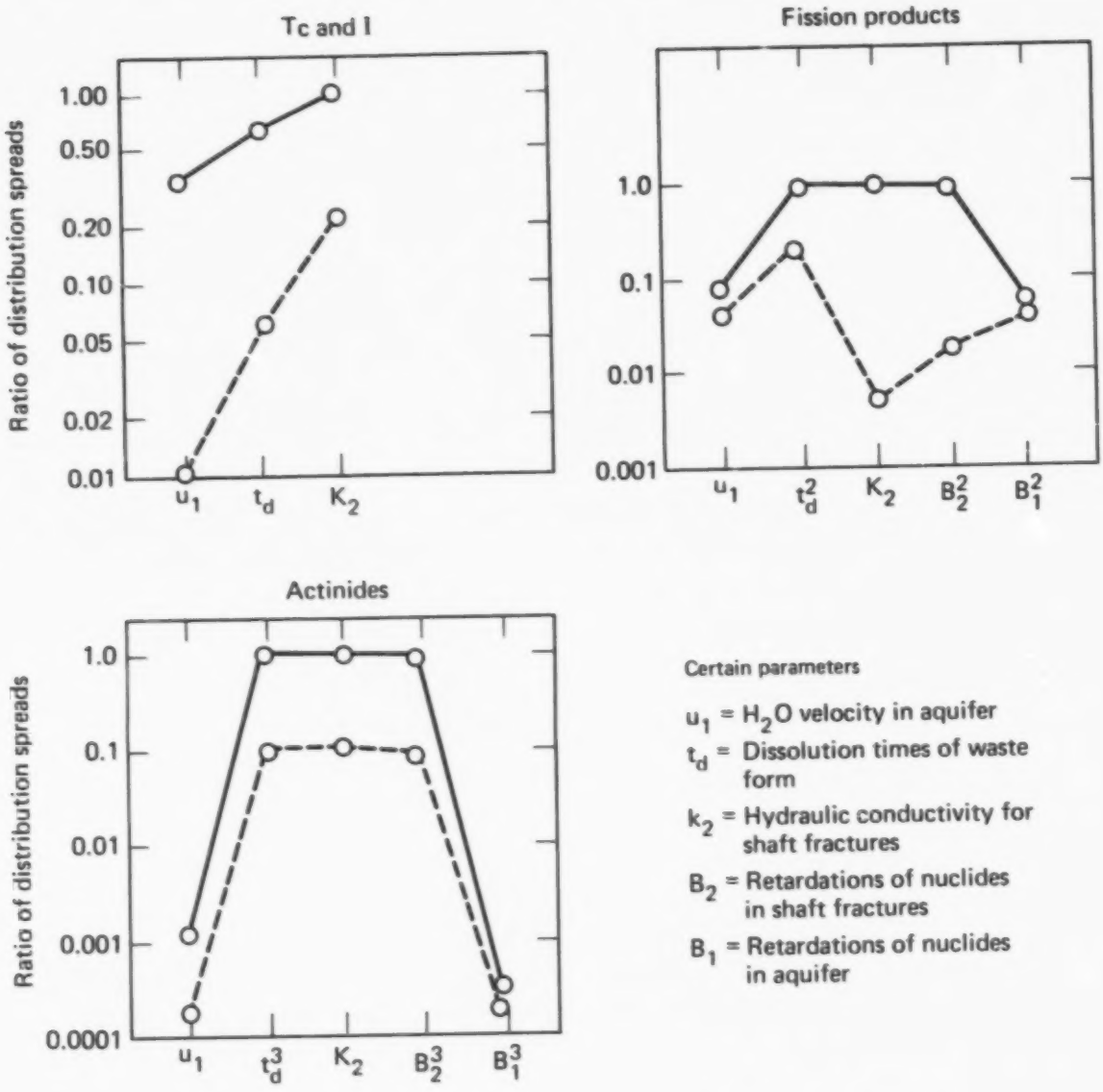

FIG. 6-12. The distribution spread shown as the ratio of the 99th to the 1st percentile; the ratio of the distribution spread is the spread with the parameter set certain divided by the spread for the base case (solid line connects results for complete system model; dashed line connects results for the single subsystem models, which contain the parameters on the abscissa).

BEST DOCUMENT AVAILABLE

example, the spread of the outcome distribution for the base uncertainty case of Tc and I (complete system) was,

$$\frac{182}{8.1} = 22.4 \quad ,$$

and the spread of the outcome distribution with u_1 certain was

$$\frac{118}{15.1} = 7.8 \quad .$$

Thus, the ratio of the spreads plotted on the graph was

$$\frac{7.8}{22.4} = 0.35 \quad .$$

A striking feature of the graphs is that the outcomes for the complete system are less sensitive to parameter uncertainties than the outcomes for the single subsystems. This effect is expected, particularly since we assumed that subsystem model parameters were independently distributed, i.e., no intersubsystem dependencies were modeled.

The complete system results show that the outcome distributions were not sensitive to setting the vertical path (repository site) subsystem model parameters certain. This is expected because the parameter distributions were selected to represent a scenario where this part of the system has been degraded substantially. Hence, the migration of nuclides is controlled by other elements of the system (waste form or aquifer). The 99th percentile ratios and the distribution spread ratios were very close to 1.0 for hydraulic conductivity (K_2) and radionuclide retardations (B_2^2 and B_2^3).

The outcome distributions were most sensitive to the water velocity (u_1) and the radionuclide retardations (B_1^2 and B_1^3) in the upper aquifer (regional subsystem model). It is noted that the sensitivities of the fission product and actinide outcome distributions were very close in value for both the complete system model and the upper aquifer (single subsystem) model. This is further evidence that the upper aquifer is dominant in determining the performance of this system under this severe scenario.

6.6 HIGH-LEVEL WASTE FORMS

This section presents sensitivity studies that vary the parameters of the waste form and package performance model to determine the effect on system performance. The sensitivity cases were selected to encompass the possible range of performance of glass and SYNROC high-level waste. This is not an assessment or comparative evaluation of waste forms. Rather, we have run several cases with different probability distributions for the parameters characterizing the waste form performance.

These results could be applied in judging the effects changes in the probability distributions of the waste form performance parameters could have on outcome probability distributions. The distributions can represent uncertainty about the performance of a waste form under specified sets of conditions. Different distributions may apply depending on the waste form, the conditions in the repository, and the information available from analytical and experimental research programs.

Thus, the results could be applied to three types of considerations:

- Selecting a waste form.
- Deciding whether to include more detail in modeling the physical conditions in the repository and their effects on waste form performance.
- Choosing whether to affect the uncertainty about performance by doing additional research.

Section 4 presents dissolution rates for glass and SYNROC waste forms at several temperatures, pressures, and chemical conditions. Typically, the experiments measure dissolution rates as $g \cdot cm^{-2} \cdot day^{-1}$. Dissolution rates of waste in a repository then depend upon the surface area-to-mass ratio. For a glass monolith, these factors are on the order of 100 ($cm^2 \cdot g^{-1} \cdot day \cdot yr^{-1}$) (Kovar [1980]).* However, this can vary depending upon the amount of cracking assumed. The range of the dissolution rate data formed the basis for selecting the various probability distributions in this parametric study.

---

*Kovar, F. R. (1980), Lawrence Livermore National Laboratory, Livermore, Calif., private communication, WFA 80-12-D.

The analysis addresses the following differences between spent fuel and high-level waste forms:

- Spatial distribution of radionuclides in the waste form.
- Radionuclide inventory.
- Dissolution rates.

These differences and their potential effects on system performance are discussed in the following paragraphs.

The analysis of the previous sections assumed that the fission products in the spent fuel were concentrated near the outside of the fuel pellets. Thus, the distribution of the dissolution times for Group-1 and Group-2 radionuclides had 1st, 50th, and 99th percentile values of 1000, 5000, and 25,000 yr, respectively, while the actinide dissolution time percentiles were 10^4, 10^5, and 10^6 yr. The waste elements in HLW glass or SYNROC would be uniformly distributed, although they might not necessarily dissolve at the same rate (see Subsection 4.2). The results in Fig. 6-13 were computed to determine the possible effects of uniform dissolution on peak release rates. The cases were computed for the spent fuel inventory of nuclides so that the effect would not be confounded by the differing inventories. The complete system model was used with the input parameter distributions in Table 6-5. In Case 3, the elements in both groups were assumed to dissolve at the same rate as the actinides.

The results show practically no improvement for the fission products (other than Tc and I) because of the relatively large values of T and S for fission products in the aquifer (median values are 5.0×10^5 and 3.1×10^5 yr, respectively). Using the larger dissolution times for Tc and I shifted the probability distributions to lower values by a factor of about 1/5 for Case 3. The effect is greater for this group because the unretarded values of T and S for Tc and I in the aquifer are about 5000 and 3100 yr, respectively. Homogeneous mixing of elements in the waste form would have a greater effect on concentrations above the repository, because the transit time and spread of the pulse are smaller for the vertical pathway.

The second difference between spent fuel and high-level waste is the inventory of nuclides. In the inventories used for HLW, reprocessing was assumed to remove all the Kr and Xe, 99.9% of the I, and 99.5% of the U and Pu. Figures 5-15 through 5-19 show the activity time for each group in spent fuel and high-level waste. The total activity of Group-2 fission products is

BEST DOCUMENT AVAILABLE

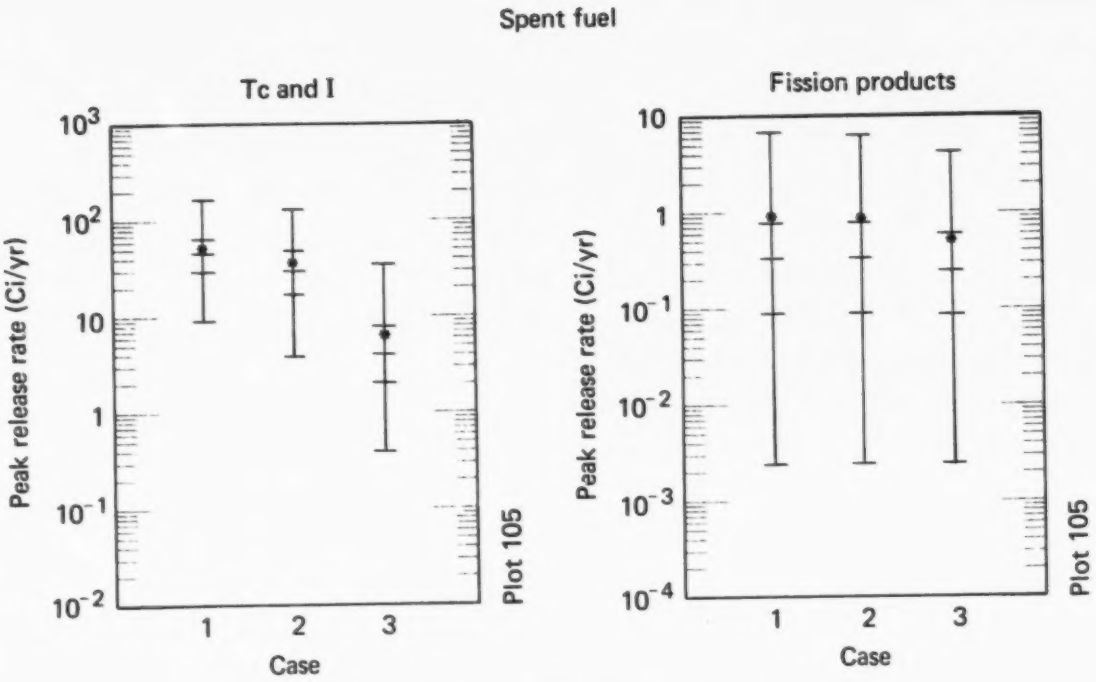

Percentiles of waste dissolution time (yr)

	1st	50th	99th
Case 1	100	5000	25,000
Case 2	1000	10,000	100,000
Case 3	10,000	100,000	1,000,000

Horizontal bars represent the 1st, 25th, 50th, 75th and 99th percentiles. *Represents the mean value.

FIG. 6-13. Performance sensitivity to the spatial distribution of waste elements in the waste form.

identical for HLW and spent fuel. Therefore, there is only one graph for this group, Fig. 5-16. The Tc and I activity is dominated by Tc until about 2.0×10^6 yr. Then, the Tc decays below the level of I as shown for spent fuel in Fig. 5-15. (Note the 10^3 Ci at 3.0×10^6 yr from the I.) The total activity of Tc and I are almost identical for spent fuel and HLW up to about 1.0×10^6 yr. The total activity of the actinides and their daughters is about a factor of 10 lower for HLW due to the removal of Pu and U and the subsequent reduction of daughter products.

The effects of differences between spent fuel and high-level waste activities are seen in comparing Figs. 6-14 and 6-15. The calculations to generate these graphs are explained in the next paragraph. There is no difference between spent fuel and high-level waste results for Tc and I, since the peak rates are determined by the activity of Tc, which is identical for the inventories. The distributions for the actinides in high-level waste are shifted down by about an order of magnitude, as expected.

The third possible difference between spent fuel and the processed forms of high-level waste is the dissolution rates in groundwater. The results in Figs. 6-15 and 6-16 can be used to indicate the potential effect of the probability distributions for the dissolution times on the probability distributions of peak release rates. The results in Fig. 6-15 were computed with the waste form subsystem model, and the results in Fig. 6-16 were computed with the complete system model used in the previous sections for bedded salt. However, a high-level waste inventory was used here.

The waste form model (used in computing the results in Fig. 6-15) represents the release as a square pulse. Since the activity curves are nonincreasing functions of time (until about 10^6 yr), then the peak rate of activity release from the waste is the quotient of the activity at the time of release initiation, divided by the dissolution time. The release initiation time was input as uncertain for all cases, with 1st, 50th, and 99th percentile values of 50, 500, and 5000 yr. The waste dissolution time was input as uncertain in each case. The median dissolution times were 10^4, 10^5, 10^6, 10^8, 10^{10}, and 10^{12} yr, respectively, for Cases 1 through 6. The distributions were lognormal with the 1st and 99th percentiles two orders of magnitude less and greater than the median, respectively. Thus, the probability distribution for dissolution time is translated along the log

BEST DOCUMENT AVAILABLE

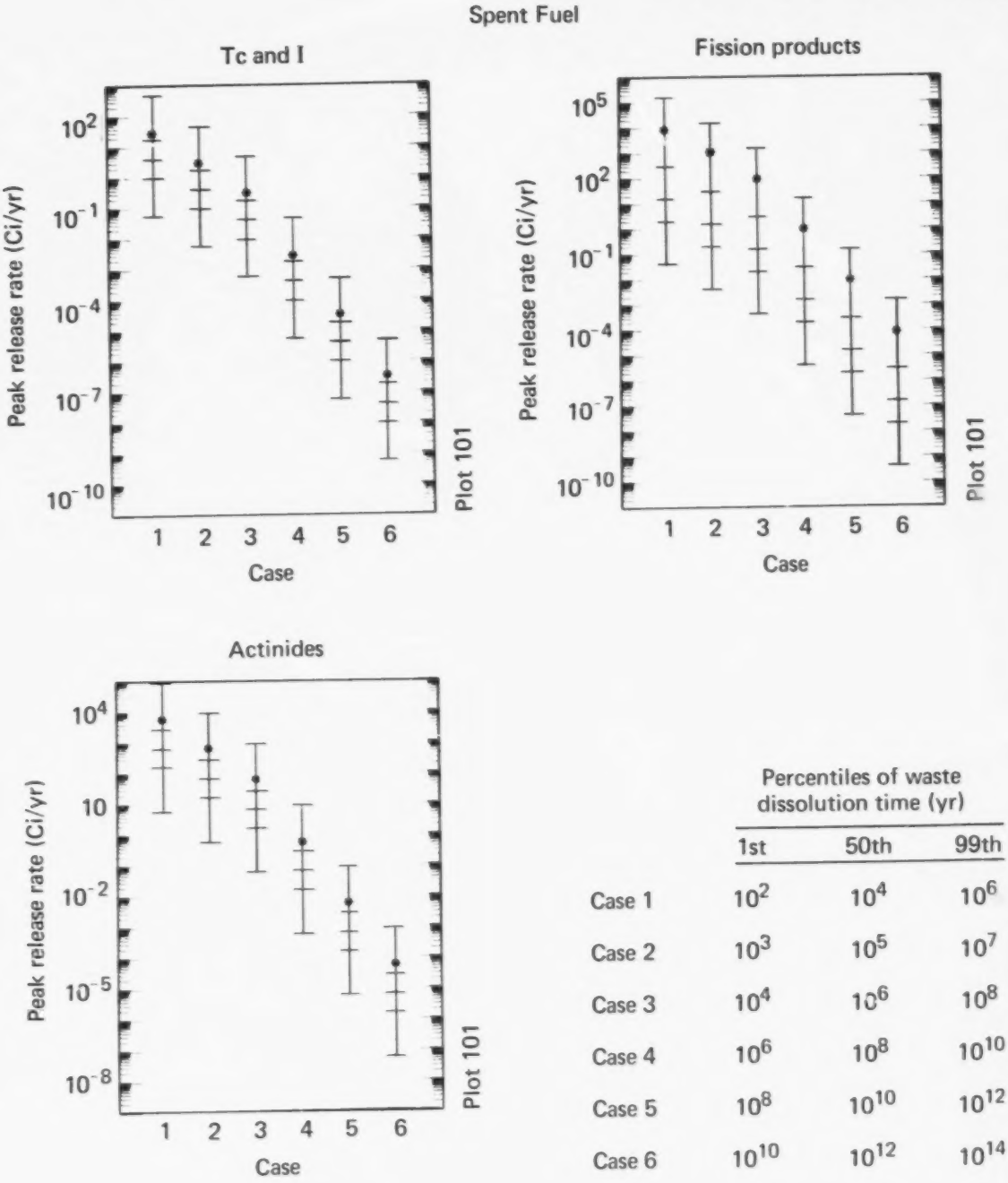

	Percentiles of waste dissolution time (yr)		
	1st	50th	99th
Case 1	10^2	10^4	10^6
Case 2	10^3	10^5	10^7
Case 3	10^4	10^6	10^8
Case 4	10^6	10^8	10^{10}
Case 5	10^8	10^{10}	10^{12}
Case 6	10^{10}	10^{12}	10^{14}

Horizontal bars represent the 1st, 25th, 50th, 75th and 99th percentiles.
*represents the mean value.

FIG. 6-14. The distributions for peak release rates computed for the waste form and package subsystem, and a spent fuel inventory (the median value of the waste dissolution time was decreased for each successive case, while the spread of the log of the probability distribution was held constant).

BEST DOCUMENT AVAILABLE

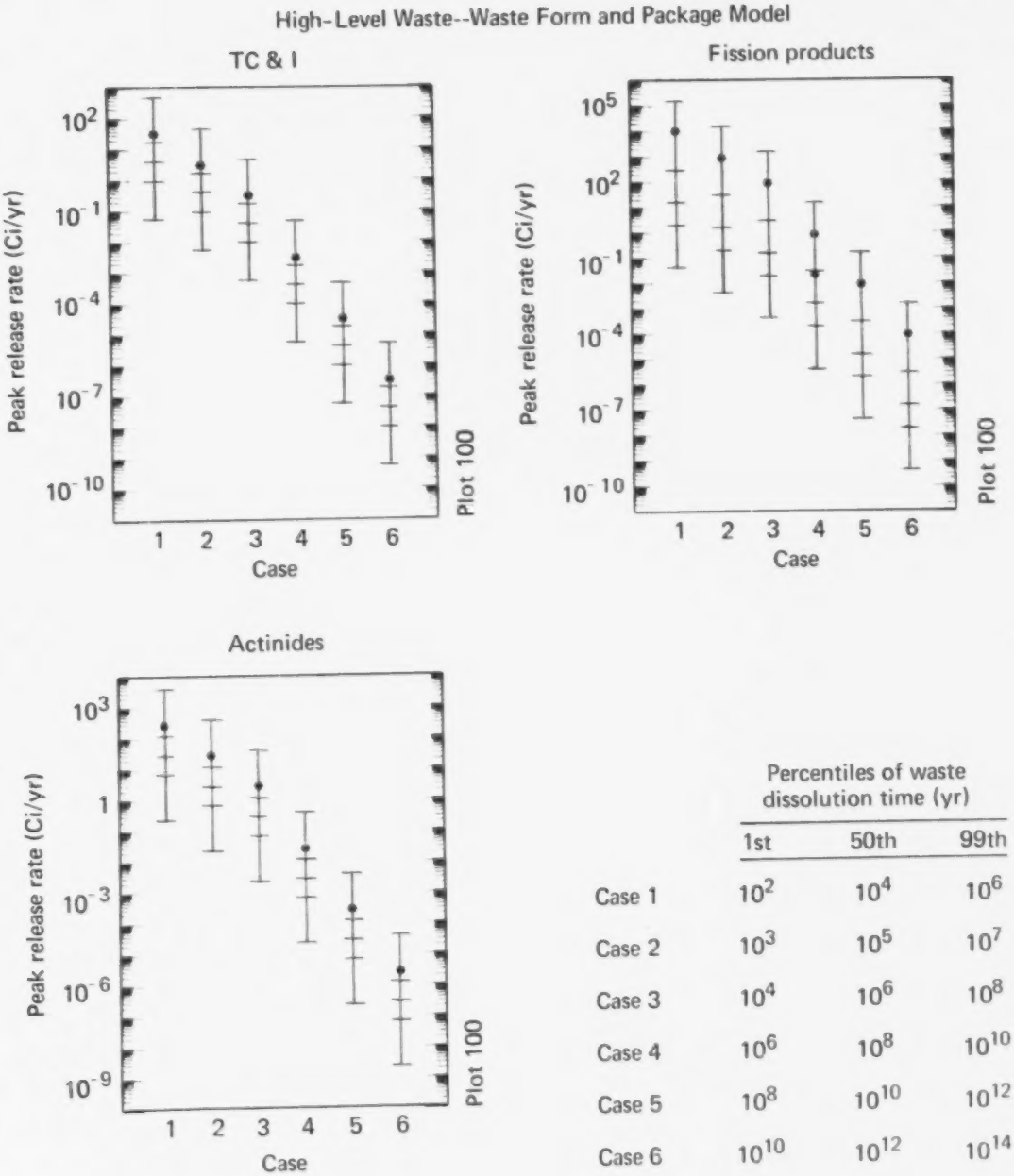

	Percentiles of waste dissolution time (yr)		
	1st	50th	99th
Case 1	10^2	10^4	10^6
Case 2	10^3	10^5	10^7
Case 3	10^4	10^6	10^8
Case 4	10^6	10^8	10^{10}
Case 5	10^8	10^{10}	10^{12}
Case 6	10^{10}	10^{12}	10^{14}

Horizontal bars represent the 1st, 25th, 50th, 75th and 99th percentiles.
*represents the mean values.

FIG. 6-15. The distributions for peak release rates computed for the waste form and package subsystem, and a high level waste inventory (the median value of the waste dissolution time was decreased for each successive case, while the spread of the log of the probability distribution was held constant; the time of release initiation was input as a lognormal distribution with 1st, 50th, and 99th percentiles for 50, 500, and 5000 yr--the same distribution was used for all cases).

BEST DOCUMENT AVAILABLE

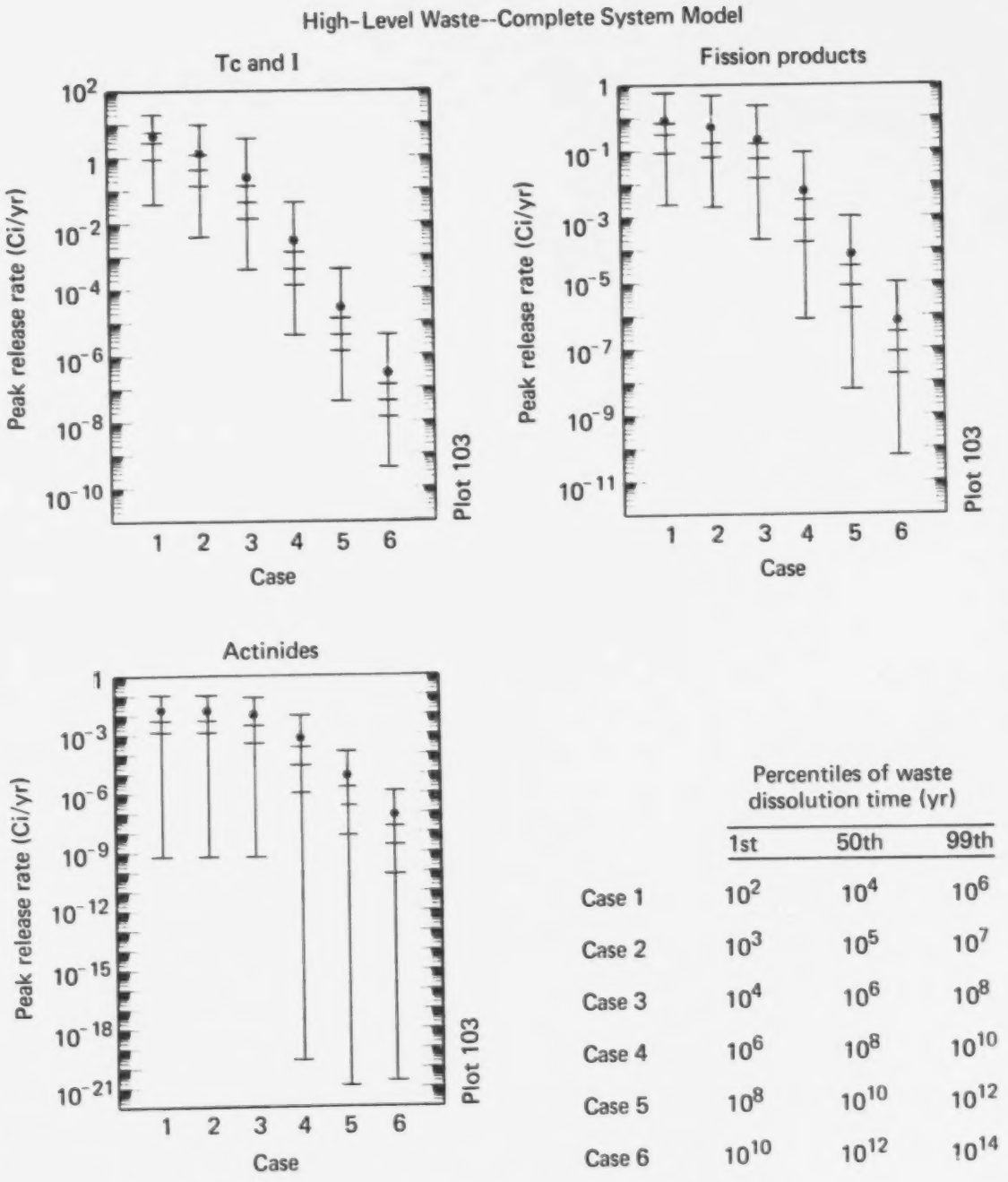

	Percentiles of waste dissolution time (yr)		
	1st	50th	99th
Case 1	10^{2}	10^{4}	10^{6}
Case 2	10^{3}	10^{5}	10^{7}
Case 3	10^{4}	10^{6}	10^{8}
Case 4	10^{6}	10^{8}	10^{10}
Case 5	10^{8}	10^{10}	10^{12}
Case 6	10^{10}	10^{12}	10^{14}

Horizontal bars represent the 1st, 25th, 50th, 75th and 99th percentiles.
*represents the mean value.

FIG. 6-16. The distributions for peak release rates computed with the complete system model and a high-level waste inventory (the median value of the waste dissolution time was decreased for each successive case).

scale of time for successive cases. As might be expected, the results show that the percentile values for distributions of the peak release rates are inversely proportional to the time location of the probability distribution at the dissolution time. If the median dissolution time is increased an order of magnitude, then the percentiles of peak rates are reduced an order of magnitude.

When the waste form is considered within the complete system model used in the previous sections, then the dissolution time may not have much effect on the release rate at the release point of the upper aquifer. The results are shown in Fig. 6-16. Increasing the waste dissolution time will not have much effect on the peak rate of release until it is comparable to the temporal width of the pulse at the end of the aquifer (i.e., the spread of the impulse response function for the vertical path and the aquifer). The results in Fig. 6-16 demonstrate this for a particular system and were computed using the complete system model. Uncertain parameters were represented by the distributions from Table 6-4, with the exception of the waste dissolution times. The same dissolution time distribution was used for all three nuclide groups, and the probability distribution was different for each case. The percentile values for each case are listed on Fig. 6-16. All other parameters were input as certain, set at the median values in Tables 6-2 and 6-3.

The peak rate of release of Tc and I decreases for all positive shifts of the dissolution time distribution. However, the shifts in the release rate distributions are not proportional to the shift in the dissolution time distribution until Case 4 (1st, 50th, and 99th percentiles are 10^6, 10^8, and 10^{10} yr). Since the spread of the waste pulse in the vertical path and the aquifer is greater for the retarded nuclides, the dissolution time does not have any substantial effect on the fission products and actinide results until Case 4. These results illustrate the point that the marginal effect of "improving" the probability distribution of the waste dissolution time depends on the performance of the other components of the system.

Figure 4-1 indicates a range of measured leach rates for various waste glasses. An effective waste surface area is required to convert the leach rates ($g \cdot cm^{-2} \cdot day^{-1}$) to waste dissolution times in years. An approximate conversion factor of 10 can be applied for an intact glass monolith about 2 ft in diam × 8 ft high. This number is also uncertain depending on the amount of cracking. Applying a factor of 10, the numbers from Figure 4-1 translate into dissolution times of 10^3-10^6 yr. Now

BEST DOCUMENT AVAILABLE

suppose that the uncertainty within this range could be reduced to give 1st and 99th percentiles within two orders of magnitude of the median. Cases 1, 2, and 3 would represent such distributions with medians 10^4, 10^5, and 10^6 yr, respectively.

The results for this system indicate less than an order of magnitude difference in results for Tc and I between these cases. They indicate even smaller differences between these cases for the fission products and actinides.

Results for SYNROC-C and SYNROC-D experiments are given in Fig. 4-1 and Table 4-1. Dissolution rates are reported for several elements at different temperatures and with different solvent compositions. These results range from about 10^{-5} g•cm^{-2}•day^{-1} to the limits of the measuring techniques at about 10^{-10} g•cm^{-2}•day^{-1}. It is not evident which results should be applied for each element over the long term. Applying a factor of 10 for conversion gives dissolution times ranging from 10^4-10^9 yr. Case 4 has a median value of 10^8 yr. We see from Fig. 6-16 that this system's performance is dominated by the waste form when the median value of the dissolution time is greater than 10^8 yr.

Again, if the release of waste (or concentrations) was measured at the top of the vertical path, the effect of changing the dissolution time would be greater.

6.7 REPOSITORIES IN BASALT

This section briefly explores some of the potential differences between repositories in bedded salt and basalt, and their possible significance to the performance of a waste isolation system. The approach is to consider each aspect of a basalt system separately within the context of the model used for bedded salt. We have not developed a separate and complete system model for basalt, nor attempted to perform a comprehensive comparison of waste isolation systems in bedded salt and basalt.

This analysis considers how differences between particular attributes of repositories in basalt and bedded salt would be reflected in the performance of the overall system. The data on basalt (see Subsection 4.3) is used to estimate which model parameters could have significantly different values in basalt. The results of the bedded salt analysis are used in judging the possible effects of differences between model parameter values for some of the

parameters. Without developing site-specific models for bedded salt and basalt, we hesitate to make any conclusion on generic differences. Also, differences in the data may depend more on the location of the site rather than the rock type. It is difficult to determine if this is the case with the limited data available to us.

6.7.1 Waste Form and Package in Basalt

The composition of the groundwater in a repository can affect the rate at which the waste dissolves. We were not able to locate any data indicating the potential differences of the dissolution rates of important elements in groundwaters for basalt and bedded salt sites. However, the results from Subsection 6.6 demonstrate how these differences may affect the repository performance.

Figure 6-15 shows that the performance of the waste form and package subsystem is directly related to the probability distributions of the dissolution rates (as expected). However, the results in Fig. 6-16 illustrate that the probability distributions for the dissolution rates may not have a significant effect on the peak rate of release into the biosphere.

The importance of any differences in the dissolution rate of waste in a basalt repository will depend on the performance of the other subsystems. If system performance is dominated by the upper aquifer (as was the system model used to generate the results in Fig. 6-16), then there is some region of the variable space for which changes in the probability distributions of dissolution will not affect system performance distributions.

However, if system performance is not dominated by the slow transport of waste from the repository corridors to waters available for human use (either in an aquifer or surface waters), then changes in the probability distributions for dissolution can have a relatively large effect on the probability distributions of the performance variables. Of course, the significance of such relative changes depends on the absolute values of the performance variables.

6.7.2 Basalt Repository Site

Comparing the data in Section 4 for basalt and bedded salt indicates some of the potential differences between these media that would affect the

BEST DOCUMENT AVAILABLE

transport of nuclides from the repository to an upper aquifer. However, without considering specific sites, it is not possible to make any conclusions that apply to the media in general. That is, variations in the system parameters between sites in the same media, may be more significant than differences between media.

The data on basalt in Subsection 4.3 indicate that the vertical hydraulic conductivity may be less than it is for the shale interbeds associated with a bedded salt repository. (In the bedded salt analysis, the vertical conductivity below the repository was assumed to be determined by the shale interbeds.) Selected data presented in Subsections 4.3 and 4.4 give vertical conductivity ranges of 0.3-6 m/yr in shale and 1×10^{-4} - 4×10^{-1} m/yr in basalt.

However, the original data source for basalt emphasizes the difficulty in measuring its vertical conductivity. Thus, a proper statement of the uncertainty about vertical conductivity should reflect more than just the range of measurements (1×10^{-4} - 4×10^{-1} m/yr). Also, if the bedded salt layer is not fractured below the repository, then the conductivity may be much less than assumed for this analysis. In that case, the bedded salt repository may have substantially less water flow.

Neither for bedded salt nor for basalt were we able to locate any data on the porosity of a shaft fracture zone. Since the waste velocity is inversely proportional to porosity, any differences in the porosity of the fracture zone between media has a significant effect on vertical transit time.

The data for the distribution coefficients of nuclides in the Umtanum member of the Columbia River basalt indicate that the retardation of uranium may be one or two orders of magnitude less than for other nuclides in the actinide group or the fission product group (other than Tc and I). Using a porosity of 2% and a density of 3 (g/cm^3), the reported K_d for uranium of 3 (ml/g) gives a retardation factor of about 450. This is greater than the median value used for the bedded salt cases. The retardations for the vertical path in the bedded salt analysis were reduced by about an order of magnitude over measured values. This is used as an estimate of the effect of brine. We could not locate any data on retardations in a brine environment. The results in Fig. 6-6 show that uncertain performance in the repository site can be sensitive to the probability distributions of the retardations.

Based on this cursory analysis, we conclude that any defensible comparison of the local transport of nuclides in bedded salt and basalt will require:

- Modeling of specific sites based on the geologic structure and site-specific data.
- Clear definitions of the scenarios (faulting, shaft seal failures, and borehole failures.
- Consideration of the relative probabilities of these scenarios at each site.

6.7.3 Regional Transport at a Basalt Site

We are particularly reluctant to make any "generic" comparison of the regional transport characteristics of basalt and bedded salt sites. The hydrology and transport parameters of aquifers associated with these media may be more strongly dependent on the location of the site (given the host rock type) than on the type of host rock.

Values of the distribution coefficients measured in sediments above the Columbia River basalt at Hanford indicate that uranium may not be retarded significantly in the aquifer at that particular site. There are also large differences between the K_d values measured for different actinide elements. This indicates a need to model the actinide group in more detail by considering individual actinide elements and their toxicities (not only activities) to determine the significance of possible low K_d's for particular actinides.

6.8 APPLICATION OF PARAMETRIC SYSTEM PERFORMANCE RESULTS TO BEDDED SALT SCENARIO

This subsection analyzes the series pathway system depicted in Fig. 6-1 using the parametric study results from Section 5. The purpose of this analysis is to demonstrate how these parametric results can be used to reach some preliminary conclusions about a system's behavior. The parameter median values from Tables 6-1 through 6-3 are used in this analysis. The graphs from Section 5 are compared to the detailed calculations in Subsection 6.4. The quantitative results agree quite well, and the qualitative conclusions (using

BEST DOCUMENT AVAILABLE

the graphs from Section 5) are consistent with earlier conclusions in Section 6.

From Table 6-2, the median values of the unretarded transit time and the ratio of transit time to spread for the vertical path are given respectively:

$$T_{50}^{*} = 1440 \text{ yr}$$
$$T/S = 3.5.$$

The ratio of T to S depends only on the ratio of length to dispersivity, both of which were assumed certain; therefore, T/S is certain as well. The corresponding quantities for the aquifer from Table 6-3 are:

$$T_{50} = 5000 \text{ yr}$$
$$(T/S)_{50} = 1.6.$$

For this pathway, the dispersivity is uncertain, so the median value for T/S is used. The system variables for the combined pathways are then [see Eq. (2-1) in Section 2]:

$$T_{50} = 6440 \text{ yr}$$

$$(T/S)_{50} = \frac{6440}{\sqrt{\frac{1440^2}{3.5} + \frac{5000^2}{1.6}}} = 2.0 \qquad (6\text{-}9)$$

The results from Section 5 are used to estimate the median values of the peak rate of release for Tc and I for each subsystem. These estimates are compared to the median values computed using the code MACRO.

From Fig. 5-8 (Group 1-SF), the waste form alone (T = 0, t_d = 5000 yr) should give a peak release rate of about 100 Ci/yr. The median value for Case 1 in Fig. 6-3 is also about 100 Ci/yr.

The median values of the peak activity release rate are computed using Table 5-1 to estimate the peak-normalized flux, and Fig. 5-15 for the total activity at the time-of-peak flux. The repository site subsystem parameter

*Subscript refers to the median value.

BEST DOCUMENT AVAILABLE

values are $t_d = 0$, T = 1440 yr, T/S = 3.5. From Table 5-1, then t_p = 1200 yr, the peak normalized flux is 1.5/T = 0.001, and the activity is 0.2×10^6 Ci. Thus, the peak release rate for Tc and I for the repository site is:

$$J^1(t_p)^* = j(t_p)H^1(t_p) \cong (0.001)(5 \times 10^5) = 500 \text{ Ci/yr.} \quad (6\text{-}10)$$

Similarly, the estimated peak release rate for the regional subsystem (with parameter values of T = 5000 yr, T/S = 2.0 and $t_d = 0$) is:

$$J^1(t_p) \cong \frac{(1.05)}{5000}(5 \times 10^5) = 100 \text{ Ci/yr.} \quad (6\text{-}11)$$

The median values from Fig. 6-3 for Cases 2 and 3 agree well with these estimates. It should be noted that the median inputs are not necessarily the same due to nonlinearities in the computations. The agreement between the two procedures is encouraging and is generally good.

It is important to reiterate how dependent these conclusions are on the assumed parameter input values. For instance, if the permeability of the vertical pathway were a factor of 10 smaller than was assumed, the transit time for the repository site would have been about 15,000 yr and the repository site would be the most important of the three barriers.

Of the three subsystem combinations shown in Table 6-9, Case 4 is still dominated by the waste form; Case 5 is equally influenced by the two component subsystems, while Case 6 is still dominated by the region. Thus, Case 5 should (and does) have the lowest median peak release rate of the three cases. The actual values for rate can be computed from Table 5-1 and Fig. 5-9 in a similar manner to the computations for the single subsystems above. When the value of T/S is neither 1 nor 10, then the figures only give the correct locations of the vertical segments of the contours. The y-axis intercepts for the horizontal segments of the contours must be computed using Table 5-1, as was done above. However, the plots can be used to bracket the possible peak release. Moreover, when the value of T/S is near one or 10, as in Case 5, then the plots can be used with no need for correction because the variation

---

*t_p stands for the time of peak, J for the release rate, j for the undecayed waste flux, and H for the activity; superscripts indicate group.

BEST DOCUMENT AVAILABLE

of the peak release is not very sensitive to T/S. Again these results are highly dependent on the assumed input parameters.

Data for the fission products is shown in Table 6-10. The retardation in the vertical path had a median value of 10, while the aquifer was assigned a median value of 100.

TABLE 6-9. The three pairwise subsystem combinations have t_d, T, T/S median values.

	t_d (yr)	T (yr)	T/S
Case 4: Waste form + vertical path	5000	1440	3.5
Case 5: Waste form + aquifer	5000	5000	1.6
Case 6: Vertical path + aquifer	0	6440	2.0

TABLE 6-10. Median values for t_d, T, and T/S for the seven fission product cases.

	t_d (yr)	T (yr)	T/S
Waste form (WF)	5×10^3	--	--
Vertical path (VP)	--	1.44×10^4	3.5
Aquifer (A)	--	5×10^5	1.6
WF + VP	5×10^3	1.44×10^4	3.5
WF + A	5×10^3	5×10^5	1.6
VP + A	--	5.1×10^5	1.6
WF + VP + A	5×10^3	5.1×10^5	1.6

BEST DOCUMENT AVAILABLE

By comparing the transit times and t_d, it is clear that the aquifer subsystem totally dominates the other two subsystems. Therefore, Cases 3, 5, 6, and 7 should all have essentially identical distributions. Moreover, the approximate median value for peak release should be computed with T/S = 1.6, $T = 5 \times 10^5$ as:

$$J^2(t_p) = g(t_p)H^2(t_p) = \frac{1.06}{5 \times 10^5}(1 \times 10^5) = 0.2 \text{ Ci/yr.} \quad (6\text{-}12)$$

This agrees with the values in Fig. 6-3. Cases 1, 2, and 4 have median values which can be computed using Fig. 5-13 or Table 5-1 and Eq. (5-1) to give approximately:

$$\text{Case 1:} \quad J(t_p) \cong \frac{10^6(0.2)}{5 \times 10^3} \cong 40 \text{ Ci/yr} \quad (6\text{-}13)$$

$$\text{Case 2:} \quad J(t_p) \cong 10^6(0.2)\ \frac{1.5}{1.44 \times 10^4} \cong 20 \text{ Ci/yr} \quad (6\text{-}14)$$

$$\text{Case 4:} \quad 10 \text{ Ci} \leq J(t_p) < 20 \text{ Ci/yr} \quad (6\text{-}15)$$

Only an estimate is given for Case 4, because the value of T/S (3.5) does not correspond to the ratio values for which contour plots exist. However, both T/S = 10 and T/S = 1 plots indicate the release rate should be larger than 10. The upper limit is imposed because Case 4 must be less than the minimum of Cases 1 and 2. From Fig. 6-3, the median peak release rates for these cases are approximately 100 Ci/yr, 20 Ci/yr, and 8 Ci/yr, respectively.

The analysis of the actinides results is identical and shows the same dominance of the aquifer transit time over the other two system parameters. Because of its similarity to the fission products, it will not be dealt with in detail.

The discussion so far has dealt with predicting the median value. However, other percentiles can be quantitatively estimated as well. This is illustrated by statistics for the vertical pathway. Since both α and L are certain, T/S is certain, and the ratio t_p/T in the Green's function is also certain (at a value of about 0.87). Therefore, from Table 5-1, the peak value of the Green's function is:

$$g(0.87;\ T/S = 3.5) = \frac{1.5}{T} \quad (6\text{-}16)$$

BEST DOCUMENT AVAILABLE

The distribution for T is lognormal. The median value of T for the vertical path is 1440 yr. The mean value of the natural logarithm of T is μ, and σ^2 is the variance of the natural logarithm of T. For the vertical path:

$\exp(\mu) = 1440$ yr, and

$$\sigma^2(\ln T) = \sigma^2(\ln K_2) + \sigma^2(\ln \theta_2) = (0.985)^2 + (0.6)^2 = (1.04)^2 \quad (6\text{-}17)$$

Here, we have ignored the head drop across the lower flaw leading into the repository, since its transmissivity is much greater than the upper flaw. Moreover, ΔH and L were assumed certain. The percentiles of T are given as:

$\exp(\mu + zT)$,

where z = 2.33, 0.67, 0, -0.67, -2.33 for the 99th, 75th, 50th, 25th, and 1st percentiles, respectively. For this specific example, these correspond to:

$$T_{99} = (1440)\ (11.3) = 16{,}270 \text{ yr} \quad (6\text{-}18)$$

$$T_{75} = (1440)\ (2.01) = 2894 \text{ yr} \quad (6\text{-}19)$$

$$T_{25} = (1440)\ (0.50) = 716 \text{ yr} \quad (6\text{-}20)$$

$$T_{01} = (1440)\ (0.089) = 127 \text{ yr} \quad (6\text{-}21)$$

Therefore, the 1st, 25th, 75th, and 99th percentiles for peak release rate for Group 1 are approximately:

$$J_{01} \cong \frac{1.5}{16{,}270}\ (0.45 \times 10^6) = 40 \text{ Ci/yr} \quad (6\text{-}22)$$

$$J_{25} \cong \frac{1.5}{2894}\ (0.45 \times 10^6) = 230 \text{ Ci/yr} \quad (6\text{-}23)$$

$$J_{75} \cong \frac{1.5}{716}\ (0.45 \times 10^6) = 940 \text{ Ci/yr} \quad (6\text{-}24)$$

$$J_{99} \cong \frac{1.5}{127}\ (0.45 \times 10^6) = 5300 \text{ Ci/yr} \quad (6\text{-}25)$$

Here we have used the fact that $H(t_p)$ for Group 1 has a constant value of 0.45 Ci/MWe/yr. From Fig. 6-3, the corresponding computed values are approximately 30, 200, 1000, and 6000, respectively.

Because the dispersivity is uncertain, the analysis of the aquifer is somewhat more complicated, therefore making t_p/T uncertain. However, the uncertainty is not large and the median value can be used with reasonable accuracy.

7. A PARALLEL PATH HYDROLOGY STUDY

In the previous sections we considered only a series of flow paths from a lower aquifer through a repository to an upper aquifer and along the upper aquifer as shown in Fig. 2-1. In this section, we consider the flow in a network with parallel pathways as shown in Fig. 7-1.

As in the previous analyses, the flow paths can represent man-made or natural flaws. In this study, only the flow or hydrology is analyzed. The transport of waste can be calculated from the flow velocities or fluxes in a relatively straightforward manner, given the necessary data. Although the pathways are pictured for a sedimentary basin having three layers, including overlying and underlying aquifers, the path segment concept is easily generalized to formations with an arbitrary number of layers or even to systems with only one aquifer, provided only that one knows all the relevant path parameters.

In this section, we first discuss the parameters (or variables) and equations that govern the flow. Then, expressions for the flow in the three paths shown in Fig. 7-1 are derived and analyzed. Finally, the results are summarized and some conclusions drawn.

7.1 PARAMETERS AND EQUATIONS

In general, the hydrology or flow is specified by the path parameters and the boundary conditions. The former are area, length, hydraulic conductivity and porosity. The latter can be any of three types: head changes across each path, total head change across a set of interconnected paths, or recharge (flow) rates into a set of paths.

This study considers only the case where the overall vertical head drops between the aquifers and horizontal gradients in the aquifers are specified. This choice does not mean that these are the preferred field measurements, but rather that the overall head drop is the most permanent condition.

The occurrence of any new pathways on the site would tend to alter individual layer head drops and individual path recharge or discharge rates, whereas overall head drops and gradient are less likely to be influenced by variations in individual path segments. Only gross climatic or geological

BEST DOCUMENT AVAILABLE

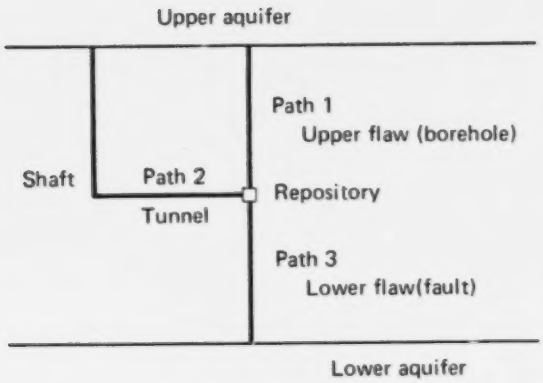

FIG. 7-1. Parallel path flow network.

BEST DOCUMENT AVAILABLE

variations can be expected to have a large effect on the overall head drops. Given this choice, the total discharge rate for the single series of paths is given by:

$$Q = \left(\sum_{i=1}^{n} TR_i^{-1} \right)^{-1} \Delta H_t \ , \tag{7-1}$$

where $TR_i = K_i A_i / L_i$, (7-2)

L = length,

A = area,

K = hydraulic conductivity,

ΔH_t = total head drop between aquifers.

TR is commonly known as the transmissivity of a flow path. Equation (7-1) follows from D'Arcy's Law:

$$\text{i)} \quad Q_i = A_i K_i \frac{\Delta H_i}{L_i} \tag{7-3}$$

water flux conservation,

$$\text{ii)} \quad Q_i = Q_{i+1} \ , \tag{7-4}$$

and the boundary condition,

$$\text{iii)} \quad \sum_{i=1}^{n} \Delta H_i = \Delta H_t \tag{7-5}$$

The D'Arcy velocity, defined as the discharge rate per unit area, is then given by

$$q_i = \frac{Q}{A_i} \ , \tag{7-6}$$

while the head drop in any given layer is

$$\Delta H_i = \frac{Q}{TR_i} \tag{7-7}$$

BEST DOCUMENT AVAILABLE

Finally, the water velocity and transit time for any path segment are given respectively by:

$$V_i = \frac{q_i}{\theta_i} = \frac{Q}{A_i \theta_i} \tag{7-8}$$

and

$$T_i = \frac{L_i}{V_i} = \frac{L_i A_i \theta_i}{Q} , \tag{7-9}$$

where θ_i = effective porosity.

In field test situations where the flow is along reasonably constrained pathways, the quantities usually measured are transmissivities and head drops. These quantities are, therefore, likely to be known with much greater accuracy than the average cross-sectional area and effective porosity, especially near a repository, where fracture rather than interstitial is likely to be the dominant flow type. Further, there is likely to be among candidate sites, a wide range of values for areas and porosities of possible flaws. For any given set of paths, it is a straightforward matter to determine probability distributions for velocities or transit times once the interdependent water fluxes, Q_i, have been extracted from the transmissivity and head measurements. The distributions for velocities usually reflect the larger uncertainties in the porosities and areas. For these reasons, the sensitivity analysis presented here focuses on the flux calculations, and especially on computing a set of interrelated fluxes for a flow network system.

7.2 ANALYSIS

For the configuration in Fig. 7-1, the zero point for head measurements is taken to be the intersection of the upper aquifer with Path 1. Specified head drops of ΔH_h and ΔH_v are assumed between the upper aquifer points for Paths 1 and 2, the upper aquifer point for Path 1, and the lower aquifer point for Path 3. These configurations with these assumptions then imply the following equations for total zero head drop for any closed loop and the

BEST DOCUMENT AVAILABL

conservation of flux at the junction of Paths 1, 2, and 3. The resistivity, R, is the inverse of the transmissivity, TR, defined by Eq. (7-10):

$$\Delta H_v = Q_1 R_1 + Q_3 R_3 = Q_1 (R_1 + R_3) + Q_2 R_3$$

$$\Delta H_h = Q_1 R_1 - Q_2 R_2 \text{ with } Q_3 = Q_1 + Q_2. \tag{7-10}$$

In matrix form:

$$\begin{pmatrix} \Delta H_v \\ \Delta H_h \end{pmatrix} = \begin{pmatrix} R_3 + R_1 & R_3 \\ R_1 & -R_2 \end{pmatrix} \begin{pmatrix} Q_1 \\ Q_2 \end{pmatrix}. \tag{7-11}$$

Solving for Q_1 and Q_2 gives:

$$Q_1 = (R_2 \Delta H_v + R_3 \Delta H_h)/D$$

$$Q_2 = (R_1 \Delta H_v - (R_1 + R_3) \Delta H_h)/D, \tag{7-12}$$

where $D = R_1 R_2 + R_1 R_3 + R_2 R_3$.

Writing these expressions in terms of transmissivities gives

$$Q_1 = TR_1 (TR_3 \Delta H_v + TR_2 \Delta H_h) / \left(\sum_1^3 TR_i \right)$$

$$Q_2 = TR_2 (TR_3 \Delta H_v - (TR_1 + TR_3) \Delta H_h) / \left(\sum_1^3 TR_i \right) . \tag{7-13}$$

And noting $Q_3 = Q_1 + Q_2$, we have

$$Q_3 = TR_3 \, [TR_1 \Delta H_v + TR_2 (\Delta H_v - \Delta H_h)] / \left(\sum_1^3 TR_i \right) .$$

BEST DOCUMENT AVAILABLE

It is often useful to have a (Taylor) series expansion for these fluxes for the case where one of the TR's is small compared to the other two. Explicitly:

$$Q_1 \underset{TR_3 \to 0}{\cong} \frac{TR_1 TR_2 \Delta H_h}{TR_1 + TR_2} + TR_3 \left[\frac{TR_1 \Delta H_v}{TR_1 + TR_2} - \frac{TR_1 TR_2 \Delta H_h}{(TR_1 + TR_2)^2} \right]$$

$$Q_2 \underset{TR_3 \to 0}{\cong} - \frac{TR_1 TR_2 \Delta H_h}{TR_1 + TR_2} + TR_3 \left[\frac{TR_2 (\Delta H_v - \Delta H_h)}{TR_1 + TR_2} + \frac{TR_1 TR_2 \Delta H_h}{(TR_1 + TR_2)^2} \right]$$

$$Q_1 \underset{TR_2 \to 0}{\cong} \frac{TR_1 TR_3 \Delta H_h}{TR_1 + TR_3} + TR_2 \left[\frac{TR_1 \Delta H_h}{TR_1 + TR_3} - \frac{TR_1 TR_3 \Delta H_v}{(TR_1 + TR_3)^2} \right]$$

$$Q_2 \underset{TR_2 \to 0}{\cong} \frac{TR_2 \left[TR_3 (\Delta H_v - \Delta H_h) - TR_1 \Delta H_h \right]}{TR_2 + TR_3}$$

$$Q_1 \underset{TR_1 \to 0}{\cong} TR_1 \frac{\left[TR_3 \Delta H_v + TR_2 \Delta H_h \right]}{TR_2 + TR_3}$$

$$Q_2 \underset{TR_1 \to 0}{\cong} \frac{TR_2 TR_3 (\Delta H_v - \Delta H_h)}{TR_2 + TR_3} + TR_1 \left[\frac{-TR_2 \Delta H_h}{TR_2 + TR_3} - \frac{TR_2 TR_3 (\Delta H_v - \Delta H_h)}{(TR_2 + TR_3)^2} \right]. \qquad (7\text{-}14)$$

The nonvanishing terms in the above limits represent the values appropriate to a subarray of the original path set (i.e., where one of the pathways is no longer present). From Eq. (7-13), it is clear that the sign (direction) of the two flow rates is a function of the ratio of horizontal head drop to vertical head drop and the ratios of various transmissivities. Explicitly:

BEST DOCUMENT AVAILABLE

$$Q_1 \begin{Bmatrix} \geq 0 \\ \leq 0 \end{Bmatrix} \quad \text{if} \quad \begin{Bmatrix} TR_3\Delta H_v \geq -TR_2\Delta H_h \\ TR_3\Delta H_v \leq -TR_2\Delta H_h \end{Bmatrix}$$

$$Q_2 \begin{Bmatrix} \geq 0 \\ \leq 0 \end{Bmatrix} \quad \text{if} \quad \begin{Bmatrix} TR_3(\Delta H_v - \Delta H_h) \geq TR_1\Delta H_h \\ TR_3(\Delta H_v - \Delta H_h) \leq TR_1\Delta H_h \end{Bmatrix} . \qquad (7\text{-}15)$$

If both ΔH_v and ΔH_h are positive (Path 2 upstream from Path 1), then Q_1 is always positive; in addition, if ΔH_v is less than ΔH_h, then Q_2 is always negative. Physically, this corresponds to the case where it is simply easier for some of the water going out Path 1 to come from the same aquifer but from upstream. If ΔH_v exceeds ΔH_h, then, depending on the ratio of TR_1/TR_3, the flow for Path 2 can be either positive or negative. If ΔH_h is negative and ΔH_v is positive (i.e., upward vertical flow, Path 2 downstream from Path 1), then Q_2 is always positive, while the direction of Q_1 is dependent on the ratio of TR_2/TR_3. In both cases for the sign of ΔH_h, the ratio of the transmissivities for two paths determines the direction of the flow for the third path. It does not depend on its own transmissivity. If $\Delta H_h = 0$ (i.e., Paths 1 and 2 are lateral to each other with respect to the direction of flow), then both Paths 1 and 2 have upward flow.

Having established these qualitative results, the question is raised: what are the first order sensitivities of the fluxes to the transmissivities TR_1, TR_2, and TR_3? To answer this question, we write the first partial derivatives in the following form:

$$\frac{\partial Q_1}{\partial TR_1} = \frac{(TR_2 + TR_3)}{\Sigma TR_i}\frac{(Q_1)}{TR_1}, \quad \frac{\partial Q_2}{\partial TR_1} = \frac{-TR_2}{\Sigma TR_i}\frac{(Q_1)}{TR_1}, \quad \frac{\partial Q_3}{\partial TR_1} = \frac{TR_3}{\Sigma TR_i}\frac{(Q_1)}{TR_1}$$

$$\frac{\partial Q_1}{\partial TR_2} = \frac{-TR_1}{\Sigma TR_i}\frac{(Q_2)}{TR_2}, \quad \frac{\partial Q_2}{\partial TR_2} = \frac{TR_1 + TR_3}{\Sigma TR_i}\frac{(Q_2)}{TR_2}, \quad \frac{\partial Q_3}{\partial TR_2} = \frac{TR_3}{\Sigma TR_i}\frac{(Q_2)}{TR_2}$$

$$\frac{\partial Q_1}{\partial TR_3} = \frac{TR_1}{\Sigma TR_i}\frac{(Q_3)}{TR_3}, \quad \frac{\partial Q_2}{\partial TR_3} = \frac{TR_2}{\Sigma TR_i}\frac{(Q_3)}{TR_3}, \quad \frac{\partial Q_3}{\partial TR_3} = \frac{TR_1 + TR_2}{\Sigma TR_i}\frac{(Q_3)}{TR_3} . \qquad (7\text{-}16)$$

BEST DOCUMENT AVAILABLE

These partial derivatives can all be bounded. In particular they are proportional to the head drop across the path corresponding to the transmissivity being varied, i.e.,

$$\frac{\partial Q_i}{\partial TR_j} \sim \Delta H_j \text{ since } \Delta H_j = \frac{Q_j}{TR_j} \quad .$$

The head drop across any path is bounded by the sum of the vertical and horizontal drops, i.e.,

$$|\Delta H_j| \leq |\Delta H_v| + |\Delta H_h| \quad .$$

The proportionality constant is less than one because it is the ratio of one or two transmissivities to the sum of all three. Thus,

$$\left| \frac{\partial Q_i}{\partial TR_j} \right| \leq |\Delta H_v| + |\Delta H_h| \quad . \tag{7-17}$$

It follows from Eq. (7-14) that for a small transmissivity in the lower path ($TR_3 \to 0$), the flow in the upper paths ($j = 1,2$) is:

$$Q_j = (-1)^{j+1} \frac{\Delta H_h}{\frac{1}{TR_1} + \frac{1}{TR_2}} \quad , \tag{7-18}$$

and therefore in this case ($TR_3 \to 0$):

$$Q_j \approx (-1)^{j+1} TR_i \, \Delta H_h \quad . \tag{7-19}$$

It follows from Eq. (7-13) that, for a large transmissivity in the lower path ($TR_3 \to \infty$), the flow in the upper paths is:

$$\begin{aligned} Q_1 &= TR_1 \, \Delta H_v \\ Q_2 &= TR_2 (\Delta H_v - \Delta H_h) . \end{aligned} \tag{7-20}$$

BEST DOCUMENT AVAILABLE

Physically, the case when $TR_3 = 0$ implies that no water flows up from the lower aquifer; therefore, the only flow is from the upstream path, through the repository and out the downstream path. Whichever transmissivity of Paths 1 and 2 is smaller will then govern the magnitude of the total flow. In the case when $TR_3 \to \infty$, the lower path admits so much flow that there is no head drop across it, and the flow in the upper paths is then governed by D'Arcy's Law. These qualitative considerations are borne out by the sensitivity results illustrated in Figs. 7-2 through 7-9. These are contour plots of equal water flux out of the "downstream" path (#1 if $\Delta H_h > 0$, #2 if $\Delta H_h < 0$) as a function of the transmissivities of the two upper pathways. The different plots correspond to different values of TR_3 and ΔH_h, while ΔH_v was set to a given value of 10 m in all cases.

To interpret these plots, it is useful to rewrite Eq. (7-13) in the form $TR_2 = f_i(Q_i, TR_i, \Delta H_v, \Delta H_h, TR_3)$:

$$TR_2 = \frac{-[TR_1 + TR_3]\, Q_2}{TR_1 \Delta H_h + Q_2 + TR_3(\Delta H_h - \Delta H_v)} \qquad (7\text{-}21)$$

$$TR_2 = \frac{TR_1(TR_3 H_v - Q_1) - Q_1 TR_3}{(Q_1 - TR_1 \Delta H_h)}$$

The level values for Q_1 and Q_2 chosen in the plots always correspond to 10^n for some integer n, while TR_3 always has the form 10^m for some integer m. With $H_v = 10$, this gives:

$$TR_2 = \frac{-[TR_1 + 10^m]\, 10^n}{TR_1 \Delta H_h + 10^n + 10^m(\Delta H_h - \Delta H_v)} \qquad (7\text{-}22)$$

$$TR_2 = \frac{TR_1(10^{m+1} - 10^n) - 10^{n+m}}{(10^n - TR_1 \Delta H_h)}$$

BEST DOCUMENT AVAILABLE

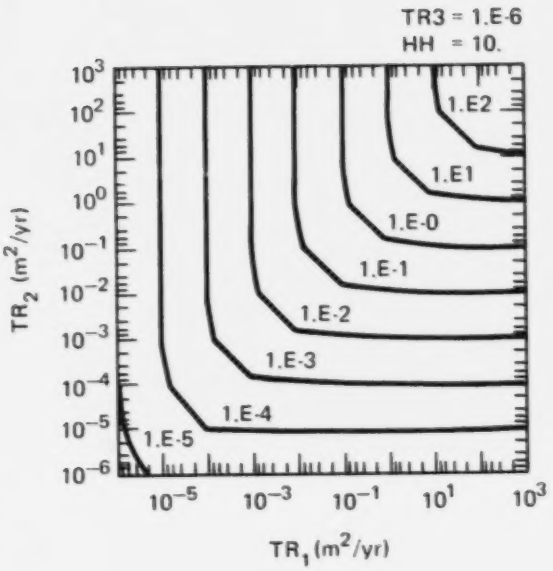

FIG. 7-2. Downstream flux, Q_1 in m^3/yr (TR3 = 1.E-6; HH = 10).

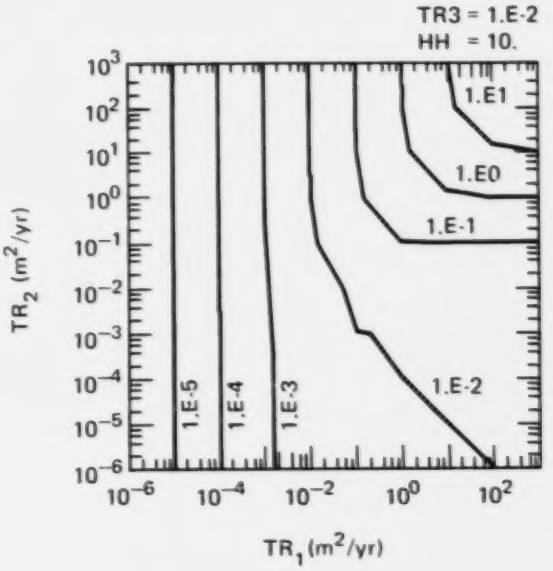

FIG. 7-3. Downstream flux, Q_1 in m^3/yr (TR3 = 1.E-2; HH = 10).

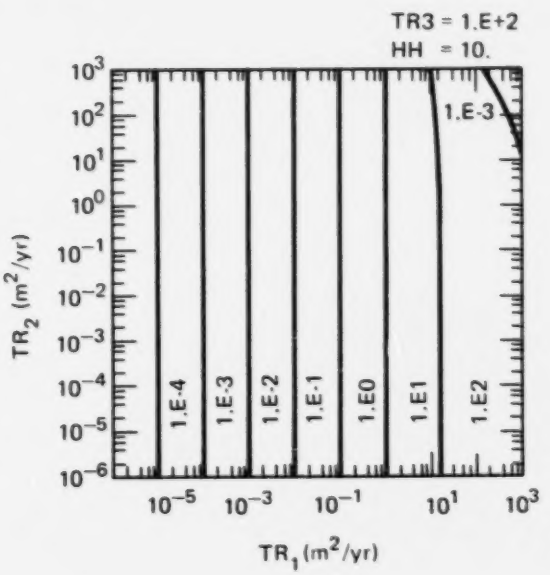

FIG. 7-4. Downstream flux, Q_1 in m^3/yr (TR3 = 1.E+2; HH = 10).

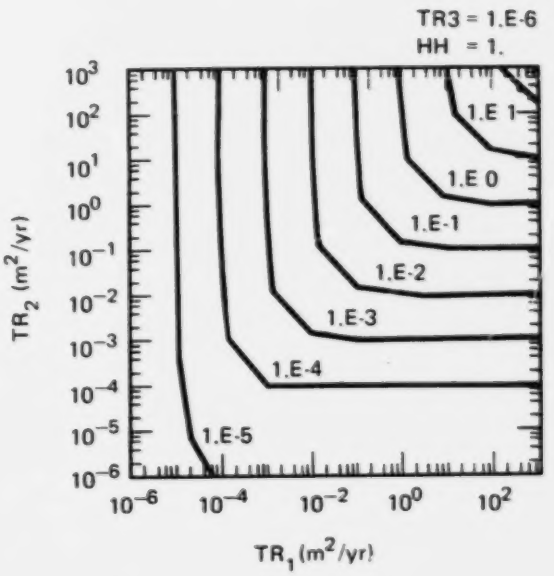

FIG. 7-5. Downstream flux, Q_1 in m^3/yr (TR3 = 1.E-6; HH = 1).

BEST DOCUMENT AVAILABLE

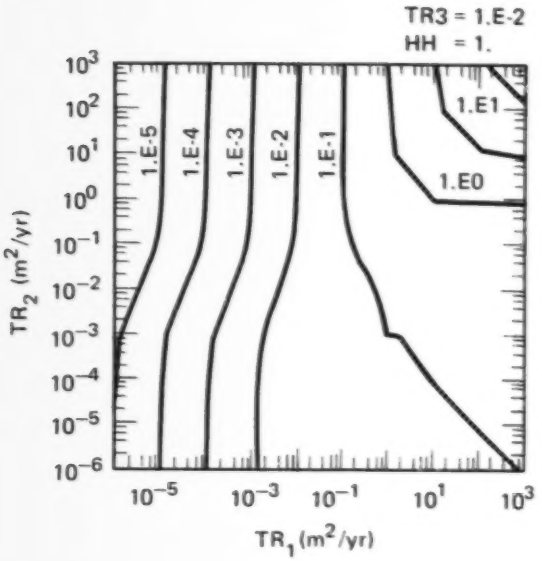

FIG. 7-6. Downstream flux, Q_1 in m^3/yr (TR3 = 1.E-2; HH = 1).

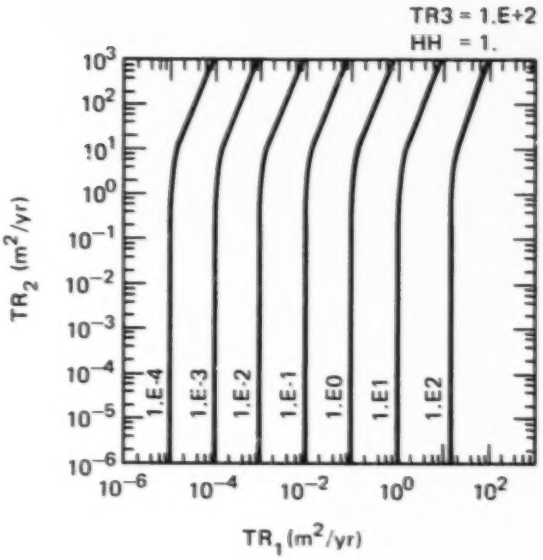

FIG. 7-7. Downstream flux, Q_2 in m^3/yr (TR3 = 1.E+2; HH = 1).

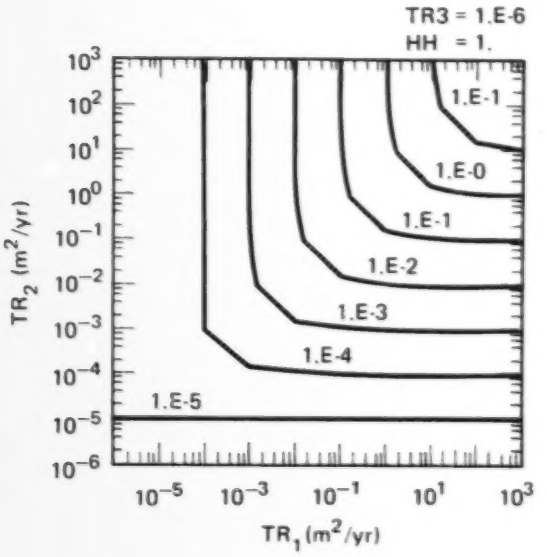

FIG. 7-8. Upstream flux, Q_2 in m^3/yr (TR3 = 1.E-6; HH = 1).

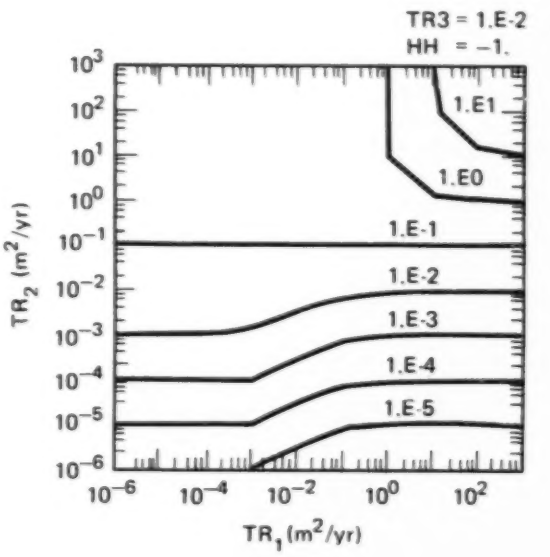

FIG. 7-9. Upstream flux, Q_2 in m^3/yr (TR3 = 1.E-2; HH = -1).

BEST DOCUMENT AVAILABLE

In Figs. 7-2 through 7-4, ΔH_h = +10 and m = -6, -2, +2, respectively. In Fig. 7-2, the form of the contour plot is then determined by the following equation:

$$TR_2 = \frac{TR_1(10^{-5} - 10^n) - 10^{n-6}}{10^n - 10TR_1} \rightarrow \begin{cases} \infty \text{ as } TR_1 \rightarrow 10^{n-1} \\ 10^{n-1} \text{ as } TR_1 >> 10^{n-1} \text{ and } n > -5 \end{cases} . \quad (7\text{-}23)$$

In Fig. 7-2, m = +2 and the equation for a contour is

$$TR_2 = \frac{TR_1(10^3 - 10^n) - 10^{2+n}}{(10^n - 10TR_1)} = \frac{1}{10^{1-n}TR_1 - 1} - 10^2 , \quad (7\text{-}24)$$

or equivalently, with TR_1 as a function of TR_2,

$$TR_1 = 10^{n-1} + \frac{10^{n-1}}{TR_2 + 10^2} \cong 10^{n-1} \text{ for } TR_2 << 10^2 . \quad (7\text{-}25)$$

These considerations are consistent with limiting forms of Eq. (7-21). For example, the cases of $TR_3 = 10^{-6}$ and $TR_3 = 10^2$, which correspond roughly to the cases where $TR_3 \rightarrow 0$ and $TR_3 \rightarrow \infty$, respectively.

Figures 7-5 through 7-7 illustrate the type of behavior obtained when the value of ΔH_h is 1 m. Compare these with the corresponding figures, where ΔH_h = 10 m indicates only one major qualitative difference. The vertical contours appropriate to regions where $TR_3 >> TR_1$ (Figs. 7-6 and 7-7) now have a kink in them (i.e., two offset vertical segments joined by a slightly sloping segment). This kink can be explained from Eq. (7-13) for Q_1 (with $TR_3 >> TR_1$): when $TR_2 << TR_3$, $Q_1 = TR_1\Delta H_v$; while when $TR_2 >> TR_3$ $(\Delta H/H_h)$, $Q_1 = TR_1\Delta H_h$. Since ΔH_v is 10 times ΔH_h, there exist two distinct vertical segments with a transition zone around $TR_2\Delta H_h = TR_3\Delta H_v$. Physically, the first case corresponds to a transmissivity for Pipe 3, which is so large that there is virtually no head drop across this path. Therefore,

BEST DOCUMENT AVAILABLE

the head drop across Path 1 is ΔH_v. The flow up Path 2 in this case is $TR_2(\Delta H_v - \Delta H_h)$, which is in accordance with the negligible head drop across Path 3. In the second case, the transmissivity in Path 2 is so large that there is no head drop across this path. This implies that the bottom of Path 1 (at the intersection with Paths 2 and 3) is at the same potential as the top of Path 2: i.e., ΔH_h. The flow in the various paths follow accordingly.

All six plots have been Q_1 plots. The corresponding Q_2 plots have not been constructed, because both ΔH_v and ΔH_h were taken positive, and for various values of transmissivities, the flow in Pipe 2 may be downward (i.e., $Q_2 < 0$). It is useful to know what value of TR_1 corresponds to the value $Q_2 = 0$ in the plots. From Eq. (15), this can be seen to occur at:

$$TR_1 = \frac{TR_3(\Delta H_v - \Delta H_h)}{\Delta H_h} \quad .$$

For $\Delta H_v = \Delta H_h$, the flow through Path 2 is always downward, while when $\Delta H_v = 10\Delta H_h$ (as in Figs. 7-2 through 7-7), then, $TR_1 = 9TR_3$ is the transition value. In Figs. 7-5, 7-6 and 7-7, the values are 9×10^{-5}, 9×10^{-1}, and 9×10^{2}, respectively. All values of TR_1 larger than these give downward flow for Q_2.

Deterministic results in this section can be used to predict many of the qualitative features of an uncertainty analysis (of the type presented in previous sections). Explicitly, when TR_3 is large, the contour results indicate that Q_j is dependent only on TR_j. Therefore, setting the other transmissivities certain would have no effect on the uncertainty of Q_j. Likewise, when TR_3 is known to be smaller than either TR_1 or TR_2, then the smaller of the two TR_i's controls the flux. As long as the probability distributions for the two TR_i's do not substantially overlap, setting the smaller TR's certain will have maximum effect, the larger TR's uncertainty having little effect.

7.3 CONCLUSIONS

Several conclusions can be drawn from the analysis of the previous subsection.

1. An upper bound can be determined for the first derivatives (first-order sensitivities) of the fluxes with respect to the transmissivities. Knowledge of the head drop in a path will allow a lower upper bound than that directly available from Eq. (7-17). These first-order sensitivities are very useful in estimating the effect of uncertainty in the measured value of any transmissivity on flux values.

2. When the transmissivity of the lower path is very low compared to the other paths, the flow is then primarily down through the upstream flaw and up through the downstream flaw. The magnitude of the flow will be governed by the smaller transmissivity.

3. When the transmissivity of the lower path is intermediate between the other two, the values of various head drops are determined by the relative magnitudes of the horizontal and vertical head drops and ratios of the two largest transmissivities. The fluxes from these head drops can then be determined from Eq. (7-7).

4. There are combinations of transmissivities and head drops that give zero flow in the upstream path. This condition does <u>not</u> depend on the transmissivity of the upstream path. It does depend, however, on the horizontal head drop between the upper outlets of the two upper paths. This last quantity, is to a certain extent, an engineerable value (as opposed to essentially all the other quantities in the analysis). For instance, if one of the flaws were a ventilation shaft or a set of exploratory boreholes, while the other flaw were the main shaft, it might be possible to choose the relative positions of the two flowpaths in such a way that the flow in a significant fraction of the repository would be very small. Careful consideration of such factors in repository design may yield significant reductions in risk.

ACKNOWLEDGMENTS

Systems Characteristics Analysis stems from a previous waste management project at LLNL. The authors wish to acknowledge those who contributed directly or indirectly to this work by their efforts in that project. We also wish to thank Dr. John D. Waddell, Project Manager at ONWI, for his continued support and guidance.

The principal analytic tool was the MACRO2 Code, developed primarily by A. M. Kaufman, and N. K. Madsen. The studies presented in Sections 5 and 7 were conducted by G. D. Pollak; the analyses in Section 6 by K. G. Feller.

We also thank L. L. Edwards and E. A. Collins for their work in support of this project. Finally, we express our gratitude to Roberta E. Burns for accomplishing all the tasks of Project Secretary in addition to the most difficult task of producing this manuscript.

*U.S. GOVERNMENT PRINTING OFFICE 1982/559-099/5345